Characterization of PIBSI Dispersants and Their PIBSA Components by Pyrene Excimer Fluorescence

by

Franklin Frasca

A thesis

presented to the University of Waterloo

in fulfillment of the

thesis requirement for the degree of

Master of Science

in

Chemistry

Waterloo, Ontario, Canada, 2020

Author's Declaration

I hereby declare that I am the sole author of this thesis. This is a true copy of the thesis, including any required final revisions, as accepted by my examiners.

I understand that my thesis may be made electronically available to the public.

Abstract

Methods are introduced to characterize the products resulting from the coupling of a polyisobutylene terminated at one end with a succinic anhydride (PIBSA) and a polyamine to generate PIBSI products where the polyamine is flanked by one or two PIB segments via a succinimide bond. The molar fraction of doubly modified PIBSA ($PIBSA_2$) molecules in two PIBSA samples (PIBSA-1 and PIBSA-2) was first determined using pyrene excimer formation (PEF) to analyse both PIBSA samples after labeling fractionated and unfractionated PIBSA samples with 1-pyrenemethylamine (PyMA) to generate PIBSA-PyMA. The ratios of succinic anhydrides, succinimides, or pyrenyl labels to the number of isobutylene units N_{SA}/N_{IB}, N_{SI}/N_{IB}, and N_{Py}/N_{IB} determined by FTIR and UV-Vis spectroscopy established that the succinic content of the unfractionated PIBSA-PyMA samples was roughly double that of the fractionated samples, suggesting a difference in the molecular weight distribution (MWD) of the samples which was confirmed by GPC analysis. Model free analysis (MFA) of the time-resolved fluorescence (TRF) decays yielded the average rate constant of pyrene excimer formation by diffusion ($<k>$) which increased linearly with $[Py]$, and the molar fraction f_{agg} of PyMA attached on $PIBSA_2$ forming excimer by direct excitation of aggregated pyrene dimers, and in turn the fraction (f_{doubly}) of $PIBSA_2$ in each sample. f_{agg} was higher for PIBSA-1 and did not change between the fractionated or unfractionated samples suggesting that $PIBSA_2$ was evenly distributed across the MWD of PIBSA. The number average degree of polymerization (X_n) was calculated for the PIBSA-PyMAs and showed a linear relationship with the rate constant (k_{diff}) describing PEF by diffusion.

Next, it was hypothesized that the composition of the mixture of a coupling reaction between PIBSA and a polyamine could be predicted with the knowledge of the ratio of the number of amines to SA units (N_{Am}/N_{SA}) available for the coupling reaction, the N_{SA}/N_{IB} ratio, and the fraction (f_{doubly}) of $PIBSA_2$ chains in the PIBSA sample. Two programs were written to simulate the products generated from the coupling of PIBSA with a diamine to form either *bis*-PIBSI (*b*-PIBSI) and higher-order PIBSI oligomers, or to only form *b*-PIBSI assuming that steric hindrance

prevented more than one PIBSA from linking to another PIBSA molecule. A set of PIBSA to hexamethylene diamine (HMDA) coupling reactions were conducted with a fractionated PIBSA-2 sample to yield the PIBSA-2-H(X) samples, where X equals the N_{Am}/N_{SA} ratio used in a coupling reaction, and generate DRI traces with GPC for use with the simulated data and the validation of the simulation programs. Parameterization of the DRI traces with sums of Gaussians enabled the determination of the fractions of PIBSA-like molecules (PLMs) and non-PIBSA-like molecules (non-PLMs) and their comparison with the fractions obtained from the simulations. This along with GPC analysis suggested that PIBSA-2 contained 30 wt% of unmaleated PIB. When assuming that the PIBSA coupling reaction could only form *b*-PIBSI, excellent agreement was found between the experimental and simulated DRI traces supporting the validity of this assumption.

Lastly, a study was conducted with a series of pyrene-labeled polyamines (Py-PAs) representative of the core of a PIBSI dispersant, to examine the relationship between the fluorescence intensity ratio of the pyrene excimer over that of the monomer (I_E/I_M), $\langle k \rangle$, and the local pyrene concentration ($[Py]_{loc}$) in the Py-PAs, and ultimately assess the usefulness of $\langle k \rangle$ for establishing a $\langle k \rangle$-*vs*-$[Py]_{loc}$ calibration curve to characterize the polyamine core of pyrene-labeled PIBSI dispersants. MFA of the TRF decays acquired with the Py-PAs yielded $\langle k \rangle$ and the analysis of the fluorescence spectra yielded I_E/I_M. Both $\langle k \rangle$ and I_E/I_M increased linearly with increasing $[Py]_{loc}$, suggesting that the $\langle k \rangle$-*vs*-$[Py]_{loc}$ plot could be used as a calibration curve for analysis of the polyamines in the PIBSI cores.

The methods detailed in this thesis expand on the use of PEF to study PIBSA-coupling procedures introduced in previous work by A. Mathew and S. Pirouz, and have resulted in a variety of interesting findings about the PIBSA samples studied herein such as the content of $PIBSA_2$ in a PIBSA sample and accurate predictions of the PIBSI coupling products taking into account f_{agg} determined by PEF. These experiments further emphasize the usefulness of PEF as a characterization method for macromolecules in general, and oil-additives specifically.

Acknowledgements

I would like to thank the Afton Chemical Corporation for the opportunity to perform this research. In addition, I would like to thank my supervisor, Professor Jean Duhamel, for his guidance and encouragement throughout the project. I would also like to thank my committee members Professors Mario Gauthier and Costas Tzoganakis for their advice on the project, as well as Afton Chemical Corporation representatives Drs. Steven Dell and David Edwards. I would also like to thank the members of the Duhamel group for providing a pleasant and helpful atmosphere in the laboratory. Finally, I would like to thank my partner Nicole for her continued support and encouragement throughout the project.

Table of Contents

List of Figures

List of Tables

List of Schemes

List of Abbreviations

a.u.	Arbitrary units
AA	Acetic acid
a_i	Pre-exponential/Pre-Gaussian factors
A^{Peak}	Absorbance at the peak of the $S_{0,0} \rightarrow S_{2,0}$ transition of a pyrene-labeled molecule
A^{Valley}	Absorbance of the valley adjacent to the peak of the $S_{0,0} \rightarrow S_{2,0}$ transition of a pyrene-labeled molecule
b-PIBSI	*bis*-PIBSI
*D**	Improperly stacked pyrene excimer
DCM	Dichloromethane
DETA	Diethylene triamine
DMSO	Dimethyl sulfoxide
dn/*dc*	Specific refractive index increment
*E**	Pyrene excimer
*E*0*	Properly stacked pyrene excimer
EGR	Exhaust gas recirculation
f_{agg}	Molar fraction of pyrene labels forming excimer by excitation of aggregated pyrenes
f_{diff}	Molar fraction of pyrene labels forming excimer by diffusion
f_{doubly}	Fraction of doubly-maleated PIB chains in a PIBSA sample
f_{free}	Molar fraction of pyrene labels emitting as free monomer

f_{inter}	Molar fraction of pyrene labels forming excimer intermolecularly
f_{intra}	Molar fraction of pyrene labels forming excimer intramolecularly
GPC	Gel permeation chromatography
HMDA	Hexamethylene diamine
HOBt	Hydroxybenzotriazole
HOSu	*N*-Hydroxysuccinimide
I_E/I_M	Ratio of excimer to monomer fluorescence intensity
$<k>$	Average rate constant of pyrene excimer formation
k_{cy}	Rate constant of end-to-end cyclization
k_{diff}	Bimolecular rate constant for PEF by diffusive encounters
m	Massic concentration
M^*	Pyrene monomer
MeOH	Methanol
MFA	Model free analysis
M_{IB}	Mass of isobutylene unit
M_n	Number average molecular weight
m-PIBSI	*mono*-PIBSI
M_{PySU}	Molar mass of 1-pyrenemethylsuccinimide unit
MS	Mass spectrometry
M_{SA}	Molar mass of succinic anhydride unit
M_w	Weight average molecular weight

MWD	Molecular weight distribution
NaCl	Sodium chloride
N_{Am}/N_{SA}	Ratio of amines-to-succinic anhydrides
N_{Py}/N_{IB}	Number of pyrenes per isobutylene unit
N_{SA}/N_{IB}	Number of succinic anhydrides per isobutylene unit
N_{SI}/N_{IB}	Number of succinimides per isobutylene unit
P_A	Peak-to-Valley ratio
PA	Polyamine
PDI	Polydispersity index
PEF	Pyrene excimer fluorescence
PEHA	Pentaethylene hexamine
PHZ	1-Pyrenebutylhydrazine
PIB	Polyisobutylene
PIBSA	Polyisobutylene terminated by succinic anhydride
$PIBSA_1$	PIBSA terminated with one SA unit
$PIBSA_2$	PIBSA terminated with two SA units at one end
PIBSI	Polyisobutylene terminated by succinimide
PLM	PIBSA-like molecule
PMA·HCl	1-Pyrenemethylamine hydrochloride
PPD	Pour point depressant
Py	Pyrene
$[Py]_{loc}$	Local pyrene concentration

Py_{agg}	Pyrene labels forming excimer by excitation of aggregated pyrenes
PyBA	1-Pyrenebutyric acid
PyBA-OSu	1-Pyrenebutyryl ester of *N*-hydroxysuccinimide
Py_{diff}	Pyrene labels forming excimer by diffusion
Py_{free}	Pyrene labels emitting as free monomer
PyLM	Pyrene-labeled macromolecule
PyMA	1-Pyrenemethylamine
Py-PA	Pyrene-labeled polyamine
RBF	Round bottom flask
SA	Succinic anhydride
SE	Succinic ester
SI	Succinimide
SSF	Steady-state fluorescence
TEPA	Tetraethylene pentamine
TETA	Triethylene tetramine
THF	Tetrahydrofuran
TRF	Time-resolved fluorescence
tri-PIBSI	PIBSI trimers
UFP	Ultrafine particle
V_{el}	Elution volume
V_H	Hydrodynamic volume
VII	Viscosity index improver

X_n	Degree of polymerization
ZDDP	Zinc dialkyldithiophosphates
ε	Molar extinction coefficient
ϕ	Quantum yield
η	Viscosity
λ_{Py}	Pyrene content
μ_i	Gaussian average
σ_i	Gaussian standard deviation
$<\tau>$	Number average lifetime of the pyrene monomer
τ_i	Decay time
τ_E	Lifetime of the pyrene excimer
τ_M	Natural lifetime of the pyrene monomer

Chapter 1

Literature Review

This thesis describes how pyrene excimer fluorescence (PEF) was applied to characterize the composition of PIBSIs, which are poly(isobutylene)s (PIBs) connected at one end to a polyamine via a succinimide and are used as oil additives, PIBSAs which are PIBs terminated at one end with a succinic anhydride and are used to prepare PIBSIs, and the polyamine core common to PIBSI dispersants. This was achieved through pyrene-labeling of the PIBSA precursors, some PIBSI dispersants, and the polyamines representative of the polyamine cores of a PIBSI dispersant. This introductory chapter begins with a discussion as to why lubricating fluids are needed, and how they have been modified to improve their properties over the years through the use of oil additives that enable them to last longer and offer more protection to the moving parts of an automobile engine. It then delves into the use of dispersants to mitigate the aggregation and deposition of insoluble particulates in an engine, followed by a description of the use and synthesis of PIBSI dispersants. This introduction continues with a review of fluorescence before discussing the use of PEF to characterize the structure and dynamics of various pyrene-labeled macromolecules (PyLMs), particularly those macromolecules being used as oil additives. The chapter concludes with an overview of the thesis objectives and summary of the research conducted in the following chapters.

1.1.1 Lubricating Oils and Additives

Lubricating oils are a necessity for machinery to operate smoothly. The thin lubricating layer that they create between moving metal parts protects them and reduces wear.[1-3] The oils used today are predominantly mineral oils, although synthetic and biologically derived oils are also available. Mineral oils are referred to as “base oil” and often make up 80-90% of the final lubricating fluid.[2] Base oils are often susceptible to oxidative and thermal degradation under the harsh conditions experienced during engine operation. As such, good lubrication is maintained over a sufficiently

long lifetime by mixing additives with the base oil to either enhance or add properties that the base oil lacks such as rust or corrosion resistance.[1-6] While additives were first introduced to decrease the frequency of oil changes, they are now employed for a variety of economical and environmental reasons such as fuel efficiency and mitigation of exhaust pollution, respectively.[2,3] Consequently, the choice of additives that are mixed into a given base oil will depend on the purpose of the final fluid. As their interactions and mechanisms of action have been studied by a variety of methods,[7-14] modern additives have imparted large improvements in both lubricant lifetime and engine efficiency.[2,3]

Some important additives found in engine oils are presented hereafter. Anti-oxidants minimize oxidative degradation of the oil by scavenging radical species.[2] Viscosity index improvers (VIIs) increase the viscosity index of the oil, which is a measure of the change in the oil viscosity with temperature, by maintaining the oil viscosity within set boundaries over a wider temperature range.[10,14,15] Polymeric dispersants stabilize polar particles generated in the oil during engine operation and prevent their aggregation or precipitation into soot and sludge.[2,3,12,15-18] Pour-point depressants (PPDs) lower the pour-point of an oil, i.e. the temperature below which an oil stops to flow, by hindering the wax left in the engine oil from forming a network upon cooling.[14,19] Anti-wear additives form films to prevent metal-on-metal contact under extreme pressures.[1,2,4] Some additives can also be designed to combine the specific properties of multiple individual additives, such as those of VIIs and dispersants[15,16,20,21] or anti-oxidants and anti-wear agents.[1,2,7,10] An important consideration in the use of oil additives is the interaction between additives which can in some cases help or hinder the functionality of the additives involved. For example zinc dialkyldithiophosphates (ZDDPs), which are commonly used in lubricating fluids to impart anti-wear properties,[1-4] are found to associate with succinimide dispersants leading to a large increase

in wear on the engine.[1,10] As such, research has focused on characterizing how different oil additives interact in order to better predict the properties of the resulting lubricating fluids[7-10] and to mitigate the loss of functionality resulting from two incompatible additives.

1.1.2 Insolubles and Their Dispersants

Soot and ultrafine particles are by-products created in an engine oil during its operation. Their polar surface induces their agglomeration in the engine oil to minimize their surface exposure to the apolar medium. Ultrafine particles (UFPs), which represent particles smaller than 100 nm, have been shown to penetrate deep into the lungs and are associated with a number of ailments.[22] They are also released through vehicle emissions.[23] These particles are formed when hot vapours generated by the engine become exposed to the lubricating fluid. The problem of UFP formation in engine oils has been exacerbated by the practice of exhaust gas recirculation (EGR), a technique which involves the recirculation of some of the exhaust gases back through the air intake before release in order to reduce the emission of nitrous oxides.[23] A diagram depicting EGR is shown in Figure 1.1. While EGR is effective in lowering nitrous oxide emissions, it results in the deposition of more particulate matter in the engine oil, which in turn reduces the lifetime of the oil by increasing its content of insoluble matter.[23] This results in an increase in viscosity known as "oil-thickening" which is detrimental to the function of the lubricant. Consequently, the reduction of the oil viscosity increased due to the presence of UFPs and other insoluble particles in lubricating fluids has been of great concern in oil formulation, and has resulted in the need for dispersants and detergents to mitigate the aggregation of insoluble matter.[24]

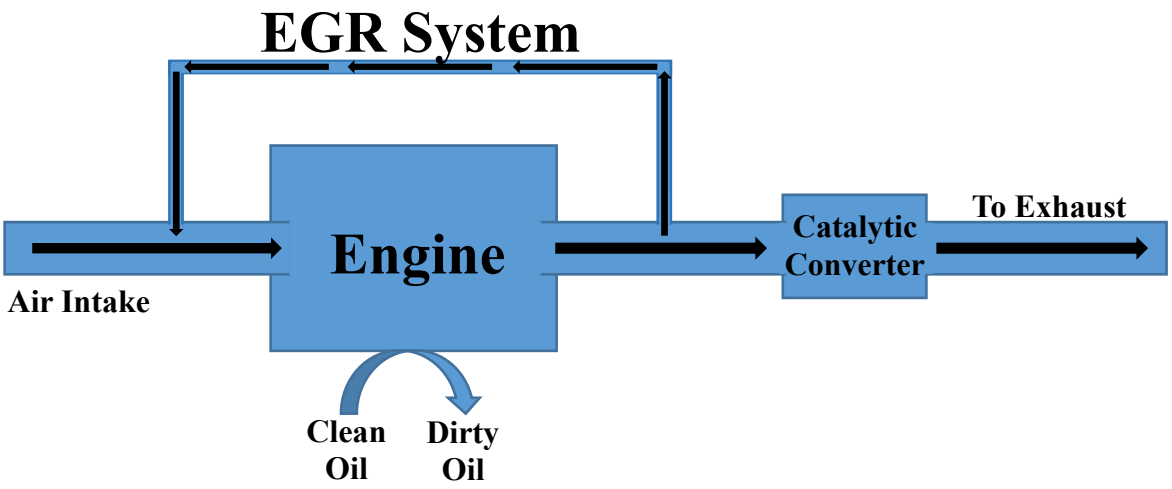

Figure 1.1. Diagram of an Exhaust Gas Recirculation system.

As mentioned previously, dispersants are polymeric additives designed to suspend insoluble matter in the oil and prevent their aggregation into particulates that would become large enough to precipitate. UFPs are a particular target of such dispersal. Dispersion is often achieved with block copolymers containing both polar and apolar segments. The apolar segment of the dispersant is typically much larger than its polar counterpart to keep the polymer soluble in the oil. The role of the smaller polar segments is to associate with the polar surface of particulate matter in the oil while the apolar segments of the dispersant extend into the oil, thus ensuring the stability of the particles.[1-4,10] Once dispersed by the additive, steric or electrostatic effects prevent further aggregation of the particles.[1-4,10] In terms of dispersant design, the apolar block should be sufficiently large with respect to the polar segment to prevent contact between the polar domains on the surface of two incoming particles, and thus prevent their aggregation and subsequent precipitation. Longer apolar blocks also aid in the solubility of dispersed particulate.[2] Conversely, a polar segment that is too small will result in a dispersant that cannot efficiently adhere to the surface of particles. Because of these and other reasons, the lubricant industry has developed

several synthetic routes and analytical methods to, respectively, produce and characterize a variety of dispersants since their inception in the 1950's.[3,25]

Dispersants were first added to engine oils in the 1950's to reduce particulate build up and to minimize the inherent thickening which arises from the presence of particulate aggregates in the lubricating fluid.[2-4,25] After observing that the utilization of dispersants increased the lifetime of both the engine and the lubricating fluid,[2-4,6] dispersants became an essential additive in lubricating oils, comprising up to 10% of some finished fluids in use today.[3] Many types of dispersants have been synthesised over the years, by mostly varying the polar segment to yield additives with different dispersancies, basicities, and solubilities which could be advantageous to different applications.[12,15-17,25-29] The polymeric dispersants of the PIBSI-type discussed in this review have a molecular weight that is often below 10 kg/mol, which is much smaller than the 25 to 500 kg/mol molecular weight of more typical dispersant polymers such as poly(alkyl methacrylate)s or styrene-diene copolymers.[2] Dispersant polymers frequently offer some VII properties along with dispersancy, but often lack sufficient dispersing capabilities to be used alone, and so are often used together with polymeric dispersants.[2] PIB is usually selected for polymeric dispersants due to its ease of manufacture and low cost.[2,3] Although most dispersants feature PIB segments, the subtle difference in properties imparted by different PIB lengths, degrees of branching, and polydispersities means that a wide variety of PIBs are being used to prepare dispersants today.[2] The moieties used to connect the polar and apolar segments of modern dispersants are often either phenol groups or succinic anhydrides (SAs), which yield Mannich-type[30] or PIBSA-based[1-4,20,31-33] dispersants, respectively. While polyamines are used in the synthesis of Mannich-type dispersants, both polyamines and polyalcohols of varying architectures can be used to link multiple PIBSA molecules together.[1-5] The choice of an amine or alcohol to generate polar groups in the

resulting dispersant decides whether a succinimide (SI) or succinic ester (SE) will be formed, although PIBSI dispersants are currently most widely used.[2,3] The high thermal and oxidative stability of PIBSA-based dispersants has led to their widespread use today over the Mannich-type equivalent, with PIBSI dispersants being preferred because their basicity induced by the amine groups provides better dispersancy than those obtained with polyalcohol polar groups.[2,3]

1.1.3 PIBSA/PIBSI

As PIBSI dispersants are the most abundantly used dispersants today, an understanding of their PIBSA blocks is important. PIBSA used to produce PIBSI dispersants is often prepared by acid-catalysed polymerization of isobutylene, using either boron trifluoride (BF_3) or aluminum trichloride ($AlCl_3$) as catalyst.[2] Depending on whether BF_3 or $AlCl_3$ is chosen, the PIB product will contain predominantly vinylidene or tri/tetrasubstituted alkenes, respectively, as shown in Figure 1.2.[2,31]

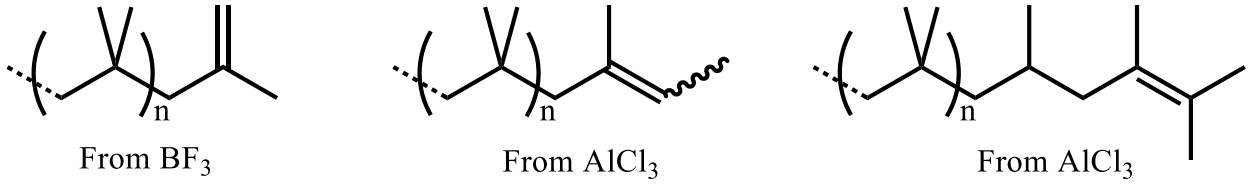

Figure 1.2. PIB products from polymerization of isobutylene with BF_3 or $AlCl_3$ catalysts.[3]

The choice of a catalyst often depends on the specifics of the final application, as different sterics about the terminal alkene result in slight differences in the chemical structure of their final products when converted to PIBSI dispersants.[2] PIBSAs with a molecular weight of 1 – 3 kg/mol are often used, which results in PIBSIs with molecular weights of 3 – 7 kg/mol. Once PIB has been polymerized, the maleic anhydride group is introduced into PIB to generate PIBSA in one of two ways, depending on how isobutylene was polymerized (see Figure 1.3).[2,3] PIB obtained from a

BF_3-catalysed polymerization requires a combination of high vinylidene content (1 vinylidene group for ~20 – 60 IB units), excess maleic anhydride, and high temperatures around 200 °C to form PIBSA.[2,3]

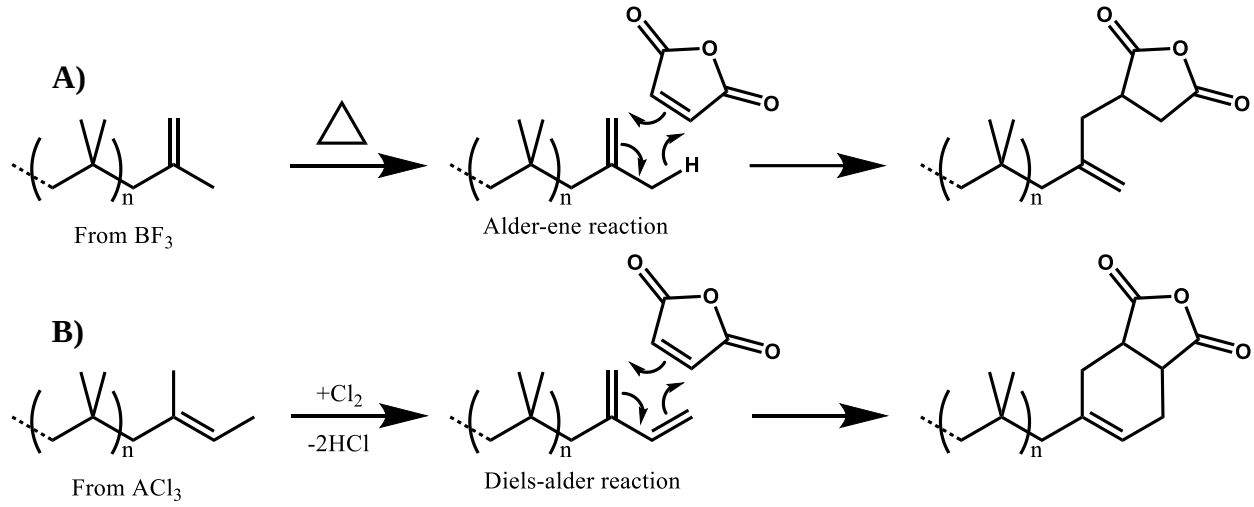

Figure 1.3. Reaction schemes for the maleation of PIB produced with A) a BF_3 and B) an $AlCl_3$ catalyst.[3]

In contrast, the PIB products generated by an $AlCl_3$-catalysed polymerization can be combined in a 1:1:1 molar ratio with chlorine and maleic anhydride without the need for high temperatures. The use of chlorine for the maleation of PIB prepared with an $AlCl_3$ catalyst leaves organic chlorides in the PIBSA product, which are an environmental concern. Consequently, maleation through the thermal pathway shown in Figure 1.3A is usually chosen despite the requirement for a higher vinylidene content.[3] As shown in Scheme 1.1, one complication associated with these syntheses is the potential occurrence of a second maleation through the alkene resulting from the first maleation. Consequently, the maleation of PIB can produce *mono*-PIBSA ($PIBSA_1$) and *bis*-PIBSA ($PIBSA_2$), which can generate a variety of complex architectures upon coupling with a polyamine core.[2,34,35]

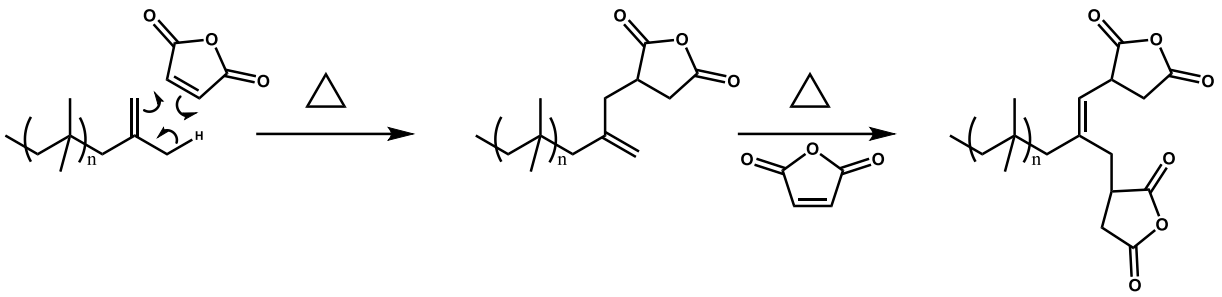

Scheme 1.1. Reaction of maleic anhydride with $PIBSA_1$ to form $PIBSA_2$.

Since the publication of the first PIBSI patents in 1965,[32,33] there has been a great deal of interest in studying how different syntheses or modifications can be applied to PIBSI dispersants in an effort to enhance their properties.[15,16,25-30] The main adjustments revolve about changing the length of the PIB chains and the size and architecture of the polyamines used to prepare the PIBSI dispersants. In practice, multiple PIBSI groups are linked by linear ethylene polyamines such as triethylene tetramine (TETA), tetraethylene pentamine (TEPA), pentaethylene hexamine (PEHA), or longer polyamines since their high amine content enhances the associative properties of the dispersant.[2,3,36] The preparation of *b*-PIBSI is shown in Scheme 1.2. While PIBSIs have been produced by reacting one and two molar equivalents (meq)s of PIBSA with a polyamine to generate *m*-PIBSI and *b*-PIBSI respectively, currently employed dispersants often feature *b*-PIBSIs as their additional PIB block provides better dispersancy compared to *m*-PIBSI.[9] *m*-PIBSI has also been shown to interact with, and thus deactivate, the commonly used ZDDP anti-wear additives to a greater extent than their *b*-PIBSI counterparts, which results in increased engine wear when using formulations with *m*-PIBSIs instead of *b*-PIBSIs.[7,10]

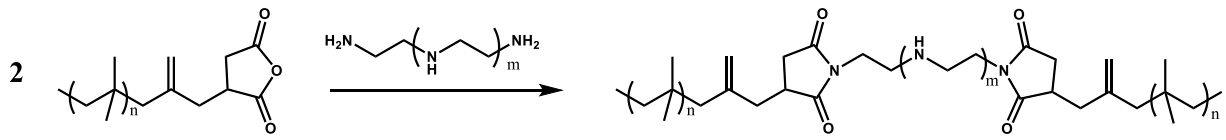

Scheme 1.2. General scheme for the synthesis of *b*-PIBSI dispersants.

The nitrogen content of a PIBSI dispersant is often a good indicator of its associative capability, but a high nitrogen content can also result in detrimental side effects. Amines are mildly basic and the basicity of an oil loaded with too many amines can damage the engine seals.[2,3] PIBSI dispersants can also be further modified to mitigate their basicity or impart new properties by reacting the amines with compounds like boric acid or ethylene carbonate.[37,38]

1.1.4 Characterization

It follows that the formulation of an engine oil with PIBSI dispersants is the result of a careful balance between a variety of factors. To be effective, the chemical composition of a PIBSI dispersant must be fully characterized in terms of its number of effective amines, molecular weight distribution (MWD) and branching level of PIB, and the average number of PIBSI units per dispersant molecule. Unfortunately, such detailed analysis remains a challenging goal.

For instance, hydrogen bonding between the amine hydrogens and the carbonyls of the succinimides constituting the PIBSI dispersants has been shown to distort the ^{1}H NMR and FTIR signals, which prevents their quantitative analysis.[39] The PIB chains are polydisperse and can be modified with more than one succinic anhydride (see Scheme 1.1), so that a PIBSI dispersant can be made of several types of PIB chains. In turn, this complicates the analysis of their MWD by gel permeation chromatography (GPC) or mass spectrometry (MS). Finally, the characterization of the small polyamine segments in a PIBSI dispersant turns out to be challenging for most traditional techniques in terms of the number of unreacted amines in the presence of such a large PIB component, which slows down the tumbling of PIBSI dispersants on the NMR time scale and dwarfs the amine signal. In recent years, fluorescence has been shown to be a useful tool in probing the structures and dynamics of various pyrene-labeled polymers such as those used as oil

additives.[39-43] Consequently, the next section provides a brief overview of fluorescence and its utility in the characterization of PIBSI dispersants.

1.2.1 Fluorescence

Fluorescence describes the emission by an excited molecule of a photon at a wavelength that is longer than that used to excite the molecule by its absorption of a photon.[44] Molecules capable of undergoing this process are called fluorophores. The Jablonski diagram shown in Figure 1.4 illustrates the different photophysical processes involved in fluorescence.[44] A dye in the lowest vibrational level of the S_0 (lowest) electronic level absorbs a photon and is excited to one of the vibrational levels of the S_1 or higher electronic levels, depending on the energy of the photon absorbed. The excited dye can then undergo internal conversion to relax down to the lowest vibrational level of the S_1 electronic level before the dye can spontaneously emit a photon of light to return to one of the vibrational levels of the S_0 electronic state; this emission is called fluorescence.[44] Photon absorption by the dye occurs on the order of femtoseconds, while internal conversion takes place within picoseconds.[44] These time scales are negligible compared to most fluorescence lifetimes, which are usually in the tens of nanoseconds range. This is certainly true for the dye pyrene which is being used intensively in this thesis and has a natural lifetime of several hundreds of nanoseconds, depending on the pyrenyl derivative and solvent used.[41,42]

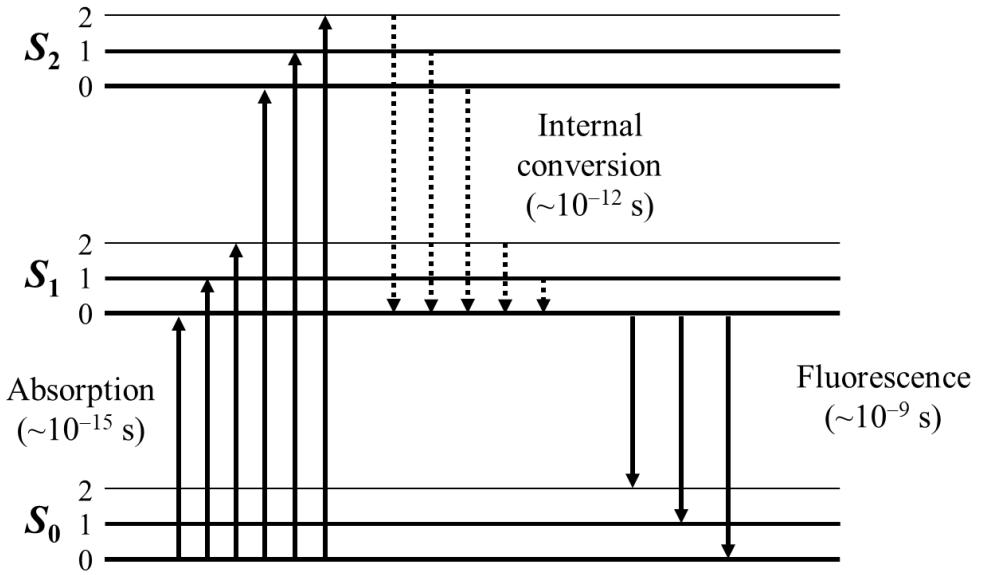

Figure 1.4. The Jablonski diagram.

1.2.2 Pyrene Excimer Fluorescence

Fluorophores are prevalent in nature, with many being found in proteins and nucleic acids.[44] The work described in this thesis used pyrene as a fluorophore due to its high quantum yield (ϕ), large molar extinction coefficient (ε), long fluorescence lifetime (τ_M), and its ability to form excimer. The large quantum yield and molar extinction coefficient mean that PyLMs can be detected at extremely low concentrations, often orders of magnitude lower than required for most other techniques.[45] The long fluorescence lifetime means that pyrene can be employed to probe slow photophysical phenomena such as excimer formation in PyLMs. The last and perhaps most important property is that an excited pyrene can form an excimer upon encounter with a ground-state pyrene, which enables the study of the internal dynamics of macromolecules labeled with pyrene. When a pyrene in the excited state fluoresces without being quenched, it decays according to its monomer lifetime τ_M, whereas a pyrene excimer species decays with its excimer lifetime (τ_E). Because τ_E is substantially different from τ_M, the two species can be identified through careful deconvolution of their time-resolved fluorescence decays.[46,47]

As previously mentioned, labeling of a macromolecule with pyrene allows one to study the internal dynamics of the PyLM by monitoring the rate constant of pyrene excimer fluorescence/formation (PEF). Such studies can be done using steady-state (SSF) and time-resolved (TRF) fluorescence. In a SSF experiment, a sample is continuously irradiated at a wavelength where the dye can be excited and its SSF spectrum is acquired. In the case of pyrene, the SSF spectrum of the pyrene monomer yields a characteristic pattern of five peaks between ~375 and ~410 nm corresponding to the $S_1 \rightarrow S_0$ transitions of pyrene with intensities that depend on the environment experienced by pyrene.[45] These five peaks are denoted as I_1 through I_5. The peaks I_1 and I_3 are often of interest due to their exceptional sensitivity to the polarity of the local environment of pyrene.[45] Figure 1.5 shows both the SSF spectra of a pyrene-labeled polyamine in THF and the scheme of PEF by both diffusive encounters between an excited and ground-state pyrene and direct excitation of pre-aggregated pyrenes.

The SSF spectra can be used to gain quantitative information about PEF efficiency by integrating the monomer (I_M) and excimer (I_E) fluorescence intensities from 372 to 378 nm and from 500 to 530 nm, respectively, to determine the ratio I_E/I_M (see Eq. 1.1).

$$\frac{I_E}{I_M} \propto k_{diff} \times [Py]_{loc} = < k > \qquad (1.1)$$

Eq. 1.1 indicates that the I_E/I_M ratio is related to both the local pyrene concentration ($[Py]_{loc}$) experienced by an excited pyrene in a PyLM and the rate constant (k_{diff}) for PEF by diffusive encounters between an excited and a ground-state pyrene. Since $[Py]_{loc}$ is difficult to determine quantitatively, the product $k_{diff} \times [Py]_{loc}$ is obtained experimentally as $<k>$, the average rate constant of PEF, through the analysis of the TRF decays.

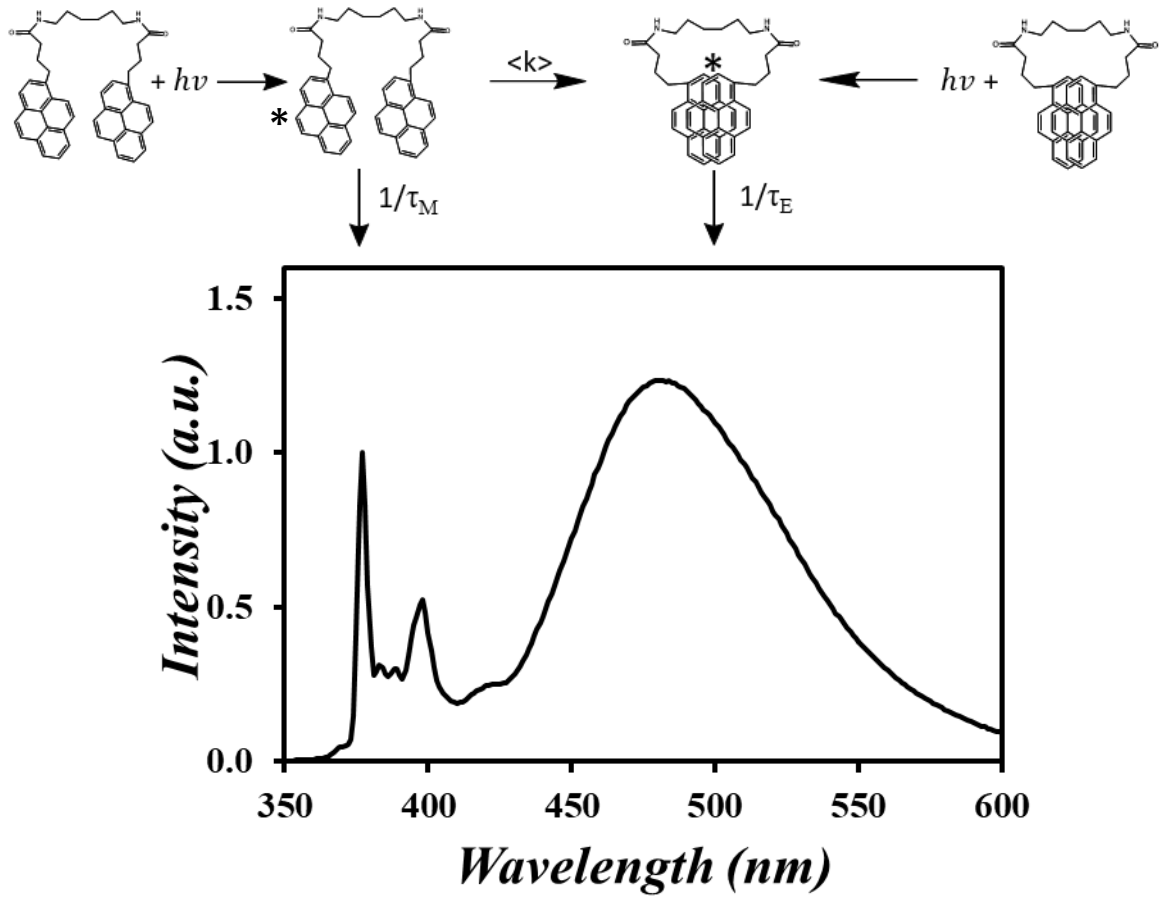

Figure 1.5. Top: Scheme of pyrene excimer formation. Bottom: Steady-state fluorescence spectrum of pyrene-labeled hexamethylenediamine normalized at 377 nm. λ_{ex} = 344 nm, [*Py*] = 2.5×10^{-6} M in THF.

TRF experiments yield the fluorescence decays of dyes. They are acquired by exciting a dye with a short pulse of light and monitoring its fluorescence intensity as a function of time. The TRF decays of the pyrene monomer and excimer can be acquired at emission wavelengths of 375 and 510 nm, respectively, using cutoff filters to block residual excitation light that might otherwise travel through the emission monochromator. The TRF decays acquired with the PyLMs that will be prepared throughout the project will be fitted according to the model free analysis (MFA).[46,47] The MFA is ideally suited for this project as the PyLMs of interest will not all have fully characterized structures as would be otherwise required for an analysis based on any other models

such as Birks' scheme, the DMD model, or the fluorescence blob model which apply mainly to monodisperse linear chains that are end-labeled with pyrene, linear oligomers end-labeled with pyrene, and macromolecules randomly labeled with pyrene.[42,46-49] In these examples, the rate constant for PEF takes a well-defined mathematical expression which is directly related to the architecture of the macromolecule of interest. By contrast, the MFA makes no assumptions about the mathematical form of the PEF rate constant and only retrieves the average rate constant $<k>$, which is related to k_{diff} and $[Py]_{loc}$ as described in Eq. 1.1.[46] Furthermore the MFA yields the molar fractions f_{diff}, f_{agg}, and f_{free} of the pyrene labels that form excimer by either diffusion (Py_{diff}) or direct excitation of pre-aggregated pyrenes (Py_{agg}), or that do not form excimer (Py_{free}) and emit as if they were free in solution with the natural monomer lifetime (τ_M), respectively. The molar fractions of the pyrene labels and $<k>$ provide quantitative information about the state of the pyrene labels covalently attached onto a macromolecule of interest, and in turn the state of the actual macromolecule. The number average lifetime of the pyrene monomer $<\tau>$ is obtained with Eq. 1.2 from the decay times (τ_i) and pre-exponential factors (a_i) retrieved from the MFA of the monomer TRF decays. These parameters are employed to calculate $<k>$ with Eq. 1.3.

$$<\tau>=\frac{\sum_{1=1}^{n} a_i\tau_i}{\sum_{1=1}^{n} a_i} \tag{1.2}$$

$$<k>=\frac{1}{<\tau>}-\frac{1}{\tau_M} \tag{1.3}$$

As indicated by Eq. 1.1, $<k>$ scales linearly with $[Py]_{loc}$. Thus $<k>$ can be used to assess how the pyrene labels are distributed inside a PyLM, providing quantitative information about the internal architecture of the macromolecule. The MFA also allows for the calculation with Eq. 1.4 of the $(I_E/I_M)^{TRF}$ ratios from the parameters obtained from the fit of the monomer and excimer TRF

decays, which affords a direct comparison for the I_E/I_M ratios obtained from the analysis of the SSF spectra. The molar fractions and <*k*> values obtained for a PyLM provide a detailed description of its conformation and dynamics. Applications of the MFA to the characterization of the macromolecule and oil additives are discussed in the next section.

$$\left(\frac{I_E}{I_M}\right)^{TRF} = \frac{\int_{t=0}^{\infty}[E^*]_{(t)}dt}{\int_{t=0}^{\infty}[Py^*]_{(t)}dt} = \frac{-f_{diff}\times\sum_{i=1}^{n} a_i \frac{\frac{1}{\tau_i}-\frac{1}{\tau_M}}{\frac{1}{\tau_i}-\frac{1}{\tau_{E0}}}\times\tau_i + \left(f_{E0}+f_{diff}\times\sum_{i=1}^{n} a_i \frac{\frac{1}{\tau_i}-\frac{1}{\tau_M}}{\frac{1}{\tau_i}-\frac{1}{\tau_{E0}}}\right)\times\tau_{E0}+f_D\times\tau_D}{f_{diff}\times\sum_{i=1}^{n} a_i\times\tau_i+f_{free}\times\tau_M} \quad (1.4)$$

1.2.4 Applications

PEF has been used to study macromolecules in general and macromolecular oil additives in particular from its inception.[39-43,46-55] PEF was first used to explore the end-to-end cyclization of pyrene end-labeled polymers by monitoring their SSF and TRF decays, and was determined to be a useful tool in probing the internal dynamics of linear chains by determining the rate constant of end-to-end cyclisation (k_{cy}).[48,49,51-59] From these initial experiments it was also shown that the purity and monodispersity of pyrene end-labeled polymers were important for the quantitative determination of k_{cy}.

More recently, PEF has been used to probe the structure and dynamics of various oil additives such as PIBSA, which is the precursor of PIBSI dispersants, EP copolymer VIIs, and poly(alkyl methacrylate) PPDs.[39-43] In one specific example, a PIBSA sample was labeled with 1-pyrenemethylamine (PyMA) and 1-pyrenebutyrylhydrazine (PHZ) to yield PIB-PyMA and PIB-PHZ, respectively, and their SSF spectra and TRF decays were acquired in both tetrahydrofuran (THF) and hexane at varying polymer concentrations.[42] An early version of the MFA was applied to fit the monomer and excimer decays to yield f_{agg}, which was plotted as a function of polymer concentration in Figure 1.6. Changing the solvent from hexane to THF led to a decrease in f_{agg}, which was attributed to a reduction in the ability of the hydrazide moiety to H-bond

intermolecularly as the polarity of the solvent was increased from hexane to THF. f_{agg} remained more or less constant in THF and its value was taken as a quantitative measure of the molar fraction of aggregated pyrenyl labels attached on oligo(maleic anhydride) segments. This study showed the significance of solvent effects on the SSF and TRF data, and demonstrated the ability of PEF to quantify the magnitude of these solvent effects on the association of the PIB-PyMA and PIB-PHZ molecules in solution.

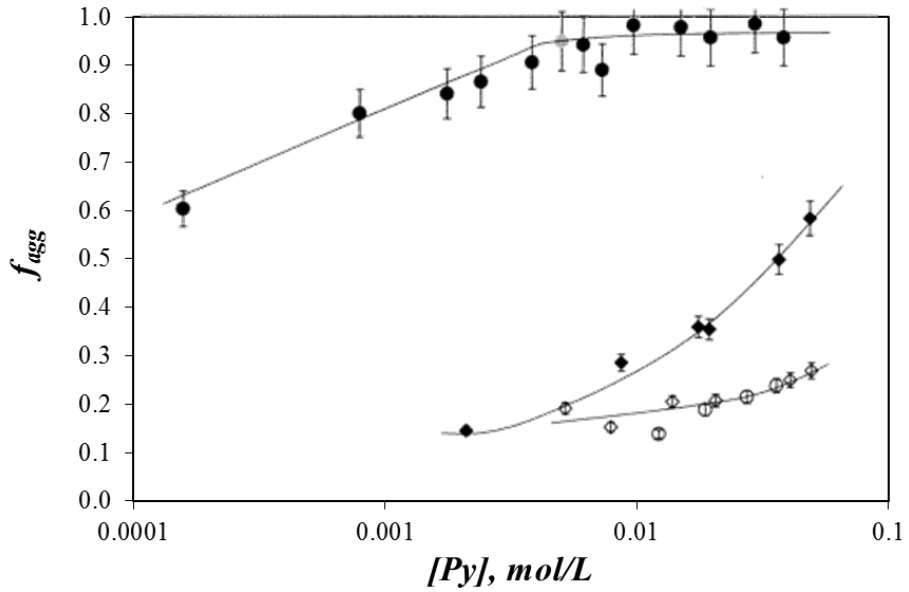

Figure 1.6. Plot of f_{agg} vs. [*Py*] for PIB-PMA (diamonds) and PIB-PHZ (circles) in THF (hollow) and hexane (filled).Reprinted with permission from 42. Copyright 2001 American Chemical Society.

Another application of PEF was to determine the molar fractions f_{intra} and f_{inter} describing the molar fractions of pyrene labels forming excimer intra- and intermolecularly, respectively, in toluene from –30 to 25 °C for an amorphous and a semicrystalline EP copolymer that had been labeled with PyMA.[41] The molar fractions were determined by taking advantage of the direct relationship that exists between the I_E/I_M ratio and $[Py]_{loc}$ described in Eq. 1.1 and measuring the

I_E/I_M ratios of a concentrated 10 g/L solution of the pyrene labeled EP copolymers and a mixture containing 0.1 g/L of the PyLMs and 10 g/L of the unlabeled EP copolymers. The large excess of unlabeled EP copolymer used in the latter solution prevented intermolecular PEF. The I_E/I_M profiles obtained for a semicrystalline EP copolymer are presented as a function of solution temperature in Figure 1.7. In the absence of intermolecular PEF, the I_E/I_M ratio increased continuously with increasing temperature in Figure 1.7A, reflecting the increase in diffusive encounters between pyrene labels. At high PyLM concentration, a clear break point was observed in the I_E/I_M profile as a function of temperature. This behaviour was attributed to the crystallization of the semicrystalline EP copolymer in solution which increased $[Py]_{loc}$ upon decreasing the solution temperature, thus resulting in an increase in I_E/I_M. The I_E/I_M profiles in Figure 1.7A were then combined to yield f_{inter} in Figure 1.7B. While f_{inter} was low at high temperature, indicating little intermolecular interactions between EP molecules, it increased steeply as the temperature was lowered and the crystallization of the semicrystalline EP copolymers led to increased intermolecular interactions. These experiments illustrated how PEF could be applied to yield quantitative information about the extent of intermolecular interactions between PyLMs in solution.

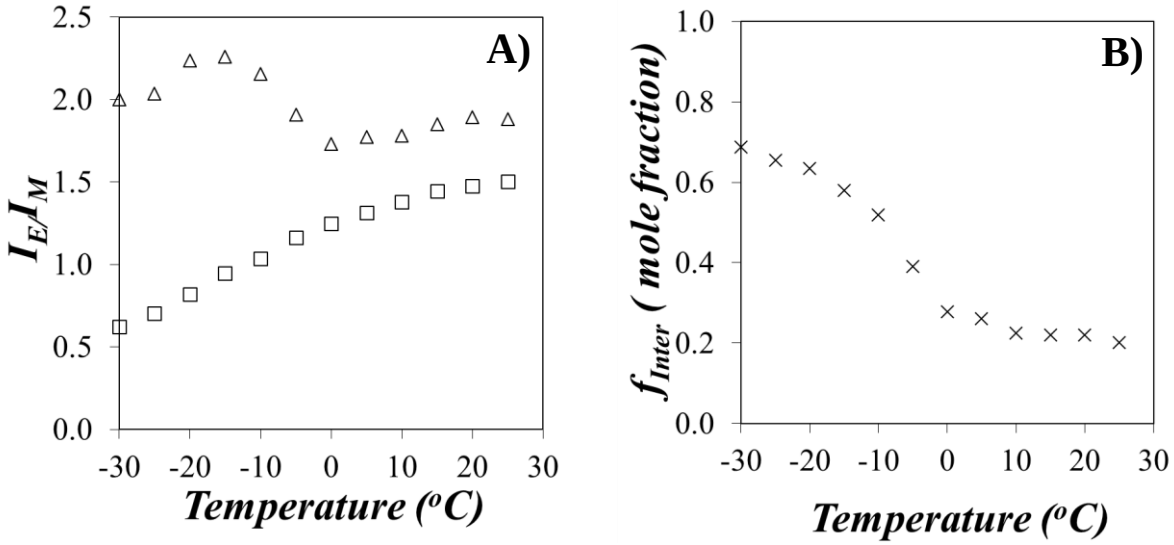

Figure 1.7. A) Plot of the I_E/I_M ratio vs. temperature of a pyrene-labeled semicrystalline EP copolymer at concentrations of (Δ) 10 g/L and (□) 0.01 g/L with 10 g/L non-labeled EP copolymer and B) plot of the molar fraction (f_{inter}) of pyrene labels forming excimer intermolecularly. Reprinted with permission from 41. Copyright 2015 American Chemical Society.

In contrast to the randomly labeled EP copolymers, the well-defined architectures of dendrimers provided an interesting challenge to characterize and understand their internal dynamics by labeling their end-groups with pyrene. While many separate experiments had been undertaken to label dendrimers with different pyrene derivatives, these studies yielded conflicting results when comparing how the I_E/I_M ratio varied with the generation number of the dendrimers.[56] Duhamel et al. were able to resolve why the I_E/I_M ratio varied so widely with the generation number in many studies by accounting for the presence of free pyrene with the MFA, yielding a linear increase in the I_E/I_M ratio obtained by SSF and TRF with increasing generation number.[56,57] The fact that the discrepancies were arising from the non-covalently attached pyrene derivatives left behind in the reaction product was confirmed by collecting the purified pyrene-labeled dendrimers

after fractionation by GPC and reacquiring the SSF spectrum and TRF decays. While the SSF spectrum of the fractionated dendrimer yielded an I_E/I_M ratio that landed on the line when plotted as a function of generation number, MFA of the decays resulted in a reduction of f_{free} from 3 to 0.1 mol% for the unfractionated and fractionated dendrimer sample, respectively. The reduction in f_{free} correlated with a 4-fold increase in the I_E/I_M ratio obtained by SSF and TRF, restoring linearity to $<k>$ w.r.t. generation number of the dendrimer. These results were also found to agree with the I_E/I_M ratio of the unfractionated sample when f_{free} was set to 0 in Eq. 1.3, further highlighting the importance of accounting for free pyrenes in the PEF analysis and the usefulness of the MFA for doing so.[57] The significance of f_{free} in the MFA was exemplified in a following publication using mixtures of dendrimers with free pyrene on the one hand, and single end-labeled PEO chains with doubly end-labeled PEO chains on the other. In both cases a notable reduction in the I_E/I_M ratios was observed when the solutions were contaminated with free pyrene or mono-labeled PEO, respectively.[58] This work has since been expanded through the analysis of more PyLMs with the MFA, yielding results consistent with those discussed previously.[59]

1.2.5 Conclusions

The nature of lubricating oils and a selection of commonly used additives were discussed in this chapter, delving into the properties and synthesis of the most commonly used dispersants today, namely PIBSI dispersants. The synthesis and methodology used to prepare PIBSI dispersants were discussed, highlighting some common problems and concerns in their characterization. The studies of various pyrene-labeled oil additives were discussed to show the usefulness of PEF for the characterization of oil additives which are often hard to probe by other techniques.

This discussion also emphasized the usefulness of the MFA in understanding the structure and dynamics of PyLMs, namely the ability to quantitatively determine the molar fractions f_{agg},

f_{diff}, and f_{free} of pyrene species in solution and the average rate constant $<k>$ for PEF, without making any assumption about the PEF process. Examples were provided to illustrate the intricate relationship that exists between the I_E/I_M ratio obtained by SSF and TRF, $<k>$ obtained from TRF, and $[Py]_{loc}$ for PyLMs. These PEF experiments provide a robust experimental means to obtain quantitative information about the internal dynamics and structure of macromolecules in solution. The importance of the MFA in assessing the existence of fluorescent impurities in the PyLM sample, such as free pyrene derivatives, was also discussed.

1.2.6 Thesis Outline and Objectives

The objective of this thesis was to assess the ability of PEF to characterize PIBSA and PIBSI molecules after they had been labeled with pyrene. A review of the characterization of different oil additives through PEF was provided in Chapter 1. Chapter 2 describes how these concepts were applied to the characterization of two PIBSA samples by labeling with PyMA. Their absorption spectra provided a measure of their number average molecular weight (M_n) while MFA of their TRF decays acquired as a function of polymer concentration yielded the molar fractions of PIBSA molecules bearing one ($PIBSA_1$) and two ($PIBSA_2$) succinic anhydrides in each PIBSA sample. Further experiments conducted in Chapter 2 also revealed that the $PIBSA_2$ content in each PIBSA sample remained constant across their MWD. This conclusion was reached after finding through the PEF experiments that the molar fractions of $PIBSA_2$ in a fractioned and unfractionated PIBSA sample were the same. Chapter 3 discusses the coupling of a PIBSA sample with varying amounts of hexamethylene diamine (HMDA) and fitting of the DRI traces obtained from GPC analysis of said samples with sums of Gaussians for the analysis of the PIBSA coupling products formed. These fits are compared to simulations of the DRI traces expected from the same PIBSA coupling reactions, taking into account f_{doubly} and the succinic anhydride content (λ_{SA}) of the PIBSA sample,

and the ratio of amines-to-succinic anhydrides (N_{Am}/N_{SA}) used in the coupling reaction. This process reveals the presence of unmaleated PIB in the PIBSA sample, and gives excellent agreement with the experimental and simulated DRI traces when assuming that the $PIBSA_2$ molecules can only form *b*-PIBSIs due to steric hindrance when coupling PIBSA with HMDA. Pyrene fluorescence was used in Chapter 4 to provide a relationship between the rate constant of pyrene excimer formation and the number of amines in a polyamine labeled with 1-pyrenebutyric acid (PyBA). These experiments are expected to provide a measure of the mean number of amines that are still available for a coupling reaction with PIBSA in a reaction mixture of PIBSA and PIBSI products. Finally, Chapter 5 summarizes the results obtained in this thesis and offers some directions for possible future work.

Chapter 2

Molar Fractions of *mono*- and *bis*-Polyisobutylene Succinic Anhydrides Determined by Pyrene Excimer Fluorescence

2.1 Outline

A procedure was established to determine the fraction (f_{doubly}) of doubly-maleated polyisobutylene ($PIBSA_2$) in a PIBSA sample constituted of *mono* ($PIBSA_1$) and $PIBSA_2$ species. To this end, two PIBSA samples (PIBSA-1 and PIBSA-2) were labeled with 1-pyrenemethylamine (PyMA). Depending on the procedure applied to purify the PIBSA-PyMA samples, different domains of the molecular weight distribution (MWD) representing the PIBSA samples could be isolated. Each PIBSA-PyMA sample was characterized by a combination of GPC, FTIR, and UV-Vis absorption analysis to yield the MWD, the number of isobutylene units per succinic anhydride (N_{SA}/N_{IB}), and pyrene content (λ_{Py}, in μmol of pyrene per gram of sample). These analyses were consistent with the expected size and chemical composition of the different PIBSA-PyMA samples. f_{doubly} was calculated from the molar fraction (f_{agg}) of pyrene labels attached onto the $PIBSA_2$ species. f_{agg} was determined through the global model free analysis (MFA) of the fluorescence decays of the pyrene monomer and excimer acquired for solutions in THF of the PIBSA-PyMA samples. Besides f_{agg}, the MFA yielded the average rate constant $<k>$ of pyrene excimer formation, which was found to increase linearly with increasing pyrene concentration as would be expected from a diffusion-controlled process. The slope of the $<k>$-*vs*-[Py] plots yielded the rate constant (k_{diff}) for excimer formation, whose value was found to correlate nicely with the size of the PIBSA-PyMA samples, taking a smaller value for a larger polymer. The MFA showed that different fractions of the MWD of the PIBSA samples yielded similar f_{agg} values across the MWD. The PIBSA-1 sample had a higher content of $PIBSA_2$ species than the PIBSA-2 sample. These experiments demonstrate the validity of the proposed PEF-based method to characterize the microstructure of PIBSA samples employed as building blocks in the preparation of the PIBSI dispersants used as oil additives.

2.2 Introduction

The automotive industry has employed engine oils for many years in order to properly lubricate the moving parts of an engine during its operation. The mineral oils, also referred to as "base oils", used in the formulation of engine oils do not provide sufficient lubrication to engines on their own due to the relatively high standard operating temperatures of engines.[1,2] It has thus become standard practice to include additives in engine oil formulations to either enhance or add properties that the base oils do not have.[1-3] Engine oils are often formulated with 10-20 wt% of additives, the remaining 80 to 90 wt% being the base oil.[1] While many different additives are used depending on the specific application of the lubricating oil, the most abundant additives in the automotive industry are dispersants which constitute up to half of the additives, or 5-10 wt% of the engine oil.[2]

Dispersants have been studied intensively since their introduction in the 1950's to mitigate particulate build up in oils, and to minimize the inherent oil thickening which arises from the presence of particulate aggregates in the lubricating fluid.[1,2,4] Dispersants consist of two large apolar chains connected by a polar linker such as a polyamine or polyalcohol. The polar cores of these constructs adhere to the polar surface of insoluble particulates and prevent further aggregation through steric stabilization.[2] The use of dispersants has been found to increase the lifetime of both the engine and the lubricating fluid, by dispersing particulate matter to prevent oil thickening.[1,2,5] Dispersants have become an integral component of lubricating fluids and their synthesis has been adjusted over the years, mostly by varying the polar segment to yield additives with different dispersancies, basicities, and solubilities which could be advantageous to different applications.[4,6-14] Although most dispersants feature PIB segments due to their ease of manufacture and cost effectiveness,[1,2] subtle differences in PIB length, degree of branching, and polydispersity mean that there is much variation in the PIB segments constituting the dispersants in use today.[1]

The moieties used to connect the polar and apolar segments of modern dispersants are often succinic anhydrides (SAs), which are usually located at the end of a PIB chain to yield PIBSAs.[15,16] Whether the polar segments bear some amines or alcohols decides if a succinimide (SI) or succinic ester (SE) will be generated upon reaction with PIBSA. Dispersants where PIB is connected to the polar core via a terminal succinimide are referred to as PIBSI dispersants, and they are currently the most widely used dispersant additives.[1]

Since the publication of the first PIBSI patents in 1965,[16,17] there has been a great deal of interest in developing syntheses or chemical modifications to prepare PIBSI dispersants with enhanced properties.[4,6,7,10,14] In practice, multiple PIBSI groups are linked by linear polyamines such as triethylene tetramine (TETA), tetraethylene pentamine (TEPA), pentaethylene hexamine (PEHA), or longer polyamines to take advantage of their high amine content and enhance the ability of the dispersant to associate with polar particulate matter in the oil.[1,2,18] The number of effective amines, the molecular weight distribution (MWD) and branching level of the PIB component, and the average number of PIBSI units per dispersant molecule are important parameters that must be fully characterized to control the architecture of a PIBSI dispersant. Unfortunately, such detailed analysis remains a challenging goal.

The PIBSA building blocks used in the production of PIBSI dispersants are often prepared by cationic polymerization of isobutylene with boron trifluoride (BF_3) as the catalyst.[1] Once PIB has been polymerized, a succinic anhydride group is introduced via an Alder-ene reaction between the PIB terminal double bond generated during the cationic polymerization and maleic anhydride to produce *mono*-PIBSA ($PIBSA_1$).[1,2] While the maleation of PIB is required to join the PIB segment to the polyamine core, this reaction can result in the formation of a small amount of doubly-maleated PIBSA ($PIBSA_2$) as shown in Scheme 2.1. When present in a PIBSA sample,

$PIBSA_2$ can lead to oligomerization during the reaction of PIBSA and a polyamine. Consequently, the presence of $PIBSA_2$ leads to a more branched PIBSI dispersant than the preferred linear *b*-PIBSI dispersants, constituted of one polyamine connected to two PIB chains.

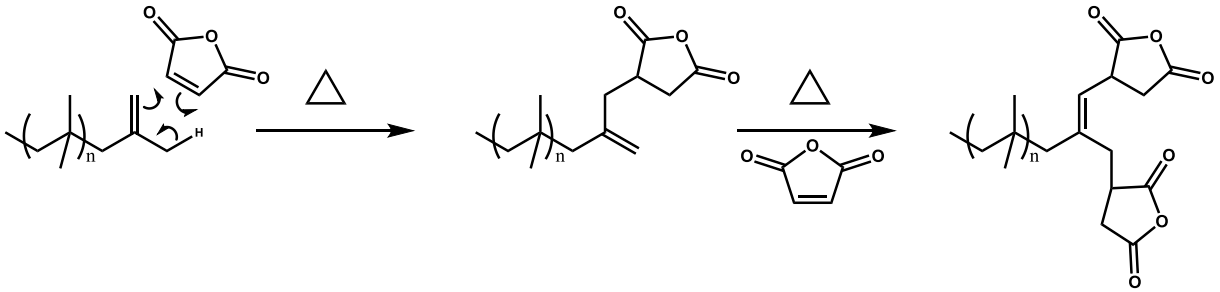

Scheme 2.1. Mechanism of the Alder-ene reaction of maleic anhydride with a vinylidene-terminated PIB.[19]

As PIBSA is the most common means to introduce the apolar PIB component into PIBSI dispersants, the characterization of the MWD, succinic anhydride content, and the fraction of $PIBSA_2$ chains of a given PIBSA sample is crucial to predict the potential reaction products and their respective architectures generated during the synthesis of *b*-PIBSI dispersants. Unfortunately, such detailed characterization is complicated by several issues. First, the low specific refractive index increment (*dn*/*dc*) and the lack of monodisperse PIB standards for low molecular weight PIB samples prevent the determination of their absolute MWD via a combination of light-scattering detection and gel permeation chromatography (GPC). Second, the low signal of succinic anhydrides (SAs) relative to the PIB chain complicates the determination of the SA content of a PIBSA sample by ^{1}H and ^{13}C NMR. Third, FTIR has been shown to yield the number of isobutylene units per succinic anhydride and/or succinimide through the SA/IB or SI/IB ratios by monitoring the relative intensity of the absorbance bands of the anhydride/succinimide with respect to the methyl groups of PIB.[20] While useful, the SI/IB ratios obtained by FTIR have also been shown to result in the inaccurate determination of the SI content, due to distortions of the

carbonyl IR absorption in the presence of H-bonding between the succinimide carbonyls and the amine protons of PIBSI dispersants.[21]

Most of the challenges affecting the characterization of PIBSA and PIBSI samples arise from the difficulty in probing the few SA units in PIBSA or amines in PIBSI dispersants against the large signal emanating from the PIB segments. A simple solution to this problem would require enhancing the signal of the functional groups present in low abundance in the PIBSA and PIBSI samples. Earlier studies have shown that the extreme sensitivity of fluorescence can be harnessed by fluorescently labeling the SA group of PIBSA or the amines of PIBSI dispersants with the dye pyrene, to provide quantitative information about the chemical composition of PIBSA and PIBSI samples.[22]

These earlier studies have led to the proposal that the molar fraction (f_{doubly}) of $PIBSA_2$ in a PIBSA sample could be determined quantitatively by reacting the SA unit of PIBSA with 1-pyrenemethylamine (PyMA) to yield PIBSI-PyMA and take advantage of the ability of an excited pyrene to form an excimer upon encounter with a ground-state pyrene. Since the labeling of $PIBSA_1$ and $PIBSA_2$ with PyMA would yield PIBSI-Py_1 and PIBSI-Py_2, where only the latter construct could form excimer intramolecularly, careful analysis of the monomer and excimer decays according to the model free analysis (MFA) should provide the molar fraction (f_{agg}) of pyrenes that form excimer intramolecularly, which could then be used to calculate f_{doubly} as $f_{agg}/(2-f_{agg})$. These concepts were applied herein by using a combination of pyrene excimer fluorescence (PEF) and GPC analysis to determine f_{doubly} quantitatively for two PIBSA samples and assess whether f_{doubly} would remain constant across the MWD of the PIBSA samples.

2.3 Experimental

Chemicals. Xylene (98.5%, Caledon Laboratory Chemicals), dodecane (anhydrous, 99%), tetrahydrofuran (THF, 99%, Sigma-Aldrich or distilled in glass, 99.9%, Fisher Chemicals), hexanes (98.5%, Sigma-Aldrich), ethyl acetate (99.7%, Sigma-Aldrich), heptane (99%, Sigma-Aldrich), methanol (MeOH, HPLC grade, Sigma-Aldrich), acetone (HPLC grade, Sigma-Aldrich), 1-pyrenemethylamine hydrochloride (PyMA.HCl, 95%, Sigma-Aldrich), and hydrochloric acid (HCl, 12.2 M, Sigma-Aldrich) were used without further purification. The two PIBSA samples, referred to as PIBSA-1 and PIBSA-2, were supplied by Afton Chemical.

Fourier-Transform Infrared (FTIR). A Bruker Tensor 27 FTIR Spectrometer was used to acquire the FTIR spectra of polymer films cast from solutions of the polymer samples deposited onto a NaCl FTIR cell after evaporating the solvent under N_2. Polymer solutions were prepared first in $CDCl_3$, and later in (cheaper) $CHCl_3$, after realizing that this solvent did not interfere with the sample absorption. The absorbance was measured from 1000 to 2000 cm^{-1} and kept around 1.0 to optimize the signal-to-noise ratio.

Gel Permeation Chromatography (GPC). The MWD of the polymer samples was determined with a Viscotek GPC max VE 2001 instrument equipped with PAS-101 and PAS-103 columns from Polyanalytik and a triple-detector array comprised of a differential refractometer, UV-Vis absorption, and light-scattering detectors using THF as the solvent. Polymer solutions were prepared with a concentration of 1 mg/mL using THF from the GPC reservoir. The polymer solutions were passed through 0.22 μm PTFE filters before injection.

UV-Visible Spectrophotometer. A Cary 100 UV-Visible spectrophotometer was used with quartz cells having a 1.0 cm path length. All absorbances were measured from 200 to 400 nm and background corrected against THF.

Steady-State Fluorescence (SSF). A Horiba QM-400 spectrofluorometer equipped with a xenon arc lamp was used to acquire the fluorescence spectra. Solutions were degassed with a gentle flow of nitrogen to evacuate oxygen, a potent quencher of pyrene fluorescence. Solutions with a pyrene concentration equal to or much larger than 2.5 μM were acquired with the right angle or front-face geometries, respectively. The front face geometry was applied for the more concentrated solutions, to minimize the inner filter effect.

Time-Resolved Fluorescence (TRF). Fluorescence decays were acquired with an IBH time-resolved fluorometer using a 340 nm nano-LED light source. The monomer and excimer decays were acquired using 370 and 495 nm cutoff filters, respectively, to minimize residual stray light from reaching the detector. All samples were degassed with a gentle flow of nitrogen for 15-20 minutes before decay acquisition to a peak maximum of 20,000 counts. The same geometry employed in the SSF measurements was applied to the TRF decay acquisition with the right angle geometry being used for the solutions with a pyrene concentration of 2.5 μM, and the front face geometry for solutions having much higher pyrene concentrations.

The monomer and excimer fluorescence decays were fitted individually with a sum of exponentials according to Equation 2.1, where *X* represents either the pyrene monomer (*M**) or excimer (*E**), with a_{xi} and τ_{xi} being the pre-exponential factors and decay times, respectively. The pyrene monomer and excimer decays were also fitted globally according to the MFA based on Equations 2.2 and 2.3, respectively.

$$[X]_{(t)} = \sum_{i=1}^{n} a_{Xi} \times \exp(-t / \tau_{Xi}) \tag{2.1}$$

$$[M^*]_{(t)} = [Py_{diff}^*]_o \sum_{i=1}^{n} a_i \times \exp(-t / \tau_i) + [Py_S^*]_o \exp(-t / 3.5\,ns) \tag{2.2}$$

$$[E^*]_{(t)} = -[Py_{diff}{}^*]_o \sum_{i=1}^{n} a_i \frac{\frac{1}{\tau_i} - \frac{1}{\tau_M}}{\frac{1}{\tau_i} - \frac{1}{\tau_{E0}}} \exp(-t/\tau_i) + \left([E0^*]_o + [Py_{diffE0}{}^*]_o \sum_{i=1}^{n} a_i \frac{\frac{1}{\tau_i} - \frac{1}{\tau_M}}{\frac{1}{\tau_i} - \frac{1}{\tau_{E0}}} \right) \exp(-t/\tau_{E0})$$

$$+ \left([D^*]_o + [Py_{diffD}{}^*]_o \sum_{i=1}^{n} a_i \frac{\frac{1}{\tau_i} - \frac{1}{\tau_M}}{\frac{1}{\tau_i} - \frac{1}{\tau_D}} \right) \exp(-t/\tau_D) \qquad (2.3)$$

In Equation 2.1, the pre-exponential factors (a_{xi}) are free to be positive or negative. In contrast, Equation 2.2 is used to fit the monomer decays globally with the excimer decays according to the MFA, and its pre-exponential factors (a_i) are normalized to unity ($\Sigma a_i = 1$) and forced to remain positive. The species $Py_S{}^*$ was added in Equation 2.2 to account for a short decay which was probably due to residual light scattering, and was handled with a short 3.5 ns lifetime that was fixed in the analysis. Furthermore, the a_i parameters and the decay times (τ_i) take the same value in Equations 2.2 and 2.3. In Equation 2.3, τ_M, which is fixed in the decay analysis, and τ_{E0} are the monomer and excimer natural lifetimes, respectively. Finally, the terms $[Py_{diffE0}{}^*]_o$, $[Py_{diffD}{}^*]_o$, $[E0^*]_o$ and $[D^*]_o$ are the concentrations at equilibrium of the pyrenyl labels forming excimers *E0** and *D** by diffusion, respectively, and are aggregated and form the excimers *E0** and *D** instantaneously upon direct excitation, respectively.

The floating parameters a_i, τ_i, τ_{E0}, $[Py_S{}^*]_o$, $[Py_{diffE0}{}^*]_o$, $[Py_{diffD}{}^*]_o$, $[E0^*]_o$ and $[D^*]_o$ were optimized according to the Marquardt-Levenberg algorithm with the sumegs33bg-9.f program and are listed in Tables A1 – 5 in Appendix A.[23] Decay fits with $\chi^2 \leq 1.30$ and residuals and autocorrelation of the residuals randomly distributed about zero were deemed acceptable.

Synthesis of fractionated PIBSA-PyMA samples (f-PIBSA-PyMA). The two PIBSA samples received from Afton Chemical, namely PIBSA-1 and PIBSA-2, were labeled with PyMA to form the 1-pyrenemethyl succinimide shown in Scheme 2.2 according to a published procedure.[22]

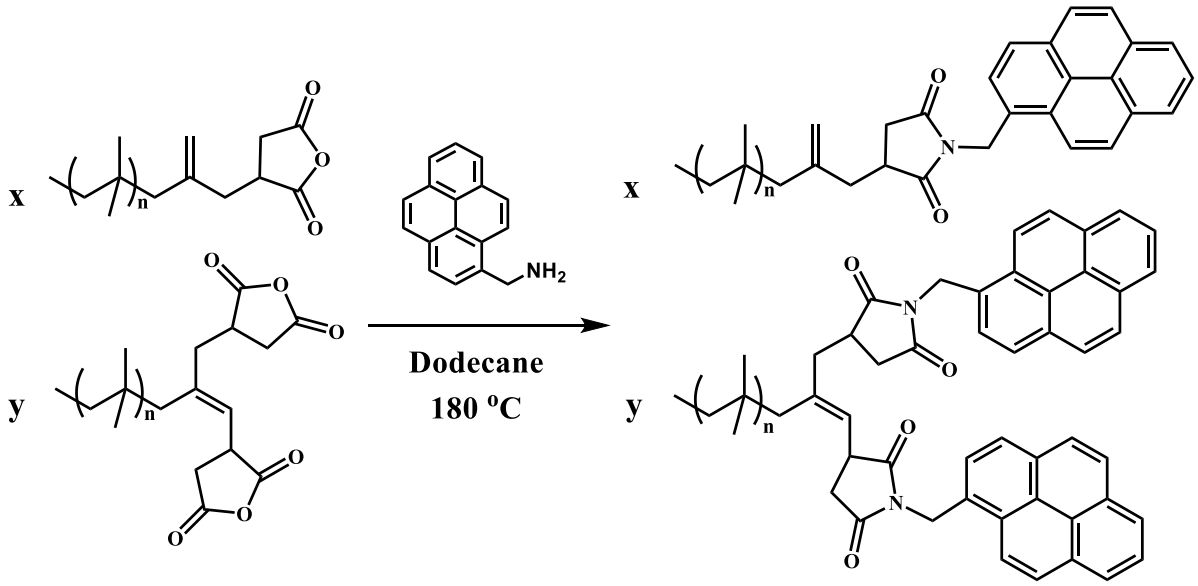

Scheme 2.2. Synthesis of PIBSA-PyMA.

PIBSA-2 (10 g) was first dissolved in THF and precipitated with acetone to yield a fractionated PIBSA-2 sample (*f*-PIBSA-2), since the low molecular weight fraction of the MWD partitioned into the solvent. The mixture was then decanted and *f*-PIBSA-2 was dried under a flow of nitrogen. *f*-PIBSA-2 (1.97 g) was dissolved in 20 mL of hot xylene, and the hot *f*-PIBSA solution was added to a 2-neck 25 mL round bottom flask (RBF) connected to a Claisen distillation head and a condenser functioning as a Dean-Stark apparatus. The whole setup was kept under nitrogen. This step was conducted to regenerate the succinic anhydride of the *f*-PIBSA-2 sample that had partially rehydrated over time, based on the presence of the succinic acid carbonyls characterized by their absorption band at 1710 cm^{-1} in Spectrum A of Figure 2.1. The Dean-Stark apparatus enabled the separation of water from the reaction mixture that was generated in xylene by dehydration of partially hydrated *f*-PIBSA-2. The dehydration proceeded by refluxing *f*-PIBSA-2

in xylene (T_b = 140-150 °C) overnight. An aliquot was taken to acquire its FTIR spectrum shown as Spectrum B in Figure 2.1. Spectrum B confirmed that the sample was fully dehydrated by the disappearance of the band at 1710 cm^{-1}, characteristic of the succinic acid carbonyls, and the appearance of the band at 1785 cm^{-1}, characteristic of the succinic anhydride carbonyls.[20] Half of the solution was stored to conduct a labeling reaction with 1-pyrenebutanol at a later date, and the remaining solution was diluted with xylene to a volume of 10 mL.

The number of succinic anhydride (N_{SA}) per isobutylene monomers (N_{IB}) of a PIBSA sample can be obtained from the analysis of its FTIR spectrum, by applying Eq. 2.4 relating the ratio N_{SA}/N_{IB} to the ratio of the absorption bands characteristic of the succinic anhydride carbonyls and the methyl swinging motion of the isobutylene monomer at 1785 and 1390 cm^{-1}, respectively.[20]

$$\frac{N_{SA}}{N_{IB}} = 0.024 \times \frac{Abs(1785\,cm^{-1})}{Abs(1390\,cm^{-1})} \qquad (2.4)$$

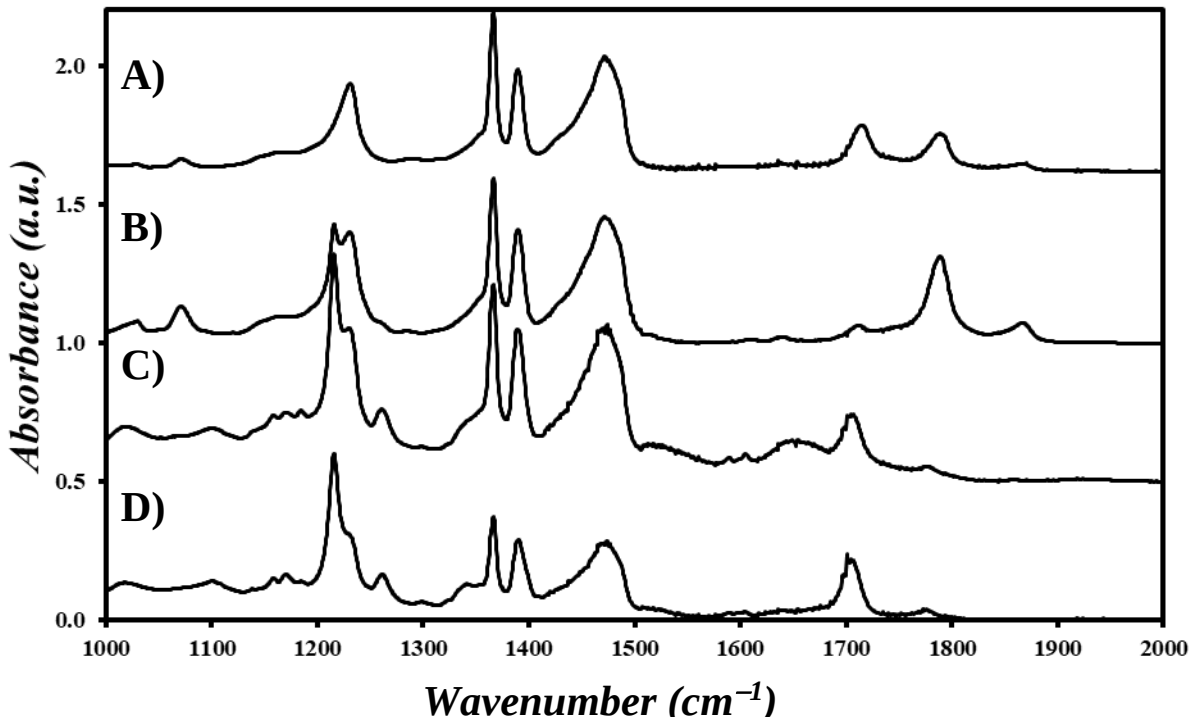

Figure 2.1. FTIR spectra of precipitated *f*-PIBSA-2. A) Post-precipitation and partially hydrated, B) dehydrated, C) before dodecane addition, and D) after dodecane addition and reflux resulting in the fully PyMA labeled *f*-PIBSA-2-PyMA sample.

Analysis of the FTIR spectrum shown as Trace B in Figure 2.1 with Eq. 2.4 yielded an N_{SA}/N_{IB} ratio of 1/54, which inferred that there were 54 isobutylene monomers for each SA unit in the *f*-PIBSA-2 sample. The amount of PyMA required to label a given mass of *f*-PIBSA-2 could be predicted from the N_{SA}/N_{IB} ratio. PyMA was prepared by dissolving PyMA·HCl (0.10 g, 1.2 meq) in 100 mL of water to which three NaOH pellets were added before extracting PyMA with repeated hexane rinses. The hexane was evaporated and the resulting PyMA was dried to completion in a vacuum oven at 60 °C. It was dissolved in hot xylene and added to the dehydrated *f*-PIBSA-2 sample to react overnight.

On the following day, an aliquot was taken from the reaction mixture and its FTIR spectrum was acquired. It is presented as Trace C in Figure 2.1. The spectrum showed a reduction in the succinic anhydride absorption band at 1785 cm^{-1} and the appearance of the succinimide band at 1705 cm^{-1} as expected, but also a moderately strong absorption at 1650 cm^{-1} which suggests the presence of a secondary amide. As shown in Scheme 2.3, the presence of a secondary amide could indicate that PyMA had opened the succinic ring, but that the amide had not closed the ring and instead halted at the succinamic acid intermediate. To aid in ring closure, 10 mL of dodecane (T_b = 216 °C) was added to the reaction, which was then gradually heated to 200-210 °C while xylene was pipetted from the elbow of the Claisen distillation head as it collected. The reaction was then left overnight, and an aliquot taken the next morning to obtain its FTIR spectrum, shown as Trace D in Figure 2.1.

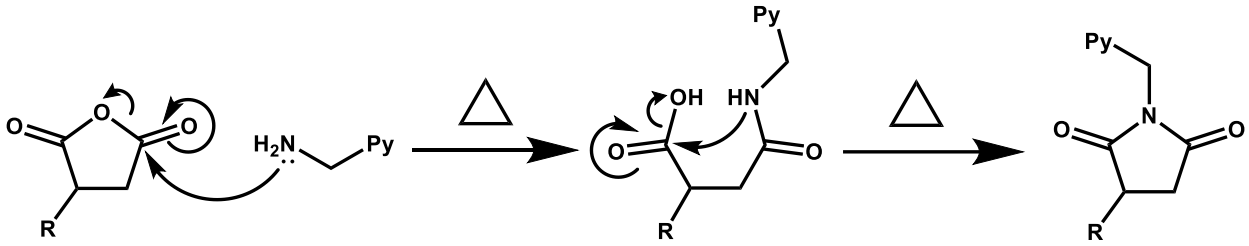

Scheme 2.3. Mechanism for 1-pyrenemethylsuccinimide formation.

Analysis of the FTIR spectrum D given in Figure 2.1 showed a reduction in secondary amide absorption at 1650 cm^{-1}, indicating that ring-closure was enhanced at the elevated temperature and that the labeling was complete, as the absorption band at 1785 cm^{-1} was absent in the spectrum and replaced by the imide absorption band at 1705 cm^{-1}. The *f*-PIBSA-2-PyMA sample was concentrated under an increased flow of nitrogen and precipitated three times with MeOH before GPC was used to confirm the removal of unreacted PyMA. The sample was then dissolved in THF and the solution transferred to a weighed 20 mL vial, before the solvent was

evaporated under a flow of nitrogen and the residue was dried in a vacuum oven overnight at 70-80 °C to yield 0.23 g of *f*-PIBSA-2-PyMA.

f-PIBSA-1-PyMA was prepared in the same manner as *f*-PIBSA-2-PyMA, although some slight modifications were applied to the procedure using insights gleaned from the previous synthesis. PIBSA-1 (10 g) was first dissolved in THF and precipitated with acetone to yield the fractionated PIBSA-1 sample (*f*-PIBSA-1) which was dried under nitrogen. *f*-PIBSA-1 (0.95 g) was dissolved in 18 mL of hot dodecane, and the hot solution was transferred to a 2-neck 100 mL RBF connected to a Dean-Stark condenser under nitrogen. The solution was heated to 190-200 °C for 6 hours before an aliquot was taken for acquisition of the FTIR spectrum (see Spectrum A in Figure A1). Spectrum A showed the same features as Spectrum B in Figure 2.1 for dehydrated *f*-PIBSA-2, thus confirming the dehydration of *f*-PIBSA-1. Using Spectrum A in Figure A1 and Equation 2.4, an N_{SA}/N_{IB} ratio of 1/49 was obtained for *f*-PIBSA-1, inferring one SA for every 49 IB units.

PyMA (0.10 g, 1.3 meq), prepared from 0.15 g (1.6 meq) of PyMA·HCl, was dissolved in dodecane (10 mL) to which 0.95 g of *f*-PIBSA-1 was added. The mixture was left to react overnight at 190-200 °C. The next morning an aliquot was taken to confirm completion of the reaction by acquiring the FTIR Spectrum B in Figure A1. Disappearance of the succinic anhydride carbonyl band at 1785 cm^{-1} demonstrated that the PyMA labeling was complete. The solution of the crude product was then concentrated and precipitated 3 times with MeOH before being dissolved in THF. After GPC confirmed the successful removal of free PyMA, the solvent was evaporated and the product was dried under vacuum at 70-80 °C overnight to yield 0.65 g of *f*-PIBSA-1-PyMA.

The effect that precipitation had on the PIBSA-PyMA samples dissolved in dodecane and precipitated with acetone is clearly illustrated in Figure 2.2, which shows that each successive

precipitation of the PIBSA samples removed a substantial portion of the low molecular weight species of the MWDs. This observation led to the conclusion that further labeling reactions with PyMA would be done without prior precipitation of the PIBSA samples to preserve their MWDs, so that f_{doubly} would be determined for their unaltered MWDs. Whether f_{doubly} would remain constant for the fractionated and unfractionated PIBSA samples would indicate whether the $PIBSA_2$ content would remain constant or show some deviation across the PIBSA MWDs. The PIBSA-PyMAs prepared after precipitation of the PIBSA samples with acetone were denoted as fractionated samples (*f*-PIBSA-PyMAs) for further reference.

Synthesis of a partially fractionated PIBSA-PyMA sample (pf-PIBSA-PyMA). PIBSA-2 (0.58 g) was dissolved in 15 mL of hot dodecane and the hot solution was heated to 200-210 °C for 4 hours in the Dean-Stark apparatus before an aliquot was taken for FTIR analysis to confirm dehydration (see Spectrum A in Figure A2). Analysis of the FTIR spectrum confirmed that the dehydration was complete and yielded an $N_{\text{SA}}/N_{\text{IB}}$ ratio of 1/32. The larger $N_{\text{SA}}/N_{\text{IB}}$ ratio indicated that the unfractionated PIBSA-2 sample (*u*-PIBSA-2) included the shorter species of the MWD. PyMA (0.11 g, 1.7 meq) was then obtained from PyMA·HCl (0.14 g, 1.8 meq), after extraction with ethyl acetate, which is a better solvent for PyMA. The dried PyMA was dissolved in xylene and added sequentially in two batches to the reaction mixture. The next day an aliquot was taken whose FTIR spectrum shown as spectrum B in Figure A2 confirmed the complete PyMA labeling of PIBSA-2 to yield PIBSA-2-PyMA.

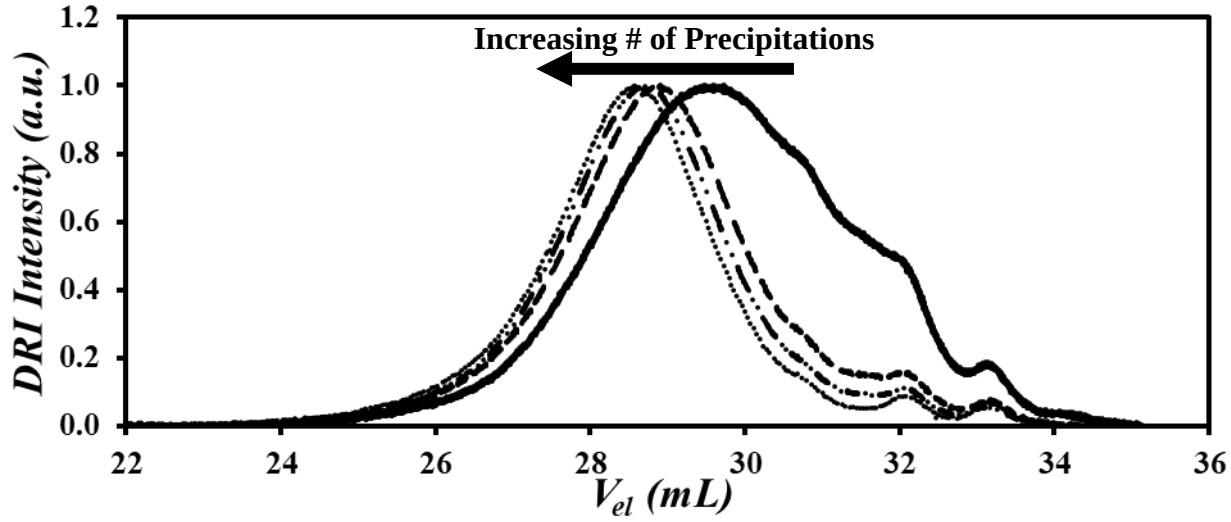

Figure 2.2. DRI traces from GPC analysis of PIBSA-2 before (solid line), and after (dashed lines) successive precipitations with acetone.

In order to better preserve the MWD of the PIBSA-2-PyMA sample during purification, a new procedure was required which would not alter its MWD while efficiently removing free PyMA. To this end, the dodecane was evaporated off the reaction mixture under a vigorous flow of nitrogen before the crude PIBSA-2-PyMA product was dissolved in heptane (80 mL) and the solution was transferred to a 125 mL separatory funnel. The free PyMA was extracted through 5 rinses with 10 mL of a MeOH/HCl (equivalent to 0.1M HCl) solution and the MeOH layer was drained between rinses. The aqueous phases were combined and found to turn turbid upon evaporation of some of the solvent. Since the lower molecular weight species in the MWD of PIBSA-2-PyMA may have partitioned into the MeOH, 20 mL of heptane was added to the MeOH/HCl solution to back-extract any low molecular weight PIBSA-2-PyMA species. This process was repeated once more before combining the back-extractions with the original organic phase and taking aliquots of the heptane and MeOH fractions. GPC was employed to compare the MWDs of the different fractions against the crude PIBSA-2-PyMA product before extraction and

the results are shown in Figures 2.3A and B for the GPC traces obtained with a UV-Vis absorption and DRI detector, respectively.

Free PyMA was detected in the crude product from the elution peak at 21.5 mL in both the DRI and UV-Vis traces. Free PyMA was not found in the heptane fraction because it had partitioned into the MeOH along with some of the smaller PIBSA-2-PyMA chains of the MWD. Although the MeOH/HCl extraction method was successful in preserving more of the PIBSA-2 MWD than was achieved earlier from precipitations with acetone, some of the shorter species of the PIBSA-2-PyMA sample were still lost after repeated extractions. The heptane was evaporated and the resulting product dried under vacuum at 70-80 °C overnight, yielding 0.57 g of partially fractionated PIBSA-2-PyMA (*pf*-PIBSA-2-PyMA) as the loss of the shortest PIBSAs meant that this sample had a MWD that was intermediate between that of *f*-PIBSA-PyMAs and the original PIBSA.

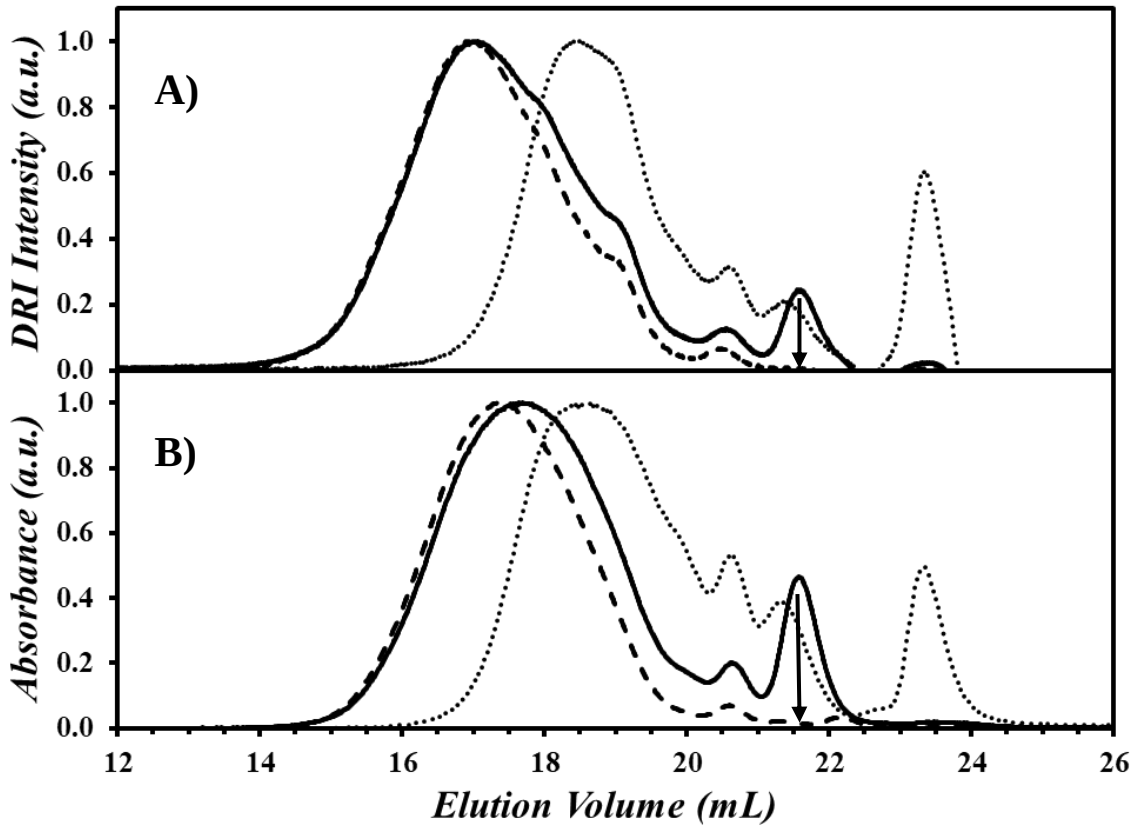

Figure 2.3. GPC traces of the non-precipitated PIBSA-2-PyMA crude product (─), heptane fraction (---), and MeOH fraction (···) as measured by the (A) DRI, and B) UV-Vis detectors, normalized to the peak maxima.

Synthesis of unfractionated PIBSA-PyMA samples (u-PIBSA-PyMA): Another purification procedure was implemented to prepare an unfractionated PIBSA-2-PyMA sample that would maintain the whole PIBSA MWD while removing free PyMA. PIBSA-2 (0.84 g) was dissolved in 20 mL of hot dodecane and added to the Dean-Stark apparatus to reflux and dehydrate overnight, yielding an N_{SA}/N_{IB} value of 1/35 (see Spectrum A in Figure A3). Then PyMA·HCl (0.16 g, 1.6 meq) was neutralized to yield 0.14 g (1.5 meq) of PyMA which was dissolved in 20 mL of xylene and added to the reaction mixture. The next morning, aliquots were taken for both FTIR and GPC analysis. GPC analysis of the crude product, shown in Figure 2.4, was used to confirm the presence

of free PyMA at an elution volume of ~21.5 mL which indicated that the reaction was complete. The FTIR Spectrum B in Figure A3 also confirmed that the reaction was complete from the absence of the succinic anhydride carbonyl band at 1785 cm^{-1}.

The reaction solvent was evaporated, and the crude product was dissolved in 125 mL of hexanes before being transferred to a separatory funnel and washed with 10 mL of 1 M HCl to extract free PyMA, after which a precipitate formed at the interface. The aqueous phase was drained. The organic phase, which was slightly turbid, was filtered via vacuum filtration and the filtrate transferred back to the separatory funnel for four more extractions and filtrations. Comparison of the product from the last two precipitations, illustrated in the inlaid plot in Figure 2.4, confirmed the successful removal of free PyMA while retaining the full PIBSA-2-PyMA MWD. The hexanes were evaporated and the sample was dried to completion under vacuum at 70-80 °C overnight to yield 0.89 g of PIBSA-2-PyMA. The PIBSA-PyMA samples isolated by this method were denoted as unfractionated PIBSA-PyMA (*u*-PIBSA-PyMA), as they represented the full MWD of the two PIBSA samples.

A sample of *u*-PIBSA-1-PyMA was then prepared by dissolving 0.91 g of PIBSA-1 in 20 mL of hot dodecane and adding the solution to a RBF connected to the Dean-Stark apparatus described earlier. The container used to hold the PIBSA-1 solution in dodecane was rinsed with another 15 mL of dodecane which was added to the RBF. The solution was refluxed for 4 hours at which point FTIR analysis confirmed that dehydration was complete, yielding an N_{SA}/N_{IB} value of 1/31 (Spectrum A in Figure A4). PyMA (0.23 g, 2.1 meq) was obtained by neutralizing 0.28 g (2.2 meq) of PyMA·HCl. PyMA was dissolved in xylene and two batches of PyMA were sequentially added to the reaction mixture. On the following morning, aliquots taken for FTIR and GPC analysis confirmed that the labeling was complete (Figures A4 and A5).

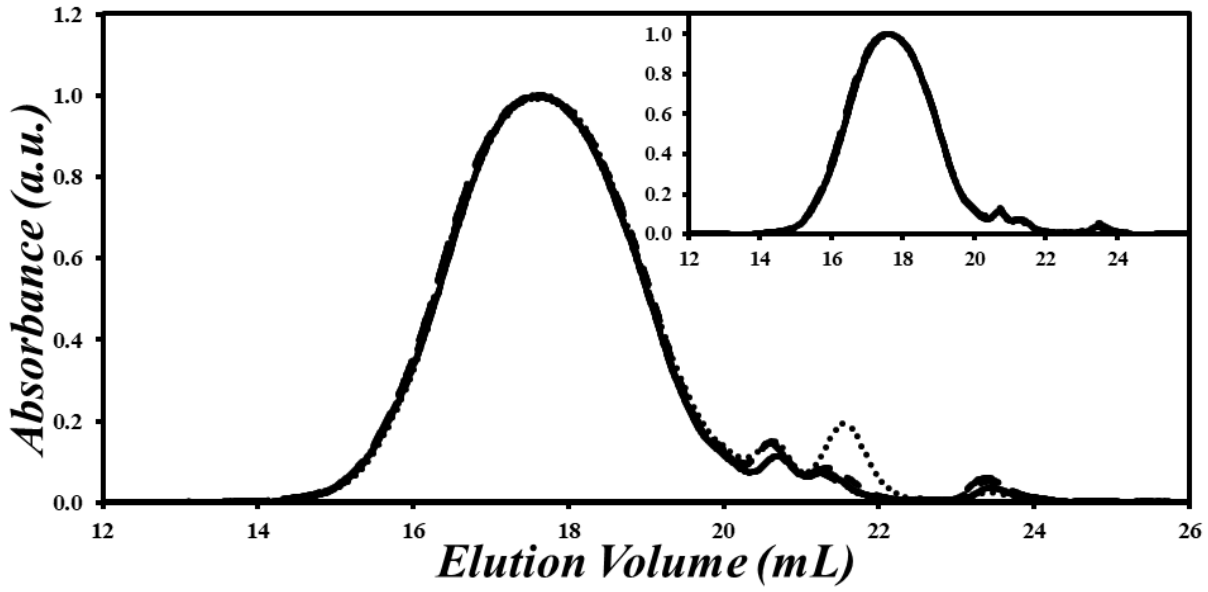

Figure 2.4. Plot of the UV-Vis absorption traces from GPC analysis of *u*-PIBSA-2-PyMA of the crude product (dotted line), after successive extractions with 1 M HCl (dashed lines) and the final product (solid line), normalized to the peak maxima. In-laid plot shows the perfectly overlapping GPC traces for the last two extractions, demonstrating that all free PyMA had been removed.

The solvent was evaporated and the crude product was dissolved in 125 mL of hexanes before being transferred to a separatory funnel where it was washed six times with 10 mL of 1 M HCl. The turbid organic phase was filtered and the filtrate was dissolved in hexanes for each wash with 1 M HCl. The GPC traces shown in Figure A5 confirmed removal of free PyMA while retaining the entire PIBSA-1-PyMA MWD. The hexanes were evaporated and the product was dried under vacuum at 70-80 °C overnight to yield 0.77 g of *u*-PIBSA-1-PyMA.

2.4 Results and Discussion

The 1-pyrenemethylsuccinimide group has been used to probe the associations of pyrene-labeled macromolecules (PyLMs) having different macromolecular architectures through PEF.[22,24,25] Each PIBSA sample was assumed to be made of a mixture of $PIBSA_1$ and $PIBSA_2$ species, which after labeling with PyMA would result in $PIBSA_1$-PyMA and $PIBSA_2$-PyMA species bearing one or two pyrenyls, respectively. In turn, their time-resolved fluorescence decays could be analysed with the MFA to determine f_{doubly}, the molar fraction of $PIBSA_2$ species in a PIBSA sample. Special care was taken to ensure that all free PyMA was removed from the PIBSA-PyMA products by using a combination of FTIR and GPC analysis. This purification step was critical for the accurate determination of f_{doubly} since any free PyMA would appear as $PIBSA_1$-PyMA in the MFA and skew f_{doubly} to lower values. The resulting PIBSA-PyMA samples were analysed by GPC, FTIR, and UV-Vis spectroscopy to determine their MWD and succinic anhydride/pyrene content. Then steady-state fluorescence (SSF) was applied to assess whether the PIBSA-PyMA samples had the spectral features expected of a pyrene derivative and f_{doubly} was determined by time-resolved fluorescence (TRF) for each PIBSA-PyMA sample.

Gel Permeation Chromatography (GPC). Although the lack of GPC standards for PIB prevented the quantitative MW determination of the polydisperse PIBSA samples, GPC analysis was effective in visualizing the effect that a given purification procedure might have on the MWD of the samples. A comparison of the GPC traces of the different PIBSA-1-PyMAs and PIBSA-2-PyMA samples obtained with the UV-Vis detector is shown in Figure 2.5.

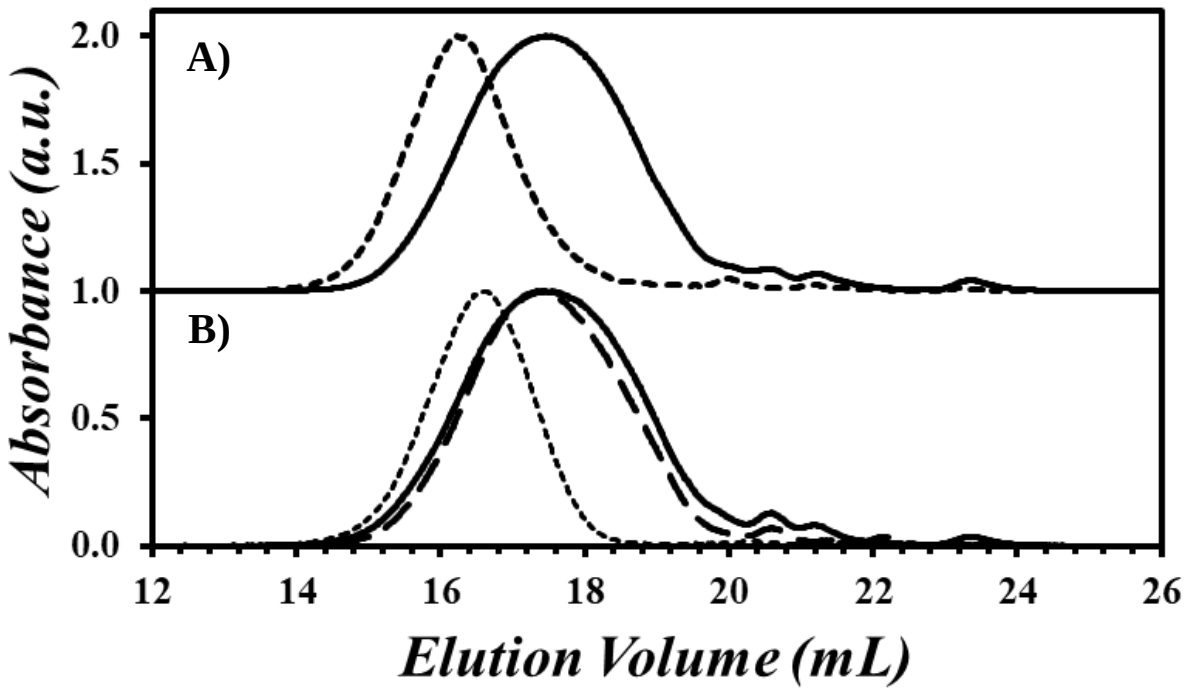

Figure 2.5. GPC traces of A) *u*-PIBSA-1-PyMA (—) and *f*-PIBSA-1-PyMA (···), and B) (—) *u*-PIBSA-2-PyMA, (---) *pf*-PIBSA-2-PyMA, and (···) *f*-PIBSA-2-PyMA as measured by the UV-Vis detector and normalized to the peak maxima.

The overlaid GPC traces in Figure 2.5 showed the difference in MWDs between the *u*-PIBSA-1-PyMA and *f*-PIBSA-1-PyMA samples and the *u*-PIBSA-2-PyMA, *pf*-PIBSA-2-PyMA, and *f*-PIBSA-2-PyMA samples. The MWDs of all fractionated samples were greatly skewed towards lower elution volumes corresponding to the higher MW species resulting from the precipitation of the PIBSA samples. Compared to the GPC trace of *f*-PIBSA-2-PyMA, the GPC trace for *pf*-PIBSA-2-PyMA was substantially shifted to lower MWs, reflecting the effect that precipitations with acetone had on the MWD of the PIBSA samples. Low MW impurities eluted from 20 to 22 mL and 23 to 24 mL for the samples purified via extraction. These impurities might have been non-maleated oligo(isobutylene) (OIB) in the PIBSA samples which could not be

removed through extraction with polar solvents. Comparison of the GPC traces obtained for the *u*-PIBSA-1-PyMA and *u*-PIBSA-2-PyMA samples in Figure 2.6 shows that these samples have similar MWDs with the same low MW components eluting between 20 and 22 mL and 23 and 24 mL. While largely absent in the *f*-PIBSA-PyMAs, the impurities contributed less to the *pf*-PIBSA-2-PyMA sample compared to the *u*-PIBSA-PyMA samples, suggesting that they were more soluble in MeOH than H_2O, as would be expected for aliphatic OIBs.

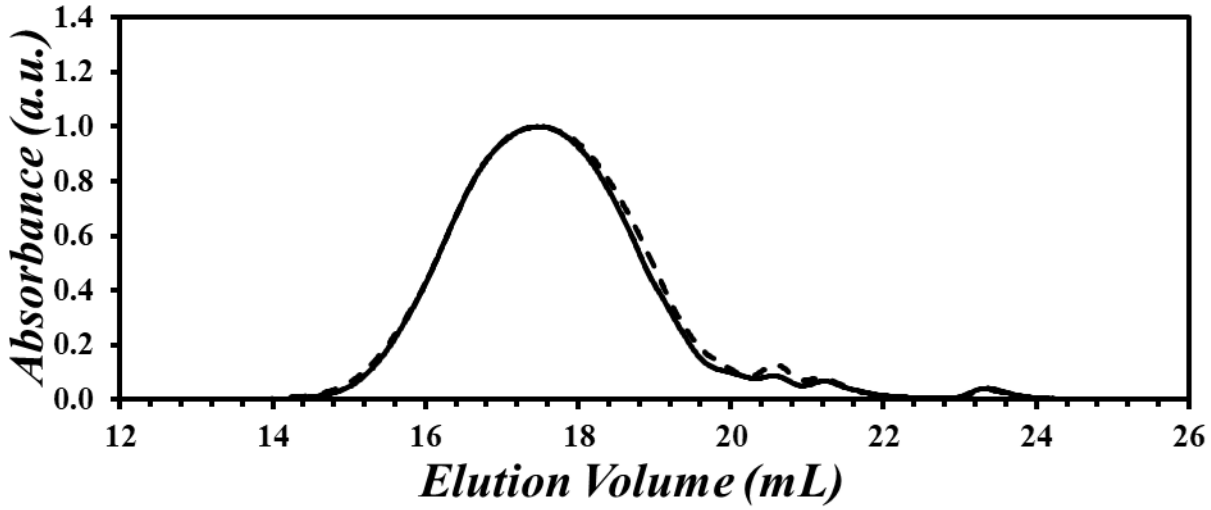

Figure 2.6. GPC traces of (—) *u*-PIBSA-1-PyMA and (---) *u*-PIBSA-2-PyMA as measured by the UV-Vis detector and normalized to the peak maxima.

The GPC traces of *u*-PIBSA-2-PyMA obtained with the DRI and UV-Vis detectors were compared in Figure 2.7. The PIBSA-PyMA samples being studied contained a set number (one or two) of pyrenyls per molecule, which led to different responses from the DRI and absorption detectors of the GPC instrument, since these detectors are sensitive to the massic and molar concentrations, respectively. The trace obtained with the DRI detector of the *u*-PIBSA-2-PyMA sample in Figure 2.7 was narrower than the trace obtained with the absorption detector, with a peak maximum shifted to lower elution volumes. These features were a direct consequence of the

architecture of the PIBSA-PyMA samples, which bore mostly one 1-pyrenemethylsuccinimide at one chain end. Thus, each species bearing a pyrenyl group generated the same absorption signal across the MWD. In contrast, the low MW species of the MWD generated much less signal with the DRI detector than the higher MW species. These comments explain why the GPC trace obtained with the DRI detector in Figure 2.7 was narrower than and shifted to the left of the GPC trace obtained with the absorption detector.

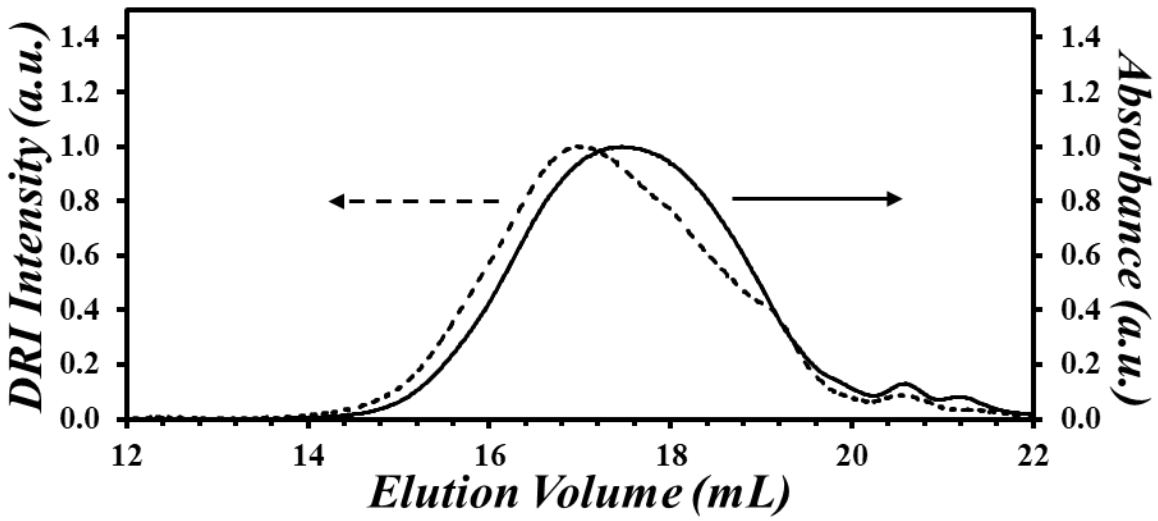

Figure 2.7. GPC traces of the *u*-PIBSA-2-PyMA sample as measured by the UV-Vis (─) and DRI (---) detectors, normalized to the peak maxima.

Fourier-Transform Infrared (FTIR). FTIR spectroscopy was used to not only monitor the dehydration and labeling of the PIBSA samples, but also quantify their N_{SA}/N_{IB} ratios according to Eq. 2.4 which helped predict the amount of PyMA required for the labeling reaction and gain information about the chemical composition of the PIBSA samples. The FTIR spectra of the *u*-PIBSA-PyMA samples are shown in Figure 2.8. The spectra for both *u*-PIBSA-PyMA samples exhibited the absorption bands expected for PIBSI samples, namely the C-H bending peaks at 1360

cm^{-1} and 1390 cm^{-1}, the methylene bending and scissoring peaks at 1225 cm^{-1} and 1465 cm^{-1}, respectively, and the asymmetric and symmetric succinimide stretching peaks at 1705 cm^{-1} and 1780 cm^{-1}, respectively.[20] The two *u*-PIBSA-PyMA samples showed similar spectra, with the *u*-PIBSA-1-PyMA sample having a slightly more intense imide absorption at 1705 cm^{-1} which implied a higher 1-pyrenemethylsuccinimide content than the *u*-PIBSA-2-PyMA sample. It is important to note that while FTIR can identify the presence of succinimide bands, these bands have been shown to suffer from artifacts due to H-bonding.[21] A comparison of all the PIBSA-PyMA samples is shown in Figure 2.9. This comparison reveals a large difference in the succinimide absorbance peak between *f*-PIBSA-PyMA and *u*-PIBSA-PyMA for both PIBSA-1-PyMA and PIBSA-2-PyMA. In particular, the *f*-PIBSA-PyMA samples showed a notably lower imide absorbance compared to the *u*-PIBSA-PyMA samples as expected from their lower succinic anhydride content resulting from the loss of the shorter PIBSA species from the precipitation with acetone.

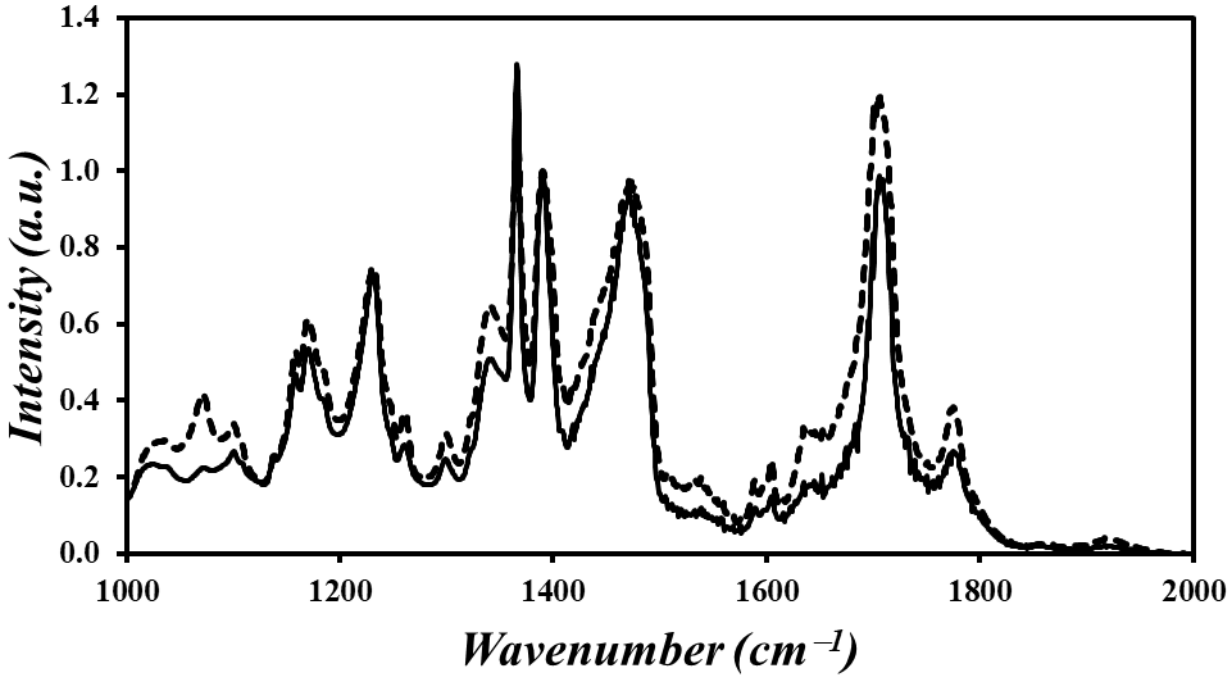

Figure 2.8. FTIR spectra of *u*-PIBSA-1-PyMA (---) and *u*-PIBSA-2-PyMA (─), normalized to 1390 cm^{-1}.

It was noted that although the reactions were conducted at temperatures that were sufficiently high to ensure efficient closure of the succinimide ring, leaving few if any amides in similar work,[21] residual absorbance in the regions from 1500 cm^{-1} to 1580 cm^{-1} and 1610 cm^{-1} to 1700 cm^{-1} suggested the existence of secondary amides in each of the PIBSA-PyMA samples. The amide bands also appeared to increase in intensity with increasing succinic anhydride content in the same manner as the imide bond.

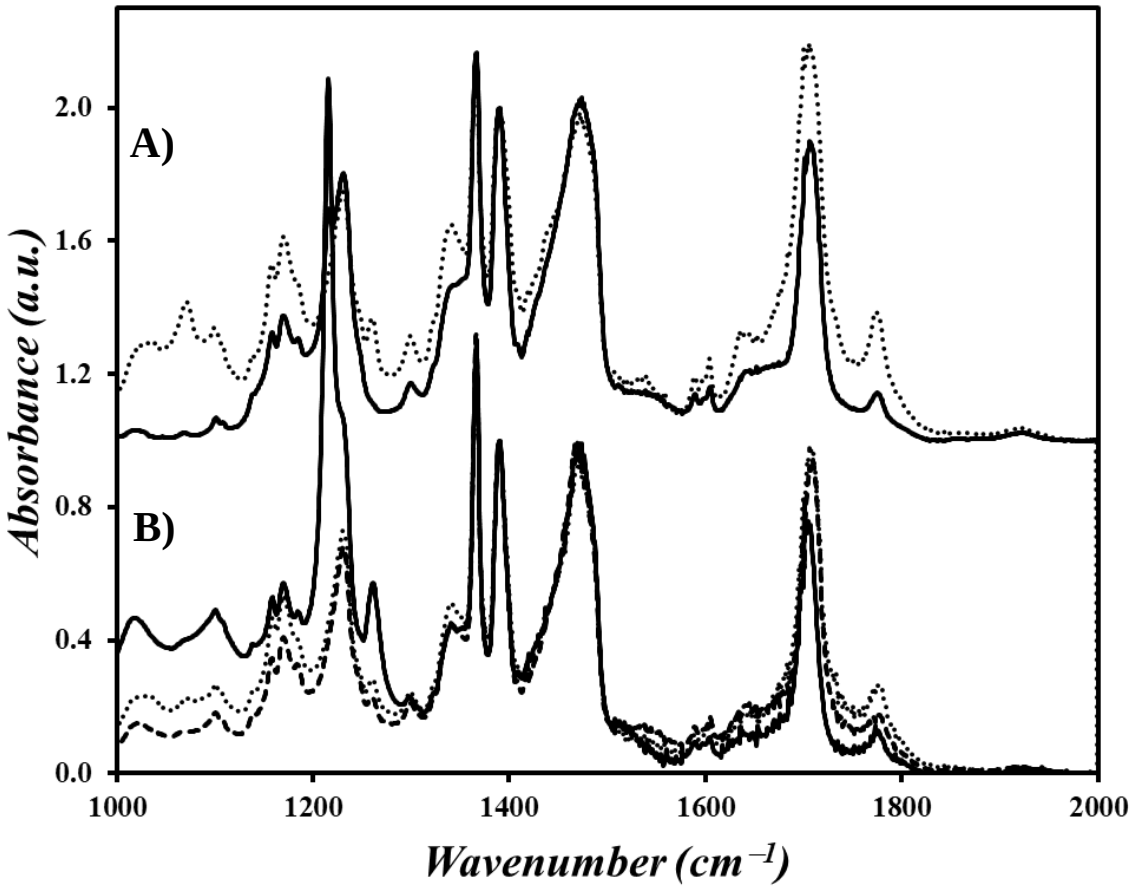

Figure 2.9. FTIR spectra of A) (—) *f*-PIBSA-1-PyMA and (···) *u*-PIBSA-1-PyMA, and B) (—) *f*-PIBSA-2-PyMA, (---) *pf*-PIBSA-2-PyMA, and (···) *u*-PIBSA-2-PyMA, normalized to 1390 cm^{-1}.

In an attempt to quantify the imide content and succinic anhydride content of the PIBSA-1-PyMA and PIBSA-2-PyMA samples, Eq. 2.5[18] was applied to determine the N_{SI}/N_{IB} ratio of the PIBSA-PyMA samples through analysis of the FTIR spectra in Figure 2.9. The N_{SI}/N_{IB} ratio gives a measure of the number of succinimides per isobutylene unit in the sample using the ratio of imide to isobutylene absorbances at 1705 cm^{-1} and 1390 cm^{-1}, respectively. Distortions of the absorbance band due to aggregation of the succinimide pendants induced by H-bonding between amine and amide hydrogens and succinimide carbonyls have also been shown to yield erroneous N_{SI}/N_{IB} ratios.[21]

$$\frac{N_{SI}}{N_{IB}} = 0.035 \times \frac{Abs(1705\ cm^{-1})}{Abs(1390\ cm^{-1})} \quad (2.5)$$

Analysis of the FTIR spectra of the dehydrated and PyMA labeled samples with Eqs 2.4 and 2.5 yielded the N_{SA}/N_{IB} and N_{SI}/N_{IB} ratios, respectively, summarized in Table 2.1. Table 2.1 reveals that the N_{SI}/N_{IB} ratios show a trend similar to that of the N_{SA}/N_{IB} ratios in that both ratios yield fewer isobutylene units per SA for the *u*-PIBSA-PyMA samples compared to the *f*-PIBSA-PyMA samples. This result was expected since the low MW species of the MWD of the *u*-PIBSA samples have a much higher N_{SA}/N_{IB} ratio than the high MW species constituting the MWD of the *f*-PIBSA samples. While there is a large difference of about 20 isobutylene units between the N_{SA}/N_{IB} ratios of the fractionated and unfractionated samples for both PIBSA-1 and PIBSA-2, the difference is lessened for the N_{SI}/N_{IB} ratios which only change by 8 and 5 isobutylene units for PIBSA-1 and PIBSA-2 respectively. This lower sensitivity of N_{SI}/N_{IB} to the PIBSA composition may be due to H-bonding from amides present in the final products, which would distort the imide absorbance band used in Eq. 2.5. This issue is avoided in the samples of dehydrated PIBSA so that the use of FTIR is justified to determine the N_{SA}/N_{IB} ratio. For each sample, the N_{SI}/N_{IB} ratio is always higher than the N_{SA}/N_{IB} ratio, similarly to what was reported in previous work.[21]

Table 2.1. Comparison of N_{SA}/N_{IB} and N_{SI}/N_{IB} ratios of PIBSA-PyMAs.

	PIBSA-1-PyMA		**PIBSA-2-PyMA**		
	Fractionated	**Unfractionated**	**Fractionated**	**Partially Fractionated**	**Unfractionated**
N_{SA}/N_{IB}	1/49.5 (± 1.0)	1/30.6 (± 1.1)	1/54.3 (± 0.6)	1/31.6 (± 1.8)	1/34.6 (± 0.5)
N_{SI}/N_{IB}	1/31.8	1/24.0	1/34.7	1/30.3	1/29.6

Since the PIBSA samples contained some $PIBSA_2$ species with two succinic anhydrides, the MW of the PIBSA-PyMA samples could not be inferred using the N_{SA}/N_{IB} ratios as the ratio of end groups to polymer chains was still unknown.

UV-Visible Absorption (UV-Vis). The pyrene contents (λ_{Py}) of the PIBSA-PyMA samples, expressed as the number of moles of 1-pyrenemethylsuccinimide per gram of pyrene-labeled sample, was determined by measuring the absorbance (*Abs*) at 344 nm of a PIBSA-PyMA sample in THF of known massic concentration (*m*). Taking the ratio $Abs/(\varepsilon \times m)$, where ε is the molar absorbance coefficient of 1-pyrenemethylsuccinimide equal to 40,600 ± 500 $M^{-1}.cm^{-1}$ at 344 nm in THF,[25] yielded λ_{Py}. In turn, λ_{Py} of the PIBSA-PyMA samples could be related to the N_{Py}/N_{IB} ratio according to Eq. 2.6 where M_{IB} and M_{PySu} were the molar mass of isobutylene (56 g/mol) and 1-pyrenemethylsuccinimide (312 g/mol), respectively. The N_{Py}/N_{IB} ratio obtained by UV-Vis absorption was compared to the N_{SA}/N_{IB} ratio obtained by FTIR in Table 2.2.

$$\frac{N_{Py}}{N_{IB}} = \frac{M_{IB}}{\lambda_{Py}^{-1} - M_{PySu}} \tag{2.6}$$

Table 2.2. Summary of λ_{Py} and the N_{Py}/N_{IB} and N_{SA}/N_{IB} ratios obtained for the PIBSA-PyMA samples.

	PIBSA-1-PyMA		**PIBSA-2-PyMA**		
	Fractionated	**Unfractionated**	**Fractionated**	**Partially Fractionated**	**Unfractionated**
λ_{Py} (µmol/g)	350 ± 6	696 ± 11	285 ± 7	486 ± 6	553 ± 2
N_{Py}/N_{IB}	1/45.5 (± 0.9)	1/20.1 (± 0.4)	1/57.0 (± 1.5)	1/31.2 (± 0.4)	1/26.7 (± 0.1)
N_{SA}/N_{IB}	1/49.5 (± 1.0)	1/30.6 (± 1.1)	1/54.3 (± 0.6)	1/31.6 (± 1.8)	1/34.6 (± 0.5)

The λ_{Py} values and N_{Py}/N_{IB} ratios between the *f*- and *u*-PIBSA-PyMA samples shown in Table 2.2 roughly doubled from 350 ± 6 μmol/g to 696 ± 11 μmol/g and from 285 ± 7 μmol/g to 553 ± 2 μmol/g for the PIBSA-1-PyMAs and PIBSA-2-PyMAs, respectively. This increase agreed with the increase in N_{SA}/N_{IB} and N_{SI}/N_{IB} ratios seen by FTIR, and the large difference in their GPC traces, which reflected the higher succinic anhydride content when retaining the whole MWD of the PIBSA samples. For the PIBSA-2-PyMAs, the λ_{Py} value and the N_{Py}/N_{IB} ratio of *pf*-PIBSA-2-PyMA sample were between those of the *f*- and *u*-PIBSA-2-PyMA samples as was seen for the N_{SA}/N_{IB} ratio obtained from FTIR. While good agreement was observed between the N_{Py}/N_{IB} and N_{SA}/N_{IB} ratios for the fractionated and partially fractionated PIBSA-PyMA samples, the N_{SA}/N_{IB} ratios for the *u*-PIBSA-PyMA samples showed a substantial difference of up to 10 isobutylene units with the N_{Py}/N_{IB} ratios. At this stage, the large errors in the calibration curve built by Walch and Gaymans[20] to obtain Eq. 2.4 particularly for the higher SA contents, suggest that Eq. 2.4 might be inaccurate for the higher SA contents obtained with the *u*-PIBSA samples.

The Peak-to-Valley ratio (P_A) obtained from the absorption spectra can also be used to obtain a qualitative measure of the level of pyrene aggregation in the PIBSA-PyMA samples, as has been shown for both pyrene-labeled polymers and for 1-pyrenemethylsuccinimides specifically.[26-28] The P_A ratio is calculated with Eq. 2.7, where A^{Peak} and A^{Valley} are the absorbance at the maximum at 344 nm and at the adjacent minimum in Figure 2.10, respectively.

$$P_A = \frac{A^{Peak}}{A^{Valley}} \tag{2.7}$$

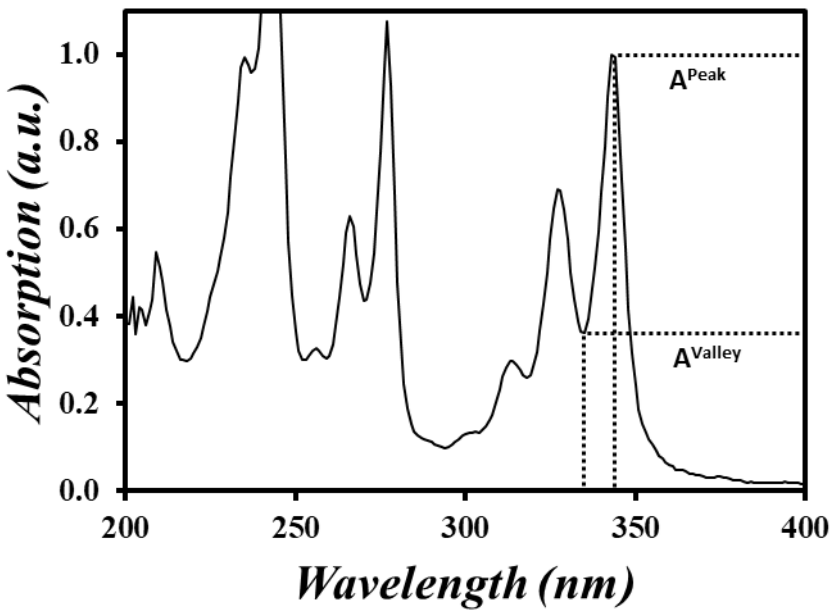

Figure 2.10. Absorption spectrum of *u*-PIBSA-1-PyMA normalized to 344 nm.

Aggregation results in a broadening of the bands in the absorption spectrum, and thus a smaller P_A ratio for samples with more aggregated pyrenes. A $P_A \geq 3$ indicates that the pyrene moieties are unassociated, while a P_A value smaller than 3 indicates the presence of pyrene aggregates in the sample. A summary of the P_A values obtained for the PIBSA-PyMA samples is given in Table 2.3.

Table 2.3. Summary of P_A values of PIBSA-PyMA samples.

	PIBSA-1-PyMA		**PIBSA-2-PyMA**		
	Fractionated	**Unfractionated**	**Fractionated**	**Partially Fractionated**	**Unfractionated**
$\boldsymbol{P_A}$	2.8 ± 0.0	2.7 ± 0.0	2.9 ± 0.0	2.8 ± 0.0	2.8 ± 0.0

The P_A values for the unfractionated samples shown in Table 2.3 are close to but smaller than 3, which indicates that both have residual pyrene aggregation. The lower P_A of 2.7 for the *u*-PIBSA-1-PyMA sample compared to the P_A value of 2.8 for the *f*-PIBSA-2-PyMA and *u*-PIBSA-2-PyMA samples suggests a slightly higher level of pyrene aggregation in the *u*-PIBSA-1-PyMA sample. As the absorbance spectra are acquired in THF, a good solvent for the PIBSA-PyMA samples, the aggregation was likely intramolecular in nature and could be attributed to $PIBSA_2$ species having two 1-pyrenemethylsuccinimide pendants.

Steady-State (SSF) and Time-Resolved Fluorescence (TRF) Measurements. The fraction of aggregated pyrenes, referred to as f_{agg} in this thesis, is related to the molar fraction of doubly modified $PIBSA_2$ species in a PIBSA sample through Equation 2.8. f_{agg} was previously determined for a PIBSA-PyMA sample using a rudimentary analysis of the pyrene monomer and excimer fluorescence decays based on sums of exponentials.[22] A more robust analysis of the fluorescence decays is now presented to determine f_{agg} for all PIBSA-PyMA samples investigated in this thesis based on the well-established MFA. The SSF spectra and TRF decays were acquired for solutions in THF of each PIBSA-PyMA sample with a pyrene concentration of 2.5 μM using the right-angle geometry. Although intermolecular PEF is impossible at such low concentrations, the SSF spectra showed trace amounts of PEF at 480 nm in Figure 2.11, indicating intramolecular PEF arising from doubly labeled $PIBSA_2$-PyMA species as suggested by the P_A ratios in Table 2.3. Unfortunately, the low PEF signal at this concentration prevented the acquisition of the excimer TRF decays, and thus the quantitative determination of f_{agg} by the MFA.

$$f_{doubly} = \frac{f_{agg}}{2 - f_{agg}} \tag{2.8}$$

Taking advantage of the ability of TRF to distinguish between the kinetic path leading to inter- and intramolecular PEF, a series of solutions in THF were prepared for each PIBSA-PyMA

sample with concentrations ranging from 2.5 g/L to 40 g/L to boost PEF. In these experiments, the rate of excimer formation by diffusion (<k>) obtained through the MFA of the decays should increase linearly with increasing pyrene concentration as predicted by Equation 2.9. However, the molar fractions f_{diff} and f_{agg} of pyrenyls forming excimer by diffusive encounters between an excited and a ground-state pyrene or direct excitation of pyrene aggregates, respectively, should remain constant over the range of PIBSA-PyMA concentrations studied, allowing the determination of f_{doubly}.

$$< k >= k_{diff} \times [Py]_{loc} \propto \frac{I_E}{I_M} \tag{2.9}$$

The SSF spectra and TRF decays were acquired using the front-face geometry to minimize artefacts induced by the inner-filter effect and reabsorption. The SSF spectra and in-laid plots of the I_E/I_M ratios of the PIBSA-PyMA samples are shown in Figure 2.11.

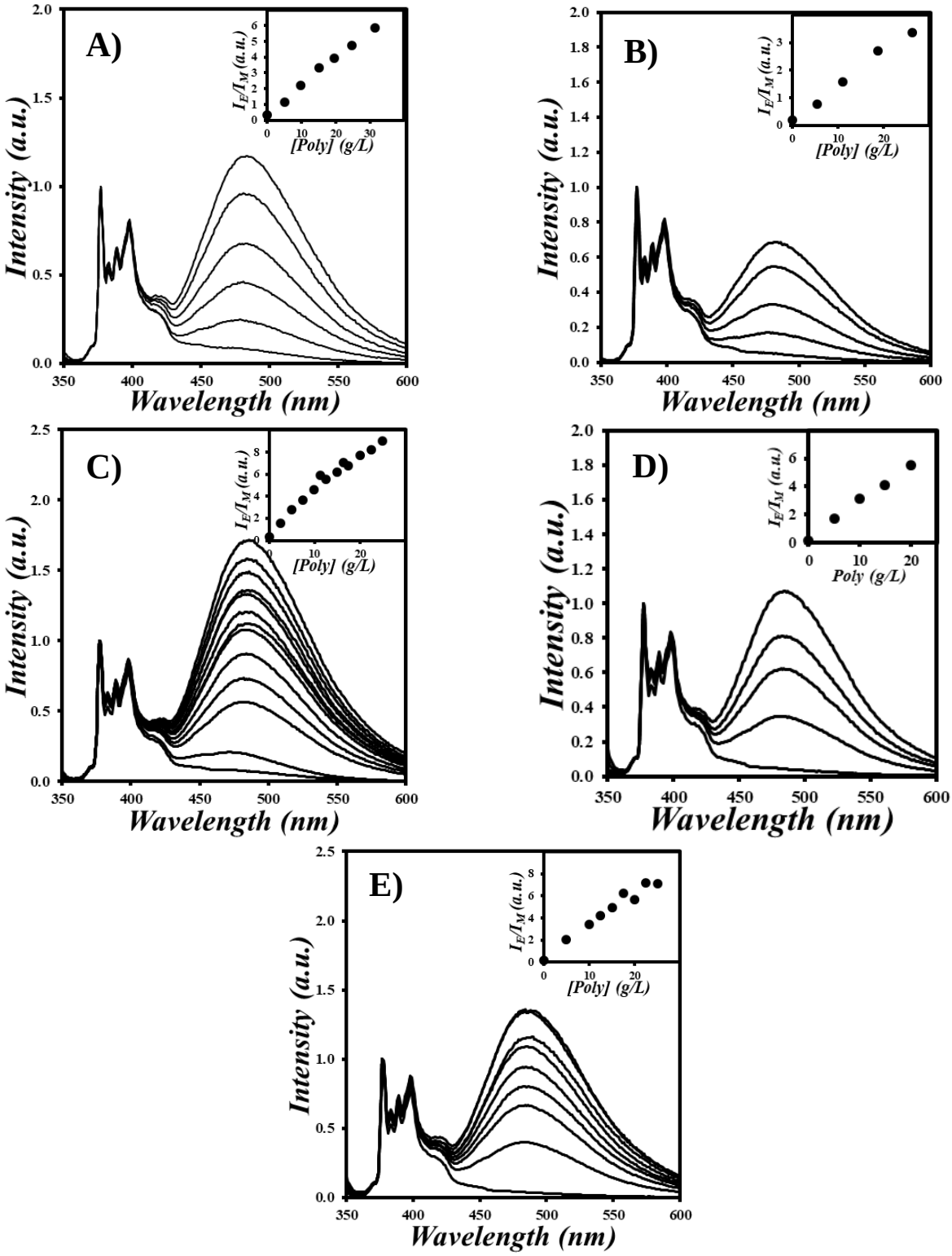

Figure 2.11. Steady-state fluorescence spectra and inlaid plots of I_E/I_M vs. the polymer concentration in g/L of A) *f*-PIBSA-1-PyMA, B) *f*-PIBSA-2-PyMA, C) *u*-PIBSA-1-PyMA, D) *pf*-PIBSA-2-PyMA, and E) *u*-PIBSA-2-PyMA in THF normalized at 377 nm.

Each set of SSF spectra in Figure 2.11 showed an increase in excimer fluorescence with an increase in polymer concentration, as reflected by the linear response of the I_E/I_M-*vs*-[PIBSA-PyMA] in the in-laid plots. The non-zero intercepts of the I_E/I_M trends were attributed to the presence of aggregated pyrenes resulting from the double labeling of the $PIBSA_2$ species. This conclusion was also supported by the presence of excimer in the fluorescence spectra acquired with a pyrene concentration of 2.5 μM shown in Figure 2.11. When the I_E/I_M-*vs*-[PIBSA-PyMA] plots were brought together in Figure 2.12A, the *u*-PIBSA-PyMA samples yielded higher I_E/I_M ratios at the same polymer mass concentration due to their higher pyrene content (see Table 2.2). The differences between the I_E/I_M-*vs*-[Py] trends narrowed substantially in Figure 2.12B compared to Figure 2.12A, indicating that the pyrene content of the samples was an important parameter controlling PEF. The overlap was not perfect however, suggesting subtle differences between the different PIBSA-PyMA samples. One such difference was related to the respective size of the different PIBSA-PyMA samples. The unfractionated samples *u*-PIBSA-1-PyMA and *u*-PIBSA-2-PyMA showed the steepest increase in I_E/I_M. This result is consistent with the unfractionated samples having a smaller averaged hydrodynamic volume (V_h) based on the GPC traces in Figure 2.5, and thus having a larger diffusion coefficient associated with a larger k_{diff} value in Equation 2.9. While qualitatively sound, the trends obtained with the I_E/I_M ratios cannot distinguish between the different pyrene species in the solution that generate excimer. Such detailed information will be obtained later on through the MFA of the TRF decays which will be presented later.

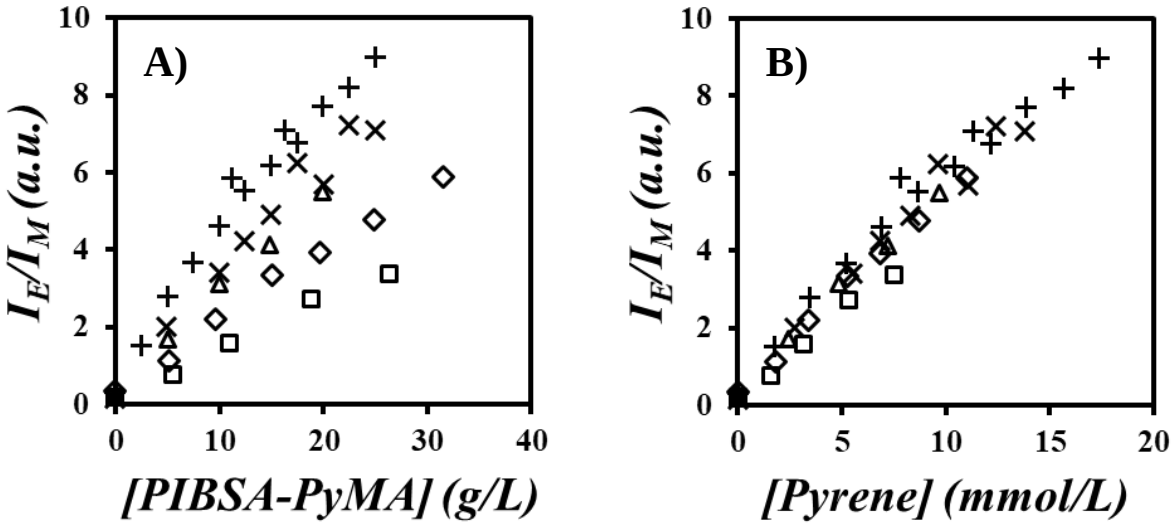

Figure 2.12. Plots of I_E/I_M vs. A) [PIBSA-PyMA] in g/L, and B) [Pyrene] in mol/L for (◆) *f*-PIBSA-1-PyMA, (◘) *f*-PIBSA-2-PyMA, (▲) *pf*-PIBSA-2-PyMA, (+) *u*-PIBSA-1-PyMA, and (×) *u*-PIBSA-2-PyMA.

The spectra in Figure 2.11 also showed some evidence of reabsorption artefacts despite the use of the front-face geometry, as seen by the poor overlap of the monomer peaks in the 370 – 410 nm region of the spectra. Distortions in the fluorescence spectra were attributed to reabsorption of the emission at 375 nm due to the large absorption of the concentrated pyrene solutions. Even though the molar absorption coefficient of pyrene is strongly reduced for the $S_0 \rightarrow S_1$ transition of pyrene at 375 nm, the minuscule absorption at 375 nm resulting from low pyrene concentrations is no longer negligible at high pyrene concentrations. Reabsorption skews the I_E/I_M ratios to higher values as it reduces the fluorescence intensity of the monomer peak at 375 nm, which is used to calculate the I_E/I_M ratio. While the fluorescence intensity of the pyrene monomer is slightly

reduced in the fluorescence spectra shown in Figure 2.11, this reduction was not enough to affect the I_E/I_M-*vs*-[Py] trends in Figure 2.12, which show a mainly linear relationship.

Once the SSF study had confirmed that the PIBSA-PyMA samples exhibited the spectral features expected from a typical PyLM, the monomer TRF decays acquired with the 2.5 μM pyrene solutions were analysed with a sum of two exponentials, where the exponential with a pre-exponential contribution over 75% was used to obtain the natural lifetime (τ_M) of the pyrene derivative for each sample. The τ_M values are listed in Table 2.4.

Table 2.4. τ_M values of the PIBSA-PyMA samples.

	PIBSA-1-PyMA		**PIBSA-2-PyMA**		
	Fractionated	**Unfractionated**	**Fractionated**	**Partially Fractionated**	**Unfractionated**
τ_M (ns)	292	283	295	276	289

The samples took an averaged τ_M value of 287 (±8) ns, comparable to the τ_M value of 290 ns reported for a PIBSA-PyMA sample in the literature.[22] The monomer and excimer TRF decays obtained at higher pyrene concentrations were fitted globally according to the MFA with the sumegs33bg-9.f program which was written in Fortran in house. The decay analysis used three exponentials to fit the monomer fluorescence decays and two excimer species *E*0* and *D** made of properly and improperly stacked pyrenyl moieties, respectively. A short-lived contribution was observed in the monomer decays, probably due to residual light scattering for these high polymer concentrations. It was handled by adding an extra exponential to fit the monomer decays with a short 3.5 ns decay time, which was fixed in the decay analysis. The MFA gave good fits (see Figure 2.13) for all PIBSA-PyMA solutions, as long as the pyrene concentration was high enough to yield a rise time in the excimer decay indicative of PEF by diffusive encounters. The monomer and

excimer fluorescence decays were fitted globally according to Equations 2.2 and 2.3, respectively. The fluorescence decay times and pre-exponential factors obtained from the MFA are summarized in Tables A1 - 5. The process of pyrene excimer formation for the PIBSA-PyMA samples was well-described by Scheme 2.4.

Scheme 2.4. Kinetic scheme of pyrene excimer formation for the PIBSA-PyMA samples.

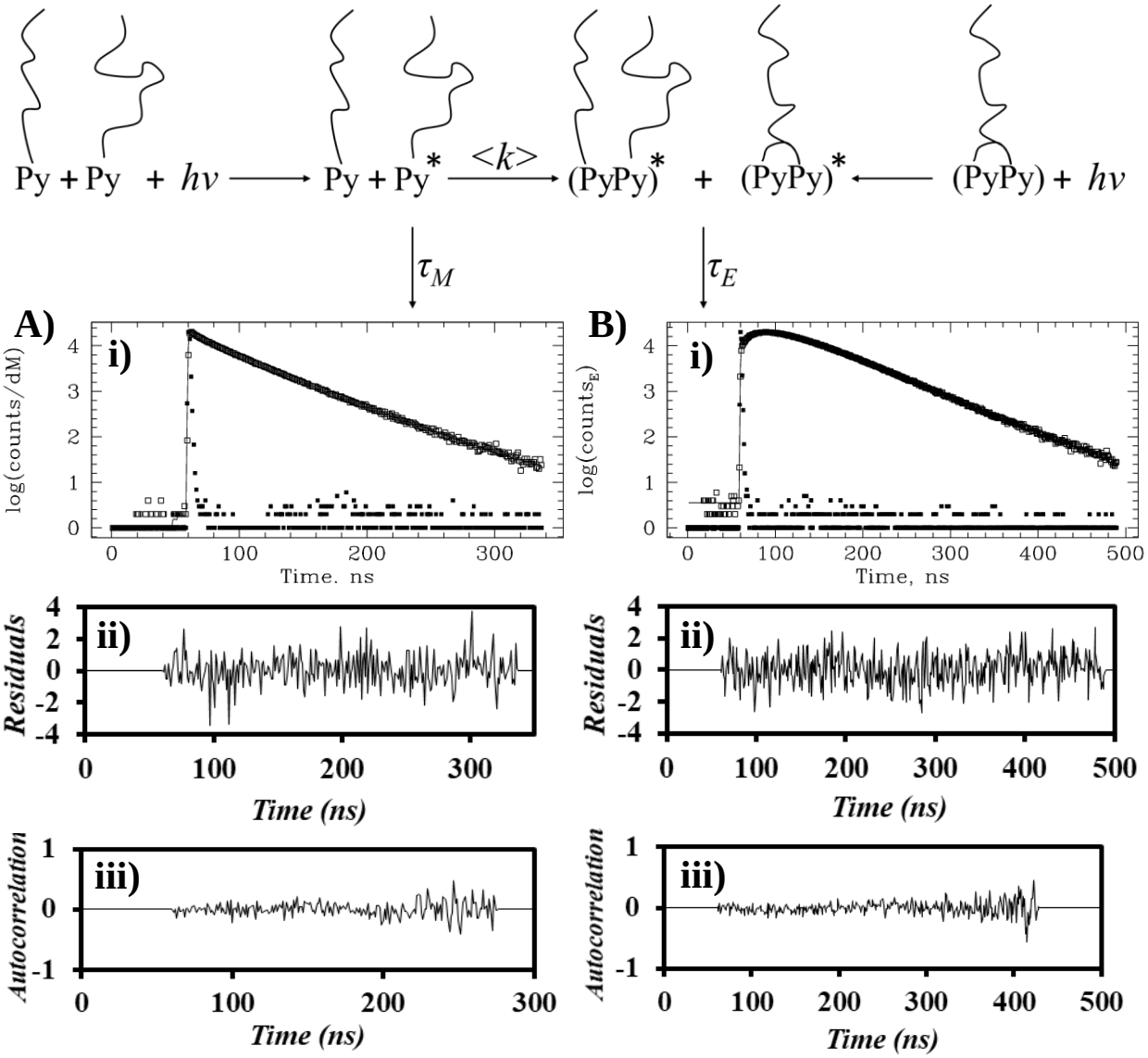

Figure 2.13. Fits of TRF i) decays, ii) residuals and iii) autocorrelation of the pyrene A) monomer and B) excimer decays of a *u*-PIBSA-1-PyMA solution in THF with a polymer concentration of 15 g/L.

The fluorescence decays of the PIBSA-PyMA solutions became shorter-lived for increasing pyrene concentrations, as expected if PEF was taking place by diffusive encounters. The number average monomer lifetime (<τ>) was calculated according to Eq. 2.10 for each PIBSA-PyMA solution using the monomer decay times and pre-exponential factors listed in Tables A1 - 5, and it was used to determine <k> from Equation 2.11, which increased linearly for increasing pyrene concentrations in Figure 2.14.

$$\langle \tau \rangle = \frac{\sum_i^n a_i \tau_i}{\sum_i^n a_i} \tag{2.10}$$

$$k_{diff} \times [Py]_{loc} = \langle k \rangle = \frac{1}{\tau_M} - \frac{1}{\langle \tau \rangle} \tag{2.11}$$

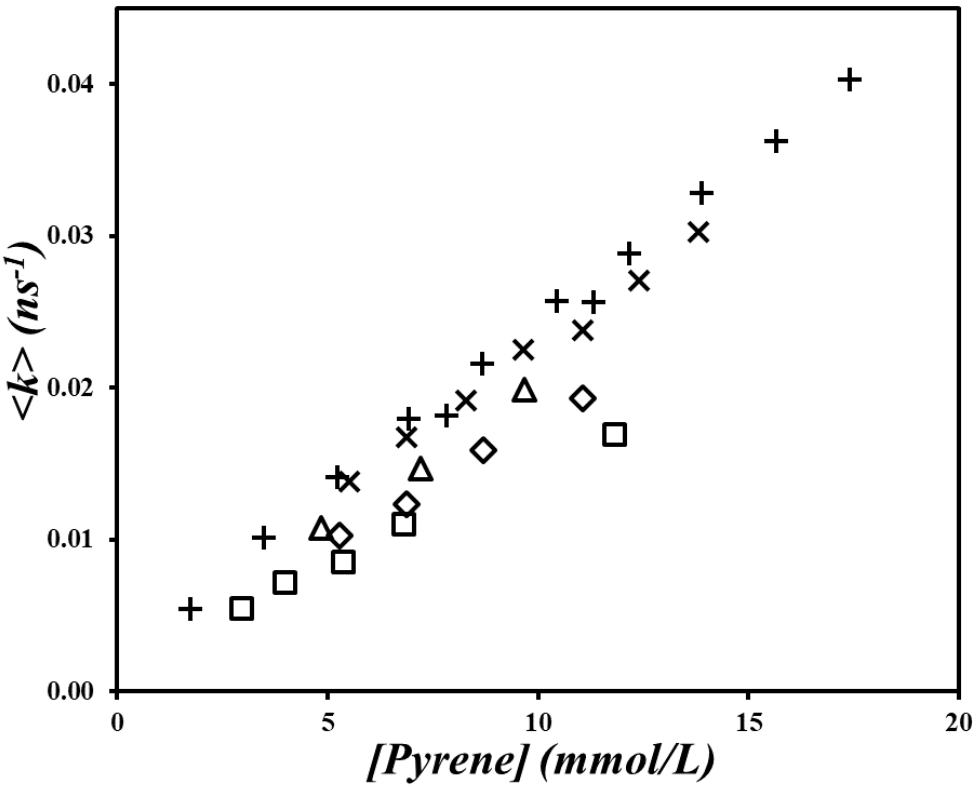

Figure 2.14. Plots of <k> vs. [Py] for (◆) *f*-PIBSA-1-PyMA, (□) *f*-PIBSA-2-PyMA, (△) *pf*-PIBSA-2-PyMA, (+) *u*-PIBSA-1-PyMA, and (×) *u*-PIBSA-2-PyMA in THF.

The parameter k_{diff} in Eq. 2.11 represents the bimolecular rate constant for diffusive encounters between the pyrene-labeled molecules in solution and is given by the slopes of the straight lines obtained from the $<k>$-vs-$[Py]$ plots in Figure 2.14. The corresponding k_{diff} values were listed in Table 2.5. Both *f*-PIBSA-PyMAs yielded lower k_{diff} values representing the slower diffusion of the longer PIBSA chains obtained after fractionation of the PIBSA samples. Similarly, k_{diff} for the *pf*-PIBSA-2-PyMA sample fell in between the high and low k_{diff} values obtained for the smaller *u*- and larger *f*-PIBSA-PyMA samples, respectively. The trend obtained with the k_{diff} values in Table 2.5 is consistent with the expected size of the PIBSA-PyMA samples.

Table 2.5. k_{diff} values for the PIBSA-PyMA samples.

	PIBSA-1-PyMA		**PIBSA-2-PyMA**		
	Fractionated	**Unfractionated**	**Fractionated**	**Partially Fractionated**	**Unfractionated**
k_{diff} ($\mu M^{-1}.ns^{-1}$)	1.80 ± 0.04	2.37 ± 0.03	1.53 ± 0.07	2.07 ± 0.04	2.24 ± 0.04

While the excimer lifetimes τ_{E1} and τ_{E2} in Tables A1 - 5 varied between 35 and 75 ns, a reasonable range of values for PEF in organic solvents, the molar fractions f_{diff} and f_{agg} of pyrene monomers forming excimer by diffusive encounters and direct excitation of pre-aggregated pyrenes, respectively, remained constant with polymer concentration. f_{agg} was obtained by summing the molar fractions f_{E0} and f_D of pyrene forming excimer by direct excitation of pyrene aggregates according to Eq. 2.11 for the PIBSA-PyMA samples at each concentration studied. The f_{agg} values were plotted as a function of pyrene concentration in Figure 2.15. The f_{agg} values were then re-arranged to yield f_{doubly} with Eq. 2.12. Both f_{agg} and f_{doubly} values were summarized in Table 2.6.

$$f_{diff} = f_{E1} + f_{E2} \tag{2.11}$$

$$f_{doubly} = \frac{f_{agg}}{2 - f_{agg}} \tag{2.12}$$

Table 2.6. f_{agg} and f_{doubly} values of PIBSA-PyMA samples.

	PIBSA-1-PyMA		**PIBSA-2-PyMA**		
	Fractionated	**Unfractionated**	**Fractionated**	**Partially Fractionated**	**Unfractionated**
f_{agg}	0.181 ± 0.006	0.165 ± 0.009	0.122 ± 0.013	0.101 ± 0.004	0.124 ± 0.010
f_{doubly}	0.100	0.090	0.065	0.053	0.066

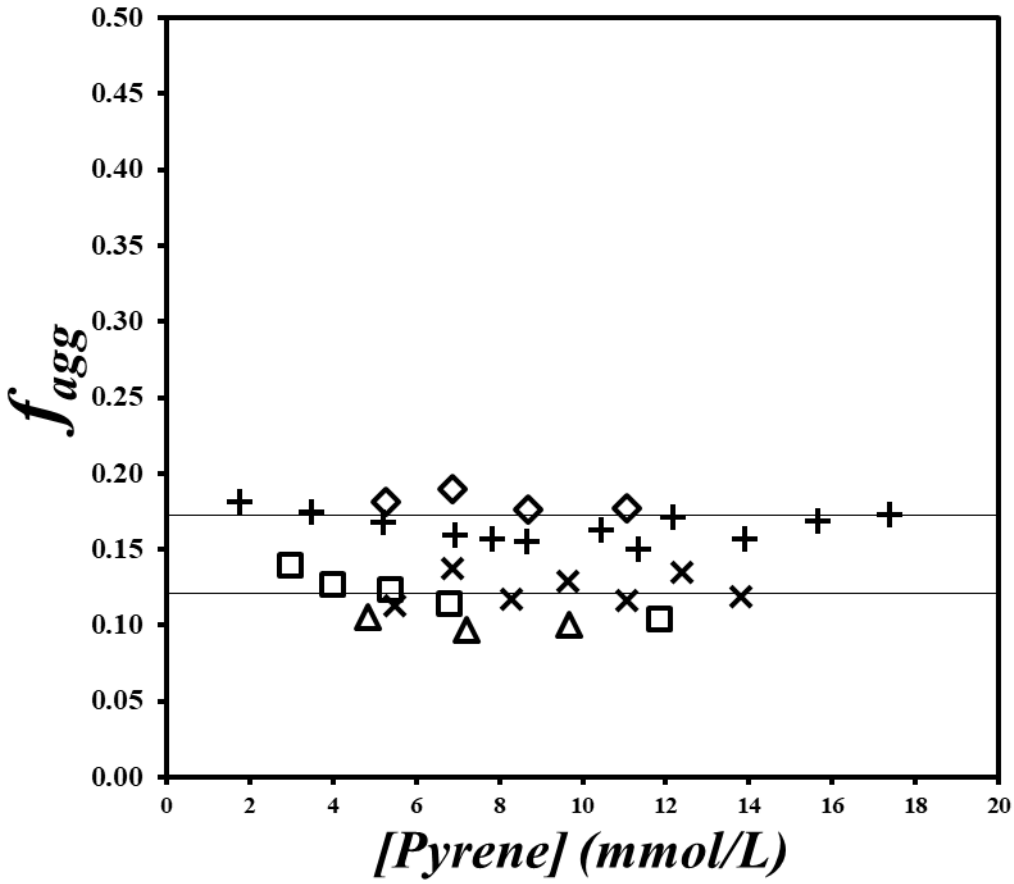

Figure 2.15. Plots of f_{agg} vs. [Py] of (◆) *f*-PIBSA-1-PyMA, (■) *f*-PIBSA-2-PyMA, (▲) *pf*-PIBSA-2-PyMA, (+) *u*-PIBSA-1-PyMA, and (×) *u*-PIBSA-2-PyMA.

For each PIBSA-PyMA sample, the f_{agg} values remained constant with pyrene concentration in Figure 2.15, indicating that they represented an intrinsic feature of the PIBSA samples. Both the *u*- and *f*-PIBSA-1-PyMA samples yielded similar f_{agg} values of 0.181 ± 0.006 and 0.165 ± 0.009, respectively. These f_{agg} values were higher than the f_{agg} values of 0.122 ± 0.013, 0.101 ± 0.004, and 0.124 ± 0.010, obtained for the *u*-, *pf*-, and *f*-PIBSA-2-PyMA samples, respectively. The consistency of f_{agg} for different samples isolated along the MWD of the unfractionated PIBSA samples inferred that the fraction of $PIBSA_2$ species in a PIBSA sample remained constant across the entire MWD of a PIBSA sample.

Now that f_{doubly} had been determined, the number average degree of polymerization (X_n) of the different PIBSA samples could be calculated with Eq. 2.13 before determining the corresponding M_n of each PIBSA from Eq. 2.14 where M_{SA} and M_{IB} represent the molar masses of a succinic anhydride moiety (99 g/mol) and isobutylene monomer (56 g/mol), respectively.

$$X_n = (1 + f_{agg}) \times \frac{\lambda_{Py}^{-1} - M_{Py}}{M_o} \tag{2.13}$$

$$M_n = (1 + f_{doubly}) \times M_{SA} + X_n \times M_{IB} \tag{2.14}$$

The resulting X_n and M_n values obtained were summarized in Table 2.6.

Table 2.7. X_n and M_n values for the PIBSA-PyMA samples.

	PIBSA-1-PyMA		**PIBSA-2-PyMA**		
	Fractionated	**Unfractionated**	**Fractionated**	**Partially Fractionated**	**Unfractionated**
X_n	50.0	21.9	60.7	32.8	28.5
M_n **(kg/mol)**	2.91	1.33	3.51	1.94	1.70

An interesting correlation could be observed between k_{diff} in Table 2.5 and X_n in Table 2.6 as shown in Figure 2.16. k_{diff} decreased with increasing degree of polymerization, as expected from a diffusion-controlled PEF where larger species diffuse more slowly. In turn, the linear relationship observed between k_{diff} and X_n suggests that it could be used as a calibration curve to predict the number average degree of polymerization of an unknown PIBSA sample based on its k_{diff} value.

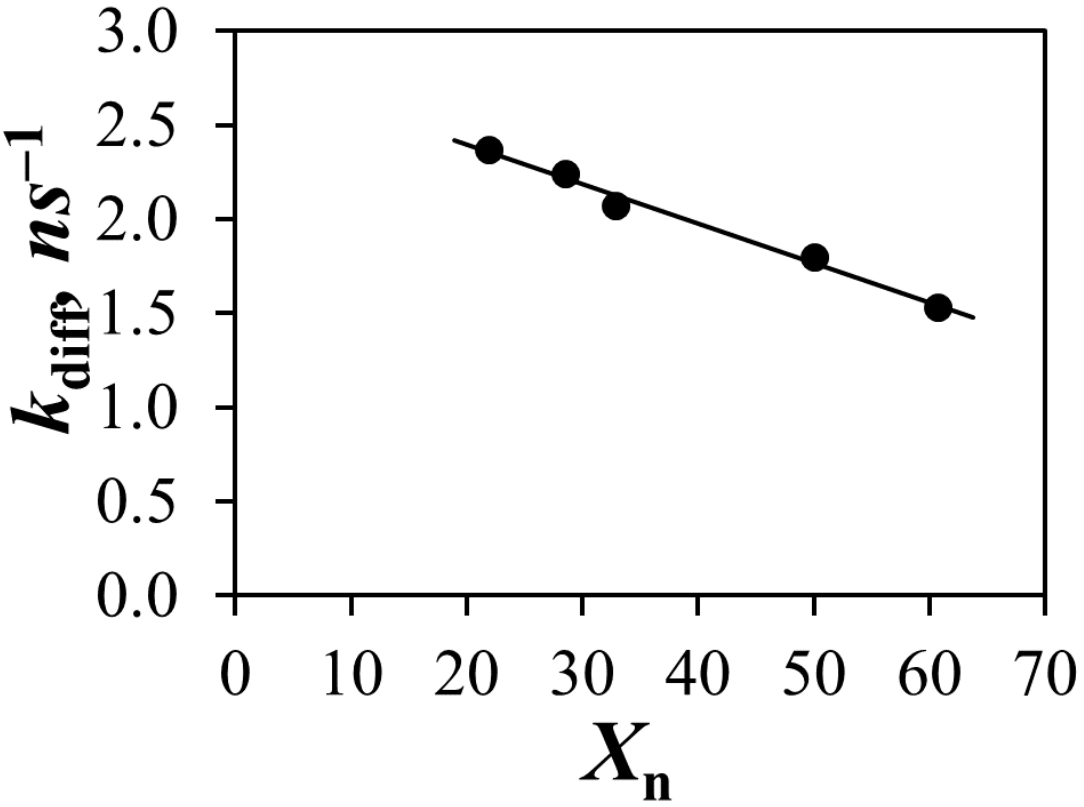

Figure 2.16. Plot of k_{diff} as a function of X_n for the five PIBSA-PyMA samples.

The M_n and f_{doubly} values represent important parameters to describe the PIBSA samples. The M_n values for the *u*-PIBSA-PyMA samples were notably lower than those for the fractionated samples as would be expected. Knowledge of f_{doubly} enables a more accurate calculation of M_n than would be possible with traditional end-group analyses which cannot distinguish doubly from singly maleated PIBSA species. Since the presence of $PIBSA_2$ in commercial PIBSAs complicates their use in dispersant manufacturing, the procedure developed in this chapter to determine f_{doubly}

represents a substantial advance in the characterization of PIBSA samples, as it should enable the prediction of the different types of architectures that can be expected for a PIBSI dispersant. These concepts will be illustrated in the following chapter.

2.5 Conclusions

Five different PIBSA-PyMA samples were prepared from the PIBSA-1 and PIBSA-2 samples which were labeled with PyMA and fractionated to different extents. Comparison of the MWD, N_{SA}/N_{IB}, and N_{Py}/N_{IB} ratios of the different PIBSA and PIBSA-PyMA samples obtained by GPC, FTIR absorption, and UV-Vis absorption analysis, respectively, showed large differences in the sample composition between the *f*- and *u*-PIBSA-PyMA samples due to precipitation. The N_{SA}/N_{IB} ratio of the dehydrated PIBSA samples obtained by FTIR yielded twice as many succinic groups when the PIBSAs were not fractionated by precipitation. Similarly, UV-Vis absorption measurements were used to determine the 1-pyrenemethylsuccinimide content (λ_{Py}) of the PIBSA-PyMA samples which was found to double when transitioning from the *f*- to *u*-PIBSA-PyMA samples. The UV-Vis absorption spectra of the PIBSA-PyMA samples provided a rough measure of the extent of pyrene aggregation through the P_A value, which was found to be close to but smaller than 3 for both *u*-PIBSA-PyMA samples which inferred residual pyrene aggregation.

SSF and TRF measurements acquired for the PIBSA-PyMA solutions in THF for concentrations ranging from 2.5 to 40 g/L yielded trends for I_E/I_M and $<k>$ which were consistent for PEF occurring mainly through diffusive encounters between an excited and a ground-state pyrene. The linear increase of $<k>$ with increasing pyrene concentration yielded k_{diff} which describes the diffusive encounters between pyrene labels. k_{diff} was found to decrease linearly with increasing degree of polymerization of the PIBSA-PyMA samples. The MFA of the TRF decays

yielded f_{doubly} values that remained constant with polymer concentration, indicating that this parameter represented an intrinsic property of the PIBSA samples. The f_{agg} values were consistently higher for the PIBSA-1-PyMA samples taking on values of 0.181 ± 0.006 and 0.165 ± 0.009 for the *f*- and *u*-PIBSA-1-PyMA fractions, respectively, than those of 0.122 ± 0.013, 0.101 ± 0.004, and 0.124 ± 0.010 obtained for the *f*-, *pf*-, and *u*-PIBSA-2-PyMAs, respectively. The similar f_{doubly} values obtained for different portions of the MWD of the PIBSA samples suggest that the proportion of $PIBSA_2$ species remains constant across the MWDs of the PIBSA-1 and PIBSA-2 samples. These results should be of interest to characterize the final architecture of polymeric oil additives such as the PIBSA dispersants, or other macromolecules generated using PIBSA as a building block.

Chapter 3

Simulation of the PIBSA/PIBSI Products Resulting from a PIBSA-HMDA Coupling Reaction

3.1 Outline

A method was implemented to predict the chemical composition resulting from the coupling of a polyisobutylene maleated at one end (PIBSA) and hexamethylene diamine (HMDA), and use it to simulate the traces that would be obtained experimentally by gel permeation chromatography (GPC) with a differential refractive index (DRI) detector. To this end, a simulation program was written that took into account the molar fraction (f_{doubly}) of PIBSA chains that were doubly maleated ($PIBSA_2$). The program randomly selected one succinic anhydride (SA) and one amine in the reaction mixture to couple them and form a PIBSI product. When all amines or SA had run out, the program stopped and summarized the number of unreacted PIBSA and mono-, bis-, tri- … PIBSI products left in the reaction mixture. A similar simulation program was implemented which assumed that steric hindrance prevented the formation of higher-order PIBSI products. Using the molecular weight distribution (MWD) of the PIBSA sample determined from GPC analysis, the MWD of the *b*-PIBSI and higher-order PIBSI products could be estimated. The MWD of PIBSA and the PIBSI products were combined with the simulation results to predict the DRI trace that would be obtained for a given coupling reaction between PIBSA and HMDA. Experimental data were generated to validate the theoretical procedure by coupling a PIBSA sample with a known f_{doubly} with HMDA for amine-to-SA ratios ($N_{\text{Am}}/N_{\text{SA}}$) varying between 0.25 and 2.00 to create PIBSA-2-H mixtures of different compositions. The PIBSA-2-H mixtures were analysed by GPC and their DRI traces were parametrized as sums of Gaussians. Excellent agreement was found between the Gaussian fits of the experimental DRI traces and the simulated DRI traces when steric hindrance was assumed to restrict the coupling reaction to the formation of *bis*-PIBSI products. This early work suggests that it might be possible to predict the chemical composition of the reaction mixture resulting from the coupling of PIBSA and more complex polyamines.

3.2 Introduction

Oils have been used for years to lubricate a variety of machinery. They work by forming a thin layer upon compression which decreases wear by reducing metal-on-metal contacts and thus increases the lifetime of any device relying on metallic moving parts, particularly automobile engines.[1-3] Engine oils consist of a mixture of base oils, often mineral oils, and additives which improve or add new properties to base oils which cannot function on their own without undergoing thermal or oxidative degradation detrimental to their performance.[2] Many oil additives can also interact with one another which can be beneficial or detrimental to an oil performance. As a result, intense research has focused on characterizing these interactions.[4-7] For example, succinimide-based dispersants can interact with metallic detergents via acid-base reactions between their polar groups.[4] While the mixture of additives can vary between different lubricating oils depending on the application, common additives for engine oils include anti-wear agents, pour point depressants, viscosity index improvers, demulsifiers, and lastly, the additive of interest for this thesis, dispersants.[4-7]

Dispersants were introduced in the 1950s to minimize oil-thickening but increased in popularity after the introduction of exhaust gas recirculation (EGR). This technique reduces nitrous oxide emissions by cycling a portion of the exhaust gases back to the intake manifold to reduce the combustion temperature and in turn the formation of nitrous oxides.[8,9] While EGR was effective in reducing nitrous oxide pollution, it resulted in a large increase in particulate deposition into the engine oil.[8] For instance, soot and ultrafine particles (UFPs) are some of the main particles which can accumulate in engine oils and will aggregate to reduce their polar surface areas in the apolar engine oil. UFPs in particular are a known emission from automobiles and they can lead to health hazards.[8,10] The increased amounts of particulates in engine oils often led to oil-thickening,

which is detrimental to lubricant function. This problem could be mitigated by the addition of dispersants which stabilize insoluble particulate in the oil to prevent further aggregation or precipitation of the said particulates. The dispersants also allowed for the removal of the dispersed particulates when replacing the oil.

Dispersants are most often block copolymers which contain both a polar core and non-polar appendages. The polar regions adhere to the polar surface of insoluble particulates in the oil, while the large apolar segments will prevent further aggregation, mainly through steric stabilization as depicted in Figure 3.1.[3,11] Steric stabilization in this context is a process by which the apolar segments of a dispersant sterically hinder encounters between the dispersed particles, thus preventing their agglomeration into larger particles that would otherwise precipitate.

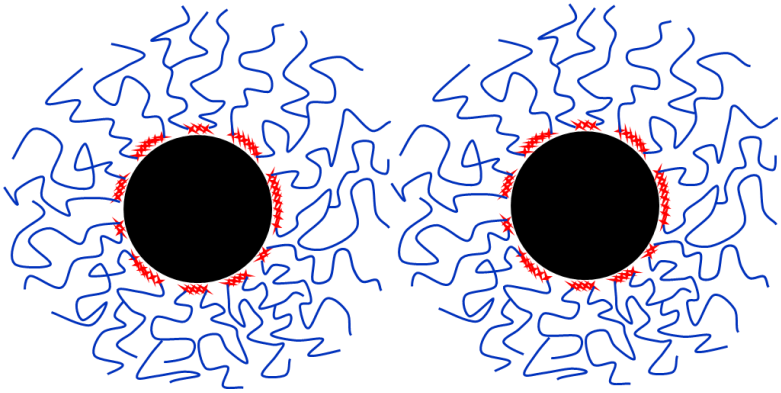

Figure 3.1. Steric stabilization of dispersed particles.

The dispersants most commonly used today are constituted of polyisobutylene (PIB) apolar segments and polyamines as the polar core. The PIB segment is usually modified through an Alder-ene reaction at high temperatures with maleic anhydride to form polyisobutylenes terminated with succinic anhydride groups (PIBSAs). Two PIBSAs can then be linked via reaction of a polyamine with two terminal SAs according to Scheme 3.1 to form *bis*-polyisobutylene succinimides (*b*-PIBSIs).[2,3,**Error! Bookmark not defined.**]

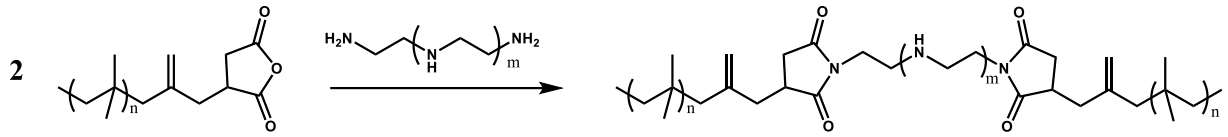

Scheme 3.1. General scheme for the synthesis of *b*-PIBSI dispersants.

Due to the presence of doubly-maleated PIBSAs ($PIBSA_2$) which have undergone the Alder-ene reaction twice, the coupling of PIBSA samples into *b*-PIBSI becomes complicated.[12] The presence of $PIBSA_2$ in PIBSA samples leads to the formation of PIBSI-trimers (*tri*-PIBSIs) or other higher-order PIBSIs during the imide coupling reaction with the bifunctional fraction of a PIBSA sample. A number of parameters can be determined to help predict the chemical composition of a reaction mixture resulting from the coupling of PIBSA and a polyamine. For instance, the succinic anhydride content of PIBSA samples can be calculated via FTIR analysis of a dehydrated PIBSA sample thanks to a calibration curve established by Walch and Gaymans,[13] and the molar fraction (f_{doubly}) of $PIBSA_2$ in a PIBSA sample can be determined via fluorescence.[14] However, the characterization of PIBSI products suffers from a variety of complications when attempting to use conventional methods such as ^{1}H NMR and FTIR spectroscopy. The signals of the amine hydrogens and succinimide carbonyls in, respectively, the ^{1}H NMR and FTIR spectra employed to characterize the PIBSI dispersants, have shown some substantial distortions due to hydrogen bonding between the two groups.[15] The lack of monodisperse low molecular weight PIB standards and the low *dn*/*dc* values for PIB in tetrahydrofuran (THF) complicate the quantitative GPC analysis with a conventional calibration curve. These issues represent difficult experimental challenges to overcome in the analysis of PIBSI products resulting from an imide coupling reaction between a PIBSA sample and a polyamine.

While the PIBSI products can be difficult to characterize, it might be possible to circumvent this problem by simulating the expected PIBSI products based on the f_{doubly} value determined from fluorescence experiments. In turn, the molecular weight distribution (MWD) of the expected PIBSI products could be used to predict the overall MWD of a PIBSI sample determined by GPC analysis. Based on these considerations, a series of coupling reactions between PIBSA and hexamethylene diamine (HMDA) were conducted with varying amine-to-succinic anhydride ratios ($N_{\text{Am}}/N_{\text{SA}}$) to produce a series of PIBSA-2-H samples whose MWD was characterized by GPC analysis of the DRI traces. Different reaction simulation programs were then applied to predict the MWD of the different PIBSI products generated by the coupling reactions conducted with different $N_{\text{Am}}/N_{\text{SA}}$ molar ratios. The simulated MWDs of the predicted PIBSI products were then transformed into a theoretical DRI trace which was then compared to the experimental DRI trace obtained for the PIBSI products. The best agreement between the simulated and experimental DRI traces was obtained by making the assumption that steric hindrance prevented the formation of high-order PIBSI constructs when they were prepared from HMDA. A complete description of the procedure is presented hereafter.

3.3 Experimental

Chemicals. Xylene (98.5%, Caledon Laboratory Chemicals), tetrahydrofuran (THF, 99%, Sigma-Aldrich or distilled in glass, 99.9%, Fisher Chemical), acetone (HPLC grade, Sigma-Aldrich), and hexamethylene diamine (HMDA, 98%, Sigma-Aldrich) were used without further purification. The PIBSA sample referred to as PIBSA-2 was supplied by Afton Chemical.

Fourier-Transform Infrared (FTIR). A Bruker Tensor 27 FTIR spectrometer was used to obtain the FTIR spectra of the polymer samples. Polymer films were prepared to acquire the FTIR spectra by depositing solutions of the polymer samples in $CHCl_3$ onto a NaCl FTIR cell and evaporating the solvent under N_2. The absorbance was then measured from 1000 to 2000 cm^{-1} and kept around 1.0 to optimize the signal-to-noise ratio.

Gel Permeation Chromatography (GPC). The MWD of the polymer samples was determined with a Viscotek GPC max VE 2001 instrument equipped with a triple-detector array and using THF as solvent. Polymer solutions were prepared with a concentration of 1 mg/mL using THF from the GPC reservoir. The solutions were filtered through 0.22 μm PTFE filters before injection.

The DRI traces were baseline corrected and could be fitted with a sum of Gaussians as a function of either elution volume (V_{el}) or degree of polymerization (X_n) using the programs *x*gauss where *x* equals *mono-, bi-, tri-, tetra-, penta-, or hexa-* to fit the DRI traces with a sum of 1 – 6 Gaussians according to Equation 3.1, respectively. This sum-of-Gaussians analysis yielded the scaling factor A and a_i, μ_i, and σ_i which represent the normalized pre-Gaussian factor, the average, and the standard deviation of the i^{th} Gaussian used to fit the data. The *x*gaussSNP program series (where *x = mono, bi,* and *tri*) was used to fit a DRI trace with Equation 3.2, divided into two sums of Gaussians. The parameters a_i, μ_i, and σ_i used in the first sum had been pre-determined from the

*x*gauss analysis of a DRI trace and were fixed in the analysis. The parameters a_j, μ_j, and σ_j used in the second sum were optimized in the analysis, along with the scaling factors *A* and *B*.

$$DRI(x) = A \times \sum_{i=1}^{n} a_i \frac{1}{\sigma\sqrt{2\pi}} exp\left(-\frac{(x-\mu)^2}{2\sigma^2}\right) \quad (3.1)$$

$$DRI(x) = A \times \sum_{i=1}^{n} a_i \frac{1}{\sigma_i\sqrt{2\pi}} exp\left(-\frac{(x-\mu_i)^2}{2{\sigma_i}^2}\right) + B \times \sum_{j=1}^{m} a_j \frac{1}{\sigma_j\sqrt{2\pi}} exp\left(-\frac{(x-\mu_j)^2}{2{\sigma_j}^2}\right) \quad (3.2)$$

In Equations 3.1 and 3.2, all pre-Gaussian and scaling factors were forced to remain positive in the analysis. All floating parameters were optimized according to the Marquardt-Levenberg algorithm for both the *x*gauss and *x*gaussSNP fitting programs.[16]

Simulations. The programs reaction3 and reaction4 were used to simulate the molar fractions of the PIBSA reactants and PIBSI products obtained at the end of a coupling reaction of a PIBSA sample and a given amount of diamine. The molecules in the coupling reaction mixture were divided into four categories. Category #1 represented the *N*1 molecules (*i*) that had only SA units and no amine ($n_{SA}(i) \neq 0$ and $n_{AM}(i) = 0$). Category #2 was for the *N*2 molecules (*j*) bearing both SA and amines available for reaction ($n_{SA}(j) \neq 0$ and $n_{AM}(j) \neq 0$). Category #3 included the *N*3 molecules (*k*) that bore no SA unit and had amines ($n_{SA}(k) = 0$ and $n_{AM}(k) \neq 0$). The products constituted Category #4 where the *N*4 molecules (*m*) were without SA or amine available for reaction ($n_{SA}(m) = 0$ and $n_{AM}(m) = 0$). Each molecule was also assigned a number (n_{PIB}) of PIB segments. At the start of the simulation, *N*1 equalled the number of $PIBSA_1$ or $PIBSA_2$ molecules having $n_{SA}(i) = 1$ or 2, respectively, where the number of $PIBSA_2$ molecules was based off the value of f_{doubly} determined by fluorescence measurements in Chapter 2. *N*2 equaled zero as no coupling had occurred. The number of diamine molecules *N*3 was determined from the experimental N_{Am}/N_{SA} ratio used for the coupling reaction. Of course, there was no product at the

beginning of the reaction and $N4$ equalled zero. As the reaction proceeded, a molecule (x) from the $N1 + N2$ species was selected randomly for its SA group and it was removed from the pool of $N1$ or $N2$ molecules and $N1$ or $N2$ turned into $N1 - 1$ or $N2 - 1$, respectively. Similarly, another molecule (y) was selected randomly for its amine from the $N2 + N3$ molecules and it was removed from the pool of $N2$ or $N3$ molecules and $N2$ or $N3$ turned into $N2 - 1$ or $N3 - 1$, respectively. The reaction took place by generating a molecule (z) with a number of SA units $n_{SA}(z) = n_{SA}(x) + n_{SA}(y) - 1$, a number of amines $n_{AM}(z) = n_{AM}(x) + n_{AM}(y) - 1$, and a number of PIB segments $n_{PIB}(z) = n_{PIB}(x) + n_{PIB}(y)$. Depending on the value of $n_{SA}(z)$ and $n_{AM}(z)$, the z molecule would be added to Category # 1 – 4 and the $N1$, $N2$, $N3$, and $N4$ values were updated accordingly. The reaction was continued until $N1 + N2$ or $N2 + N3$ would equal zero.

Two programs were implemented based on this concept. The program reaction3 simulated the coupling of PIBSA with a diamine by reacting SAs and amines at random, and output the number of unreacted PIBSAs, *m*-, *b*-, *tri*-, and *tet*-PIBSIs, and mono- and diamines after coupling had consumed all available amines or all available succinic anhydrides from the starting materials. This simulation provided the molar fractions of PIBSAs/*m*-PIBSIs, *b*-PIBSIs, *tri*-PIBSIs, *tet*-PIBSIs … after coupling a PIBSA sample with HMDA, which could be used with their corresponding MWDs to simulate the DRI traces obtained from the products of a given PIBSA coupling reaction.

The program reaction4 worked similarly to reaction3 but assumed that steric hindrance prevented the reaction of a doubly modified $PIBSA_2$ with more than one other PIBSA molecule (either $PIBSA_1$ or $PIBSA_2$), essentially limiting the PIBSI products to contain only *m*- and *b*-PIBSI species. In order to use the molar fractions obtained with the programs reaction3 and reaction4 to simulate the DRI traces expected from a reaction between a PIBSA sample and a given number of

diamines, the MWDs of the *b*-PIBSI and other higher-order PIBSI products needed to be determined.

The MWD of higher-order PIBSI oligomers was obtained with the prod-dis2 coupling program. The program works by taking the MWD of the unimer, namely PIBSA, given by the probability $P_1(i)$ of having a degree of polymerization i of the unimer obtained from the GPC analysis of the PIBSA sample. The probability $P\mathrm{x}(i)$ of a higher-order (X) PIBSI product can then be obtained by applying Equation 3.3, where the probability $P_{\mathrm{X\text{-}1}}(i)$ represents the MWD of the X-1 order PIBSI product. For example, coupling the MWD ($P_1(i)$) of PIBSA with itself yields the MWD ($P_2(i)$) of *b*-PIBSI, coupling the MWDs of ($P_1(i)$) PIBSA and ($P_2(i)$) *b*-PIBSI yields the MWD ($P_3(i)$) of *tri*-PIBSI, etc.

$$P_{\mathrm{X}}(i) = \sum_{k=1}^{i} P_1(k) \times P_{\mathrm{X\text{-}1}}(i+1-k) \tag{3.3}$$

The function $P_1(i)$ needed to be extracted from the GPC data obtained with the PIBSA sample. This task was not straightforward as the low molecular weight PIBSA did not scatter enough to use the light scattering detector of the GPC instrument to determine its absolute MWD, and short PIB standards with narrow MWD were not available to generate a calibration curve. The procedure applied for GPC to calibration with the DRI detector is described in the following section.

Calibration of the GPC instrument with polydisperse PIB standards. A calibration curve was established by using the fairly polydisperse PIB standards **1**, **2**, and **3** from Polymer Source whose M_{n} and M_{w} values were listed in Table 3.1. Assuming that the calibration curve could be approximated by the polynomial of degree n shown in Equation 3.4, M_{n} and M_{w} could then be expressed in Equations 3.5 and 3.6 as a function of the polynomial constants b_{i} from Equation 3.4 and the DRI(V_{el}) trace showing the DRI signal of the PIB standards as a function of elution volume

(V_{el}) obtained from GPC analysis. A second order polynomial (n = 2 in Equation 3.4) was deemed satisfactory for the calibration curve. The program cal-2 was then used to optimize the pre-factors b_i in Equation 3.4 with the Marquardt-Levenberg algorithm to obtain the target M_n and M_w values of the three PIB standards based on their DRI(V_{el}) traces and Equations 3.5 and 3.6.

$$Ln(M) = \sum_{i=0}^{n} b_i V_{el}^i \tag{3.4}$$

$$M_n = \frac{\int_o^\infty DRI(V_{el})\,dV_{el}}{\int_o^\infty DRI(V_{el}) \exp(-\sum_{i=0}^{n} b_i V_{el}^i)\,dV_{el}} \tag{3.5}$$

$$M_w = \frac{\int_0^\infty DRI(V_{el}) \exp(\sum_{i=0}^{n} b_i V_{el}^i)\,dV_{el}}{\int_0^\infty DRI(V_{el})\,dV_{el}} \tag{3.6}$$

Table 3.1. M_n and M_w values of the PIB standards used for the GPC calibration and determined using the calibration curve from cal-2.

	Known		**From calibration curve**	
PIB standards	M_n (kg/mol)	M_w (kg/mol)	M_n (kg/mol)	M_w (kg/mol)
1	1.0	1.5	1.2	2.4
2	3.2	5.0	2.9	5.3
3	6.0	7.8	5.6	7.7

Unlike the standard GPC calibration method using standards with narrow MWDs, the program cal-2 takes the baseline-corrected DRI traces of the PIB standards having broad MWDs and optimizes the b_i parameters in Equation 3.4 to yield M_n and M_w that would be as close as possible to those of the PIB standards **1**, **2**, and **3**. The known M_n and M_w values in Table 3.1 are seen to agree fairly well with those determined using the calibration curve from cal-2 (see Equation

B1 in Appendix B), albeit with a larger deviation for the M_w values of 1.5 and 2.4 for PIB standard **1**. The probability $P_1(i)$ of having a degree of polymerization i for the PIBSA unimer in Equation 3.3 could then be approximated by Equation 3.7, where the function $DRI_{PIBSA}(V_{el})$ corresponds to the GPC trace obtained for the PIBSA sample with the DRI detector.

$$P_1(i) = \frac{1}{\int_0^{\infty} DRI_{\text{PIBSA}}(V_{el}) \exp(\sum_{i=0}^{n} a_i V_{el}^i) dV_{el}} \times \frac{DRI_{\text{PIBSA}}(V_{el})}{\exp\left(2 \times \sum_{i=0}^{n} a_i V_{el}^i\right) \times \sum_{i=1}^{n} i a_i V_{el}^{i-1}} \tag{3.7}$$

The function $P_1(i)$ could then be used with the program prod-dis2 to simulate the MWDs of the *b*-PIBSI, *tri*-PIBSI, and *tet*-PIBSI. First the *m*-PIBSA was coupled to itself to yield $P_2(i)$ for *b*-PIBSI, then *m*-PIBSA was coupled to *b*-PIBSI to yield $P_3(i)$ for *tri*-PIBSI, and *m*-PIBSA was coupled to *tri*-PIBSI to yield $P_4(i)$ *tet*-PIBSI. It is worth noting that $P_4(i)$ for *tet*-PIBSI could also be obtained by combining two $P_2(i)$ functions of *b*-PIBSI and that it was identical to the $P_4(i)$ function obtained from combining $P_1(i)$ for PIBSA and $P_3(i)$ for *tri*-PIBSI, as expected. These MWDs were then converted back into weight fractions ($w_i(V_{el})$) with the GPC calibration curve to simulate the DRI traces expected from different PIBSI oligomers, the molar fractions of which were predicted with the programs reaction3 and reaction4.

Synthesis of PIBSA-2-HMDA samples (PIBSA-2-H). The PIBSA-2 sample received from Afton Chemical was reacted with varying amounts of HMDA to form *m*-PIBSI, *b*-PIBSI, and possibly other higher-order PIBSI products enabled by the presence of $PIBSA_2$, according to Scheme 3.2. The N_{Am}/N_{SA} ratio was varied from 0.25 to 2.0 to study how this ratio would affect the proportions of reactants and products generated during the coupling reactions. The proportion of PIBSA should decrease when the N_{Am}/N_{SA} ratio increases from 0.25 to 1.0, as more amine is provided for coupling

of the PIBSAs into *b*-PIBSIs, while the proportion of *m*-PIBSI should increase when the N_{Am}/N_{SA} ratio increases from 1.0 to 2.0, as PIBSAs are 'capped' by the excess amines, resulting in more *m*-PIBSIs bearing a free amine. The reaction with an N_{Am}/N_{SA} ratio of 0.5 is explained in more detail as an example.

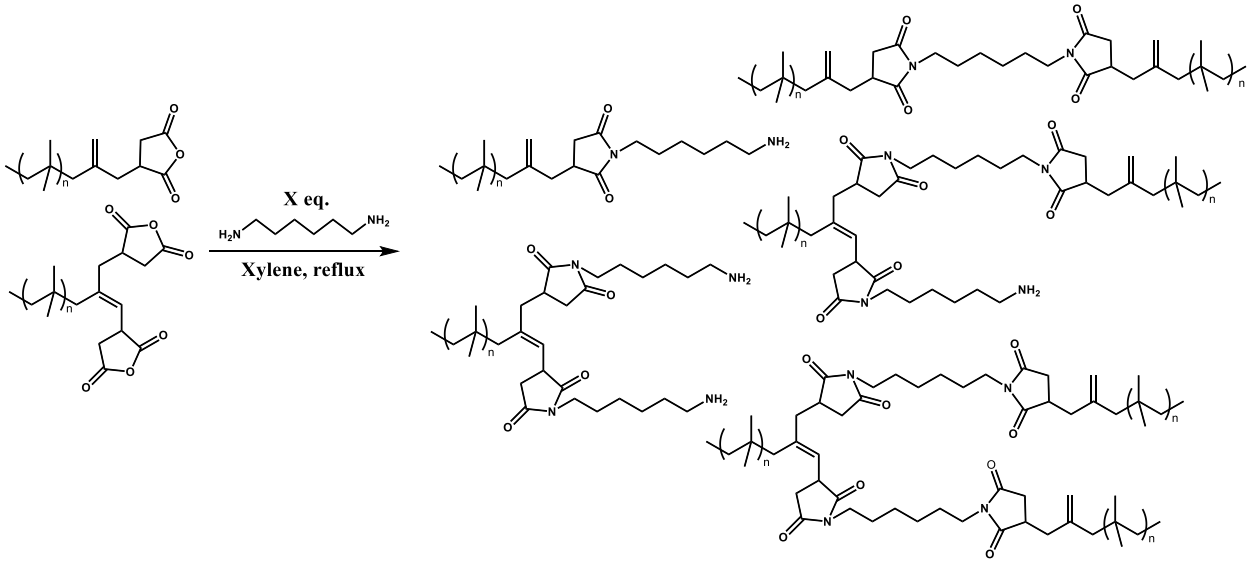

Scheme 3.2. Synthesis of PIBSI-HMDA.

PIBSA-2 was dissolved in THF and precipitated with acetone to remove low molecular weight impurities along with the low molecular weight fraction of the MWD. The mixture was then decanted and PIBSA-2 dried overnight under vacuum at 70 °C. PIBSA-2 (0.93 g) was dissolved in 20 mL of hot xylene and the hot PIBSA solution was added to a 100 mL round bottom flask (RBF) which was connected to a Dean-Stark condenser and kept under nitrogen. The solution was refluxed overnight in an oil bath at 175 °C to dehydrate the partially-hydrated PIBSA-2 sample and regenerate succinic anhydride from the succinic acid groups. An aliquot was taken the next day to acquire an FTIR spectrum (see Spectrum A in Figure 3.2), to confirm dehydration of the PIBSA via disappearance of the absorbance peak at 1710 cm^{-1}, characteristic of the succinic acid carbonyl.

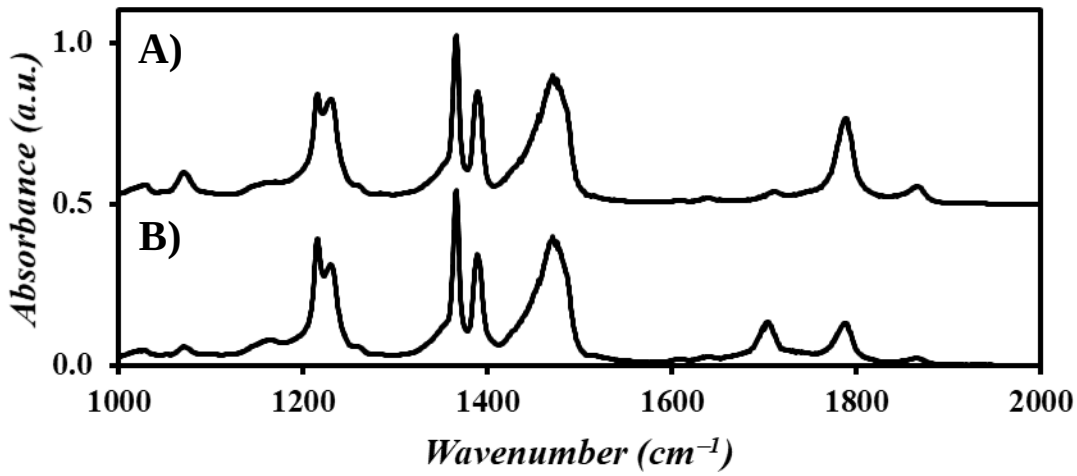

Figure 3.2. FTIR spectra of precipitated PIBSA-2: A) Dehydrated and B) after HMDA coupling using an N_{Am}/N_{SA} ratio of 0.5.

The succinic anhydride content (λ_{SA}) of the PIBSA sample, which is the number of moles of succinic anhydride per gram of PIBSA, can be calculated with Equations 3.8 and 3.9.[13]

$$\frac{N_{SA}}{N_{IB}} = 0.024 \times \frac{Abs(1785\,cm^{-1})}{Abs(1390\,cm^{-1})} \tag{3.8}$$

$$\lambda_{SA} = \left(M_{SA} + \left({}^{N_{SA}}/_{N_{IB}} \right)^{-1} \times M_{IB} \right)^{-1} \tag{3.9}$$

Equation 3.8 yields the number of succinic anhydrides per isobutylene unit in the PIBSA sample using the ratio of the absorbance at 1785 cm^{-1} for the succinic anhydride carbonyl over that at 1390 cm^{-1} for the methyl swinging motions in the PIBSA backbone. Equation 3.9 yields the number of moles of succinic anhydride per gram of PIBSA. M_{SA} and M_{IB} in Equation 3.9 represent the molar mass of the succinic anhydride (99 g/mol) and isobutylene monomer (56 g/mol), respectively. Application of Equations 3.8 and 3.9 yielded a λ_{SA} value of 0.315 mmol/g for this precipitated, and thus fractionated, PIBSA-2 sample, which was used to calculate the appropriate

amount of HMDA to add to the reaction according to the N_{Am}/N_{SA} ratio of interest, in this case 0.5. HMDA (8.7 mg, 0.075 mmol) was dissolved in 20 mL of hot xylene and added to the dehydrated PIBSA-2 sample to react overnight at reflux. The next morning an aliquot was taken from the reaction mixture to acquire an FTIR spectrum, shown as Spectrum B in Figure 3.2. The FTIR spectrum confirmed the completion of the reaction from the presence of the imide absorption band at 1705 cm^{-1}. The spectrum also lacked the strong amide absorption at 1650 cm^{-1}, which would have indicated incomplete cyclization of the succinamic acids into succinimides, as observed in the labeling of PIBSA-2 with 1-pyrenemethylamine in Chapter 2. Dodecane was used in Chapter 2 to increase the reaction temperature and complete the imide formation, eliminating the amide absorption band at 1650 cm^{-1}. The HMDA coupling reaction product lacked an amide absorption and displayed intense imide and anhydride absorptions, without the need for higher temperatures afforded by using dodecane as solvent. This result could be due to the increased nucleophilic character of the amines connected to an electron-donating alkyl chain in HMDA as compared to amines connected to the electron-withdrawing pyrene group in 1-pyrenemethylamine. Since the N_{Am}/N_{SA} ratio was below 1, the final product would include both succinimide and succinic anhydride groups as there are not enough amines to react with each succinic anhydride group, as is seen from the succinimide and succinic anhydride absorption bands in Spectrum B in Figure 3.2. After the reaction was complete, the reaction mixture was condensed and dissolved in THF before being transferred to a 20 mL vial. The THF was evaporated under a flow of nitrogen before the polymer product was dried to completion in a vacuum oven at 70 °C overnight to yield the PIBSA-2-H-0.5 sample. After being removed from the vacuum oven, the PIBSA-2-H-0.5 sample was dissolved in THF for GPC analysis, the results of which are discussed in the following section.

PIBSA-2-H samples were prepared for N_{Am}/N_{SA} ratios ranging from 0.25 to 2.0 in increments of 0.25, and the different samples were characterized by FTIR and GPC in an identical manner.

3.4 Results and Discussion

The coupling of PIBSA with varying amine equivalents to generate higher-ordered PIBSIs has already been studied to determine the optimal amine-to-PIBSA molar ratio to produce *b*-PIBSI dispersants.[15] However, the complication of having doubly modified PIBSA molecules ($PIBSA_2$) was not considered in this earlier study. Since the presence of $PIBSA_2$ complicates the prediction of the nature of the PIBSI products obtained from the coupling reaction between PIBSA and polyamines, it was theorized that the population of PIBSI products resulting from the reaction of a PIBSA sample and a polyamine could be determined quantitatively by applying the following procedure. First, the molar fraction (f_{doubly}) of bi- ($PIBSA_2$) substituted PIBSA molecules in a given PIBSA sample was determined by conducting the pyrene excimer fluorescence (PEF) experiments described in Chapter 2 on a PIBSA sample that had been reacted with 1-pyrenemethylamine. Second, the SA content of the PIBSA sample was determined by FTIR measurements according to Equations 3.8 and 3.9. Third, the population of PIBSI products obtained during the coupling reaction between a given number of SA and amine groups could be predicted by simulation. Fourth, the MWD of the higher order PIBSI products could be predicted by mathematically coupling the MWDs of lower order PIBSI products as described in Equation 3.3. Fifth, the MWD of the PIBSA reactant and PIBSI products in a given reaction mixture could be estimated from the MWD of the individual PIBSA and PIBSI constituents of the overall population as predicted by simulation, and it could be compared with the MWD experimentally determined by GPC analysis of the reactants and products obtained in a given coupling reaction. Good agreement in the fifth

step of the procedure validates the assumptions made to conduct the coupling reaction *in silico* and suggests that the same assumptions rule the reaction of a PIBSA sample with a polyamine. How this procedure was implemented is described hereafter.

Fourier-Transform Infrared (FTIR). FTIR spectroscopy was used to monitor the coupling of PIBSA with HMDA at different N_{Am}/N_{SA} ratios, by monitoring the absorption bands of the succinic anhydride and succinimide groups. The FTIR spectra of the PIBSA-2-H(*X*) coupling products, where *X* is the N_{Am}/N_{SA} ratio applied in a given coupling reaction, are shown in Figure 3.3. The FTIR spectra in Figure 3.3 shared most of the same features, notably the characteristic PIB peaks from the methyl swinging motions at 1365 and 1390 cm^{-1} and methylene bending and scissoring peaks at 1225 and 1465 cm^{-1}, respectively.[13] The PIBSA-2-H(2) sample had a small amide peak at 1650 cm^{-1} which was not as prevalent in the other samples with lower N_{Am}/N_{SA} ratios, possibly due to its increased amine content as compared to the other samples.

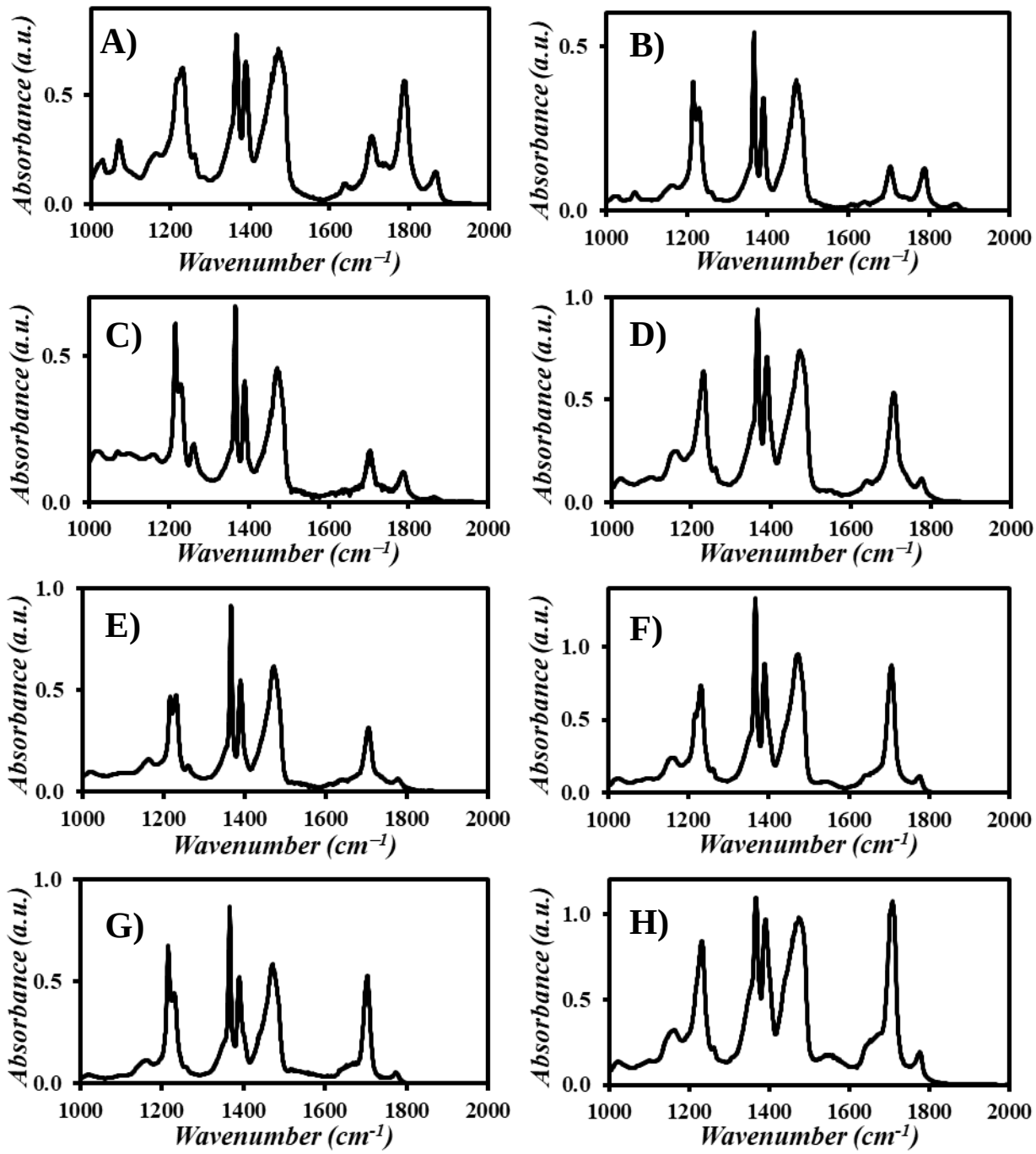

Figure 3.3. FTIR spectra of the PIBSA-2-H(*X*) products obtained with N_{Am}/N_{SA} ratios of A) 0.25, B) 0.5, C) 0.75, D) 1.0, E) 1.25, F) 1.5, G) 1.75, and H) 2.0.

While H-bonding has been shown in previous work to distort the FTIR spectra of PIBSIs,[15] some interesting comparisons can be made when looking at the range of N_{Am}/N_{SA} ratios studied. The absorbance of the succinic anhydride carbonyl at 1785 cm^{-1} decreased with respect to that of the PIB bands for increasing N_{Am}/N_{SA} ratios as expected, while the anhydride absorbance was practically absent for reactions with an N_{Am}/N_{SA} ratio greater than 1. The succinimide absorbance at 1705 cm^{-1} was weak for the PIBSA-2-H(0.25) product, and increased relatively to that of the PIB bands for increasing N_{Am}/N_{SA} ratios as expected. A quantitative comparison of the succinic anhydride and succinimide absorbances against the PIB absorption band at 1390 cm^{-1} is shown in Figure 3.4.

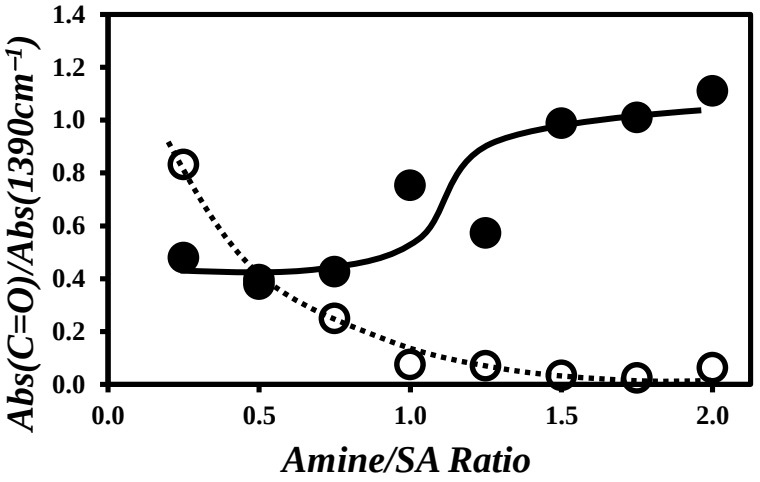

Figure 3.4. Plot of the ratios (○) Abs(1785 cm^{-1})/Abs(1390 cm^{-1}) and (●) Abs(1705 cm^{-1})/Abs(1390 cm^{-1}) for the PIBSA-2-H(*X*) reaction products.

The trends in Figure 3.4 showed that the absorbance of the succinic anhydride carbonyl decreased sharply for increasing N_{Am}/N_{SA} ratios from 0.25 to 1.0 and was relatively constant and close to nil for N_{Am}/N_{SA} ratios between 1.0 and 2.0. The non-zero values of the SA carbonyl absorbance observed for N_{Am}/N_{SA} ratios greater than 1 could be due to the weak secondary

absorption band of the succinimide at 1775 cm^{-1}, which increased in intensity for increasing N_{Am}/N_{SA} ratios. The absorbance of the succinimide carbonyl increased sharply for N_{Am}/N_{SA} ratios above 1, as more amine was available for conversion of the succinic anhydrides into succinimides. All in all, the FTIR spectra showed that the coupling reactions between PIBSA and HMDA were efficient and that the IR absorbance of the succinimide and succinic anhydride carbonyls followed the expected trends.

Gel Permeation Chromatography (GPC). The lack of monodisperse PIB standards for GPC prevented the determination of the MWD of the different PIBSA and PIBSI species by conventional calibration. A calibration curve was established for the GPC instrument with three polydisperse PIB standards as described in the Experimental section. The *x*gauss and *x*gaussSNP fitting programs were used to fit the DRI traces obtained for the PIBSA-2-H(*X*) samples by GPC with sums of Gaussians, thus providing a mathematical representation of the DRI traces that could be more easily processed later on.

The DRI trace for the dehydrated PIBSA-2 sample was first fitted with a sum of 4 gaussians using the tetragauss program, to eliminate the solvent peaks from the DRI profile. The experimental DRI trace and gaussian fit of the data are shown in Figure 3.5. The sum of four Gaussians used to represent the DRI profile of the PIBSA-2 sample could then be fixed in the analysis of the DRI traces conducted with the *x*gaussSNP programs to determine the contribution of the PIBSI products whose MWD was different from that of PIBSA.

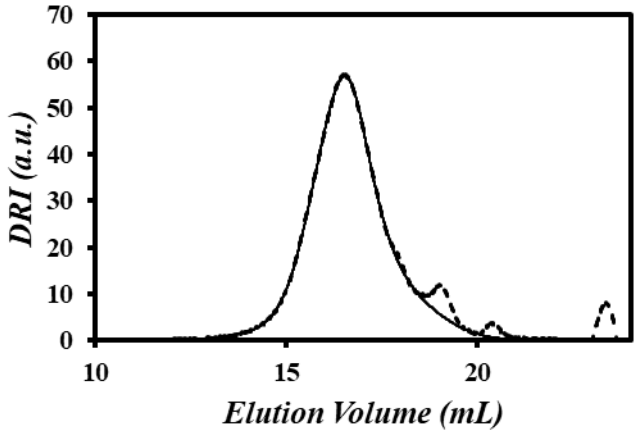

Figure 3.5. Plot of the (- - -) DRI trace and (──) gaussian fit of a dehydrated PIBSA-2 sample as a function of elution volume. The contribution of the solvent peaks at 19, 20, and 24 mL were eliminated from the calculation.

The sum of Gaussians used to represent the PIBSA trace in Figure 3.5 was then fixed in the analysis with the monogaussSNP, bigaussSNP, and trigaussSNP programs used to simulate the DRI traces of the PIBSA-2-H(*X*) samples for each N_{Am}/N_{SA} ratio. These programs used a sum of one, two, and three additional Gaussians, respectively, on top of the sum of four Gaussians used to represent the PIBSA contribution to the DRI traces. The aim was to use the smallest number of Gaussians to properly fit the DRI trace of each PIBSA-2-H(*X*) sample and assess the contribution of the PIBSA (or *m*-PIBSI) samples in the DRI traces. The DRI traces were fitted first with the monogaussSNP program and the quality of the fit of the experimental DRI trace was assessed by reviewing the sum of squared differences between the experimental DRI trace and the *x*gaussSNP fit, which represented the error on the fit. If the fit was poor, the next xgaussSNP program using an additional Gaussian, in this case bigaussSNP, was used to fit the DRI trace, and this process was repeated until good agreement was obtained between the experimental DRI trace and the fit with a sum of Gaussians. For example, the PIBSA-2-H(0.25) sample was first fitted with

monogaussSNP, yielding an error value of 775. The error values obtained using bigaussSNP and trigaussSNP with the experimental DRI trace of the PIBSA-2-H(0.25) sample were 68 and 50, respectively, which showed that the bigaussSNP gave a much better quality of fit than monogaussSNP, and that the two additional Gaussians from bigaussSNP were sufficient for a good fit, as there was little change in the error value using a third Gaussian. This was also confirmed by visual inspection of the fit in Figure 3.6A. In the end, the DRI trace of the PIBSA-2-H(0.25) sample could be properly fitted with a sum of two additional Gaussians with bigaussSNP, while the PIBSA-2-H(*X*) samples with N_{Am}/N_{SA} ratios ranging from 0.5 to 2.0 required three additional Gaussians with trigaussSNP for a good fit. The DRI traces overlaid with their fits with sums of Gaussians are shown in Figure 3.6 for each PIBSA-2-H(*X*) sample. The parameters retrieved from these fits with sums of Gaussians are listed in Tables B1 and B2 in Appendix B.

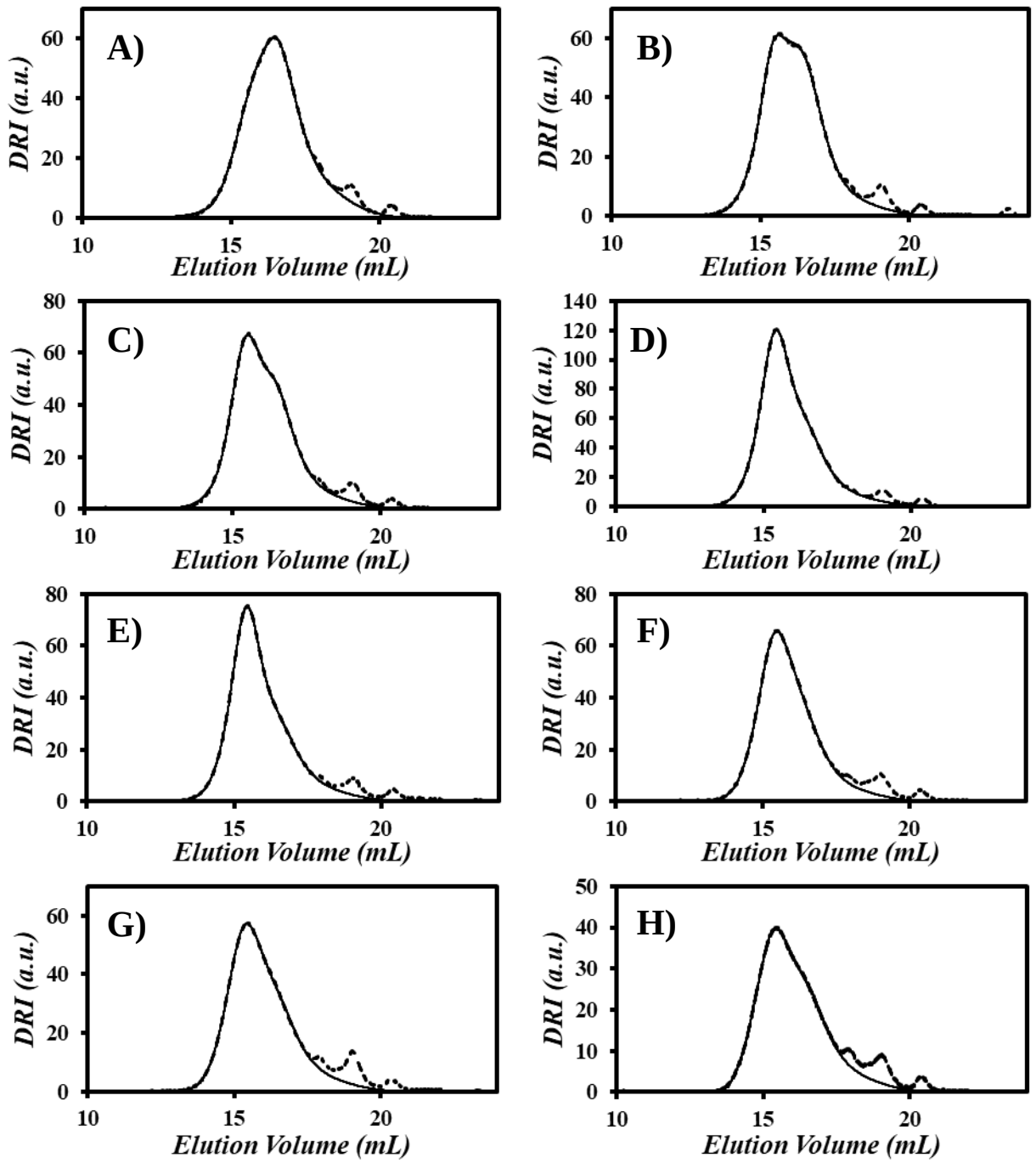

Figure 3.6. Experimental DRI traces (- - -) from GPC analysis of the PIBSA-2-H(*X*) products and their fit with a sum of Gaussians (——) obtained for N_{Am}/N_{SA} ratios of A) 0.25, B) 0.5, C) 0.75, D) 1.0, E) 1.25, F) 1.5, G) 1.75, and H) 2.0.

Since the fits of the DRI traces with a sum of Gaussians in Figure 3.6 gave a good representation of the PIBSA/PIBSI species without the solvent peaks in the PIBSA-2-H(*X*) samples, they were used in all further comparisons of the experimentally obtained DRI traces. An example of the traces obtained by fitting the PIBSA-2-H(1.0) DRI trace with trigaussSNP and the comparison of the fits with sums of Gaussians of the PIBSA-2-H(*X*) samples having N_{Am}/N_{SA} ratios ranging from 0.25 to 1.0 and from 1.0 to 2.0 are shown in Figure 3.7A, B, and C, respectively. In these analyses, PIBSA and *m*-PIBSI are assumed to have a same MWD and both molecules are referred to as PIBSA-like molecules (PLMs).

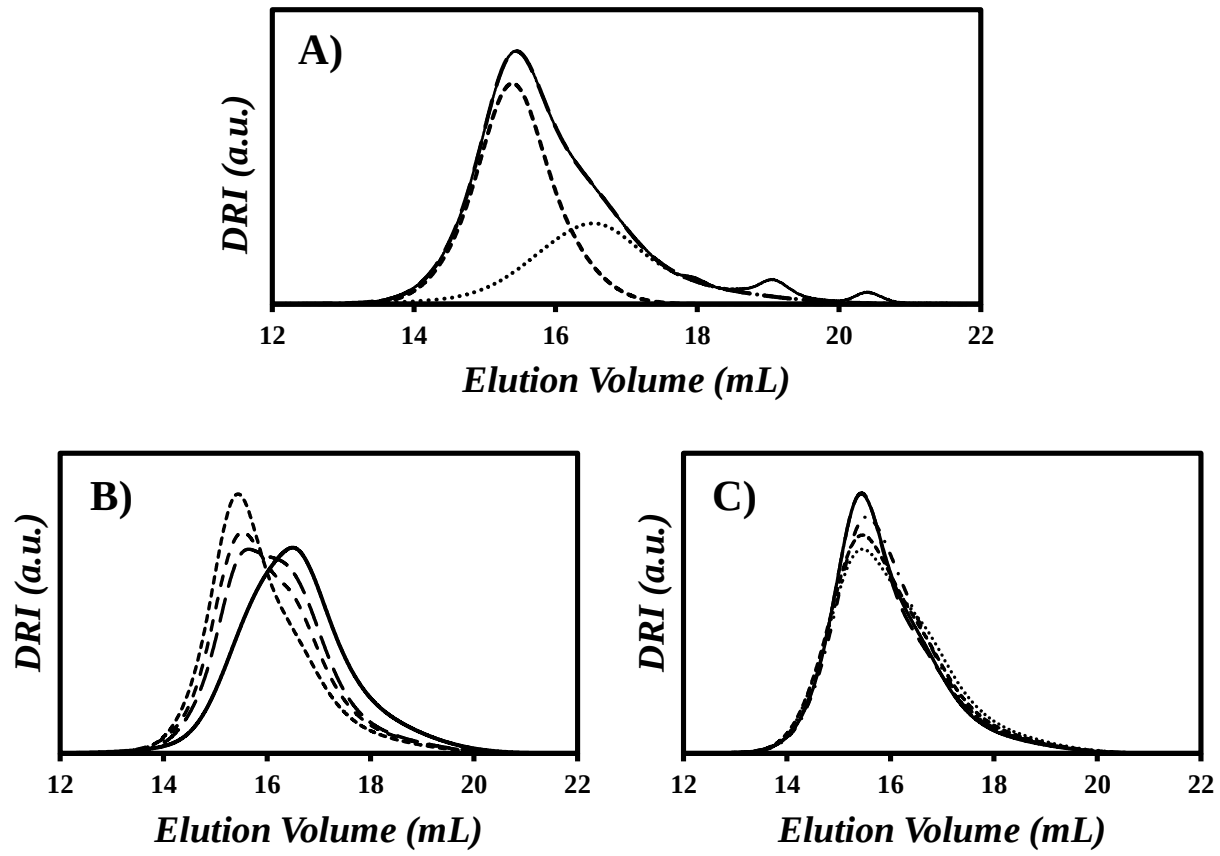

Figure 3.7. A) An example of the quality of the (– – –) fit with a sum of Gaussians of (———) the DRI trace of PIBSA-2-H(1.0), (·····) the contribution from PIBSA-like molecules, and (– – – –) the contribution from non-PIBSA like molecules. Fits with sums of Gaussians for the PIBSA-2-H(*X*) samples with N_{Am}/N_{SA} ratios of B) (———) 0.25, (– – – –) 0.5, (– – –) 0.75, and (·····) 1.0, and C) (———) 1.0, (– · –) 1.25, (– – –) 1.5, (– – – –) 1.75, and (·····) 2.0, normalized to a sum of 1.

The traces in Figure 3.7A show the trigaussSNP fit which combines the DRI trace of the PIBSA-2 sample which was fixed in the analysis with an additional sum of three Gaussians to yield the final fit with the respective contributions of the PLMs and non-PLMs to the PIBSA-2-H(1.0) sample. The comparison of the traces in Figure 3.7B and C revealed some interesting trends

for the PIBSA-2-H(*X*) products. The MWD shifted to lower elution volumes when the N_{Am}/N_{SA} ratio increased from 0.25 to 1.0 in Figure 3.7B, as would be expected if more diamines were added to favor the coupling to two PIBSAs into one *b*-PIBSI. It was also noticeable that a substantial contribution from PLMs was found in the DRI trace of the PIBSA-2-H(1.0) sample, which should have favored coupling of all PIBSA species into higher-ordered PIBSIs with the nominal number of diamines available. Similarly, a non-negligible contribution from PLMs was found in the DRI traces in Figure 3.7C, whose contribution increased when the N_{Am}/N_{SA} ratio increased from 1.0 to 2.0, although to a much lesser extent than the decrease in the contribution from PLMs seen for the N_{Am}/N_{SA} ratios between 0.25 and 1.0. This result showed that having an N_{Am}/N_{SA} ratio above 1.0 did not mean that the coupling reaction would necessarily favor the formation of *m*-PIBSI over that of *b*-PIBSI or higher-ordered PIBSIs. The high MW region of the DRI traces in Figure 3.7C appeared to have roughly the same front in the low V_{el} region and peak maximum, inferring that the same higher-ordered PIBSI products were generated at N_{Am}/N_{SA} ratios ≥ 1. To further examine this conclusion, the contribution of the non-PLMs in the DRI traces, determined by fitting the DRI traces of the PIBSA-2-H(*X*) samples with the *x*gaussSNP programs, were overlaid in Figure 3.8A and B for N_{Am}/N_{SA} ratios between 0.25 and 1.0 and between 1.0 and 2.0, respectively. It must be reiterated at this point that PIBSA and *m*-PIBSI were assumed to share a same MWD and DRI trace in this analysis, and they are referred to as PIBSA-like molecules (PLMs) in the remainder of this chapter.

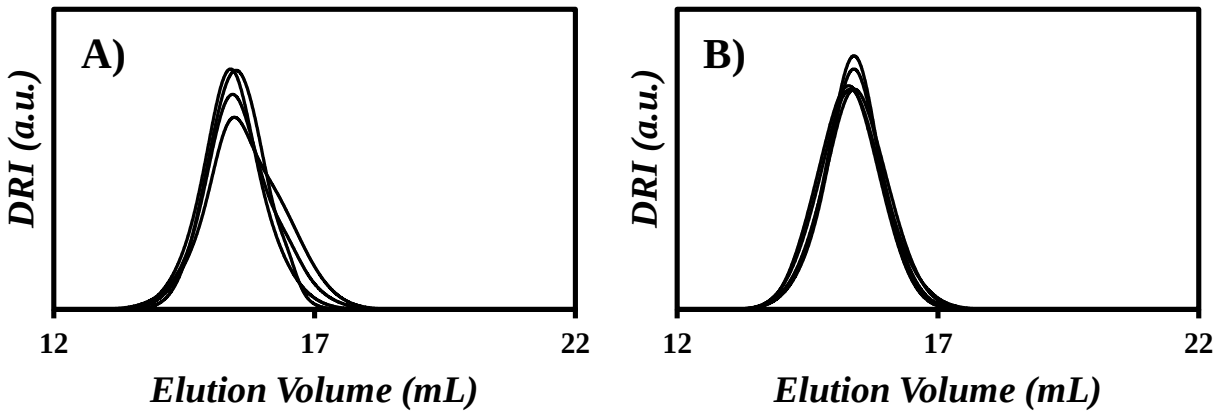

Figure 3.8. Overlaid DRI contribution of the non-PIBSA fractions of the PIBSA-2-H(*X*) samples with N_{Am}/N_{SA} ratios of A) 0.25, 0.5, 0.75, and 1.0, and B) 1.0, 1.25, 1.5, 1.75, and 2.0, normalized to a sum of 1.

The traces in Figure 3.8B showed that the non-PLMs in the PIBSA-2-H(*X*) samples had roughly the same MWD for all N_{Am}/N_{SA} ratios ≥ 1, inferring that the coupling reaction must be producing the same higher-order PIBSI products regardless of the N_{Am}/N_{SA} ratio. The non-PIBSA contribution in the DRI traces for the N_{Am}/N_{SA} ratios of 0.5 and 0.75 shown in Figure 3.8A all had a shoulder in the low MW region of the MWDs, where PIBSA is expected to elute. This observation would imply that the fraction of PLMs in these samples was underestimated, even more so for the PIBSA-2-H(0.5) sample, which had a larger shoulder.

The main conclusion from such an analysis would be that the DRI traces could be decomposed into just two contributions, one contribution from PLMs, referring to PIBSA or *m*-PIBSI which would be indistinguishable, and another contribution from a same higher-order PIBSI product assigned to *b*-PIBSI. To elaborate further on this proposal, the DRI traces obtained from the *x*gaussSNP fits were fitted with a linear regression assuming that they were the sum of two contributions, one from PLMs and the other from the non-PLMs portion of the PIBSA-2-H(1.0)

sample. A comparison of the weight fractions (*wt-f*) of the PLM contribution obtained by applying a sum of Gaussians fit or a linear regression to the DRI traces of the PIBSA-2-H(X) samples are shown in Figure 3.9. When plotted against the N_{Am}/N_{SA} ratio in Figure 3.9, the weight fractions of PLMs in the PIBSA-2-H(*X*) samples compared fairly well regardless of the fitting method.

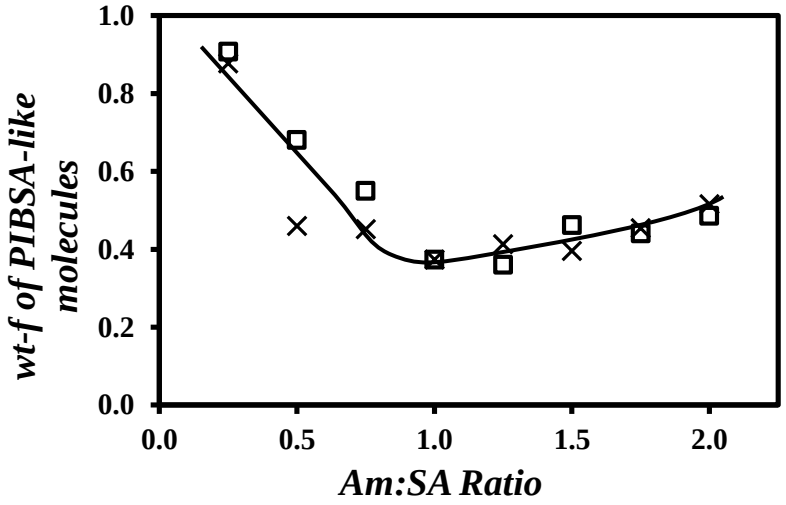

Figure 3.9. Plots of the weight fraction (*wt-f*) of PIBSA-like molecules in the PIBSA-2-H(*X*) samples determined by fitting the DRI traces with (×) *x*gaussSNP and a (□) linear regression.

Review of Figure 3.9 indicated that the weight fractions showed more scatter when they were determined with the *x*gaussSNP programs than with the linear regression. This was probably a consequence of the larger number of degrees of freedom available when fitting the DRI traces with a sum of Gaussians with three floating parameters (a_i, μ_i and σ_i in Equations 3.1 and 3.2) for each Gaussian, versus just two pre-Gaussian factors when applying the linear regression. The weight fractions obtained from the fits based on a linear regression showed a steady decrease when the N_{Am}/N_{SA} ratio increased from 0.25 to 1.0, before increasing slightly when the N_{Am}/N_{SA} ratio increased from 1.0 to 2.0. It was also interesting to note that the weight fraction of the PLMs never went below 36 wt% for any N_{Am}/N_{SA} ratio by either fitting method. This was a strange result at

first glance, as an N_{Am}/N_{SA} ratio should exist where all available PIBSA molecules should be coupled to form *b*-PIBSI or higher-ordered PIBSI products. This discrepancy suggested that the PIBSA-2 sample might contain a portion of unmodified PIB which had not been successfully maleated. The unmodified PIB would then appear as PLMs in the DRI traces, as it would not be able to form *b*-PIBSI during the coupling reaction. This development will be discussed in the next section.

The DRI traces obtained by applying a linear regression with one contribution from PLMs and another from the non-PLM portion of the DRI trace obtained with the PIBSA-2-H(1.0) sample were compared in Figure 3.10. While there were some slight deviations from the experimental data near the peak maxima as in Figures 3.10B and H, the regression fits gave a fairly good representation of the DRI traces of each PIBSA-2-H(*X*) sample. The good agreement between the experimental and fitted DRI traces using two set contributions supported the earlier suggestion that the coupling reaction between PIBSA and HMDA might be producing the same higher-order PIBSI product regardless of the N_{Am}/N_{SA} ratio applied. The good agreement between the results obtained from the fit of the DRI traces with a linear regression or the *x*gaussSNP programs suggested that the proposed analysis could successfully characterize the products of the PIBSA-HMDA coupling reactions based only on a GPC instrument with a DRI detector and the Gaussian fitting programs developed in house.

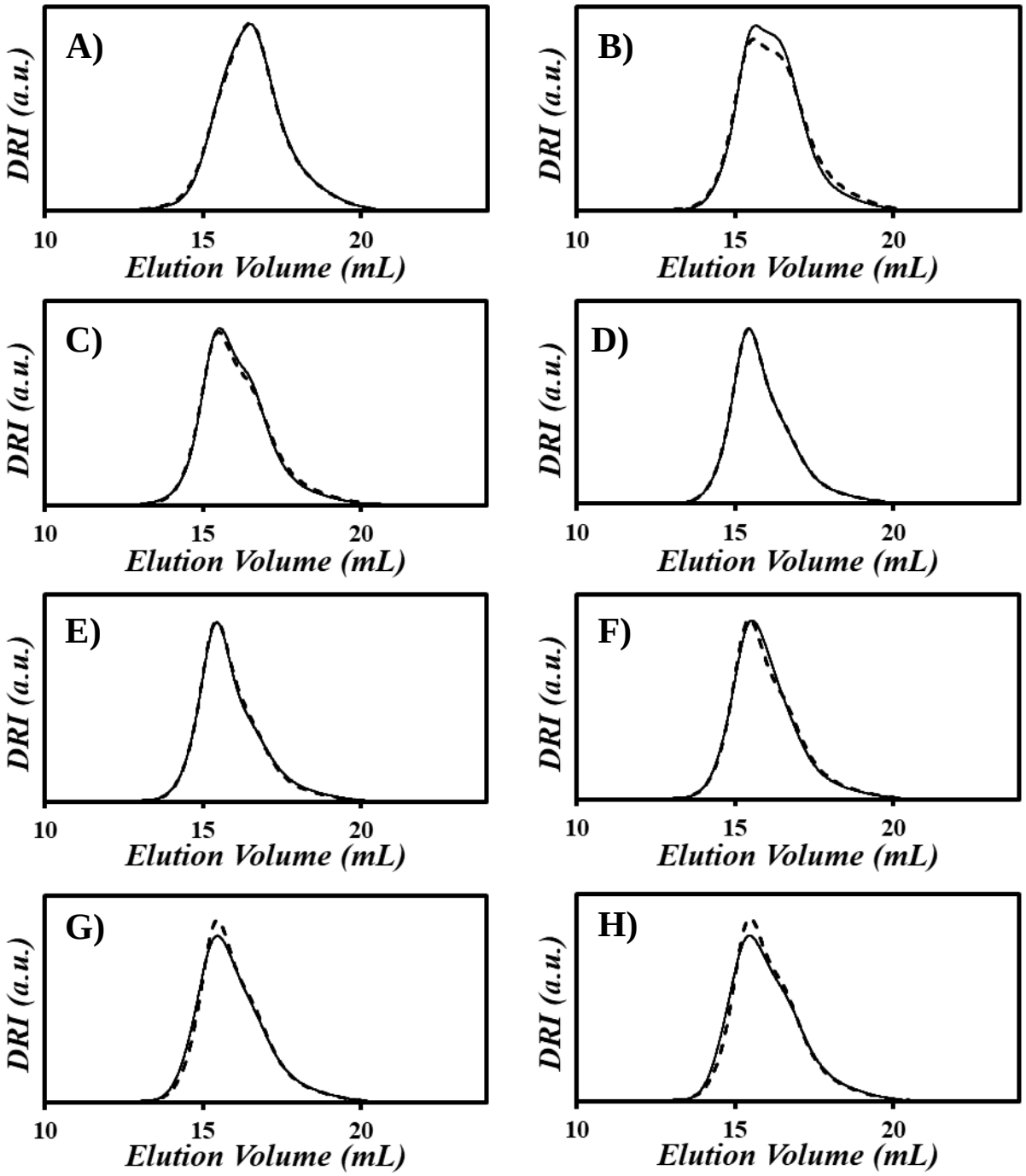

Figure 3.10. Comparison of the fits obtained with (———) the *x*gaussSNP programs and (- - - -) the linear regression analysis of the PIBSA-2-H(*X*) samples with N_{Am}/N_{SA} ratios of A) 0.25, B) 0.5, C) 0.75, D) 1.0, E) 1.25, F) 1.5, G) 1.75, and H) 2.0.

Now that the DRI traces of each PIBSA-2-H(*X*) sample had been examined by applying two different fitting procedures, the results could be compared with some simulated data. This was done to assess whether a reaction simulation program could be developed which would accurately predict the MWD, and in turn the chemical composition of PIBSI products. The program took into account both f_{doubly} for the PIBSA sample and the $N_{\text{Am}}/N_{\text{SA}}$ ratio to be used in the reaction, without requiring a series of coupling reactions to be run such as those undertaken previously.

Simulations. While the fits with sums of Gaussians and linear regressions have enabled the quantitative characterization of the PIBSA-2-H(*X*) samples, it might be more useful from a synthetic point of view to predict the products of a coupling reaction between PIBSA and a polyamine. To evaluate the feasibility of this proposal, the coupling programs reaction3 and reaction4 were created to simulate the products of a coupling reaction between PIBSA and HMDA, and take into account the molar fraction (f_{doubly}) of doubly modified PIBSA_2 in the PIBSA sample and the $N_{\text{Am}}/N_{\text{SA}}$ ratio used in the reaction. Since the non-PLM fractions of the PIBSA-2-H(*X*) samples shared a common MWD in Figure 3.8, the proposal was made that the PIBSA-HMDA coupling reactions might yield the same higher-order PIBSI product regardless of the $N_{\text{Am}}/N_{\text{SA}}$ ratio. The similarity of the non-PLM products suggested that only *b*-PIBSA dimers were formed, possibly due to the short span of HMDA giving rise to steric hindrance when trying to couple two PIBSAs to the same PIBSA_2 molecule. HMDA is 8 atoms long, compared to the more industrially relevant pentaethylene hexamine (PEHA) which is 16 atoms long. The longer span of PEHA could allow the formation of higher-order PIBSI through the bifunctional PIBSA_2 species. If steric hindrance were preventing the formation of *tri*-PIBSA or higher-order PIBSI products in the PIBSA-HMDA coupling reactions, only *b*-PIBSI dimers would be formed, which would result in the same non-PIBSA fraction in all the DRI profiles, regardless of $N_{\text{Am}}/N_{\text{SA}}$ ratio, as was noted in

the GPC analysis described in the previous section. While this would eliminate the possibility of higher-order structures such as *tri*-PIBSI, the f_{doubly} value for the PIBSA sample of interest would still need to be taken into consideration in simulations to account for the extra succinic anhydride in $PIBSA_2$ which would consume the amines of HMDA, but not append an additional PIBSA if the neighboring succinic group had already coupled another PIBSA to form *b*-PIBSI. To further study this possibility, the reaction3 program was created to simulate the fractions of *m*-PIBSA, *b*-PIBSA, *tri*-PIBSA and higher-order PIBSIs, expected from the coupling of a PIBSA sample with a known f_{doubly} fraction of $PIBSA_2$ species with a number of HMDA molecules, determined by the N_{Am}/N_{SA} ratio. Similarly, the reaction4 program was created to simulate the fractions of PLM*s* and *b*-PIBSI expected from the coupling of a PIBSA with a known f_{doubly} and a given N_{Am}/N_{SA} ratio, while assuming that a $PIBSA_2$ molecule could react with two diamines but only one other PIBSA molecule, due to steric hindrance which limits the products to only *m*-PIBSI and *b*-PIBSI.

The reaction3 and reaction4 programs were both used with a f_{doubly} value of 0.065, determined for *f*-PIBSA-2 in the previous chapter, since the PIBSA-2-H(*X*) samples were precipitated with acetone before the HMDA coupling in a similar manner to the *f*-PIBSA-2-PyMA sample of the previous chapter. Each of the reaction3 and reaction4 programs were carried out with 1000 PIBSA molecules using N_{Am}/N_{SA} ratios of 0.25, 0.5, 0.75, 1.0, 1.25, 1.5, 1.75, 2.0. For each coupling reaction, the number of product molecules with different numbers of PIB segments (n_{PIB}) were compiled and they are listed in Table 3.2.

Table 3.2. PIBSI products simulated by the reaction3 and reaction4 programs.

N_{Am}/N_{SA} ratio	reaction3.f					reaction4.f		
	PIBSA	*m*-PIBSI	*b*-PIBSI	*tri*-PIBSI	*tet*-PIBSI	PIBSA	*m*-PIBSI	*b*-PIBSI
0.25	739	0	123	5	0	742	0	129
0.50	481	0	240	13	0	492	0	254
0.75	234	0	337	28	2	254	0	373
1.00	0	1	410	49	8	34	0	483
1.25	0	128	380	32	4	0	130	435
1.50	0	231	339	29	1	0	234	383
1.75	0	290	313	28	0	0	294	353
2.00	0	345	295	19	2	0	350	325

Both simulation programs yielded expected trends, showing that the fraction of PLMs decreased steeply for increasing N_{Am}/N_{SA} ratios from 0.25 to 1.0, before increasing gently for increasing N_{Am}/N_{SA} ratios from 1.0 to 2.0. A large fraction of *b*-PIBSI products persisted for N_{Am}/N_{SA} ratios ≥ 1, similarly to what was noted upon review of the fractions of PLMs obtained from the fits of the DRI traces acquired with the PIBSA-2-H(*X*) samples in Figures 3.9 and 3.10. This would suggest that the coupling reaction stops at the *b*-PIBSI product, possibly due to steric hindrance preventing the formation of higher-order PIBSI products from $PIBSA_2$. It was also important to note that both programs predicted a negligible fraction of PLMs at an N_{Am}/N_{SA} ratio of 1, in contrast to the GPC results for PIBSA-2-H(*X*), which all seemed to contain a substantial contribution of PLMs regardless of the N_{Am}/N_{SA} ratio. The reaction3 program produced the highest number of higher-ordered PIBSI products at a N_{Am}/N_{SA} ratio of 1 as compared to any other N_{Am}/N_{SA} ratio, since the reaction mixture contained the exact number of amines required to couple all PIBSAs without excess diamines.

Comparison of the PIBSA DRI trace with that of two PIB standards with M_n's equal to 1.0 kg/mol and 3.2 kg/mol in Figure B1 suggested that the PIBSA trace represented a MWD that was much closer to the 1.0 than to the 3.2 kg/mol PIB standard. This observation contradicted the

conclusion reached in Chapter 2 that based on the f_{doubly} and λ_{Py} values, the fractionated PIBSA-2 sample (*f*-PIBSA-2) used in these coupling experiments had an M_n of 3.5 kg/mol. The difference in M_n, along with the strong contribution from PLMs in each of the PIBSA-2-H(*X*) samples, suggested that some unmaleated PIB was present in the PIBSA-2 sample. Without succinic groups to form imide linkages with HMDA, and assuming that it shared a same MWD with PIBSA, this unmaleated PIB species would contribute to the DRI traces of all PIBSA-2-H(*X*) samples, which would explain why the weight fractions of PLMs never dropped below 36 wt% in Figure 3.9. The weight fraction of PIB (w_{PIB}) in the PIBSA-2 sample was calculated for each N_{Am}/N_{SA} ratio used to prepare the PIBSA-2-H(*X*) samples with Equation 3.10.

$$w_{PIB} = \frac{w_1(2 - f_1) - f_1}{2(1 - f_1)} \tag{3.10}$$

In Equation 3.10, w_1 and f_1 represent the weight fraction of PLMs determined for a PIBSA-2-H(*X*) sample by GPC analysis at a given N_{Am}/N_{SA} ratio, and the molar fraction of PLMs determined by reaction3 or reaction4 for a given N_{Am}/N_{SA} ratio, respectively. The weight fraction w_{PIB} was calculated for each N_{Am}/N_{SA} ratio and it is plotted in Figure 3.11.

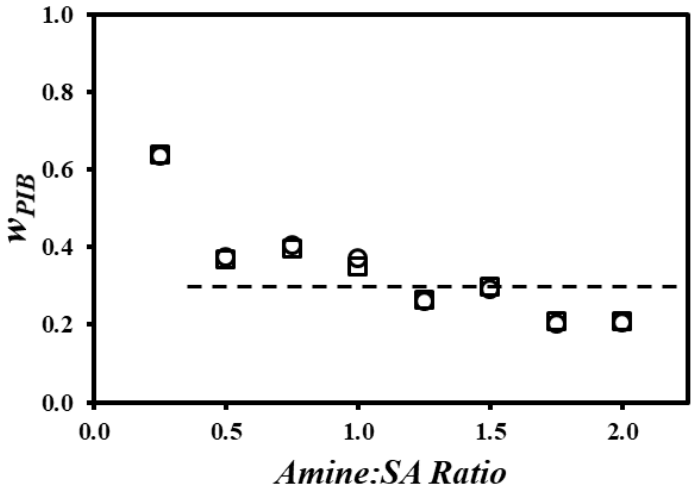

Figure 3.11. Weight fractions of unmaleated PIB obtained with (□) reaction3 and (○) reaction4.

Beside the w_{PIB} value obtained for an N_{Am}/N_{SA} ratio of 0.25 which was probably an outlier, the w_{PIB} values shown in Figure 3.11 remain fairly constant with N_{Am}/N_{SA} ratio and took an average value of 0.30 ± 0.08 when calculated with reaction3 or reaction4. This analysis suggested that 30 wt% of the PIBSA-2 sample was unmaleated PIB. The weight fraction of the PLMs in the PIBSA-2-H(X) samples obtained from the regression fits in Figure 3.9 were compared in Figure 3.12 to the same weight fractions obtained by adding w_{PIB} to that obtained from the reaction3 and reaction4 simulations. Without adding w_{PIB} in Figure 3.12, the weight fraction of PLMs obtained from the simulations showed a similar trend as that obtained experimentally by GPC analysis, but the weight fractions were shifted to lower values. Upon adding w_{PIB} to the weight fractions obtained from the simulation programs, excellent agreement between the simulated and experimental weight fractions was obtained.

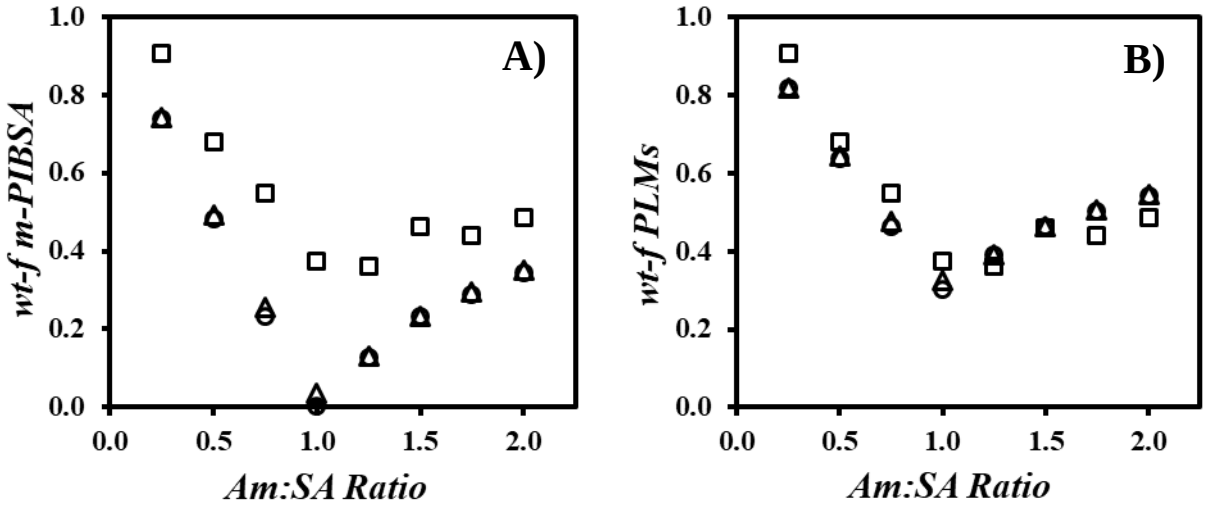

Figure 3.12. Weight fractions obtained from (□) regression fits and simulations with (○) reaction3 or (△) reaction4 plotted as a function of the N_{Am}/N_{SA} ratio A) without w_{PIB} and B) with w_{PIB}.

The excellent agreement found in Figure 3.12B between the weight fraction of PLMs obtained by GPC analysis and upon adding w_{PIB} = 0.30 to the weight fraction of PLMs obtained by the simulation programs suggests that 30 wt% of the PIBSA-2 is unmaleated PIB. Little difference was also found between the weight fractions determined by simulating a coupling reaction that would (reaction3) or would not (reaction4) yield higher order PIBSI products, probably because f_{doubly} was fairly small and equal to 0.065.

The weight fractions determined from the simulation programs, including w_{PIB} = 0.30, could be used to predict the MWD of the PIBSA-2-H(*X*) samples for each N_{Am}/N_{SA} ratio. Doing this, however, would require the DRI traces for each PIBSI product found in a given sample. As shown earlier, the contribution of non-PLMs to the DRI traces was found to be a good representation of the *b*-PIBSI product. To obtain the MWD of the higher order PIBSI products, the procedure described in the Experimental section was applied with Equation 3.3.

The resulting DRI traces corresponding to individual PIBSI products are shown in Figure 3.13 as they would be expected to appear from a GPC run. The MWD of *b*-PIBSI, *tri*-PIBSI, and *tet*-PIBSI products showed an increase in MW with increased coupling, along with a narrowing of MWD with increasing PIBSI-order, as seen by a decrease in the PDI of the simulated MWDs from 1.76 to 1.12 going from *m*-PIBSI to *tet*-PIBSI.

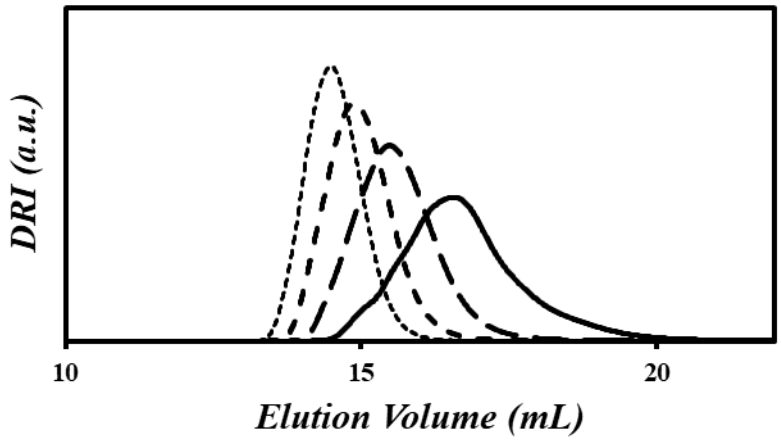

Figure 3.13. The simulated DRI traces of (———) *m*-PIBSI, (– – –) *b*-PIBSI, (– – – –) *tri*-PIBSI, and (·····) *tet*-PIBSI after conversion to $w_i(V_{el})$, normalized to a sum of 1.

Now that the DRI traces had been obtained for each of the high order PIBSI products, the simulation programs could be used to predict the DRI traces of the PIBSA-2-H(*X*) samples and compare them to the corresponding experimental DRI traces fitted with the *x*gaussSNP programs for each N_{Am}/N_{SA} ratio. Figures B2 and B3 in Supporting Information show the results that were obtained with the reaction3 and reaction4 programs. In particular, the experimental DRI traces obtained for N_{Am}/N_{SA} ratios of 0.25, 1.0 and 2.0 were compared to the simulated DRI traces obtained with reaction3 and reaction4 in Figure 3.14.

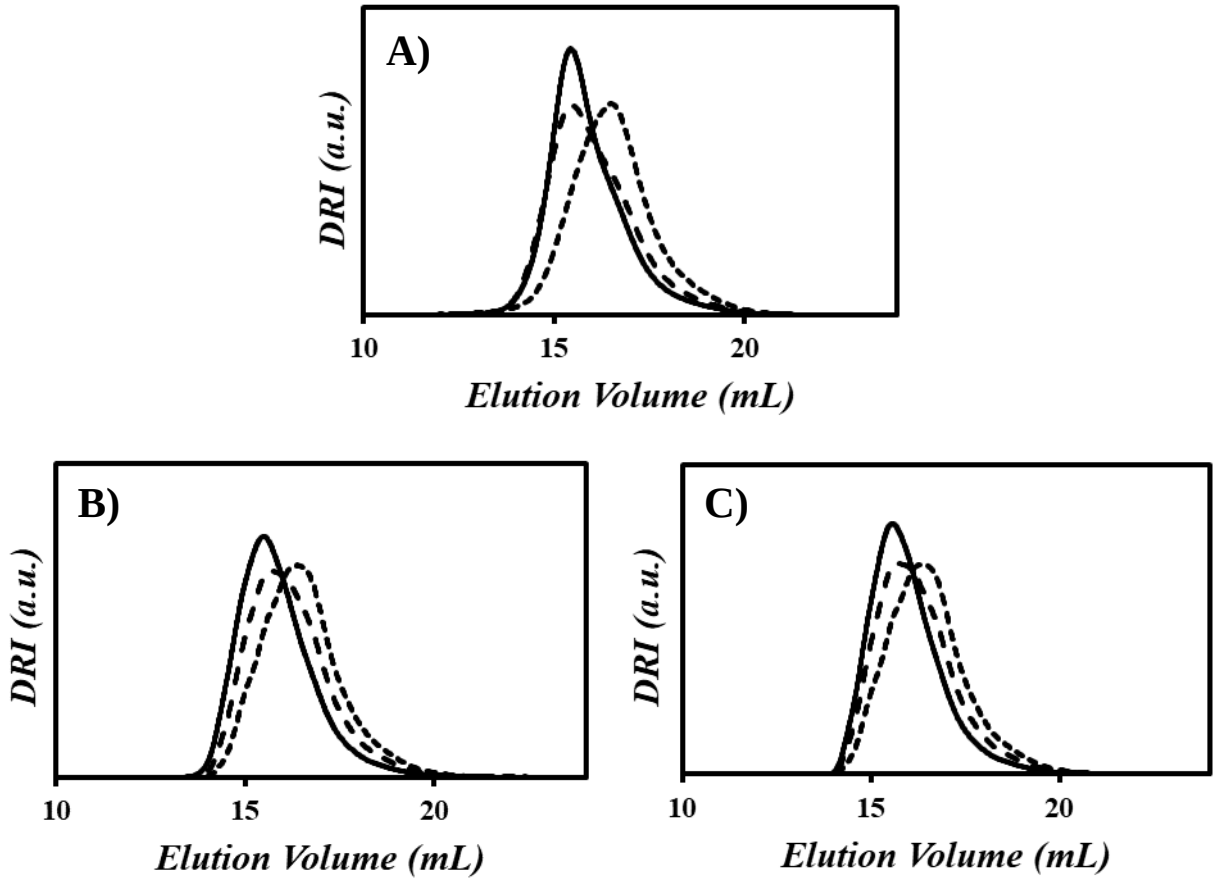

Figure 3.14. DRI traces of the PIBSA-2-H(*X*) samples obtained A) experimentally after Gaussian fits of DRI traces, and simulated B) with reaction3, and C) reaction4. N_{Am}/N_{SA} ratios of (▬▬▬) 0.25, (———) 1.0, and (– – –) 2.0, normalized to a sum of 1.

Comparisons of Figure 3.14B and C illustrated the key difference between the reaction3 and reaction4 programs. The presence of higher-order PIBSI products shifted the high MW front of the DRI traces obtained with reaction3 to the left. The simulations with reaction4 yielded DRI traces for the PIBSA-2-H(*X*) samples with $X = 1.0$ or 2.0 that had a similar high MW front, which more closely resembled the experimental data in Figures 3.7 and 3.14A. This similarity was partly by design, since reaction4 does not allow for the formation of *tri*- or higher-ordered PIBSI products. This discussion led to the conclusion that the non-PLM fraction of each PIBSA-2-H(*X*)

sample was comprised essentially of *b*-PIBSI. The DRI traces in Figure 3.14B and C also showed a notable shift to high MW when the N_{Am}/N_{SA} ratio increased from 0.25 to 1.0, and a much lesser shift back to low MW when the N_{Am}/N_{SA} ratio increased from 1.0 to 2.0, as had been noted for the experimental data in Figure 3.7. For a better comparison with the experimental data, simulated DRI traces were generated using the DRI traces of the PLMs and *b*-PIBSI using reaction4. The comparison between the simulated and experimental DRI traces is shown in Figure 3.15 for each N_{Am}/N_{SA} ratio.

The simulated DRI traces in Figure 3.15 displayed very good agreement with the experimental DRI traces fitted with the *x*gaussSNP programs. Overall, the combination of molar fractions of the PIBSA and HMDA reactants and PIBSI products simulated using reaction4 with the DRI traces predicted for the PLMs and *b*-PIBSI products provided a good estimate of the experimental DRI traces obtained with the PIBSA-2-H(*X*) samples for each N_{Am}/N_{SA} ratio. Since the GPC instrument had been calibrated with broad PIB standards, the DRI traces could then be converted into MWDs. These simulations and calculations used the experimental N_{Am}/N_{SA} ratio, the SA content of the PIBSA-2 sample, and the molar fraction f_{doubly} for PIBSA-2 which had been determined by fluorescence in Chapter 2.

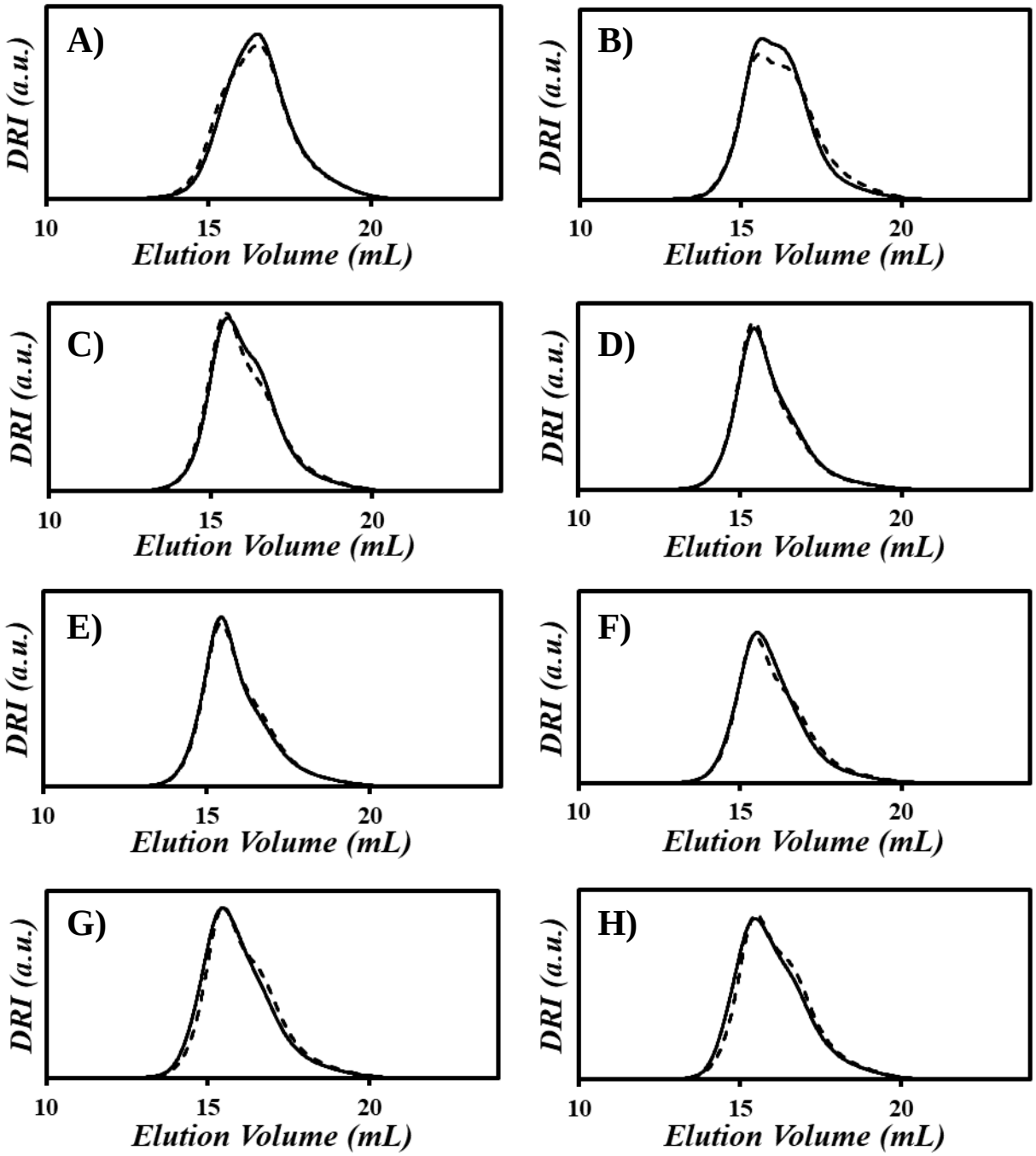

Figure 3.15. Comparison of (———) the simulated DRI traces obtained from the molar fractions obtained with reaction4, w_{PIB} = 0.30, and the DRI traces of PIBSA and *b*-PIBSI and (- - - -) the experimental DRI traces fitted with the *x*gaussSNP programs of the PIBSA-2-H(*X*) products. The N_{Am}/N_{SA} ratios equal A) 0.25, B) 0.5, C) 0.75, D) 1.0, E) 1.25, F) 1.5, G) 1.75, and H) 2.0.

The DRI traces shown in Figure 3.15 were then analyzed using the calibration curve (Equation B1) generated for the GPC instrument to obtain the M_n, M_w, and PDI values for the PIBSA-2-H(*X*) reaction mixtures. They are plotted as a function of the N_{Am}/N_{SA} ratio in Figure 3.16.

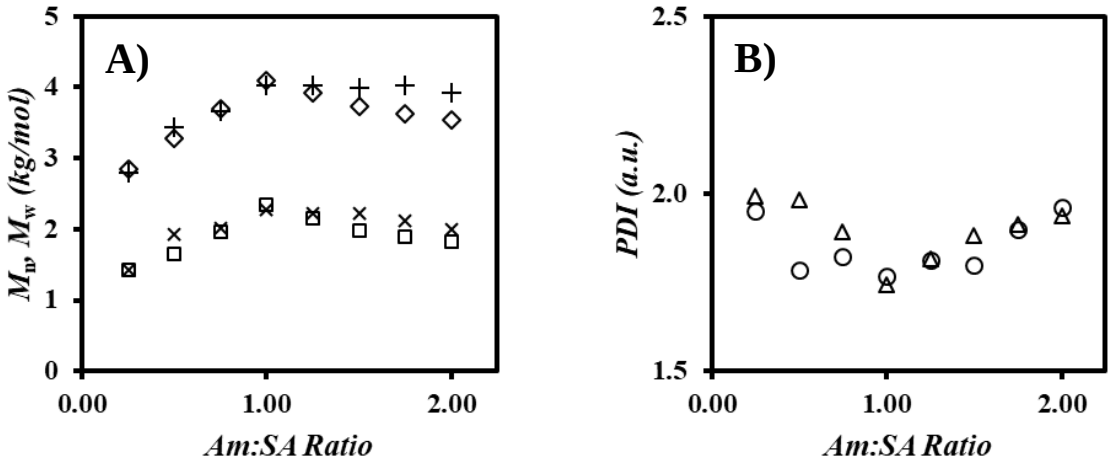

Figure 3.16. Plot of A) (□,×) M_n and (◇,+) M_w and B) (○,△) PDI of the PIBSA-2-H(*X*) samples as a function of the N_{Am}/N_{SA} ratio. (□, ◇, △) simulations and (×, +, ○) experiments.

The M_n and M_w values of the PIBSA-2-H(*X*) samples were determined from the DRI traces that were obtained experimentally and through simulations. M_n and M_w increased when the N_{Am}/N_{SA} ratio increased from 0.25 to 1.0, before decreasing slightly when the N_{Am}/N_{SA} ratio increased from 1.0 to 2.0. These trends mirrored the large decrease in the experimental weight fraction of PLMs upon increasing the N_{Am}/N_{SA} ratio from 0.25 to 1.0 before showing a slight increase when the N_{Am}/N_{SA} ratio increased further from 1.0 to 2.0 as seen in Figure 3.10. Both trends reflected the shift towards the formation of more *b*-PIBSI product as the N_{Am}/N_{SA} ratio increased from 0.25 to 1.0, before more *m*-PIBSI was generated when the N_{Am}/N_{SA} ratio increased

from 1.0 to 2.0. In summary, the experimental results seem to agree remarkably well with the simulated data.

Now that the PIBSA-2 sample was known to consist of 30 wt% of unmaleated PIB, the M_n determined for the fractionated *f*-PIBSA-2-PyMA sample in Chapter 2 could be reassessed according to Equation 3.11 by taking into account the w_{PIB}, the molar fraction ($f_{doubly} = 0.065$), and the succinic anhydride content ($\lambda_{SA} = 0.315$ mmol/g).

$$M_n = \frac{(1 - w_{PIB})(1 + f_{doubly})}{\lambda_{SA}} \tag{3.11}$$

The M_n value obtained with Equation 3.11 equalled 2.4 kg/mol. For comparison against the calculated M_n, the DRI trace of the *f*-PIBSA-2-PyMA was analysed with the calibration curve (Equation B1) to determine M_n experimentally which yielded an M_n of 2.0 K for the *f*-PIBSA-2-PyMA sample. While the decrease in the M_n value of PIBSA from 3.5 to 2.4 kg/mol when calculated in Chapter 2 and 3 without and with the w_{PIB} contribution of 30 wt%, respectively, is reasonable, the difference between the M_n value of 2.4 and 2.0 kg/mol when determined mathematically and experimentally, respectively, suggests that while this could be attributed to differences between PIB and PIBSA in establishing the calibration curve, the GPC characterization of PIBSA might require further adjustments.

3.5 Conclusions

A series of eight PIBSA-2-H(*X*) samples were prepared by reacting a PIBSA-2 sample with varying amounts of HMDA to generate different mixtures of PIBSA reactants and PIBSI products. The DRI traces from GPC analysis of the PIBSA-2-H(*X*) samples were fitted with sums of

Gaussians using a series of fitting programs designed in-house to provide a mathematical representation of the MWDs of the PIBSA-2-H(*X*) samples. This analysis, where the MWD of the PLMs was fixed to that of PIBSA, enabled the quantification of the weight fraction of the PLMs in each sample. The non-PLM portion of the gaussian fits was found to have roughly the same MWD, suggesting that the PIBSI products shared a similar MWD regardless of the N_{Am}/N_{SA} ratio used to prepare the PIBSA-2-H(*X*) samples. This observation led to the proposal that the non-PLM portion of the PIBSA-2-H(*X*) sample represented the *b*-PIBSI product. The absence of higher order PIBSI products was speculated to be due to steric hindrance which prevented the short HMDA linker from coupling multiple PIBSAs to a same $PIBSA_2$ molecule. The weight fraction of the PLMs was found to decrease sharply from 91 to 36 wt% as the N_{Am}/N_{SA} ratio increased from 0.25 to 1.0, before increasing to 49 wt% as the N_{Am}/N_{SA} ratio was increased further from 1.0 to 2.0. It was noted that the weight fraction of the PLMs was always substantially larger than zero for all N_{Am}/N_{SA} ratios. Interestingly, the MWD of the fractionated PIBSA-2 sample used in these coupling reactions appeared to be of a considerably lower MW than suggested form the FTIR and fluorescence analysis conducted in Chapter 2. All these observations suggested the presence of unmaleated PIB in the PIBSA-2 sample, which appeared as PLMs in the GPC analysis of the PIBSA-2-H(*X*) samples.

The reaction3 and reaction4 programs were used to simulate the number of PIBSA and HMDA molecules that would be consumed and the type of PIBSI products that would be formed during the coupling reaction of PIBSA with HMDA. These simulation programs took into account the N_{Am}/N_{SA} ratio and f_{doubly} of the PIBSA-2 sample. Comparison of the weight fraction of PLMs obtained by simulation and experimentally through GPC analysis confirmed the proposal that a substantial amount of unmaleated PIB was present in the PIBSA-2 sample. Comparison of the

simulation and GPC analysis results enabled the calculation of the weight fraction (w_{PIB}) of unmaleated PIB in the PIBSA-2 sample, which was found to equal 0.30 (±0.08). Excellent agreement was reached between the weight fractions of PLMs determined through GPC analysis of the experimental DRI traces and the weight fractions determined with the coupling simulation programs, when the 30 wt% unmaleated PIB was accounted for and assuming that unmaleated PIB and PLMs shared the same MWD as PIBSA.

A calibration curve was generated for the GPC analysis based on three PIB standards with a broad MWD, which was applied to simulate the MWDs of *b*-PIBSI and higher-order PIBSI products expected from the coupling reaction. These simulated traces were used with the reaction3 and reaction4 coupling programs to simulate the DRI traces expected for each PIBSA-2-H(*X*) sample. The reaction4 simulations were a better match for the experimental data and supported the claim that only *b*-PIBSI was formed.

The DRI traces of PIBSA and *b*-PIBSI were used with their molar fractions obtained through the reaction4 program to simulate the expected DRI traces of the PIBSA-2-H(*X*) samples for each N_{Am}/N_{SA} ratio. The simulated DRI traces in Figure 3.15 matched surprisingly well those obtained experimentally for the PIBSA-2-H(*X*) samples. The set of fitting and coupling programs appears to provide a powerful tool to predict the MWD of PIBSI coupling products, by taking into account the N_{Am}/N_{SA} ratio and f_{doubly} of the PIBSA sample. These fitting and simulation procedures should be of great value to scientists working on the coupling of PIBSA samples and polyamines to obtain a desired PIBSI product.

Chapter 4

Correlating Local Pyrene Concentration to the Rate of Excimer Formation in Pyrene-Labeled Polyamines

4.1 Outline

A library of pyrene-labeled polyamines (Py-PAs) was synthesized and their ability to form an excimer by encounter of an excited and a ground-state pyrene was characterized by steady-state and time-resolved fluorescence. The linear relationship expected to exist between the fluorescence intensity ratio (I_E/I_M) of the excimer over that of the monomer, the rate of pyrene excimer formation by fluorescence ($\langle k \rangle$), and the local pyrene concentration ($[Py]_{loc}$) for pyrene-labeled macromolecules was investigated for the PyPAs. This relationship could provide an experimental means of probing the polyamine core of a polyisobutylene succinimide (PIBSI) sample by simple labeling with pyrene. The labeling of four polyamines and *n*-hexylamine with 1-pyrenebutyric acid (PyBA) yielded four Py-PAs with different $[Py]_{loc}$ and a model compound, respectively. ^{1}H NMR was used to confirm the chemical composition of the Py-PAs and model compound before they were studied by fluorescence to yield the I_E/I_M ratios and $\langle k \rangle$ values for each Py-PA sample in THF, DMF, and DMSO. The I_E/I_M ratios varied linearly with the $[Py]_{loc}$ in each solvent, and for each Py-PA, I_E/I_M increased as the solvent viscosity decreased. Model free analysis (MFA) of the monomer and excimer fluorescence decays of the Py-PA samples yielded a small molar fraction f_{agg} of aggregated pyrene labels, indicating that the Py-PAs were well-solubilized in each solvent. The MFA also yielded a large molar fraction (f_{diff}) of pyrene labels forming excimer by diffusive pyrene-pyrene encounters. $\langle k \rangle$ was found to increase linearly with $[Py]_{loc}$ for each solvent, similarly to the I_E/I_M ratios. This result suggests that the linear trends of I_E/I_M and $\langle k \rangle$ versus $[Py]_{loc}$ could serve as calibration curves in the analysis of small pyrene-labeled molecules, as is usually expected for pyrene-labeled macromolecules.

4.2 Introduction

PIBSI dispersants can be viewed as block copolymers composed of two large blocks of polyisobutylene terminated at one end with succinic anhydride (PIBSA) connected to a much smaller polyamine core. The use of PIBSI dispersants as engine oil additives has continuously increased over the past 30 years due to their good dispersancy for particulates and good thermal stability at the high operating temperatures of an engine.[1,2] The scheme of PIBSI formation is shown in Scheme 4.1.

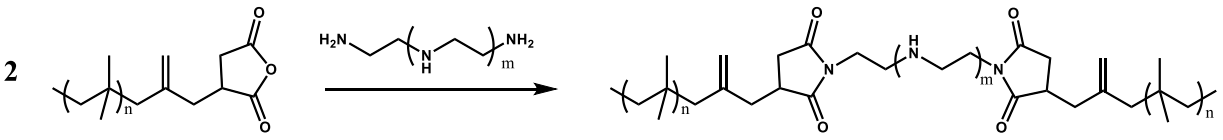

Scheme 4.1. General scheme for the synthesis of b-PIBSI dispersants.

The characterization of PISI dispersants by conventional methods remains a difficult task due to a variety of complications.[3] The PIBSA block used to prepare PIBSI has a broad molecular weight distribution (MWD) and can result in a variety of PIBSI structures due to the presence of doubly-maleated $PIBSA_2$ in a given PIBSA sample. The broad MWD and the presence of $PIBSA_2$ molecules complicate the analysis of PIBSI products via gel permeation chromatography (GPC) and mass spectrometry (MS). While FTIR has been shown to provide the content of succinic anhydride in a PIBSA sample, H-bonding between the polyamine protons and the succinimide carbonyls has been shown to distort the FTIR spectra of PIBSIs, which complicates the analysis of the PIBSI dispersant products via FTIR.[3] Furthermore, the polyamines used in an industrial setting are often of low purity and can have unknown architectures. Tumbling of the small polyamine core of PIBSI dispersants is also greatly slowed by the large PIB overhangs, which

often results in weak and broad ^{1}H NMR signals further complicating the characterization of the polyamine core. Conversely, fluorescence suffers from none of the aforementioned limitations and could be used to probe the small polar region of PIBSI dispersants through specific labeling of amines in the polyamine core. One possible limitation of fluorescence, beyond the obvious fluorescence labeling step, is the fluorescence quenching ability of nitrogen-containing groups, although this problem can be accounted for by conducting control quenching experiments.

In recent years, pyrene excimer fluorescence/formation (PEF) has proven to be a useful tool for the characterization of the structure and dynamics of pyrene-labeled macromolecules (PyLMs) in solution, enabling the characterization of macromolecules in solution that would be difficult to probe by other techniques.[3-12] The change in fluorescence induced by the formation of an excimer upon the encounter between an excited and a ground-state pyrene allows one to probe the local pyrene concentration ($[Py]_{loc}$) of PyLMs, since the rate of PEF depends directly on $[Py]_{loc}$. Previous studies conducted with pyrene-labeled dendrimers have yielded a mathematical expression of $[Py]_{loc}$, shown in Equation 4.1, which should apply to any PyLM.[10,12]

$$[Py]_{loc} = \frac{\#\ of\ G.S.Pyrenes}{\frac{4}{3}\pi\left(\frac{\langle L_{Py}{}^2\rangle^{1/2}}{2}\right)^3} \qquad (4.1)$$

In Equation 4.1, $\langle L_{Py}{}^2\rangle^{1/2}$ represents the average end-to-end distance between pyrene labels on the PyLM. Analysis of the steady-state fluorescence (SSF) spectra of a PyLM yields qualitative information about its PEF efficiency by monitoring the fluorescence intensity of the pyrene excimer over that of the monomer, namely the I_E/I_M ratio. In contrast, Model Free Analysis of the time-resolved fluorescence (TRF) decays of a PyLM yields the molar fractions of the different pyrene species contributing to PEF and the rate constant of PEF by diffusion, $\langle k \rangle$. The scheme for PEF and a corresponding SSF spectrum are shown in Figure 4.1.

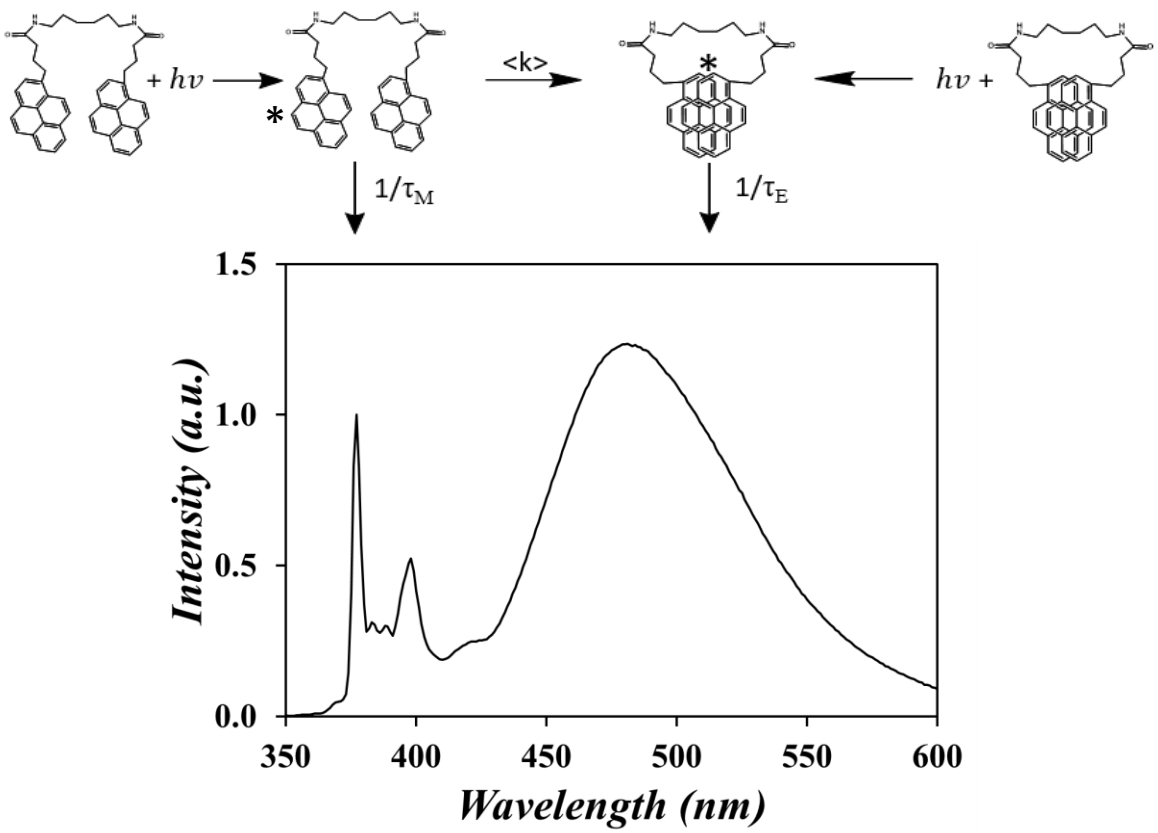

Figure 4.1. Top: Kinetic scheme of pyrene excimer formation. Bottom: Steady-state fluorescence spectrum of pyrene-labeled hexamethylenediamine normalized at 377 nm. λ_{ex} = 344 nm, [Py] = 2.5×10^{-6} M in THF.

The kinetic scheme in Figure 4.1 indicates that PEF can occur either by diffusive encounters between an excited and a ground-state pyrene with an average rate constant <*k*> (kinetic path on the left), or by direct excitation of a pyrene aggregate which occurs instantaneously (kinetic path on the right). The I_E/I_M ratio provides a measure of the PEF efficiency for a given PyLM.

The I_E/I_M ratio is obtained by dividing the fluorescence intensity of the excimer (I_E) by that of the monomer (I_M) taken from 372 to 378 nm and 500 to 530 nm, respectively, in the SSF spectrum of a PyLM. The Model Free Analysis (MFA) for the global analysis of the monomer and

excimer TRF decays yields the molar fractions f_{diff}, f_{agg}, and f_{free} of pyrene labels forming excimer by diffusion or direct excitation of pyrene aggregates, and emitting as isolated pyrene monomer with the natural fluorescence lifetime (τ_M), respectively.[9] The molar fractions f_{diff}, f_{agg}, and f_{free} give greater insight into the kinetic path toward PEF. The molar fraction f_{free}, in particular, enables the isolation of the contribution of a small amount of pyrene monomer impurity in the analysis of a PyLM whose behavior is characterized by the molar fractions f_{diff} and f_{agg}.[10] The number average monomer lifetime ($<\tau>$) obtained after eliminating the contribution of the isolated pyrene labels (f_{free}) can be used to calculate $<k>$ according to Equation 4.2. Previous work has shown that both the I_E/I_M ratio and $<k>$ for PyLMs are predicted to be proportional to $[Py]_{loc}$ based on Equation 4.3.[12]

$$< k >= \frac{1}{< \tau >} - \frac{1}{\tau_M} \tag{4.2}$$

$$\frac{I_E}{I_M} \propto k_{diff} \times [Py]_{loc} = < k > \tag{4.3}$$

The linear relationship between the I_E/I_M ratio, $<k>$, and $[Py]_{loc}$, where $[Py]_{loc}$ is expressed by Equation 4.1, has only been demonstrated quantitatively for a series of pyrene-labeled dendrimers.[12] It would be a worthwhile achievement to extend the validity of this relationship to other pyrene labeled molecules. To this end, a series of pyrene-labeled polyamines (Py-PAs) were prepared and their SSF spectra and TRF decays were analyzed to yield the I_E/I_M ratio and $<k>$ value for each Py-PA sample in different solvents. If the linear relationship held for the Py-PAs prepared with the polyamines used in the synthesis of PIBSI dispersants, similar SSF and TRF experiments could be applied to probe the local environment of polyamines constituting the core of PIBSI dispersants by labeling them with a pyrene derivative. Such experiments have the

potential to overcome the limitations of more traditional analytical techniques, and would provide a more accurate picture of the structure and dynamics of the polyamine core of a PIBSI dispersant.

4.3 Experimental

Chemicals. Hexamethylene diamine (HMDA, 98%, Sigma-Aldrich), diethylenetriamine (DETA, 99%, Sigma-Aldrich), diaminodecane (97%, Sigma-Aldrich), *n*-hexylamine (99%, Sigma-Aldrich), 1-pyrenebutyric acid (PyBA, 97%, Sigma-Aldrich), triethylamine (TEA, 99.5%, Sigma-Aldrich), diisopropylcarbodiimide (DIC, 99%, Sigma-Aldrich), dicyclohexylcarbodiimide (DCC, 99%, Sigma-Aldrich), hydroxybenzotriazole monohydrate ($HOBt{\cdot}H_2O$, ACS grade, Advanced ChemTech), cyanuric chloride (99%, Sigma-Aldrich), *N*-hydroxysuccinimide (HOSu, 98%, Sigma-Aldrich), acetic acid (AcOH, glacial, Fisherbrand), hydrochloric acid (HCl, conc. 12.2M, Sigma-Aldrich), sodium bicarbonate ($NaHCO_3$, ACS grade, Anachemia), sodium hydroxide (NaOH, 97%, Sigma-Aldrich), sodium sulfate (Na_2SO_4, 99%, EMD Millipore), chloroform ($CHCl_3$, HPLC grade, 99.8%, Sigma-Aldrich), deuterated chloroform ($CDCl_3$, anhydrous, 99.8%, Sigma-Aldrich), dimethylformamide (DMF, 99.8%, Sigma-Aldrich), ethyl acetate (HPLC grade, 99.7%, Sigma-Aldrich), isopropanol (HPLC grade, Sigma-Aldrich), dichloromethane (DCM, HPLC grade, 99.8%, Sigma-Aldrich), methanol (MeOH, HPLC grade, 99.9%, Sigma-Aldrich), hexanes (98.5%, Sigma-Aldrich), tetrahydrofuran (THF, 99%, Sigma-Aldrich or distilled in glass, 99.9%, Fisher Chemical), and acetone (HPLC grade, Sigma-Aldrich) were used without further purification.

Proton Nuclear Magnetic Resonance (^1H NMR). ^{1}H NMR spectra of the pyrene-labeled molecules in $CDCl_3$ were acquired on a Bruker 300 MHz NMR instrument at sample concentrations of ~5 – 10 mg/mL to achieve a sufficient signal-to-noise ratio.

Steady-State Fluorescence (SSF). A Horiba QM-400 spectrofluorometer equipped with a xenon arc lamp was used to acquire the fluorescence spectra. Solutions were degassed with a gentle flow of nitrogen to evacuate oxygen which is a potent quencher of pyrene fluorescence.

Time-Resolved Fluorescence (TRF). Fluorescence decays were acquired with an IBH time-resolved fluorometer using a 340 nm nano-LED light source. The monomer and excimer decays were acquired using 370 and 495 nm cutoff filters, respectively, to minimize residual stray light from reaching the detector. All samples in THF were degassed with a gentle flow of nitrogen for 15-20 minutes and samples in DMF or DMSO were degassed for 40-45 minutes before decay acquisition with 20,000 counts at the peak maximum. The same right-angle geometry was employed as in the SSF measurements.

The monomer and excimer fluorescence decays could be fitted individually with a sum of exponentials according to Equation 4.4 where *X* represents either the pyrene monomer (*M**) or excimer (*E**), with a_{xi} and τ_{xi} being the pre-exponential factors and decay times, respectively. The pyrene monomer and excimer decays could also be fitted globally according to the MFA based on Equations 4.5 and 4.6, respectively.

$$[X]_{(t)} = \sum_{i=1}^{n} a_{Xi} \times \exp(-t/\tau_{Xi}) \tag{4.4}$$

$$[M^*]_{(t)} = \left[Py_{diff}{}^*\right]_o \sum_{i=1}^{n} a_i \times exp(-t/\tau_i) + \left[Py_{free}{}^*\right]_o exp(-t/\tau_M) \tag{4.5}$$

$$[E^*]_{(t)} = -[Py_{diffE0}{}^*]_o \sum_{i=1}^{n} a_i \frac{\frac{1}{\tau_i} - \frac{1}{\tau_M}}{\frac{1}{\tau_i} - \frac{1}{\tau_{E0}}} \exp(-t/\tau_i) + \left([E0^*]_o + [Py_{diffE0}{}^*]_o \sum_{i=1}^{n} a_i \frac{\frac{1}{\tau_i} - \frac{1}{\tau_M}}{\frac{1}{\tau_i} - \frac{1}{\tau_{E0}}} \right) \exp(-t/\tau_{E0})$$

$$-[Py_{diffD}{}^*]_o \sum_{i=1}^{n} a_i \frac{\frac{1}{\tau_i}-\frac{1}{\tau_M}}{\frac{1}{\tau_i}-\frac{1}{\tau_D}} \exp(-t/\tau_i) + \left([D^*]_o + [Py_{diffD}{}^*]_o \sum_{i=1}^{n} a_i \frac{\frac{1}{\tau_i}-\frac{1}{\tau_M}}{\frac{1}{\tau_i}-\frac{1}{\tau_D}} \right) \exp(-t/\tau_D) \quad (4.6)$$

In Equation 4.4, the pre-exponential factors (a_{xi}) are free to be positive or negative, depending on whether a monomer or excimer decay was considered, with the former requiring solely positive pre-exponential factors while the latter might need some negative pre-exponential factors. In contrast, Equation 4.5 is used to fit the monomer decays globally with the excimer decays according to the MFA, and its pre-exponential factors (a_i) are normalized to unity ($\Sigma a_i = 1$) and forced to remain positive. Furthermore, the analysis program was designed so that the a_i parameters and the decay times (τ_i) took the same values in Equations 4.5 and 4.6. In Equation 4.6, τ_{E0} and τ_D are the natural lifetimes of excimer species resulting from good and poor overlap of two pyrene labels, respectively. The terms $[Py_{diffE0}{}^*]_o$, $[Py_{diffD}{}^*]_o$, $[E0^*]_o$ and $[D^*]_o$ are the concentrations at equilibrium of the pyrenyl labels that form one of the two excimers *E0** and *D** by diffusion and are aggregated, and form the excimers *E0** and *D** instantaneously upon direct excitation, respectively. The term $[Py_{free}{}^*]_o$ in Equation 4.5 represents isolated pyrenyl labels that cannot form excimer.

The floating parameters a_i, τ_i, τ_{E0}, τ_D, $[Py_{diff}]_o$ ($=[Py_{diffE0}{}^*]_o+[Py_{diffD}{}^*]_o$), $[Py_{free}]_o$, $[Py_{diffE0}{}^*]_o$, $[Py_{diffD}{}^*]_o$, $[E0^*]_o$, and $[D^*]_o$ were optimized according to the Marquardt-Levenberg algorithm with the program sumegs10bg (n = 2, no *D** species), sumegs33bg (n = 3), and sumegs35bg (n = 2). The application of a given program for the MFA of the TRF decays depended on the complexity of the PyLM, a molecule with a higher pyrene content being likelier to require more exponentials and two types of excimer to properly fit the fluorescence decays. The fitting parameters retrieved

from these analyses are listed in Table A1 as supporting information (SI).[13] The quality of the decay fits was deemed satisfactory as long as the χ^2 was lower than 1.30 and the residuals and autocorrelation of the residuals were randomly distributed about zero.

The a_i and τ_i parameters were re-arranged in Equation 4.7 to yield the average rate constant $<k>$ for PEF. The pre-exponential factors $[Py_{diff}^*]_o$, $[Py_{free}^*]_o$ in Equation 4.5 and $[Py_{diffE0}^*]_o$, $[Py_{diffD}^*]_o$, $[E0^*]_o$, and $[D^*]_o$ in Equation 4.6 could be re-arranged to yield the molar fractions f_{diffE0}, f_{diffD}, f_{free}, f_{E0}, and f_D of all the pyrene species in the solution as shown in Equations 4.8 – 4.12. The sum of f_{diffE0} and f_{diffD} (= f_{diff}) and the sum of f_{E0} and f_D (= f_{agg}) represented the pyrene species that formed excimer by diffusive encounters or via direct excitation of a pyrene aggregate, respectively. The rate constant $<k>$ and the molar fractions (f_{diff}, f_{free}, f_{agg}) provided a complete description of the PyLM.

$$< k >= \frac{\sum_{i=1}^{n} a_i}{\sum_{i=1}^{n} a_i \tau_i} - \frac{1}{\tau_M} \tag{4.7}$$

$$f_{diffE0} = \frac{[Py_{diffE0}^*]_o}{[Py_{diffE0}^*]_o + [Py_{diffD}^*]_o} \times \frac{1}{1 + \frac{[Py_{free}^*]_o}{[Py_{diff}^*]_o} + \frac{[E0^*]_o + [D^*]_o}{[Py_{diffE0}^*]_o + [Py_{diffD}^*]_o}} \tag{4.8}$$

$$f_{diffD} = \frac{[Py_{diffD}^*]_o}{[Py_{diffE0}^*]_o + [Py_{diffD}^*]_o} \times \frac{1}{1 + \frac{[Py_{free}^*]_o}{[Py_{diff}^*]_o} + \frac{[E0^*]_o + [D^*]_o}{[Py_{diffE0}^*]_o + [Py_{diffD}^*]_o}} \tag{4.9}$$

$$f_{free} = (f_{diffE0} + f_{diffD}) \times \frac{[Py_{free}^*]_o}{[Py_{diff}^*]_o} \tag{4.10}$$

$$f_{E0} = \frac{[E0^*]_o}{[Py_{diffE0}^*]_o + [Py_{diffD}^*]_o} \times \frac{1}{1 + \frac{[Py_{free}^*]_o}{[Py_{diff}^*]_o} + \frac{[E0^*]_o + [D^*]_o}{[Py_{diffE0}^*]_o + [Py_{diffD}^*]_o}} \tag{4.11}$$

$$f_D = \frac{[D^*]_o}{[Py_{diffE0}^*]_o + [Py_{diffD}^*]_o} \times \frac{1}{1 + \frac{[Py_{free}^*]_o}{[Py_{diff}^*]_o} + \frac{[E0^*]_o + [D^*]_o}{[Py_{diffE0}^*]_o + [Py_{diffD}^*]_o}} \quad (4.12)$$

Synthesis of N-*hexyl*-4-*(pyren*-1-*yl)butanamide (Py₁-HA)*: 1-Pyrenebutyric acid (PyBA, 0.10 g, 0.35 mmol, 1.2 eq) and hydroxybenzotriazole (HOBt·H_2O, 0.05 g, 0.35 mmol, 1.2 eq) were added to 15 mL of dichloromethane (DCM) where they dissolved quickly under stirring. Hexylamine (39 µL, 0.29 mmol, 1.0 eq) was added dropwise to the reaction mixture over 1 minute before adding *N*,*N*'-diisopropylcarbodiimide (DIC, 53 µL, 0.34 mmol, 1.2 eq) dropwise over 1 minute in the same manner. The reaction vessel was wrapped in aluminum foil to minimize photobleaching of the pyrene moieties and left to stir overnight. The next morning 3 drops of glacial acetic acid (AcOH) were added to the reaction mixture to convert any remaining DIC to diisopropyl urea (DIU). The reaction mixture was condensed on a rotary evaporator to a volume of ~1.5 mL and purified via silica gel chromatography using a 4:1 DCM:ethyl acetate solvent mixture shifting to pure DCM. The purification yielded 88.7 mg of a white flaky solid upon evaporation of the solvent under a flow of nitrogen. As ^{1}H NMR showed the presence of an impurity, the product was dissolved in chloroform ($CHCl_3$) and precipitated with hexanes. The precipitate was isolated by suction filtration (Whatman #1) and dried to completion in a vacuum oven at room temperature overnight to yield a white cakey solid. (73.5 mg, 67%) ^{1}H NMR (300 MHz, $CDCl_3$): δ = 8.37 – 7.80 (m, 9H), 5.32 (br. s, 1H), 3.41 (t, J = 7.1 Hz, 2H), 3.21 (q, J = 6.5 Hz, 2H), 2.32 – 2.16 (m, 4H), 1.51 – 1.38 (m, 2H), 1.35 – 1.22 (m, 6H), 0.86 (br. t, J = 6.7 Hz, 3H) ppm (see ^{1}H NMR spectrum in Figure C1 in Appendix C).

Synthesis of N,N*'-(hexane*-1,6-*diyl)bis(*4-*pyren*-1-*yl)butanamide (Py₂-HMDA).* PyBA (0.10 g, 0.35 mmol, 1.0 eq) and HOBt·H_2O (0.06 g, 0.38 mmol, 1.1 eq) were added to 5 mL of stirring

dichloromethane (DCM) followed by hexamethylene diamine (HMDA, 0.02 g, 0.16 mmol, 0.5 eq). DCM (5 mL), ethyl acetate (5 mL), and dimethylformamide (2 mL) were added to the reaction mixture to aid the dissolution of the reactants before adding DIC (53 μL, 0.34 mmol, 1.0 eq) dropwise over 1 minute. The reaction vessel was wrapped in aluminum foil and the brown solution was left to stir overnight. The next morning the reaction mixture appeared lighter in color. AcOH was added to quench any remaining DIC. The reaction mixture was transferred to a separatory funnel with 40 mL of ethyl acetate and washed twice with 75 mL of aqueous HCl (1M), twice with 50 mL of an aqueous sodium bicarbonate solution ($NaHCO_3$, 1M), and twice with 50 mL of brine (a 50:50 w/w solution of H_2O:NaCl). A precipitate in the organic phase was isolated with suction filtration using a Whatman #5 filter paper and dissolved in tetrahydrofuran (THF) for precipitation twice from methanol (MeOH). The precipitate was isolated in the same manner as before and dried in a vacuum oven overnight to yield a cakey beige solid. (47.4 mg, 44 %) ^{1}H NMR (300 MHz, $CDCl_3$): δ = 8.32 – 7.80 (m, 18H), 5.42 (br. s, 2H), 3.34 (t, J = 7.2 Hz, 4H), 3.20 (q, J = 6.6 Hz, 4H), 2.28 – 2.13 (m, 8H), 1.47 – 1.34 (m, 4H), 1.33 – 1.22 (m, 4H) ppm (see ^{1}H NMR spectrum in Figure C2).

Synthesis of N,N*'-(decane*-1,10-*diyl)bis(*4-*pyren*-1-*yl)butanamide (Py$_2$-DEC).* 1-Pyrenebutyric acid (PyBA, 0.21 g, 0.70 mmol, 1.0 eq) and triethylamine (TEA, 0.12 mL, 0.86 mmol, 1.2 eq) were dissolved in 18 mL of stirring acetone. Cyanuric chloride (TCT, 0.04 g, 0.21 mmol, 0.33 eq) was dissolved in acetone (2 mL) and added to the reaction mixture. Some precipitate formed after 2.5 hours and diaminodecane (0.05 g, 0.31 mmol, 0.5 eq) was added to the reaction mixture which was then sonicated to help disperse the amine. A large amount of precipitate evolved rapidly upon sonication, and the reaction mixture was left to stir overnight while being covered in aluminum foil. The reaction mixture was condensed under a flow of nitrogen and transferred with 20 mL of

DCM to a separatory funnel. The organic phase was washed three times with 6 mL of aqueous HCl (1 M), five times with 8 mL of an aqueous sodium hydroxide solution (NaOH, 1 M), and three times with 6 mL of brine before being dried over sodium sulfate (Na_2SO_4). Decanting and evaporating some of the solvent from the organic phase yielded a white precipitate. This precipitate was isolated via suction filtration over a Whatman #5 filter paper and dried overnight in a vacuum oven at room temperature to yield a white cakey solid. (10.2 mg, 5 %) ^{1}H NMR (300 MHz, $CDCl_3$): δ = 8.38 – 7.78 (m, 18H), 5.31 (br. s, 2H), 3.38 (t, J = 7.2 Hz, 4H), 3.19 (q, J = 7.2 Hz, 4H), 2.29 – 2.09 (m, 8H), 1.48 – 1.33 (m, 4H), 1.31 – 1.17 (m, 12H) ppm (see ^{1}H NMR spectrum in Figure C3).

Synthesis of N,N*'-(azanediylbis(ethane*-2,1-*diyl))bis(*4-*pyren*-1-*yl)butanamide*) *(Py_2-DETA).* PyBA (0.12 g, 0.35 mmol, 1.1 eq) and HOBt·H_2O (0.59 g, 0.38 mmol, 1.2 eq) were dissolved in 20 mL of stirring DCM. Diethylene triamine (DETA, 17 µL, 0.16 mmol, 0.5 eq) and dicyclohexylcarbodiimide (DCC, 0.07 g, 0.33 mmol, 1.0 eq) were added sequentially to the reaction mixture and left to stir overnight after wrapping the reaction vessel in aluminum foil. AcOH was added to quench DCC to form its corresponding dicyclohexyl urea (DCU) before rotary evaporation of the reaction mixture yielded a white DCU precipitate which was removed via successive vacuum filtrations with a Whatman #5 filter paper and evaporation of some of the solvent. The filtrate was condensed under a flow of nitrogen to a minimal solvent volume (~4-5 mL) and precipitated twice from ether. The precipitate was again isolated via suction filtration with Whatman #5 filter paper before it was dissolved in $CHCl_3$ (10 mL) for transfer to a separatory funnel. The organic layer was washed four times with an aqueous $NaHCO_3$ solution (1M) and four times with brine before drying over Na_2SO_4. The organic layer was decanted, the solvent was evaporated under a flow of nitrogen, and the product was dried to completion under vacuum

overnight yielding an orange flaky solid. (33.8 mg, 34 %) ^{1}H NMR (300 MHz, $CDCl_3$): δ = 8.29 – 7.77 (m, 18H), 5.89 (br. s, 2H), 3.34 – 3.23 (m, 8H), 2.68 (t, J = 5.5 Hz, 4H), 2.24 – 2.06 (m, 8H) ppm (see ^{1}H NMR spectrum in Figure C4).

Synthesis of 1-*Pyrenebutyric acid* N-*hydroxysuccinimide ester (PyBA-OSu).* PyBA (1.00 g, 3.49 mmol, 1 eq), *N*-hydroxysuccinimide (HOSu, 0.55 g, 4.77 mmol, 1.4 eq), and DCC (0.94 g, 4.58 mmol, 1.0 eq) were added sequentially to 50 mL of stirring DCM and dissolved quickly before being left to stir overnight in the reaction vessel wrapped in aluminum foil. The next morning AcOH was added to convert DCC to DCU which formed immediately as noted by a white precipitate which was removed via suction filtration with a Whatman #5 filter paper and subsequent elution of the filtrate through celite. The filtrate was condensed under a flow of nitrogen before precipitation with isopropanol. It was dried in a vacuum oven overnight and yielded a yellow-brown solid. (1.22 g, 91 %) ^{1}H NMR (300 MHz, $CDCl_3$): δ = 8.33 – 7.89 (m, 9H), 3.50 (t, J = 7.8 Hz, 2H), 2.88 (s, 4H), 2.73 (t, J = 7.0 Hz, 2H), 2.33 (quintet, J = 7.8 Hz, 2H) ppm (see ^{1}H NMR spectrum in Figure C5).

Synthesis of N,N-*bis(*2-*(*4-*(pyren*-1-*yl)butanamido)ethyl)*-4-*(pyren*-2-*yl)butanamide (*Py_3*-DETA).* PyBA-OSu (0.16 g, 0.41 mmol, 4 eq) was dissolved in stirring THF (20 mL). DETA (11 μL, 0.10 mmol, 1.0 eq) was added to the reaction mixture dropwise over 1 minute during which the solution went turbid. The reaction mixture was left to stir overnight with the reaction vessel wrapped in aluminum foil. The day after, the THF was evaporated under a flow of nitrogen before dissolving the crude product in DCM (10 mL) and transferring the solution to a separatory funnel. The organic phase was washed three times with 5 mL of aqueous NaOH (1 M) before drying over Na_2SO_4 and precipitating the supernatant with cold diethyl ether. The precipitate was isolated with suction filtration and dissolved in minimal $CHCl_3$ (1 mL) for purification via silica gel chromatography

using a 3:1 acetone:DCM solvent mixture before switching to acetone upon emergence of a green fluorescent band. The solvent of this fluorescent elution band was evaporated under a flow of nitrogen and the product was kept in a vacuum oven at 60 °C overnight to yield a white-yellow crystalline solid. (0.26 g, 28 %) ^{1}H NMR (300 MHz, $CDCl_3$): δ = 8.20 – 7.62 (m, 27H), 6.30 (br. s, 2H), 3.55 – 3.40 (m, 4H), 3.36 – 3.14 (m, 10H), 2.39 – 2.21 (dt, J_t = 6.9, J_d = 25.0 Hz, 4H), 2.18 – 2.00 (m, 8H) ppm (see ^{1}H NMR spectrum in Figure C6).

4.4 Results and Discussion

Earlier studies have established PEF as a useful analytical tool in the characterization of macromolecules in solution such as linear polymers or highly branched dendrimers.[7,10,12] The usefulness of PEF stems from the relationship that exists between the efficiency of PEF and $[Py]_{loc}$, as $[Py]_{loc}$ is directly related to the local density of the macromolecules to which pyrene is covalently bound. The PEF efficiency is reflected by the I_E/I_M ratio and $\langle k \rangle$ obtained from the analysis of the fluorescence spectra and decays of PyLMs, respectively. Although the linear relationship between I_E/I_M and $\langle k \rangle$ is well-accepted in the scientific community, it has only been validated once with a series of pyrene-labeled dendrimers.[12] To expand the validation of this important relationship, PyBA was used to label hexylamine (HA) and various polyamines (PAs) to generate the model compound Py_1-HA and some Py-PA samples, respectively. After confirmation of the chemical composition of the Py_1-HA and Py-PA samples by ^{1}H NMR (see Figures C1 – 6), SSF and TRF measurements were undertaken to investigate the nature of the relationship between the I_E/I_M ratio, $\langle k \rangle$, and $[Py]_{loc}$ which was calculated based on Equation 4.1 for each Py-PA sample.

Steady-State (SSF) and Time-Resolved (TRF) Fluorescence Measurements. The SSF spectra of the Py-PA samples were acquired in THF, DMF, and DMSO and they are shown in Figure 4.2. The fluorescence spectra exhibited the characteristic fluorescence peaks of the pyrene monomer between 370 and 410 nm, and the broad structureless fluorescence of the excimer centered at 480 nm. An increase in $[Py]_{loc}$ from Py_2-DEC, to Py_2-HMDA, Py_2-DETA, and Py_3-DETA resulted in an increase in the excimer fluorescence intensity with respect to the monomer. The excimer fluorescence of a given Py-PA was most intense in THF, and least intense in DMSO, which had the lowest and highest solvent viscosity, respectively. This was to be expected since a less viscous solvent should more easily allow for PEF via diffusion during the lifetime of pyrene, resulting in a more intense excimer fluorescence band. The PEF efficiency could be quantified by determining the I_E/I_M ratio for each sample in each solvent.

The I_E/I_M ratios were compared in Figure 4.3 to the $[Py]_{loc}$ values calculated for each Py-PA according to Equation 4.1, and summarized in Table 4.1.

Table 4.1. $[Py]_{loc}$ values calculated for the Py-PA samples according to Equation 4.1.

Sample	**Py_2-HMDA**	**Py_2-DEC**	**Py_2-DETA**	**Py_3-DETA**
$[Py]_{loc}$ ($Å^{-3}$)	0.015	0.011	0.017	0.042

SSF and TRF measurements were conducted at a pyrene concentration of 2.5×10^{-6} M, which eliminated the possibility of intermolecular excimer formation, for each of Py_1-HA and the Py-PA samples in THF, DMF, and DMSO. The SSF spectra for the Py-PAs are shown in Figure 4.2.

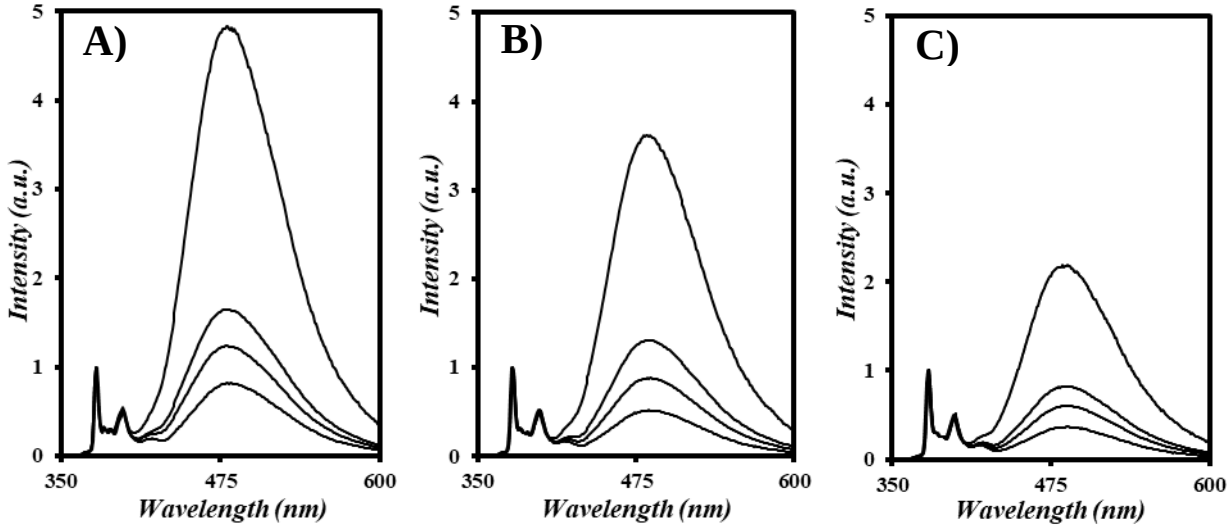

Figure 4.2. SSF spectra of the Py-PAs in A) THF, B) DMF, and C) DMSO from top to bottom: Py_3-DETA, Py_2-DETA, Py_2-HMDA, and Py_2-DEC. [*Py*] = 2.5×10^{-6} M. λ_{ex} = 344 nm.

The I_E/I_M ratio trends in Figure 4.3 matched the qualitative observations made in Figure 4.2. The I_E/I_M ratio increased most steeply with increasing $[Py]_{loc}$ in THF, the least viscous solvent which facilitated diffusive pyrene-pyrene encounters, and the most gradually in DMSO, which was the most viscous solvent in the study. I_E/I_M was found to increase linearly with increasing $[Py]_{loc}$.

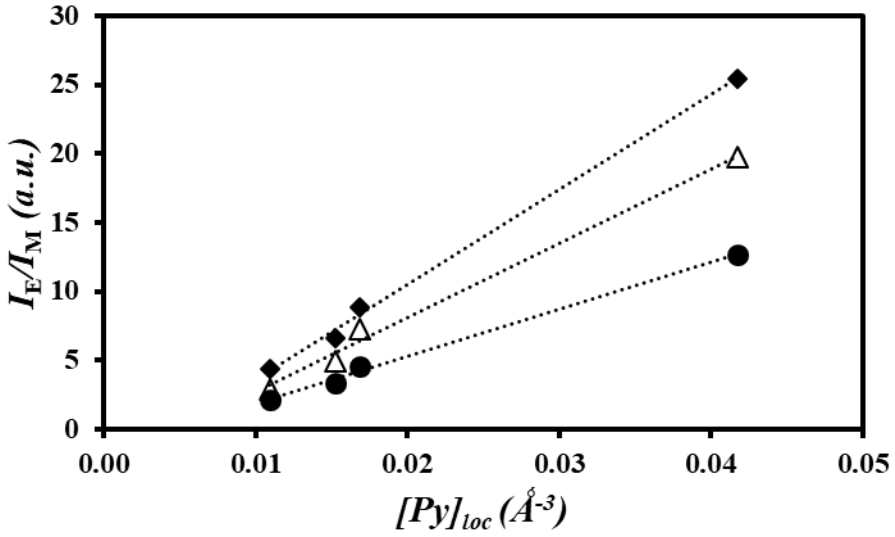

Figure 4.3. Plot of I_E/I_M vs. $[Py]_{loc}$ for the Py-PAs at a pyrene concentration of 2.5 μM in (◆) THF, (▲) DMF, and (●) DMSO.

The TRF decay analysis began by fitting the fluorescence decays of Py_1-HA with a sum of two exponentials (n = 2 in Equation 4.4) to determine the natural lifetime of the pyrenyl label (τ_M) in the different solvents. The decay analysis showed a main pre-exponential contribution (0.93 ±0.04) for the long-lived component, and its decay time was assigned to the lifetime of pyrene in that solvent. The τ_M values retrieved from this analysis are listed in Table 4.2.

Table 4.2. τ_M values obtained with TRF analysis of the Py_1-HA sample.

Solvent	**THF**	**DMF**	**DMSO**
τ_M (ns)	203	175	137

Now that the τ_M value had been determined for the model compound in each solvent of interest, it could be fixed in Equations 4.5 and 4.6 to fit the monomer and excimer TRF decays with the MFA. MFA of the monomer and excimer TRF decays yielded a good fit, as illustrated in

Figure 4.4. The parameters a_i and τ_i retrieved from the MFA of the fluorescence decays were used to calculate <*k*> with Equation 4.7 for each of the Py-PA samples. The pre-exponential factors, fluorescence decay times, and <*k*> values determined for the Py-PAs in each solvent are listed in Table C1. The molar fractions f_{diff}, f_{agg}, and f_{free} determined by global analysis with the MFA are plotted as a function of $[Py]_{loc}$ for the Py-PAs in THF, DMF, and DMSO in Figure 4.5.

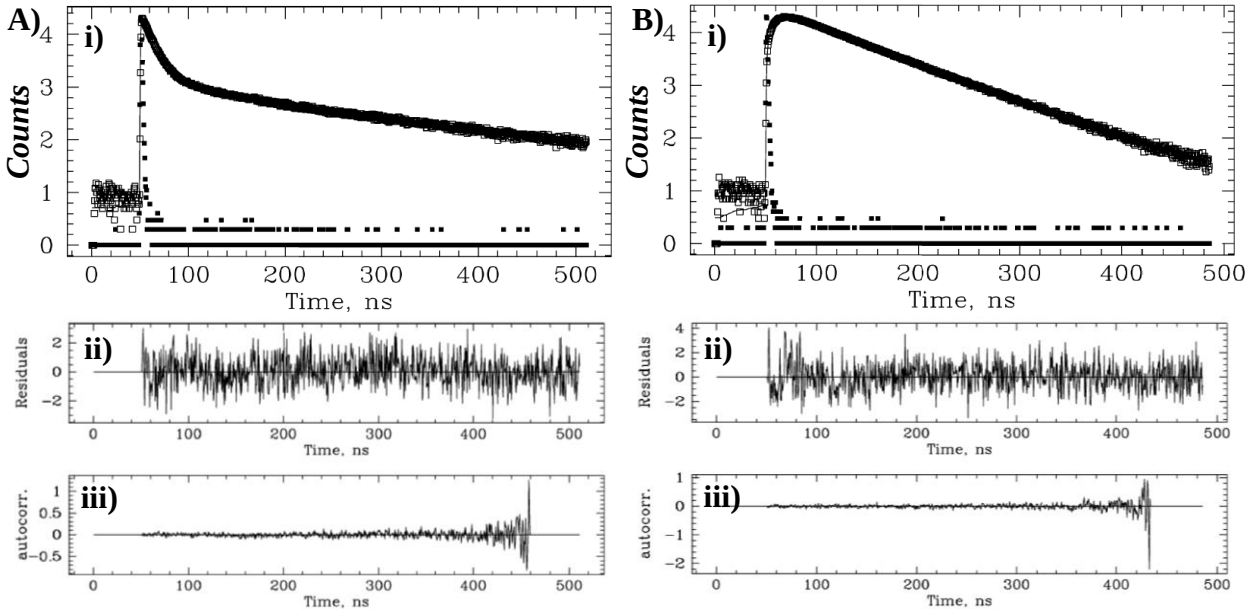

Figure 4.4. Example of TRF decay fit according to the MFA: i) decays, ii) residuals, and iii) autocorrelation of the residuals for the pyrene A) monomer (λ_{em} = 375 nm) and B) excimer (λ_{em} = 510 nm) decays of a Py_2-HMDA solution in THF. $[Py] = 2.5\times10^{-6}$ M, λ_{ex} = 344 nm, χ^2 = 1.27.

The molar fractions f_{diff}, f_{agg}, and f_{free} shown in Figure 4.5 represent the fractions of pyrenyl labels forming excimer by diffusion (Py_{diff}), involved in pyrene aggregates (Py_{agg}), and isolated in solution and emitting as monomer with the natural lifetime τ_M, respectively. Each molar fraction remained fairly constant regardless of the Py-PA sample, and in turn the $[Py]_{loc}$ or solvent used.

The low f_{agg} values (≤ 0.11) indicated that THF, DMF, and DMSO were good solvents for the Py-PA samples without excessive aggregation of the pyrene moieties. The low f_{free} values (≤ 0.06) showed that the Py-PA samples were of high purity and did not have appreciable amounts of singly pyrene-labeled Py-PA contaminants which would fluoresce as free monomer. The high f_{diff} values (≥ 0.88) also alluded to the good solubility of the Py-PA samples in the selected solvents.

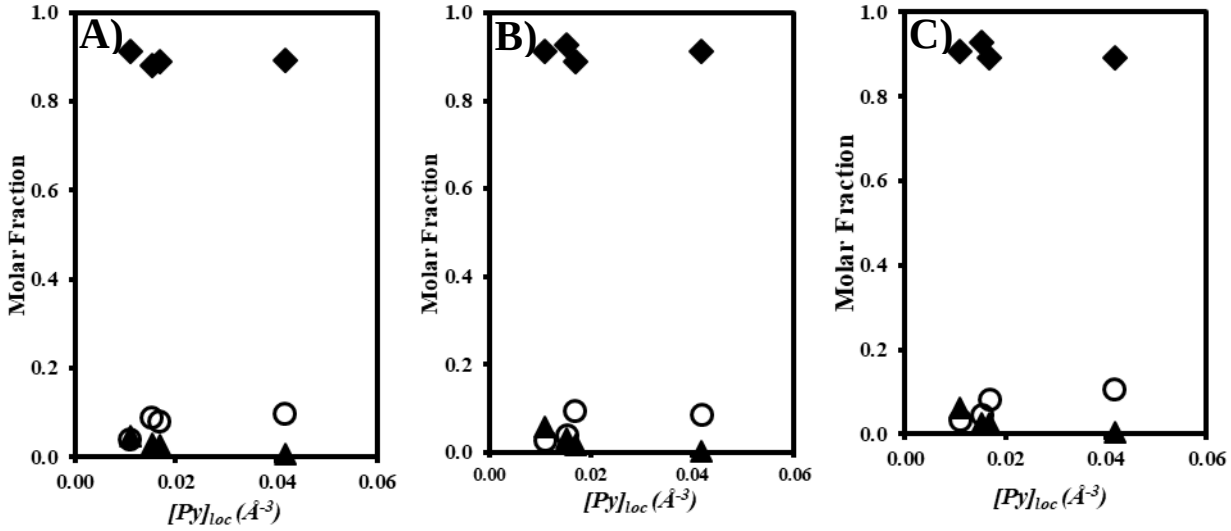

Figure 4.5. Molar fractions (◆) f_{diff}, (○) f_{agg}, and (▲) f_{free} vs. $[Py]_{loc}$ obtained by MFA of the fluorescence decays acquired for the Py-PA samples in A) THF, B) DMF, and C) DMSO.

The $\langle k \rangle$ value for each Py-PA sample was plotted as a function of $[Py]_{loc}$ in Figure 4.6.

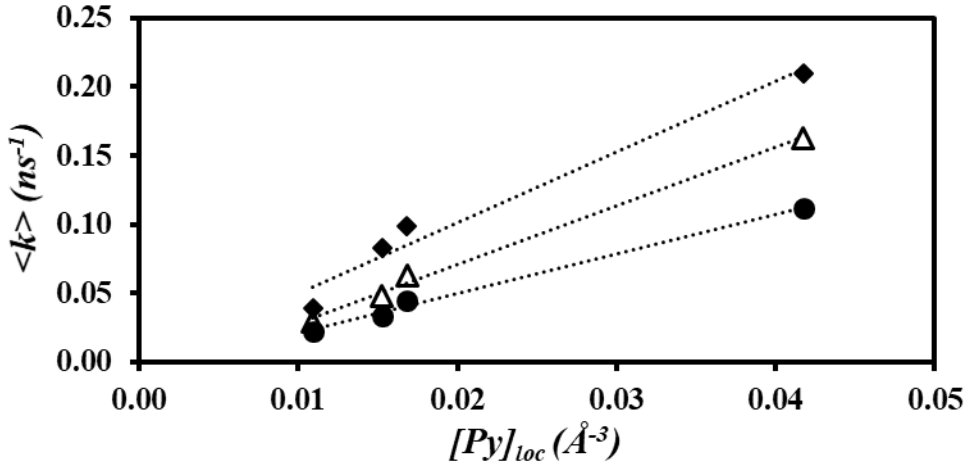

Figure 4.6. Plot of <*k*> vs. $[Py]_{loc}$ for the Py-PA samples in (◆) THF, (△) DMF, and (●) DMSO.

<*k*> was found to increase linearly with increasing $[Py]_{loc}$ in Figure 4.6, suggesting that a calibration curve could be established between <*k*> and $[Py]_{loc}$ for Py-PA samples. The different trends seen between solvents were consistent with those noted in Figure 4.3, with THF resulting in the steepest increase in <*k*> with $[Py]_{loc}$ and DMSO the smallest. The linear relationships observed between the I_E/I_M ratio, <*k*>, and $[Py]_{loc}$ were expected from Eq. 4.3. For further comparison, the k_{diff} value was calculated for the Py-PA samples in each solvent studied and summarized in Table 4.3.

Table 4.3. k_{diff} values calculated for the Py-PA samples in THF, DMF, and DMSO with Eq. 4.3.

Solvent	**THF**	**DMF**	**DMSO**
$\boldsymbol{k_{diff}}$ **(Å^3.ns^{-1})**	5.1 ± 0.6	4.3 ± 0.2	2.9 ± 0.2
$\boldsymbol{\eta}$ **(mPa.s)**	0.46	0.79	1.99

The rate constants for diffusive encounters between pyrene labels listed in Table 4.3 further exemplified the effects of solvent viscosity with THF, the least viscous solvent of the three,

yielding the highest k_{diff} for the Py-PA samples and conversely, the lowest k_{diff} being obtained in more viscous DMSO. While the k_{diff} values listed in Table 4.3 indicate that k_{diff} decreases with increasing solvent viscosity, k_{diff} is far from being inversely proportional to solvent viscosity as would be theoretically expected for a rate constant describing a diffusion-controlled process. The reason for this discrepancy lies in the probability (p) of forming excimer upon encounter between an excited and a ground-state pyrene. Because p depends on the solvent, being larger in DMSO than in DMF, this factor complicated the direct comparison of the $<k>$ values between solvents.[14] Nevertheless, the $<k>$ values obtained for different PyLMs can be compared in a same solvent since all constructs share a same p value.

4.5 Conclusions

A library of four Py-PA samples and a Py_1-HA model compound were prepared by labeling hexylamine, HMDA, diaminodecane, and DETA with PyBA. The chemical composition of the different Py-PAs was confirmed by ^{1}H NMR. The SSF spectra of the Py-PA samples were acquired at a pyrene concentration of 2.5×10^{-6} M in THF, DMF, and DMSO. The fluorescence spectra reflected an increase in excimer formation with increasing $[Py]_{loc}$ and decreasing η, and a linear trend was obtained in each solvent studied by plotting the I_E/I_M ratio as a function of $[Py]_{loc}$. TRF measurements using dilute solutions of the Py_1-HA model compound in THF, DMF, and DMSO yielded τ_M which was fixed in the MFA of the TRF decays acquired with the Py-PA samples. The molar fractions f_{diff}, f_{agg}, and f_{free} obtained with the MFA of the monomer and excimer TRF decays retained similar values for all Py-PA samples and solvents used ($f_{diff} \geq 0.88$, $f_{agg} \leq 0.11$, and $f_{free} \leq 0.06$). This set of molar fractions suggested that THF, DMF, and DMSO were good solvents for the Py-PA samples which formed excimer mainly by diffusion. Linear $<k>$-*vs*-$[Py]_{loc}$ trends were

obtained for each solvent. These plots were used to determine k_{diff} which was found to increase with decreasing solvent viscosity. However, k_{diff} was not inversely proportional to solvent viscosity due to the solvent-dependent probability of PEF. Nevertheless, the linear trends obtained for both the I_E/I_M ratio and $<k>$ as a function of $[Py]_{loc}$ for these Py-PA samples suggest that Equation 4.3 could be used to build a calibration curve that would relate $<k>$ to $[Py]_{loc}$ for pyrenyl labels covalently attached onto polyamines either free in solution as in Chapter 4 or linking two PIBSA molecules in a PIBSI dispersant.

Chapter 5

Summary and Future Work

5.1 Summary of Thesis

Polyisobutylene succinimide (PIBSI) dispersants are an important component of engine oils which have seen increased use over the past 30 years.[1] To improve their properties, a better understanding is required of the chemical composition of both their succinic anhydride terminated polyisobutylene (PIBSA) precursors and polyamine cores. The polyamines used industrially are often of a low purity and have a variety of structures, meaning that the polar core of PIBSI dispersants is often poorly defined. Since the polar core is mostly involved in interactions with dispersed particulate or other oil additives, a greater understanding of the structure of a given PIBSI core is of great interest to those involved in dispersant design. Beside the poorly defined polyamine core of PIBSI dispersants, the presence of doubly-maleated PIBSA molecules ($PIBSA_2$) in PIBSA precursors add another layer of complication to the study of the succinic anhydride-to-polyamine coupling process to form PIBSI products. As such, the aim of this thesis was to use pyrene excimer formation (PEF) to gain further insights into the structure of PIBSI dispersants and their constituting PIBSA precursors by capitalizing on the work of Drs. Anna Mathew and Solmaz Pirouz in this area.[2,3]

The first goal of this thesis was to establish a procedure to determine the molar fraction (f_{doubly}) of doubly maleated $PIBSA_2$ chains in a PIBSA sample. It was implemented by considering two PIBSA samples, namely PIBSA-1 and PIBSA-2, which were labeled with 1-pyrenemethylamine (PyMA) in a manner similar to that reported in a previous study to yield several PIBSA-PyMA samples.[2]

PIBSA-1 and PIBSA-2 were labeled with PyMA to yield a fractionated *f*-PIBSA-1-PyMA and *f*-PIBSA-2-PyMA sample via precipitation of the PIBSA starting material, followed by the removal of low MW impurities and free PyMA from the PIBSA-PyMA reaction mixtures with

acetone. This fractionation was later found to result in a large shift of the molecular weight distribution (MWD) toward higher MWs with respect to the unprecipitated PIBSA precursor. By using extractions instead of precipitations, unfractionated *u*-PIBSA-1-PyMA and *u*-PIBSA-2-PyMA samples and one partially fractionated *pf*-PIBSA-2-PyMA sample were obtained. Analysis via FTIR yielded the N_{SA}/N_{IB} and N_{SI}/N_{IB} ratio of the number of SA and SI units over the number of isobutylene units for each PIBSA and PIBSA-PyMA sample, respectively. These ratios were found to increase two-fold from the *f*-PIBSA-PyMA to the *u*-PIBSA-PyMA samples. Similarly, the pyrene content (λ_{Py}) of the *u*-PIBSA-PyMA samples was double that of the *f*-PIBSA-PyMA samples. Analysis of the Peak-to-Valley ratio (P_A) by UV-Vis absorption measurements yielded $P_A < 3$ ($2.7<P_A<2.9$) for each PIBSA-PyMA sample which suggested some aggregation of the pyrenyl labels. The differences in MWD inferred by all FTIR and UV-Vis measurements were confirmed upon comparison of the DRI traces of the *f*- and *u*-PIBSA-PyMA samples obtained by gel permeation chromatography (GPC) analysis. They revealed a substantial loss of the lower MW portion of the PIBSA MWD for the *f*-PIBSA-PyMAs, and a very slight loss of the smallest MWs for the *pf*-PIBSA-2-PyMA sample. Analysis of the SSF spectra of solutions of the PIBSA-PyMA samples in THF revealed some reabsorption of the $S_0 \rightarrow S_1$ transition band and yielded linear trends when plotting I_E/I_M as a function of [*Py*]. Model free analysis (MFA) of the time-resolved fluorescence (TRF) decays of the PIBSA-PyMA samples yielded the average rate constant ($<k>$) of PEF and the molar fraction of aggregated pyrenes (f_{agg}). $<k>$ increased linearly with increasing [*Py*] while f_{agg} remained constant for each PIBSA-PyMA sample. The f_{agg} values were also fairly consistent with *f*- and *u*-PIBSA-1-PyMA taking values of 0.181 ± 0.006 and 0.165 ± 0.009, respectively, and the *f*-, *pf*-, and *u*-PIBSA-2-PyMA samples yielding f_{agg} values of 0.122 ± 0.013, 0.101 ± 0.004, and 0.124 ± 0.010, respectively. The PIBSA-1 sample yielded a higher f_{agg} value

and the consistency in f_{agg} regardless of whether the sample was fractionated or unfractionated suggested that $PIBSA_2$ was evenly distributed over the MWD of the PIBSA samples. The slope of the $<k>$-*vs*-[*Py*] plots yielded the bimolecular rate constant for PEF (k_{diff}) for each sample and k_{diff} was found to decrease linearly with increasing degree of polymerization as expected.

The second goal of this thesis was to investigate if the molar fractions of the mixtures resulting from the coupling reaction of a polyamine and a PIBSA sample could be predicted from the knowledge of f_{agg} determined by PEF measurements and the N_{Am}/N_{SA} and N_{SA}/N_{IB} ratios. To this end, a set of eight PIBSA-2-H(*X*) samples, where *X* equals N_{Am}/N_{SA}, were prepared by varying the N_{Am}/N_{SA} ratio from 0.25 to 2.0 in 0.25 increments. Comparison of the DRI traces of the PIBSA-2-H(*X*) samples from GPC revealed a shift towards higher MWs for N_{Am}/N_{SA} ratios increasing from 0.25 to 1.0, and a less significant shift back to lower MWs for N_{Am}/N_{SA} ratios increasing from 1.0 to 2.0. Fitting the DRI traces with sums of Gaussians provided mathematical expressions for each DRI trace which yielded the weight fractions (*wt-f*'s) of the PIBSA-like molecules (PLMs) which had the same MWD as PIBSA and the non-PIBSA-like molecules (non-PLMs) which had a MWD different from that of PIBSA. The *wt-f* of PLMs decreased from 0.91 to 0.36 for N_{Am}/N_{SA} ratios increasing from 0.25 to 1.0, before increasing slightly from 0.36 to 0.49 for N_{Am}/N_{SA} ratios increasing from 1.0 to 2.0. The *wt-f* of PLMs did not approach 0 for any N_{Am}/N_{SA} ratio contrary to what would have been expected upon using a N_{Am}/N_{SA} ratio of 1.0 which should favour complete coupling of PIBSA into *b*-PIBSI. When compared to PIB standards by GPC analysis, the MW of the PIBSA samples was notably lower than that calculated in Chapter 2, possibly due to differences in the initial precipitation of PIBSA before coupling. It was also noted that the non-PLM portion of each Gaussian fit of the DRI traces shared roughly the same MWD which inferred that the same PIBSI products were being produced in the PIBSA-HMDA coupling reaction regardless of

N_{Am}/N_{SA} ratio. It was hypothesized that the traces of the non-PLMs for the PIBSA-2-H(*X*) samples represented the MWD of the *b*-PIBSI product, and that steric hindrance could arise from the relatively short HMDA linker preventing coupling of more than one PIBSA to another PIBSA molecule, despite the presence of $PIBSA_2$. This conclusion led to the suggestion that these coupling reactions with a longer linker such as diaminododecane which may relieve steric hindrance, would enable the formation of higher-order PIBSI products.

Once the experimental data was analyzed, the simulation programs reaction3 and reaction4 were written in *Fortran* to couple *in silico* PIBSA samples and diamines to simulate a PIBSA-diamine coupling reaction producing PIBSI dispersants. These simulations took into account the ratios N_{Am}/N_{SA} and N_{SA}/N_{IB} and the molar fraction f_{doubly} of the PIBSA sample. The program reaction3 allowed oligomerization of the PIBSAs into *trimer*-PIBSI (*tri*-PIBSI) and higher-ordered PIBSIs with $PIBSA_2$. In contrast, the program reaction4 limited PIBSA coupling to the formation of *m*-PIBSI and *b*-PIBSI so that the reaction mixture could only contain PIBSA, *m*-PIBSI, and *b*-PIBSI present in different amounts depending on the N_{Am}/N_{SA} ratio used. These programs yielded the *wt-f*'s of PLMs and non-PLMs for each N_{Am}/N_{SA} ratio. In these simulations, PIBSA and *m*-PIBSI were viewed as PLMs, and their *wt-f*'s were compared to those found. The simulated *wt-f* s did reach 0 at a N_{Am}/N_{SA} ratio of 1, but otherwise showed the same sharp decrease for N_{Am}/N_{SA} ratios increasing from 0.25 to 1.0 followed by a slight increase for N_{Am}/N_{SA} ratios increasing from 1.0 to 2.0. This discrepancy along with others all suggested the presence of unmaleated PIB in the PIBSA-2 sample. Comparison of the *wt-f*'s of PLMs obtained by GPC analysis and the number fractions of PLMs obtained from the simulations suggested a *wt-f* of unmaleated PIB (w_{PIB}) of 0.30 (±0.08) for PIBSA-2. When the presence of 30 wt% of unmaleated PIB was assumed to contribute to the *wt-f* of the PLMs, great agreement was found between the plots of the experimental and

simulated *wt-f*'s of the PLMs as a function of the N_{Am}/N_{SA} ratio. A calibration curve was established with three broad MWD PIB standards to estimate the MWD of some PIBSI coupling products such as *b*-PIBSI, *tri*-PIBSI etc. based off the known MWD of PIBSA-2. Using the simulated MWDs of the PIBSI products with the simulated number fractions of PIBSI products, the profiles using the reaction4 program were shown to match the experimental data more closely than those produced with reaction3. As such, the DRI trace of the non-PLMs obtained from the PIBSA-2-H(1.0) sample was selected to represent *b*-PIBSI and the DRI traces of the PIBSA-2-H(*X*) reaction mixtures were simulated by using the experimentally determined DRI traces of PIBSA and *b*-PIBSI. This approach gave excellent agreement between the experimental and simulated DRI traces. In summary, the simulation programs appear to be a useful tool to predict the formation of PIBSI products by simply taking into account the ratios N_{Am}/N_{SA} and N_{SA}/N_{IB} and f_{doubly} of the PIBSA sample.

The third goal of this thesis was to assess whether PEF could be applied to probe the local concentration of amines in the polyamine core of a PIBSI dispersant. To this end, a series of pyrene-labeled polyamines (Py-PAs) were prepared by labeling hexylamine, hexamethylene diamine, diaminodecane, and the primary or all amines of diethylenetriamine (DETA) with 1-pyrenebutyric acid (PyBA) to generate Py_1-HA, Py_2-HMDA, Py_2-DEC, Py_2-DETA, and Py_3-DETA, respectively. Their I_E/I_M ratio and $<k>$ value were monitored as a function of $[Py]_{loc}$. Py_1-HA was first used to acquire the natural monomer lifetime (τ_M) of the Py-PAs which was fixed in the MFA of the TRF decays of the Py-PAs in THF, DMF, and DMSO. Analysis of the SSF spectra of the Py-PAs showed that the I_E/I_M ratio increased linearly with increasing $[Py]_{loc}$, as predicted theoretically. MFA of the TRF decays acquired with each Py-PA sample in THF, DMF, and DMSO yielded the molar fractions f_{diff}, f_{agg}, and f_{free} which gave fairly consistent values. The

fractions f_{diff} and f_{agg} were always large (≥ 0.88) and small ($f_{agg} \leq 0.11$), respectively, which suggested good solubility of the Py-PAs in the solvents used in the PEF experiments. MFA of the monomer and excimer TRF decays also confirmed the linear relationship between $<k>$ and $[Py]_{loc}$, thus suggesting that a calibration curve could be established with these samples to evaluate the amine content of other pyrene-labeled polyamines such as those in a PIBSI dispersant core.

In summary, this thesis has investigated the use of different methods to tackle some of the experimental challenges associated with the characterization of PIBSA/PIBSI molecules. While a variety of instruments and methodologies were used throughout this work, PEF was shown to be a powerful tool for probing some of the intricate and subtle differences between PIBSA samples. Simulation programs have been developed to take advantage of the parameter f_{doubly} which was determined by PEF experiments to better predict the products of a coupling reaction between PIBSA and a polyamine. The work with the Py-PAs suggests that the pyrene-labeling of the polyamine cores of PIBSIs could glean further insights into their complex structure. The experiments presented in this thesis have further established the usefulness of PEF for the characterization and understanding of oil additives.

5.2 Future Work

Dispersants remain an important engine oil additive today and are thus of interest for further characterization. In Chapters 2 and 3, the fraction f_{doubly} was calculated for a PIBSA sample and subsequently used to accurately predict the MWD of PIBSA-HMDA coupling products as they would appear in the DRI traces obtained from a GPC instrument. While the simulation program reaction4 gave the best agreement when assuming that steric hindrance prevented the formation of *tri*-PIBSI or higher-order PIBSI products, it would be reassuring to further validate this assumption

by repeating the coupling experiments with a longer diamine such as diaminodecane to see if the steric hindrance is alleviated. Expanding the reaction programs to incorporate other amine architectures such as triamines could be more useful for predicting the products of industrial coupling reactions using polyamines of unknown compositions.

While the relationships between the I_E/I_M ratio, $<k>$, and $[Py]_{loc}$ were shown to be linear over the $[Py]_{loc}$ range studied here, the library of Py-PAs could be expanded to cover a wider range of $[Py]_{loc}$ values, thus expanding the utility of such a calibration curve. This curve could also be used to analyze the SSF and TRF data obtained with pyrene-labeled polyamines constituting the core of PIBSIs.

Letters of Copyright Permission

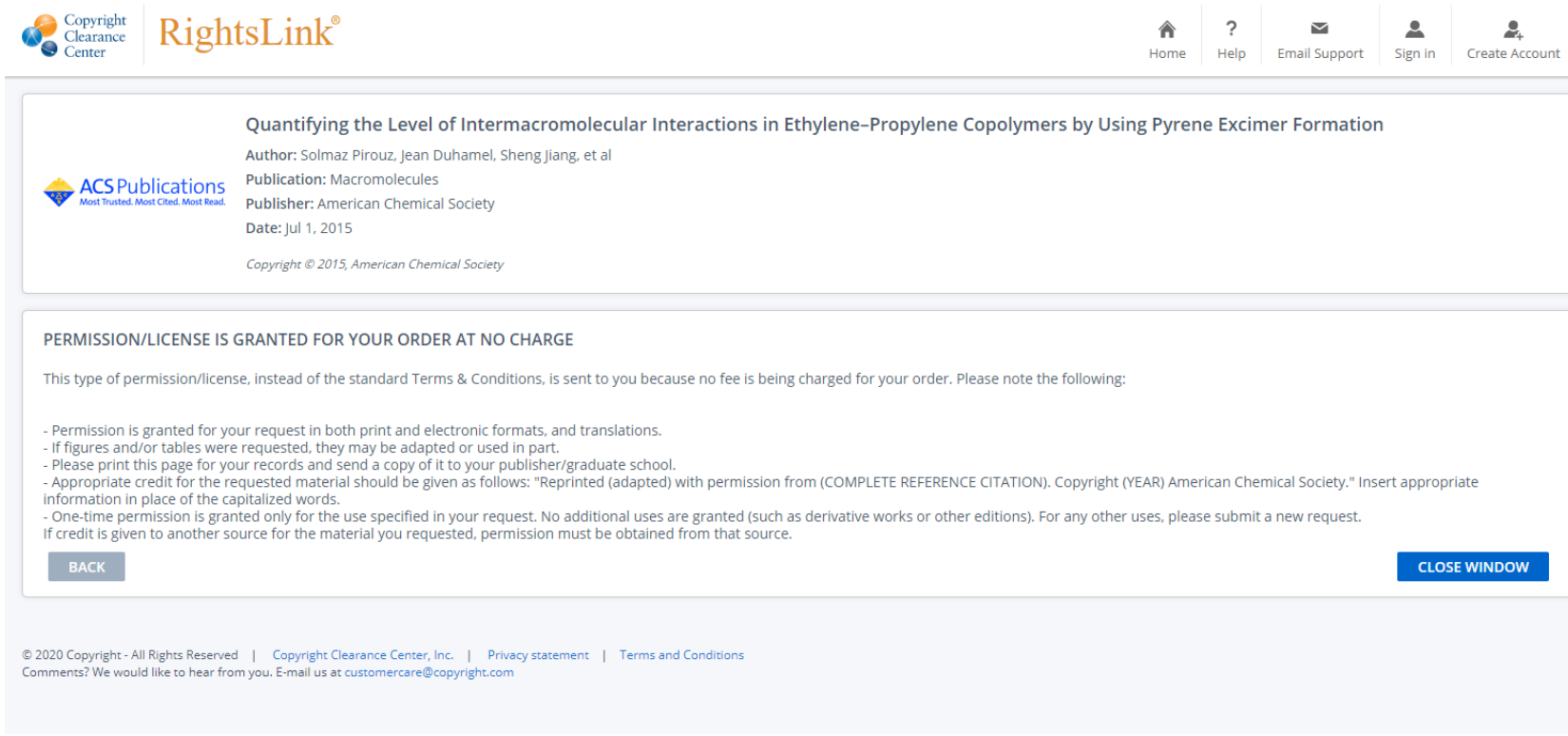

Copyright Clearance Center | RightsLink®

Home | Help | Email Support | Sign in | Create Account

ACS Publications
Most Trusted. Most Cited. Most Read.

Quantifying the Level of Intermacromolecular Interactions in Ethylene–Propylene Copolymers by Using Pyrene Excimer Formation

Author: Solmaz Pirouz, Jean Duhamel, Sheng Jiang, et al
Publication: Macromolecules
Publisher: American Chemical Society
Date: Jul 1, 2015

Copyright © 2015, American Chemical Society

PERMISSION/LICENSE IS GRANTED FOR YOUR ORDER AT NO CHARGE

This type of permission/license, instead of the standard Terms & Conditions, is sent to you because no fee is being charged for your order. Please note the following:

- Permission is granted for your request in both print and electronic formats, and translations.
- If figures and/or tables were requested, they may be adapted or used in part.
- Please print this page for your records and send a copy of it to your publisher/graduate school.
- Appropriate credit for the requested material should be given as follows: "Reprinted (adapted) with permission from (COMPLETE REFERENCE CITATION). Copyright (YEAR) American Chemical Society." Insert appropriate information in place of the capitalized words.
- One-time permission is granted only for the use specified in your request. No additional uses are granted (such as derivative works or other editions). For any other uses, please submit a new request.

If credit is given to another source for the material you requested, permission must be obtained from that source.

BACK | CLOSE WINDOW

References

Chapter 1

1. Pawlak, Z. In *Tribochemistry of lubricating oils;* Elsevier: Warsaw, **2003**, Vol. 45, 217-20.
2. Rizvi, S. Q. A.; edited by Rudnick, L. R. In *Chemistry and Applications: Lubricant Additives*. CRC Press, Boca Raton: Florida, 2017, pp 1-65.
3. Seddon, E. J.; Friend, C. L.; Roski, J. P. In *Chemistry and Technology of Lubricants*. Edited by Mortier, R. M.; Malcolm, F. F.; Orszulik, S. T. Springer: Netherlands, 2010, pp 213-236.
4. Rizvi, S. Q. A.; edited by Shah, R. J. In *Fuels and Lubricants Handbook*: Technology, Properties, Performance and Testing. ASTM International, West Conshohocken: PA, 2003, pp 199-248.
5. Arumugam, S.; Ellappan, R. The effect of Corrosion Inhibitor on Corrosion of Automotive Materials in Biodegradable Engine Oil. From *IOP Conf. Series: Materials Science and Engineering* 390, 2018.
6. Trigg, H. S.; Norris, H. D.; White, R. V. Antirust Agent. USP 2,540,800, 1951.
7. Inoue, K.; Watanabe, H. Interactions of Engine Oil Additives. *ASLE Transactions* **2008**, *26*, 189-199.
8. Matsuoka, M.; Arifuku, T.; Aoki, M.; Coy, C. R. The Determination of Additive Effects in a Japanese Valve Train Wear Test Using an Orthogonal Statistical Design. *SAE Paper* **1983**, 831761.
9. Fox, M. F.; Pawlak, Z.; Picken, D. J. Inverse Micelles and Solubilization of Proton Donors in Hydrocarbon Formulations. *Tribol. Int.* **1991**, *24*, 341-349.

10. Willermet, P. A. Some Engine Oil Additives and their Effects on Antiwear Film Formation. *Tribol. Lett.* **1998**, *5*, 41-47.
11. Sen, A.; Rubin, I. D. Molecular Structures and Solution Viscosities of Ethylene-Propylene Copolymers. *Macromolecules* **1990**, *23*, 2519-2524.
12. Forbes, E. S.; Neustadter, E. L. The Mechanism of Action of Polyisobutenyl Succinimide Lubricating Oil Additives. *Tribology* **1972,** *5*, 72-77.
13. Fang. L.; Zhang, X.; Ma, J.; Zhang, B. Investigation in to a Pour Point Depressant fo Shengli Crude Oil. *Ind. Eng. Chem. Res.* **2012**, *51*, 11605-11612.
14. Pendersen, K. S.; Rønningsen, H. P. Influence of Wax Inhibitor on Wax Appearance Temperature, Pour Point, and Viscosity of Waxy Crude Oils. *Energy Fuels* **2002**, *17*, 321-328.
15. Coleman, L. E. Lubricant Containing Nitrogen-Containing Ester USP 3,702,300, 1972.
16. Coleman, L. E. Nitrogen-Containing Ester and Lubricant Containing the Same. USP 3,933,761, 1976.
17. Meinhardt, N. A.; Davis, K. E. Novel Carboxylic Acid Acylating Agents, Derivatives Thereof, Concentrate and Lubricant Compositions Containing the Same, and Processes for Their Preparation. USP 4,234,435, 1980.
18. Tomlinson, A.; Danks, T. N.; Heyes, D. M.; Taylor, S. E.; Moreton, D. J. Interfacial Characterization of Succinimide Surfactants. *Langmuir* **1997**, *13*, 5881-5893.
19. Heilman, W. J.; Wilburn, B. E. Olefin Polymer Pour Point Depressants. USP 5,188,724, 1993.
20. Rudnick, L. R.; Bartz, W. J. In *Synthetics, Mineral Oils, and Bio-Based Lubricants;* Chemistry and Technology. CRC Press, Boca Raton: Florida, 2020, pp 359-376.

21. Cook, S. J.; O'Connor, S. P. European Patent 0,365,288 Application 1.

22. Gwinn, M. R.; Vallyathan, V. Nanoparticles: Health Effects – Pros and Cons. *Environ. Health Perspect.* **2006**, *114*, 1818-1825.

23. Aldajah, S.; Ajayi, O. O.; Fenske, G. R.; Goldblatt, I. L. Effect of Exhaust Gas Recirculation (EGR) Contamination of Diesel Engine Oil on Wear. *Wear* **2007**, *263*, 93-98.

24. Bardasz, E. A.; Cowling, S. V.; Ebeling, V. L.; George, H. F.; Graf, M. M.; Kornbrekke, R. E.; Ripple, D. E. Understanding Soot Mediated Oil Thickening Through Designed Experimentation – Part 1: Mack EM6-287, GM 6.2L. *SAE Technical Paper* **1995**, 925527.

25. Morris, J. R.; Roach, J. R. Lubricating Oils Containing Metal Derivatives of Cyclic Imides. USP 2,628,942, 1953.

26. Drummond, A. Y.; Anderson, R. G.; Stuart, F. A. Alkenyl Succinimides of Piperazines. USP 3,024,237, 1962.

27. Mekewi, M. A. Synthesis and Characterization of Antioxidants and Detergent Dispersant Based on some Poluisobutylene Copolymers. *Mat. Res. Innovat.* **2002**, *6*, 214-217.

28. Ahmed, N. S.; Nassar, A. M.; Abdel-Hameed, H. S.; El-Kafrawy, A. F. Preparation, Characterization, and Evaluation of some Ashless Detergent/Dispersant Additives for Lubricating Engine Oil. *Appl. Petrochem. Res.* **2015**, *6*, 49-58.

29. Tomlinson, A.; Danks, T. N.; Heyes, D. M.; Taylor, S. E.; Moreton, D. J. Interfacial Characterization of Succinimide Surfactants. *Langmuir* **1997**, *13*, 5881-5893.

30. Otto, F. P. High Molecular Weight Mannich Bases as Engine Oil Additives. USP 3,368,972, 1968.

31. Harrison, J. J.; Young, D. C.; Mayne, C. L. 2D-INADEQUATE Structural Assignment of Polybutene Oligomers. *J. Org. Chem.* **1997**, *62*, 693-699.

32. Le Suer, W. M.; Norman, G. R. Reaction Product of High Molecular Weight Succinic Acids and Succinic Anhydrides with an Ethylene Polyamine. USP 3,172,892, 1965.

33. Stuart, F. A.; Anderson, R. G.; Drummond, A. Y. Alkenyl Succinimides of Tetraethylene Pentamine. USP 3,202,678, 1965.

34. Pucci, A.; Rausa, R.; Ciardelli, F. Aggregation-Induced Luminescence of Polyisobutylene Succinic Anhydrides and Imides. *Macromol. Chem. Phys.* **2008**, *209*, 900-906.

35. Walch, E.; Gaymans, R. J. Telechelic Polyisobutylene with Unsaturated End Groups and with Anhydride End Groups. *Polymer* **1994**, *35*, 1774-1778.

36. Shen, Y.; Duhamel, J. Micellization and Adsorption of a Series of Succinimide Dispersants. *Langmuir* **2008**, *24*, 10665-10673.

37. Wollenburg, R. H.; Plavac, F.; Erdman, T. R. Modified Succinimides. USP 4,612,132, 1986.

38. Karol, T. J.; Magaha, H. S. Borate Esters of Hydrocarbyl-Substituted Mono and Bis-Succinimides Containing Polyamine Chain Linked Hydroxyacyl Groups and Lubricating Oil Compositions Containing Same. USP 4,554,086, 1985.

39. Pirouz, S.; Wang, Y.; Chong, M.; Duhamel, J. Characterization of the Chemical Composition of Polyisobutylene-Based Oil-Soluble Dispersants by Fluorescence. *J. Phys. Chem. B.* **2014**, *118*, 3899-3911.

40. Pirouz, S.; Wang, Y.; Chong, M.; Duhamel, J. Chemical Modification of Polyisobutylene Succinimide Dispersants and Characterization of Their Associative Properties. *J. Phys. Chem. B* **2015**, *119*, 12202-12211.

41. Pirouz, S.; Jiang, S.; Duggal, A.; Duhamel, J. Quantifying the Level of Intermolecular Interactions in Ethylene-Propylene Copolymers by Using Pyrene Excimer Formation. *Macromolecules* **2015**, *48*, 4620-4630.

42. Mathew, A. K.; Duhamel, J. Maleic Anhydride Modified Oligo(isobutylene): Effect of Hydrogen Bonding on Its Associative Strength in Hexane Characterized by Fluorescence Spectroscopy. *Macromolecules* **2001**, *34*, 1454-1469.

43. Gholami, K.; Jiang, S.; Duhamel, J. Probing the Interactions between Mimics of Pour Point Depressants (PPDs) and Viscosity Index Improvers (VIIs) in Engine Oil Using Fluorescently Labeled PPDs *Macromolecules.* **2019**, *52*, 2651-2658.

44. Lakowicz, J. R. *Principles of Fluorescence Spectroscopy.* 3rd ed. Springer: New York, NY, USA, 2006.

45. Kalyanasundaram, K.; Thomas, J. K. Environmental Effects on Vibronic Band Intensities in Pyrene Monomer Fluorescence and their Application in Studies of Micellar Systems. *J. Am. Chem. Soc.* **1977**, *99*, 2039-2044.

46. Fowler, M. A.; Duhamel, J.; Bahun, G. J.; Adronov, A.; Zaragoza-Galán, G.; Rivera, E. Studying Pyrene-Labeled Macromolecules with the Model-Free Analysis. *J. Phys. Chem. B* **2012**, *116*, 14689-14699.

47. Duhamel, J. Global Analysis of Fluorescence Decays to Probe the Internal Dynamics of Fluorescently Labeled Macromolecules. *Langmuir* **2014**, *30*, 2307-2324.

48. Zachariasse, K.; Kühnle, W. Intramolecular Excimers. *J. Photochem.* **1976**, *5*, 166-167.

49. Zachariasse, K. A.; Busse, R.; Duveneck, G.; Kühnle, W. Intramolecular Monomer and Excimer Fluorescence with Dipyrenylpropanes: Double-exponential *Versus* Triple-exponential Decays. *J. Photochem.* **1985**, *28*, 237-253.

50. Mathew, A. K.; Siu, H.; Duhamel, J. A Blob Model to Study Chain Folding by Fluorescence. *Macromolecules* **1999**, *32*, 7100-7108.

51. Cuniberti, C.; Perico, A. Intramolecular Excimers and Micro-Brownian Motion of Flexible Polymer Molecules in Solution. *Eur. Polym. J.* **1977**, *13*, 369-374.

52. Redpath, T.; Richards, D. H.; Winnik, M. A. The Dynamics of End-to-End Cyclization in Polystyrene Probed by Pyrene Excimer Formation. *Macromolecules* **1980**, *13*, 328-335.

53. Winnik, M. A.; Redpath, A. E. C.; Paton, K.; Danhelka, J. Cyclization dynamics of polymers: 10 Synthesis, fractionation, and fluorescent spectroscopy of pyrene end-capped polystyrenes. *Polymers.* **1984**, *25*, 91-99.

54. Jao, T. C.; Mishra, M. K.; Rubin, I. D. Studies on Ethylene-Propylene Copolymer in Hydrocarbon Solvents by Fluorescence Probe Method. *J. Macromol. Sci. Part A Pure Appl. Chem.* **1992**, *29*, 283-292.

55. Winnik, F. M. Photophysics of Preassociated Pyrenes in Aqueous Polymer Solutions and in Other Organized Media. *Chem. Rev.* **1993**, *93*, 587-614.

56. Duhamel, J. Internal Dynamics of Dendritic Molecules Probed by Pyrene Excimer Formation. *Polymers* **2012**, *4*, 211-239.

57. Yip, J.; Bahun, G. J.; Duhamel, J.; Adronov, A. A Study of the Dynamics of the Branch Ends of a Series of Pyrene-Labeled Dendrimers Based on Pyrene Excimer Formation. *J. Phys. Chem. B* **2010**, *114*, 10254-10265.

58. Chen, S.; Bahun, G. J.; Duhamel, J.; Adronov, A. Quantifying the Presence of Unwanted Fluorescent Species in the Study of Pyrene-Labeled Macromolecules. *J. Phys. Chem. B* **2011**, *115*, 9921-9929.

59. McNelles, S. A.; Thoma, J. L.; Adronov, A.; Duhamel, J. Quantitative Characterization of the Molecular Dimensions of Flexible Dendritic Macromolecules in Solution by Pyrene Excimer Fluorescence. *Macromolecules* **2018**, *51*, 1586-1590.

Chapter 2

1. Rizvi, S. Q. A.; edited by Rudnick, L. R. In *Chemistry and Applications:* Lubricant Additives. CRC Press, Boca Raton: Florida, 2017, pp 45-65.

2. Seddon, E. J.; Friend, C. L.; Roski, J. P. In *Chemistry and Technology of Lubricants*. Eds. Mortier, R. M.; Malcolm, F. F.; Orszulik, S. T. Springer: Netherlands, 2010, pp 213-236.

3. Pawlak, Z. In *Tribochemistry of lubricating oils;* Elsevier: Warsaw, **2003**, *45*, 217-20.

4. Morris, J. R.; Roach, J. R. Lubricating Oils Containing Metal Derivatives of Cyclic Imides. USP 2,628,942, 1953.

5. Trigg, H. S.; Norris, H. D.; White, R. V. Antirust Agent. USP 2,540,800, 1951.

6. Coleman, L. E. Lubricant Containing Nitrogen-Containing Ester USP 3,702,300, 1972.

7. Coleman, L. E. Nitrogen-Containing Ester and Lubricant Containing the Same. USP 3,933,761, 1976.

8. Forbes, E. S.; Neustadter, E. L. The Mechanism of Action of Polyisobutenyl Succinimide Lubricating Oil Additives. *Tribology* **1972,** *5,* 72-77.

9. Meinhardt, N. A.; Davis, K. E. Novel Carboxylic Acid Acylating Agents, Derivatives Thereof, Concentrate and Lubricant Compositions Containing the Same, and Processes for Their Preparation. USP 4,234,435, 1980.

10. Drummond, A. Y.; Anderson, R. G.; Stuart, F. A. Alkenyl Succinimides of Piperazines. USP 3,024,237, 1962.

11. Mekewi, M. A. Synthesis and Characterization of Antioxidants and Detergent Dispersant Based on some Poluisobutylene Copolymers. *Mat. Res. Innovat.* **2002**, *6,* 214-217.

12. Ahmed, N. S.; Nassar, A. M.; Abdel-Hameed, H. S.; El-Kafrawy, A. F. Preparation, Characterization, and Evaluation of some Ashless Detergent/Dispersant Additives for Lubricating Engine Oil. *Appl. Petrochem. Res.* **2015**, *6,* 49-58.

13. Tomlinson, A.; Danks, T. N.; Heyes, D. M.; Taylor, S. E.; Moreton, D. J. Interfacial Characterization of Succinimide Surfactants. *Langmuir* **1997,** *13,* 5881-5893.

14. Otto, F. P. High Molecular Weight Mannich Bases as Engine Oil Additives. USP 3,368,972, 1968.

15. Harrison, J. J.; Young, D. C.; Mayne, C. L. 2D-INADEQUATE Structural Assignment of Polybutene Oligomers. *J. Org. Chem.* **1997**, *62,* 693-699.

16. Le Suer, W. M.; Norman, G. R. Reaction Product of High Molecular Weight Succinic Acids and Succinic Anhydrides with an Ethylene Polyamine. USP 3,172,892, 1965.

17. Stuart, F. A.; Anderson, R. G.; Drummond, A. Y. Alkenyl Succinimides of Tetraethylene Pentamine. USP 3,202,678, 1965.

18. Shen, Y.; Duhamel, J. Micellization and Adsorption of a Series of Succinimide Dispersants. *Langmuir* **2008**, *24*, 10665-10673.

19. Pucci, A.; Rausa, R.; Ciardelli, F. Aggregation-Induced Luminescence of Polyisobutylene Succinic Anhydrides and Imides. *Macromol. Chem. Phys.* **2008**, *209*, 900-906.

20. Walch, E.; Gaymans, R. J. Telechelic Polyisobutylene with Unsaturated End Groups and with Anhydride End Groups. *Polymer* **1994**, *35*, 1774-1778.

21. Pirouz, S.; Wang, Y.; Chong, M.; Duhamel, J. Characterization of the Chemical Composition of Polyisobutylene-Based Oil-Soluble Dispersants by Fluorescence. *J. Phys. Chem. B.* **2014**, *118*, 3899-3911.

22. Mathew, A. K.; Duhamel, J. Maleic Anhydride Modified Oligo(isobutylene): Effect of Hydrogen Bonding on Its Associative Strength in Hexane Characterized by Fluorescence Spectroscopy. *Macromolecules* **2001**, *34*, 1454-1469.

23. Press, W. H.; Flannery, B. P.; Teukolsky, S. A.; Vetterling, W. T. *Numerical Recipes. The Art of Scientific Computing (Fortran Version)*; Cambridge University Press: Cambridge, 1992.

24. Gholami, K.; Jiang, S.; Duhamel, J. Probing the Interactions between Minics of Pour Point Depressants (PPDs) and Vicosity Index Improvers (VIIs) in Engine Oil Using Fluorescently Labeled PPDs *Macromoleculs.* **2019**, *52*, 2651-2658.

25. Pirouz, S.; Jiang, S.; Duggal, A.; Duhamel, J. Quantifying the Level of Intermacromolecular Interactions in Ethylene-Propylene Copolymers by Using Pyrene Excimer Formation. *Macromolecules*, **2015**, *48*, 4620-4630.

26. Winnik, F. M. Photophysics of Preassociated Pyrenes in Aqueous Polymer Solutions and in Other Organized Media. *Chem. Rev.* **1993**, *93*, 587-614.

27. Kiarash Gholami, MSc Thesis, Associations between Oil Additives in Base Oils Probed by Pyrene Excimer Fluorescence. University of Waterloo, **2017**.

28. Solmaz Pirouz, PhD Thesis, Quantitative Characterization of Polymeric Engine Oil Additives in Solution by Fluorescence. University of Waterloo, **2015**.

Chapter 3

1. Pawlak, Z. In Tribochemistry of lubricating oils; Elsevier: Warsaw, Poland, 2003; Vol. 45.
2. Rizvi, S. Q. A.; edited by Rudnick, L. R. In Chemistry and Applications: Lubricant Additives. CRC Press, Boca Raton: Florida, **2017**, pp 45-65.
3. Seddon, E. J.; Friend, C. L.; Roski, J. P. In Chemistry and Technology of Lubricants. Eds. Mortier, R. M.; Malcolm, F. F.; Orszulik, S. T. Springer: Netherlands, **2010**, pp 213-236.
4. Inoue, K.; Watanabe, H. Interactions of Engine Oil Additives. ASLE Transactions **2008**, *26*, 189-199.
5. Matsuoka, M.; Arifuku, T.; Aoki, M.; Coy, C. R. The Determination of Additive Effects in a Japanese Valve Train Wear Test Using an Orthogonal Statistical Design. SAE Paper **1983**, 831761.
6. Willermet, P. A. Some Engine Oil Additives and their Effects on Antiwear Film Formation. Tribol. Lett. **1998**, *5*, 41-47.
7. Fox, M. F.; Pawlak, Z.; Picken, D. J. Inverse Micelles and Solubilization of Proton Donors in Hydrocarbon Formulations. Tribol. Int. **1991**, *24*, 341-349.
8. Aldajah, S.; Ajayi, O. O.; Fenske, G. R.; Goldblatt, I. L. Effect of Exhaust Gas Recirculation (EGR) Contamination of Diesel Engine Oil on Wear. Wear **2007**, *263*, 93-98.
9. Yu, R. C.; Syed, M. S. Effects of Injection Timing and Exhaust Gas Recirculation on Emissions from a D.I. Diesel Engine. *SAE Technical Paper* **1981**, 811234.

10. Gwinn, M. R.; Vallyathan, V. Nanoparticles: Health Effects – Pros and Cons. Environ. Health Perspect. **2006**, *114*, 1818-1825.
11. Rizvi, S. Q. A.; edited by Shah, R. J. In Fuels and Lubricants Handbook: Technology, Properties, Performance and Testing. ASTM International, West Conshohocken: PA, **2003**, pp 199-248.
12. Pucci, A.; Rausa, R.; Ciardelli, F. Aggregation-Induced Luminescence of Polyisobutylene Succinic Anhydrides and Imides. Macromol. Chem. Phys. **2008**, *209*, 900-906.
13. Walch, E.; Gaymans, R. J. Telechelic Polyisobutylene with Unsaturated End Groups and with Anhydride End Groups. Polymer **1994**, *35*, 1774-1778.
14. Mathew, A. K.; Duhamel, J. Maleic Anhydride Modified Oligo(isobutylene): Effect of Hydrogen Bonding on Its Associative Strength in Hexane Characterized by Fluorescence Spectroscopy. Macromolecules **2001**, *34*, 1454-1469.
15. Pirouz, S.; Wang, Y.; Chong, M.; Duhamel, J. Characterization of the Chemical Composition of Polyisobutylene-Based Oil-Soluble Dispersants by Fluorescence. J. Phys. Chem. B. **2014**, *118*, 3899-3911.
16. Press, W. H.; Flannery, B. P.; Teukolsky, S. A.; Vetterling, W. T. Numerical Recipes. The Art of Scientific Computing (Fortran Version); Cambridge University Press: Cambridge, **1992**.

Chapter 4

1. Rizvi, S. Q. A.; edited by Rudnick, L. R. In *Chemistry and Applications: Lubricant Additives*. CRC Press, Boca Raton: Florida, 2017, pp 1-65 & 452-458.

2. Seddon, E. J.; Friend, C. L.; Roski, J. P. In *Chemistry and Technology of Lubricants*. Edited by Mortier, R. M.; Malcolm, F. F.; Orszulik, S. T. Springer: Netherlands, 2010, pp 213-236.

3. Pirouz, S.; Wang, Y.; Chong, M.; Duhamel, J. Characterization of the Chemical Composition of Polyisobutylene-Based Oil-Soluble Dispersants by Fluorescence. *J. Phys. Chem. B.* **2014**, *118,* 3899-3911.

4. Redpath, T.; Richards, D. H.; Winnik, M. A. The Dynamics of End-to-End Cyclization in Polystyrene Probed by Pyrene Excimer Formation. *Macromolecules* **1980**, *13*, 328-335.

5. Winnik, M. A.; Redpath, A. E. C.; Paton, K.; Danhelka, J. Cyclization dynamics of polymers: 10 Synthesis, fractionation, and fluorescent spectroscopy of pyrene end-capped polystyrenes. *Polymers.* **1984**, *25*, 91-99.

6. Jao, T. C.; Mishra, M. K.; Rubin, I. D. Studies on Ethylene-Propylene Copolymer in Hydrocarbon Solvents by Fluorescence Probe Method. *J. Macromol. Sci. Part A Pure Appl. Chem.* **1992**, *29*, 283-292.

7. Mathew, A. K.; Siu, H.; Duhamel, J. A Blob Model to Study Chain Folding by Fluorescence. *Macromolecules* **1999**, *32*, 7100-7108.

8. Mathew, A. K.; Duhamel, J. Maleic Anhydride Modified Oligo(isobutylene): Effect of Hydrogen Bonding on Its Associative Strength in Hexane Characterized by Fluorescence Spectroscopy. *Macromolecules* **2001**, *34,* 1454-1469.

9. Siu, H.; Duhamel, J. Comparison of the Association Level of a Pyrene-Labeled Associative Polymer Obtained from an Analysis Based on Two Different Models. *J. Phys. Chem. B* **2005**, *109*, 1770-1780.

10. Yip, J.; Bahun, G. J.; Duhamel, J.; Adronov, A. A Study of the Dynamics of the Branch Ends of a Series of Pyrene-Labeled Dendrimers Based on Pyrene Excimer Formation. *J. Phys. Chem. B* **2010**, *114*, 10254-10265.

11. Gholami, K.; Jiang, S.; Duhamel, J. Probing the Interactions between Mimics of Pour Point Depressants (PPDs) and Viscosity Index Improvers (VIIs) in Engine Oil Using Fluorescently Labeled PPDs *Macromolecules.* **2019**, *52*, 2651-2658.

12. McNelles, S. A.; Thoma, J. L.; Adronov, A.; Duhamel, J. Quantitative Characterization of the Molecular Dimensions of Flexible Dendritic Macromolecules in Solution by Pyrene Excimer Fluorescence. *Macromolecules* **2018**, *51*, 1586-1590.

13. Press, W. H.; Flannery, B. P.; Teukolsky, S. A.; Vetterling, W. T. *Numerical Recipes. The Art of Scientific Computing (Fortran Version)*; Cambridge University Press: Cambridge, 1992.

14. Hall, T.; Whitton, G.; Casier, R.; Gauthier, M.; Duhamel, J. Arborescent Poly(*L*-glutamic acid)s as Standards To Study the Dense Interior of Polypeptide Mesoglobules by Pyrene Excimer Fluorescence. *Macromolecules* **2018**, *51*, 7914-7923.

Chapter 5

1. Rizvi, S. Q. A.; edited by Rudnick, L. R. In *Chemistry and Applications: Lubricant Additives*. CRC Press, Boca Raton: Florida, 2017, pp 1-65 & 452-458.

2. Mathew, A. K.; Duhamel, J. Maleic Anhydride Modified Oligo(isobutylene): Effect of Hydrogen Bonding on Its Associative Strength in Hexane Characterized by Fluorescence Spectroscopy. *Macromolecules* **2001**, *34*, 1454-1469.

3. Pirouz, S.; Wang, Y.; Chong, M.; Duhamel, J. Characterization of the Chemical Composition of Polyisobutylene-Based Oil-Soluble Dispersants by Fluorescence. *J. Phys. Chem. B.* **2014**, *118*, 3899-3911.

Appendices

Appendix A – Supporting Information for Chapter 2

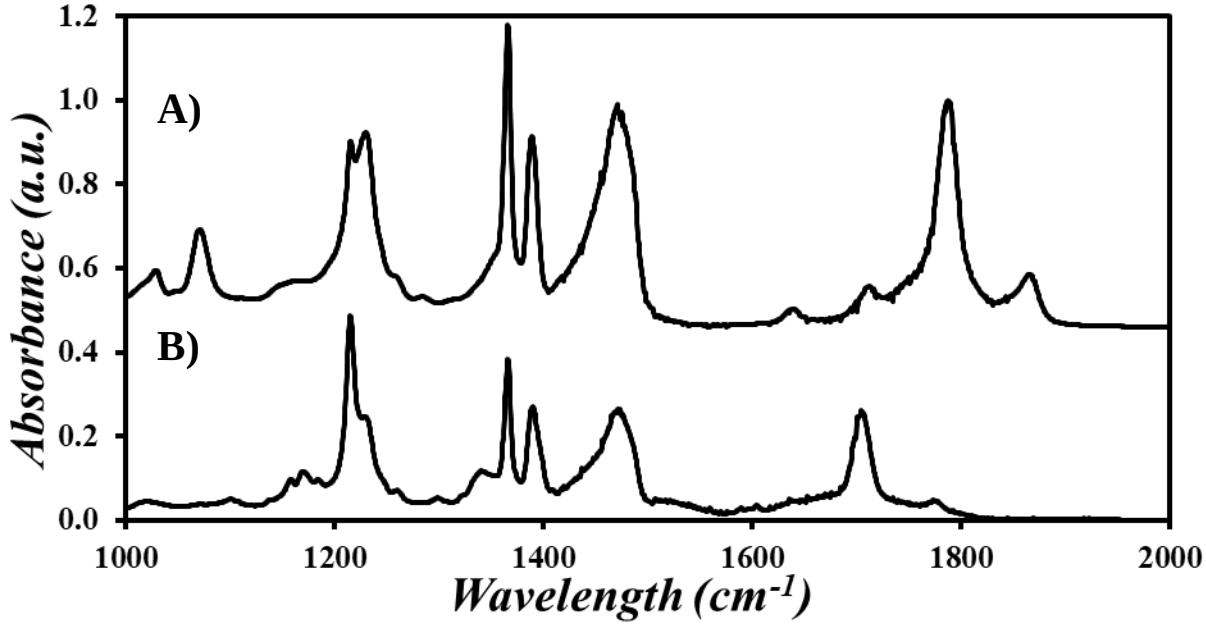

Figure A1. FTIR spectra of fractionated PIBSA-1 that was A) dehydrated and B) PyMA-labeled.

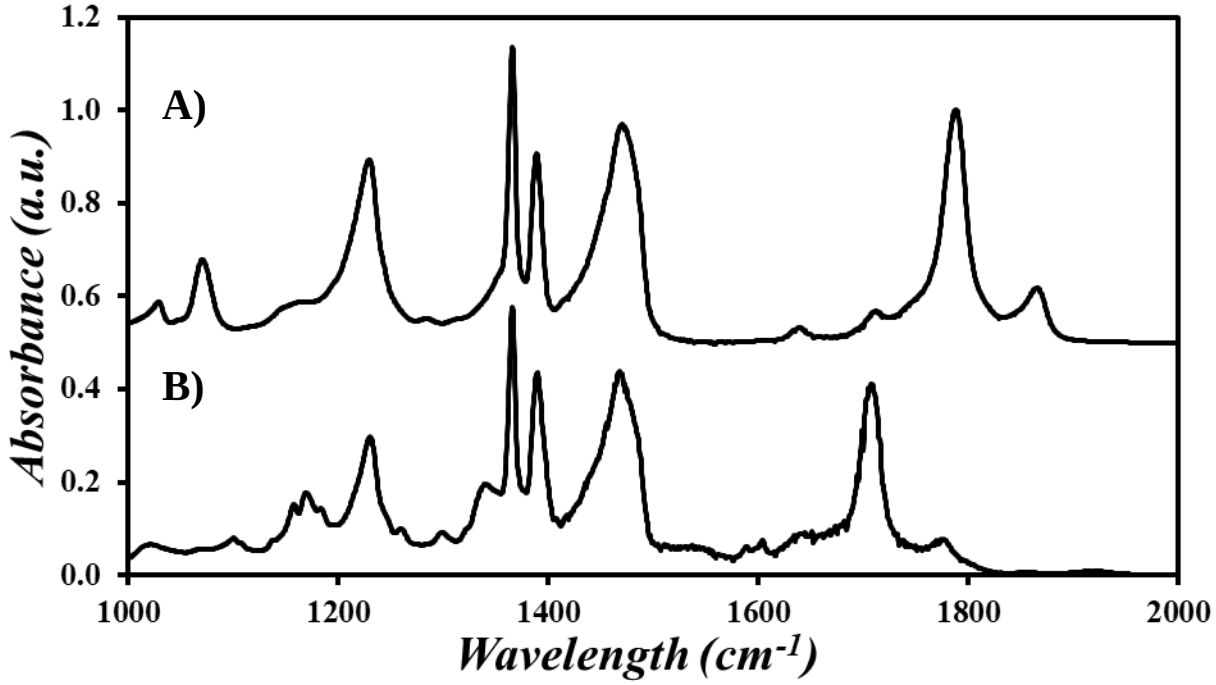

Figure A2. FTIR spectra of partially fractionated PIBSA-2 that was A) dehydrated and B) PyMA-labeled.

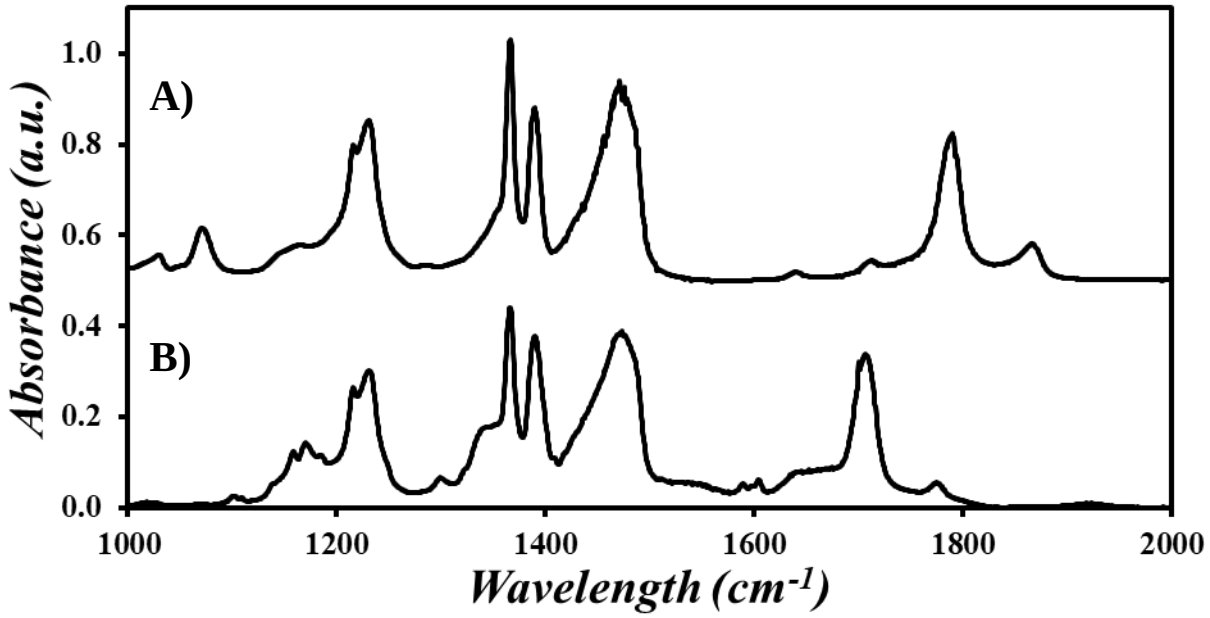

Figure A3. FTIR spectra of unfractionated PIBSA-2 that was A) dehydrated and B) PyMA-labeled.

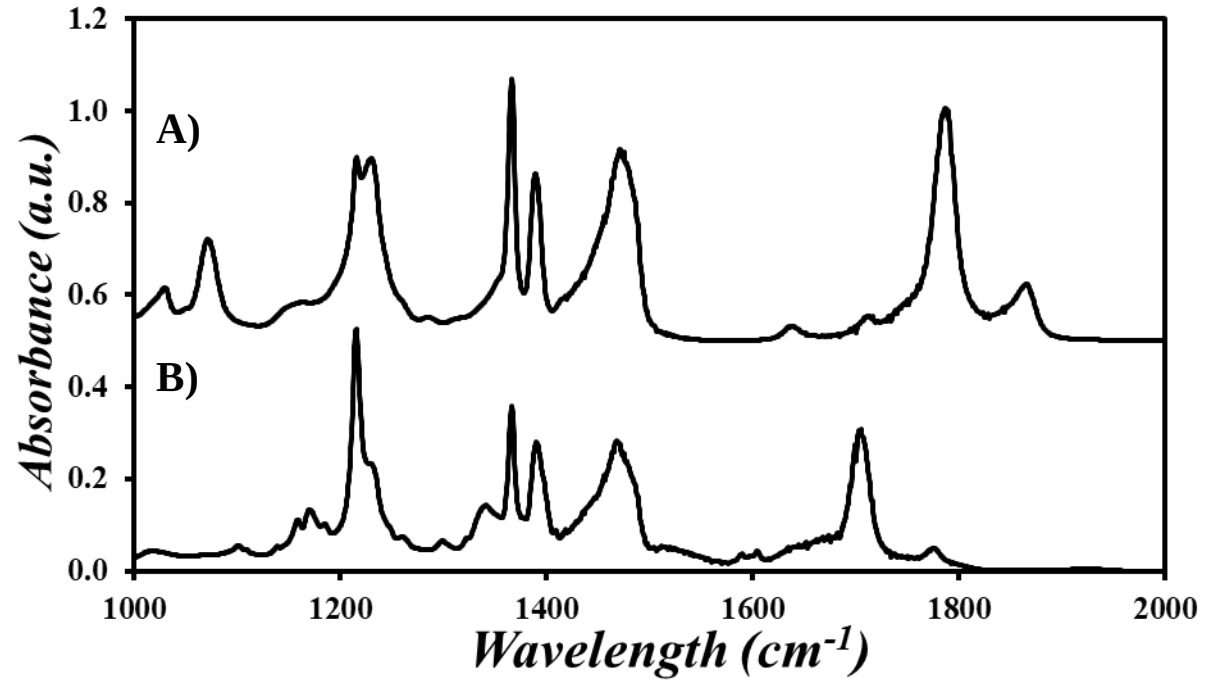

Figure A4. FTIR spectra of unfractionated PIBSA-1 that was A) dehydrated and B) PyMA-labeled.

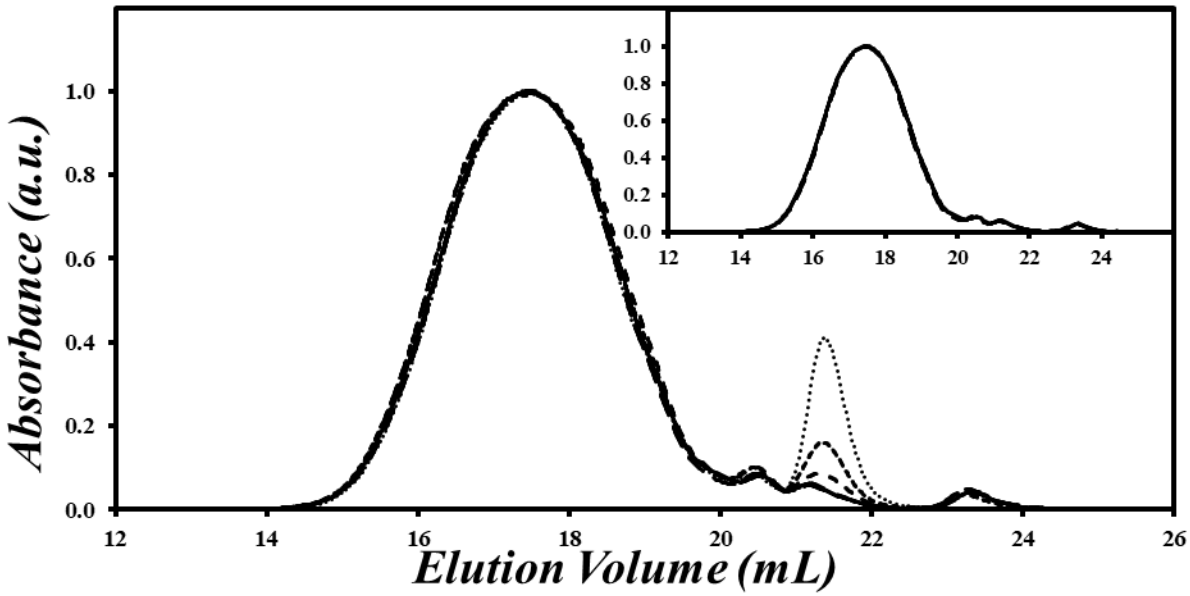

Figure A5. GPC analysis of *u*-PIBSA-1-PyMA with the UV-Vis absorption detector of the crude product (dotted line), successive extractions with 1 M HCl (dashed lines) and the final product (solid line), normalized to the peak maxima. Insert: GPC traces of *u*-PIBSA-1-PyMA after the last two extractions.

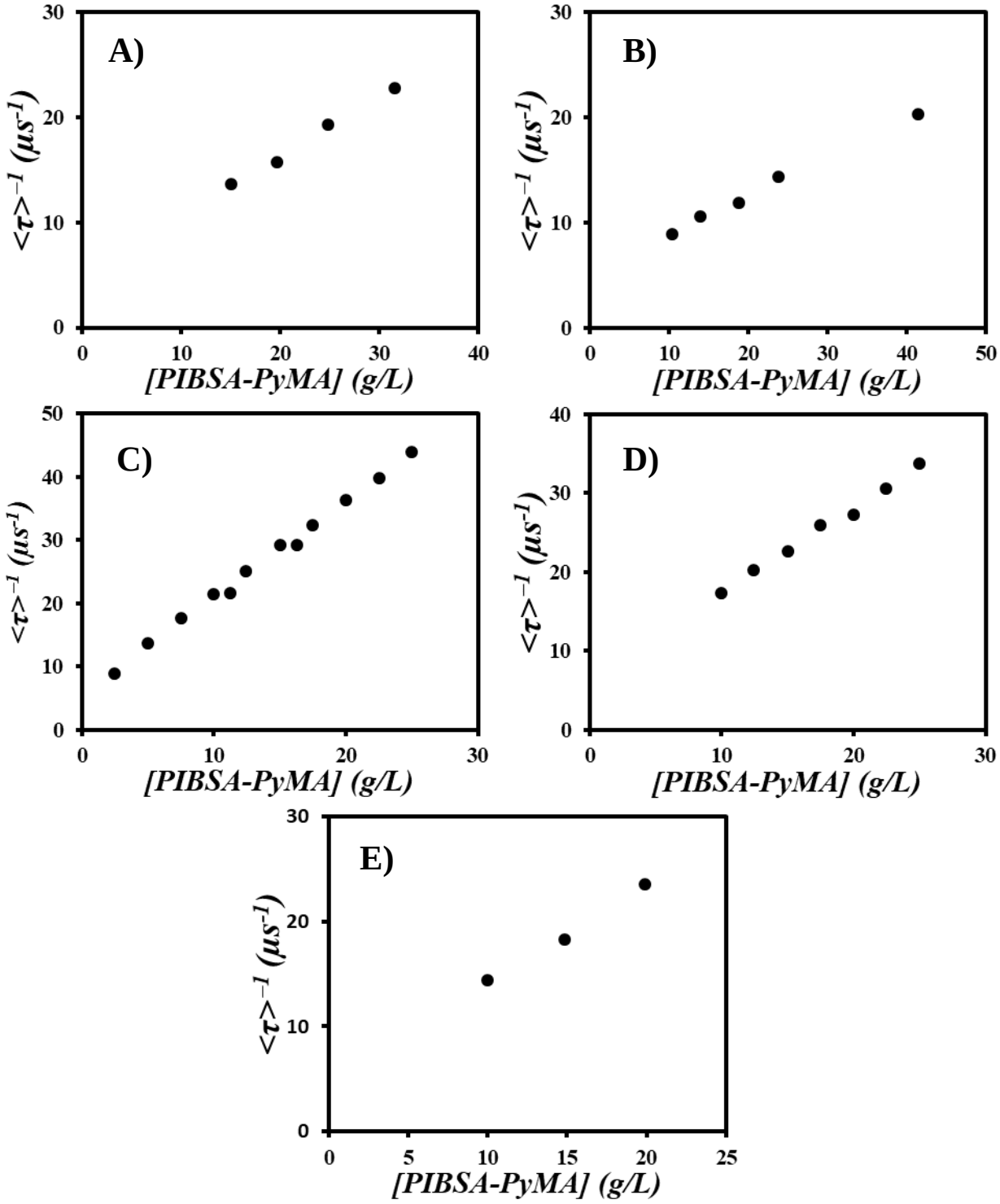

Figure A6. Plots of $<\tau>^{-1}$ vs. [*PIBSA-PyMA*] for A) *f*-PIBSA-1-PyMA, B) *f*-PIBSA-2-PyMA, C) *u*-PIBSA-1-PyMA, D) *u*-PIBSA-2-PyMA, and E) *pf*-PIBSA-2-PyMA.

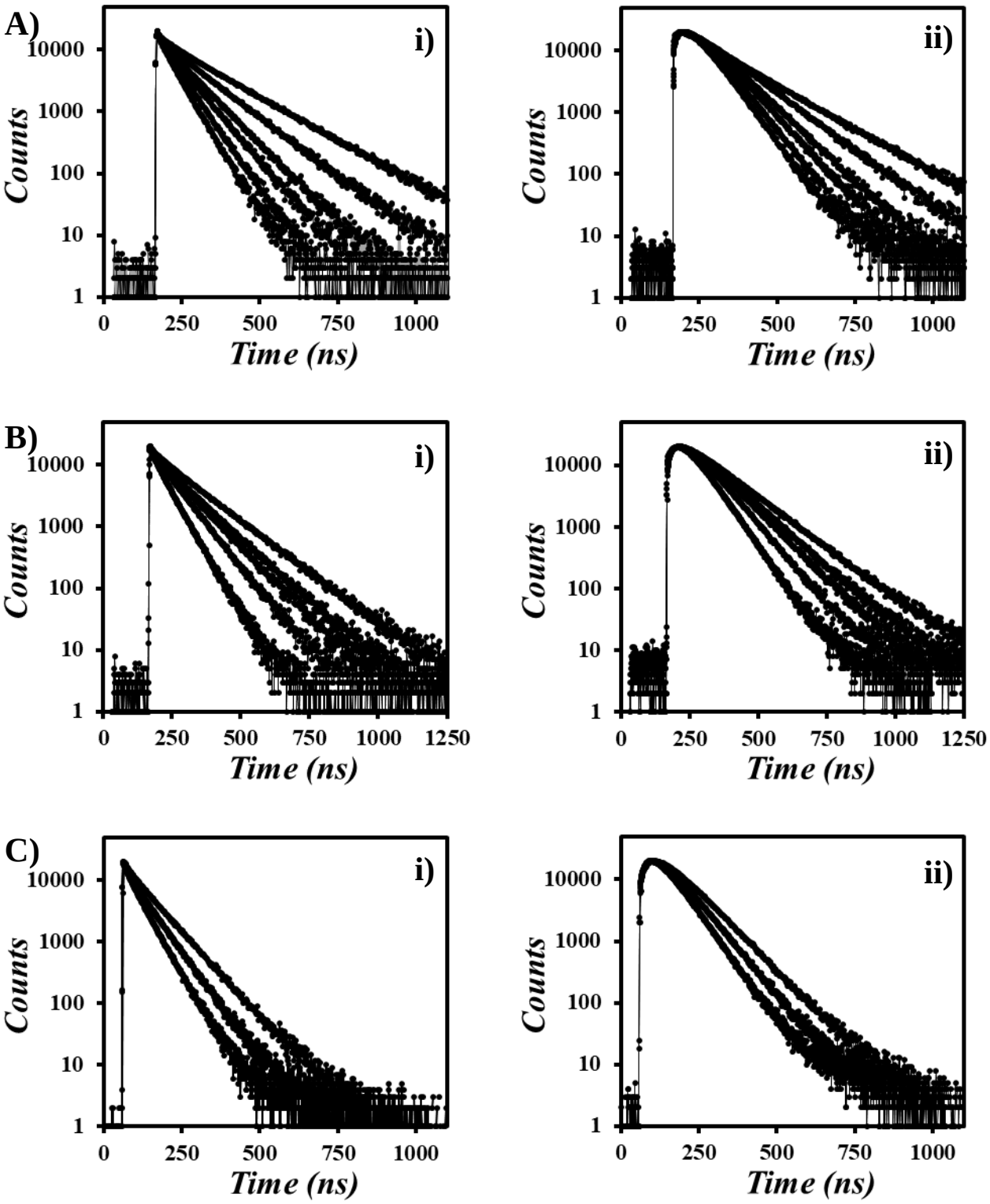
A)
i)
ii)
B)
i)
ii)
C)
i)
ii)
Counts
Time (ns)
10000
1000
100
10
1
0
250
500
750
1000
1250

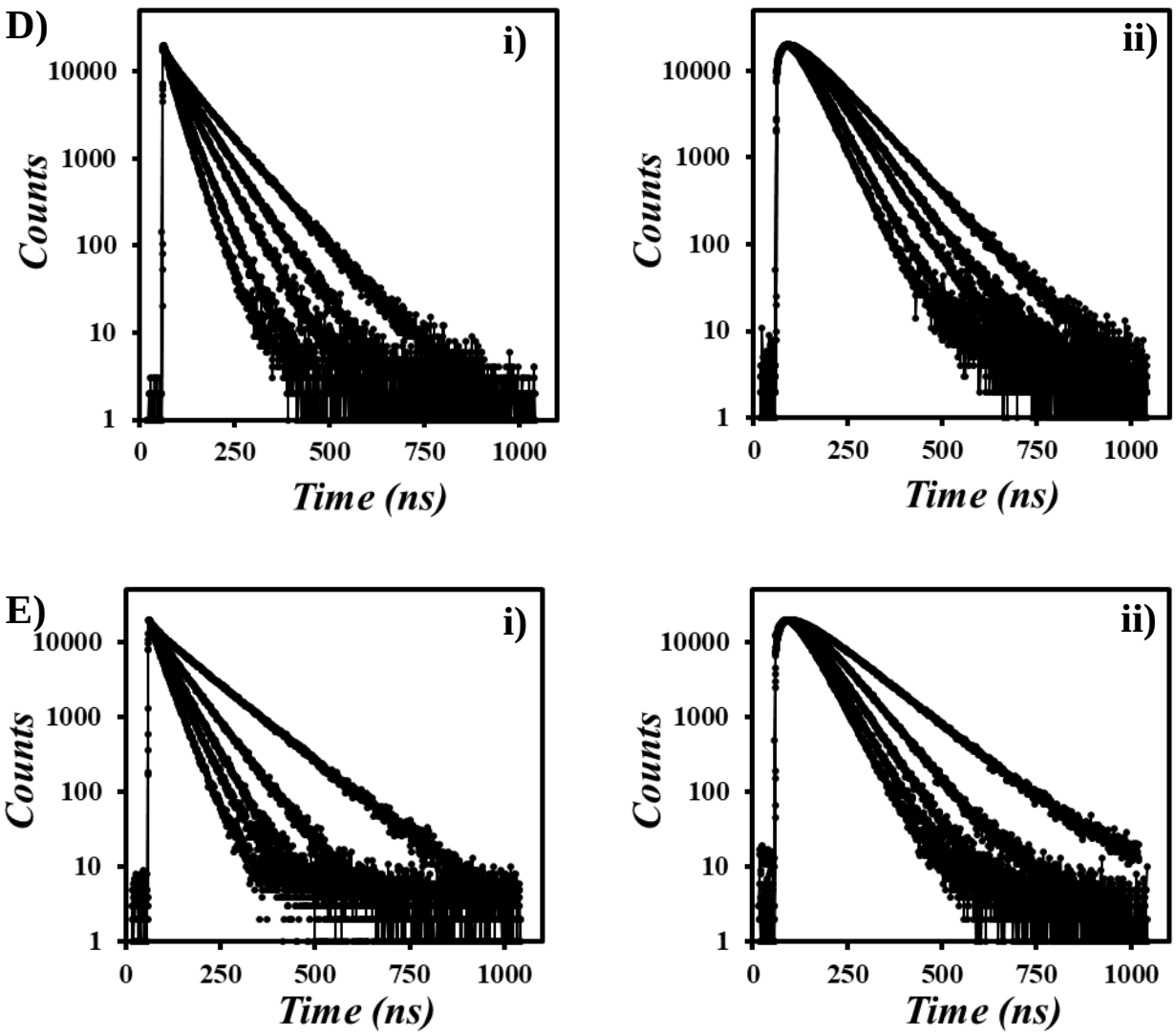

Figure A7. TRF decays of the pyrene i) monomer and ii) excimer of A) *f*-PIBSA-1-PyMA, B) *f*-PIBSA-2-PyMA, C) *pf*-PIBSA-2-PyMA, D) *u*-PIBSA-1-PyMA and E) *u*-PIBSA-2-PyMA solutions in THF with polymer concentrations varying from 2.5 to 40 g/L.

Table A1. Pre-exponential factors and decay times retrieved from MFA with Equations 2.2 and 2.3 for *f*-PIBSA-1-PyMA.

[Py] (mmol/ L)	[Poly] (g/L)	a_{M1}	a_{M2}	a_{M3}	a_{MS}	τ_{M1} (ns)	τ_{M2} (ns)	τ_{M3} (ns)	τ_{MS} (ns)	f_{diffE0}	f_{diffD}	f_{E0}	f_D	τ_{E0} (ns)	τ_D (ns)	χ^2
5.27	15.06	0.08	0.21	0.49	0.23	16.45	60.24	87.60	3.50	0.11	0.71	0.14	0.04	78.88	52.07	1.02
6.87	19.63	0.10	0.03	0.63	0.24	20.09	44.15	71.43	3.50	0.16	0.65	0.00	0.19	70.57	47.39	1.04
8.70	24.84	0.09	0.58	0.14	0.19	14.03	52.26	74.63	3.50	0.25	0.58	0.04	0.14	62.61	46.87	1.08
11.05	31.57	0.06	0.19	0.54	0.20	11.47	31.94	52.16	3.50	0.27	0.55	0.00	0.17	59.16	44.57	1.00

Table A2. Pre-exponential factors and decay times retrieved from MFA with Equations 2.2 and 2.3 for *f*-PIBSA-2-PyMA.

[Py] (mmol/ L)	[Poly] (g/L)	a_{M1}	a_{M2}	a_{M3}	a_{MS}	τ_{M1} (ns)	τ_{M2} (ns)	τ_{M3} (ns)	τ_{MS} (ns)	f_{diffE0}	f_{diffD}	f_{E0}	f_D	τ_{E0} (ns)	τ_D (ns)	χ^2
2.95	10.34	0.03	0.13	0.70	0.14	11.11	44.59	129.39	3.50	0.22	0.64	0.14	0.00	85.36	62.08	1.04
3.98	13.95	0.11	0.23	0.48	0.18	30.93	93.55	108.42	3.50	0.34	0.54	0.13	0.00	70.35	52.84	1.06
5.36	18.78	0.08	0.39	0.34	0.20	26.53	78.29	103.28	3.50	0.31	0.57	0.12	0.00	72.82	47.41	1.07
6.79	23.78	0.08	0.59	0.16	0.17	22.54	70.02	91.18	3.50	0.45	0.44	0.11	0.00	59.95	45.57	1.06
11.82	41.42	0.07	0.59	0.13	0.20	16.13	49.01	67.75	3.50	0.49	0.41	0.06	0.04	58.71	43.58	1.02

Table A3. Pre-exponential factors and decay times retrieved from MFA with Equations 2.2 and 2.3 for *pf*-PIBSA-2-PyMA.

[Py] (mmol/ L)	[Poly] (g/L)	a_{M1}	a_{M2}	a_{M3}	a_{MS}	τ_{M1} (ns)	τ_{M2} (ns)	τ_{M3} (ns)	τ_{MS} (ns)	f_{diffE0}	f_{diffD}	f_{E0}	f_D	τ_{E0} (ns)	τ_D (ns)	χ^2
4.84	9.96	0.13	0.61	0.05	0.21	31.33	76.40	83.99	3.50	0.51	0.39	0.11	0.00	59.63	43.10	1.02
7.21	14.84	0.04	0.26	0.49	0.21	17.08	42.70	64.02	3.50	0.25	0.65	0.09	0.01	62.72	42.59	1.15
9.67	19.90	0.07	0.29	0.47	0.17	15.53	36.81	50.16	3.50	0.01	0.89	0.09	0.01	74.49	44.83	1.01

Table A4. Pre-exponential factors and decay times retrieved from MFA with Equations 2.2 and 2.3 for *u*-PIBSA-1-PyMA.

[Py] (mmol/ L)	[Poly] (g/L)	a_{M1}	a_{M2}	a_{M3}	a_{MS}	τ_{M1} (ns)	τ_{M2} (ns)	τ_{M3} (ns)	τ_{MS} (ns)	f_{diffE0}	f_{diffD}	f_{E0}	f_D	τ_{E0} (ns)	τ_D (ns)	χ^2
1.74	2.50	0.08	0.14	0.63	0.15	11.47	48.47	139.05	3.50	0.40	0.42	0.07	0.11	84.23	52.10	1.04
3.48	5.01	0.13	0.42	0.31	0.14	18.15	73.61	96.02	3.50	0.44	0.39	0.15	0.02	65.13	44.65	1.05
5.22	7.50	0.11	0.39	0.34	0.16	16.18	53.44	73.11	3.50	0.32	0.51	0.17	0.00	61.20	42.81	1.08
6.93	9.96	0.09	0.21	0.54	0.16	11.42	36.45	56.27	3.50	0.28	0.56	0.16	0.00	57.57	42.28	1.00
7.82	11.23	0.11	0.17	0.56	0.17	15.54	37.47	54.51	3.50	0.23	0.61	0.15	0.00	59.36	43.96	1.08
8.66	12.45	0.06	0.24	0.54	0.16	10.48	29.38	47.82	3.50	0.23	0.61	0.02	0.13	55.97	41.11	1.00
10.43	14.99	0.06	0.49	0.31	0.14	8.89	30.51	45.12	3.50	0.28	0.56	0.11	0.05	52.98	38.93	0.98
11.33	16.27	0.06	0.21	0.58	0.15	9.37	24.05	40.61	3.50	0.02	0.83	0.10	0.05	68.35	43.48	1.06
12.17	17.48	0.40	0.12	0.33	0.15	38.00	13.95	28.18	3.50	0.00	0.83	0.06	0.11	72.52	41.40	1.15
13.89	19.96	0.05	0.32	0.48	0.15	6.33	21.75	33.34	3.50	0.45	0.39	0.05	0.11	46.74	34.14	1.00
15.67	22.51	0.08	0.43	0.35	0.15	10.83	21.99	32.04	3.50	0.22	0.61	0.07	0.10	49.98	36.19	1.13
17.39	24.99	0.06	0.38	0.43	0.13	6.98	18.94	28.36	3.50	0.03	0.80	0.09	0.08	52.89	37.64	1.18

Table A5. Pre-exponential factors and decay times retrieved from MFA with Equations 2.2 and 2.3 for *u*-PIBSA-2-PyMA.

[Py] (mmol/ L)	[Poly] (g/L)	a_{M1}	a_{M2}	a_{M3}	a_{MS}	τ_{M1} (ns)	τ_{M2} (ns)	τ_{M3} (ns)	τ_{MS} (ns)	f_{diffE0}	f_{diffD}	f_{E0}	f_D	τ_{E0} (ns)	τ_D (ns)	χ^2
5.50	9.95	0.04	0.11	0.72	0.13	10.36	31.00	64.47	3.50	0.18	0.71	0.10	0.01	60.02	45.53	1.07
6.88	12.45	0.14	0.11	0.54	0.22	23.69	51.93	55.72	3.50	0.22	0.65	0.13	0.01	55.20	45.15	1.17
8.29	15.00	0.11	0.21	0.54	0.14	19.14	45.80	48.72	3.50	0.29	0.59	0.12	0.00	51.04	39.17	1.03
9.65	17.47	0.10	0.19	0.54	0.17	18.54	32.49	44.27	3.50	0.54	0.33	0.05	0.08	50.80	40.42	1.19
11.06	20.02	0.11	0.19	0.58	0.11	18.24	32.11	41.86	3.50	0.41	0.48	0.09	0.03	45.78	35.33	1.04
12.40	22.43	0.06	0.47	0.25	0.21	17.44	30.64	40.42	3.50	0.23	0.63	0.00	0.14	53.24	38.92	1.10
13.81	24.99	0.04	0.31	0.52	0.14	9.08	23.81	34.54	3.50	0.58	0.30	0.02	0.09	46.56	35.40	0.95

Appendix B – Supporting Information for Chapter 3

Equation B1. The expression for the GPC calibration curve determined with cal-2.

$$Ln(M_i) = 0.867 \times 10^{-3} \times {V_{el}}^2 - 0.742 \times V_{el} + 19.638 \quad \text{(B1)}$$

Table B1. Pre-Gaussian factors, averages, and standard deviations retrieved from the fit of the DRI trace of the PIBSA-2 sample as a function of (V_{el}) weight tetragauss according to Equation 3.1.

Sample	A	a_1	μ_1	σ_1	a_2	μ_2	σ_2	a_3	μ_3	σ_3	a_4	μ_4	σ_4
PIBSA-2	127.94	0.082	15.563	1.357	0.601	16.399	0.738	0.036	16.661	0.348	0.281	17.505	1.199

Table B2. Pre-Gaussian factors, averages, and standard deviations retrieved from the fit of the DRI traces of the PIBSA-2-H(*X*) samples as a function of (V_{el}) with *x*gaussSNP (*x* = *bi*, *tri*) according to Equation 3.2.

Sample	A	B	a_1	μ_1	σ_1	a_2	μ_2	σ_2	a_3	μ_3	σ_3
PIBSA-2-H(0.25)	128.933	18.076	0.982	15.494	0.546	0.018	16.497	0.169			
PIBSA-2-H(0.5)	68.705	80.864	0.120	14.898	0.493	0.170	15.385	0.319	0.710	15.919	0.728
PIBSA-2-H(0.75)	68.352	82.959	0.307	15.378	0.390	0.679	15.623	0.787	0.014	16.500	0.244
PIBSA-2-H(1)	86.580	145.510	0.465	15.292	0.621	0.225	15.377	0.345	0.310	15.675	0.684
PIBSA-2-H(1.25)	59.696	84.819	0.351	15.246	0.644	0.186	15.401	0.330	0.463	15.447	0.568
PIBSA-2-H(1.5)	54.950	83.962	0.029	14.716	0.572	0.051	15.333	0.287	0.920	15.45	0.629
PIBSA-2-H(1.75)	59.568	71.565	0.189	14.785	0.507	0.070	15.267	0.322	0.741	15.477	0.583
PIBSA-2-H(2.0)	50.175	47.09	0.230	14.729	0.445	0.096	15.257	0.322	0.674	15.484	0.550

Table B3. Pre-Gaussian factors, averages, and standard deviations retrieved from the fit of the simulated MWDs obtained for *m*-, *b*-, *tri*- and *tet*- PIBSI as a function of (X_n) with *x*gauss (*x* = *tri*, *tetra*, and *hexa*) according to Equation 3.1.

Sample	A	a_1	μ_1	σ_1	a_2	μ_2	σ_2	a_3	μ_3	σ_3	a_4	μ_4	σ_4	a_5	μ_5	σ_5	a_6	μ_6	σ_6
m-PIBSI	1	0.035	6.255	2.915	0.075	12.449	4.813	0.389	25.024	9.493	0.279	42.226	11.117	0.099	64.046	12.363	0.123	83.911	27.440
b-PIBSI	1	0.248	45.376	15.897	0.468	70.931	19.921	0.180	106.477	20.869	0.104	141.887	28.265						
tri-PIBSI	1	0.307	80.834	22.931	0.365	115.124	27.527	0.319	154.906	41.19									
tet-PIBSI	1	0.301	109.921	25.700	0.254	144.889	24.429	0.268	180.667	30.317	0.168	223.106	43.006						

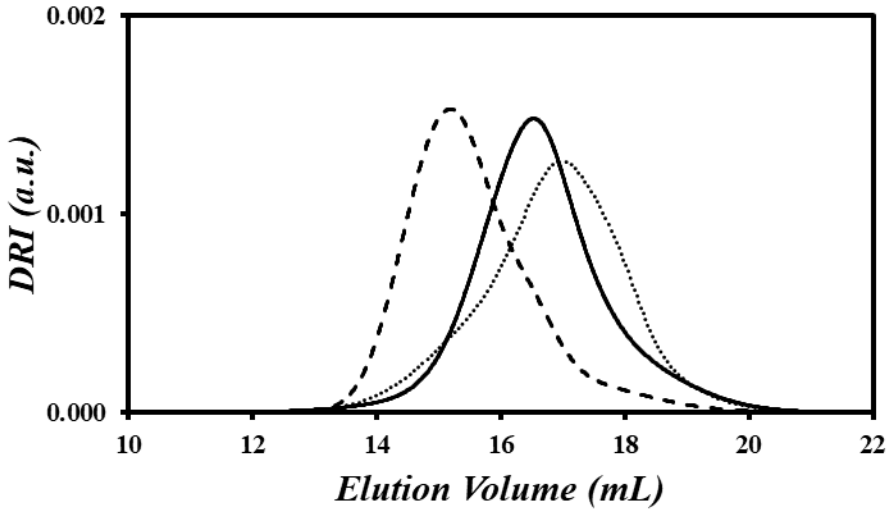

Figure B1. Gaussian fits of the DRI traces of (solid) a dehydrated PIBSA-2 sample, (dashed) a PIB standard with M_n = 3.2 K and PDI = 1.3, and (dotted) a PIB standard with M_n = 1.0 K and PDI = 1.5, normalized to a sum of 1.

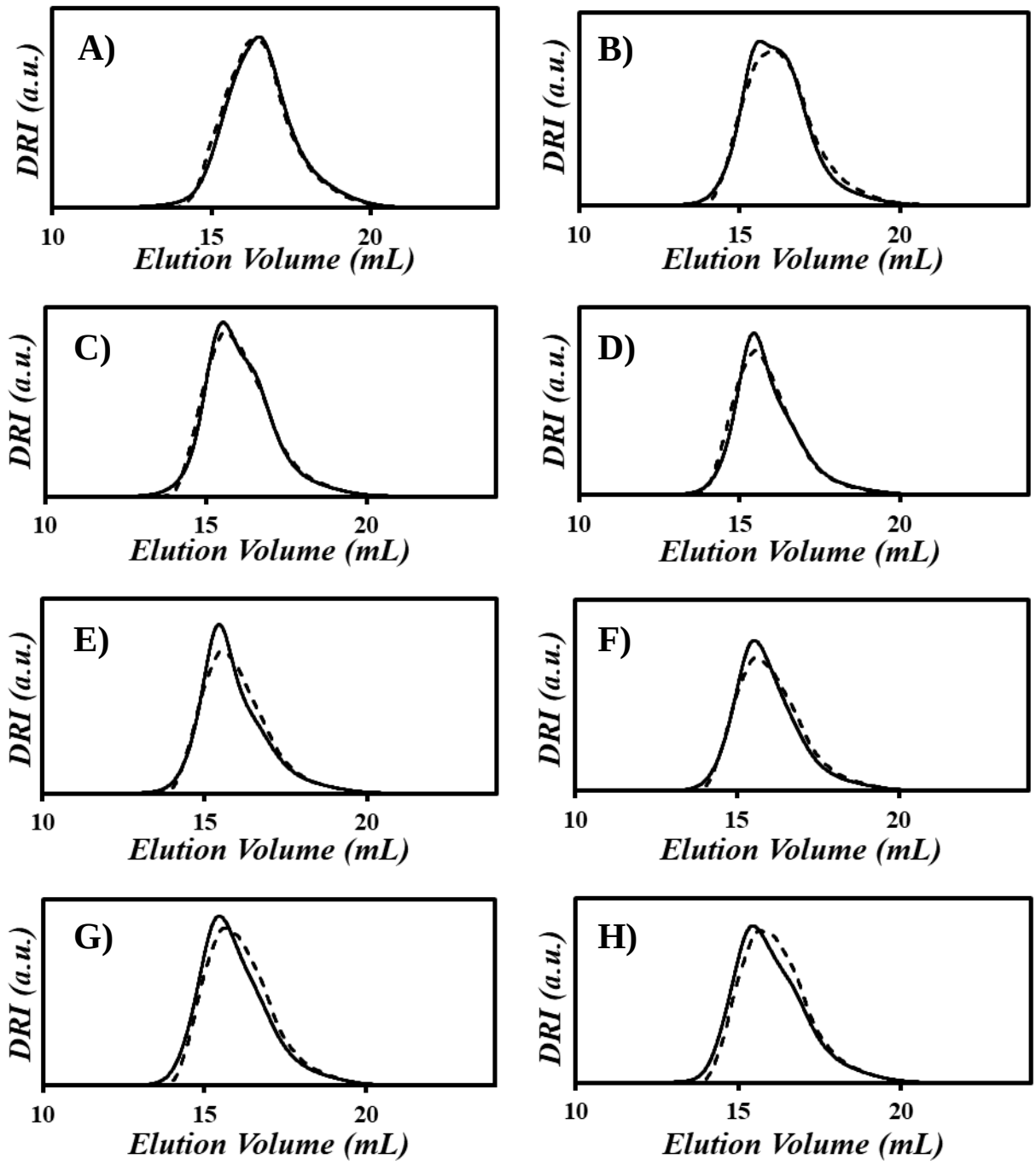

Figure B2. Comparison of (- - - -) the simulated DRI traces obtained from the molar fractions determined with reaction3, and w_{PIB} = 0.30 using the simulated traces of *m*-, *b*-, *tri*-, and *tet*-PIBSI from prod-dis2 and (———) the experimental DRI traces fitted with the *x*gaussSNP programs of the PIBSA-2-H(*X*) products. The N_{Am}/N_{SA} ratios equal A) 0.25, B) 0.5, C) 0.75, D) 1.0, E) 1.25, F) 1.5, G) 1.75, and H) 2.0.

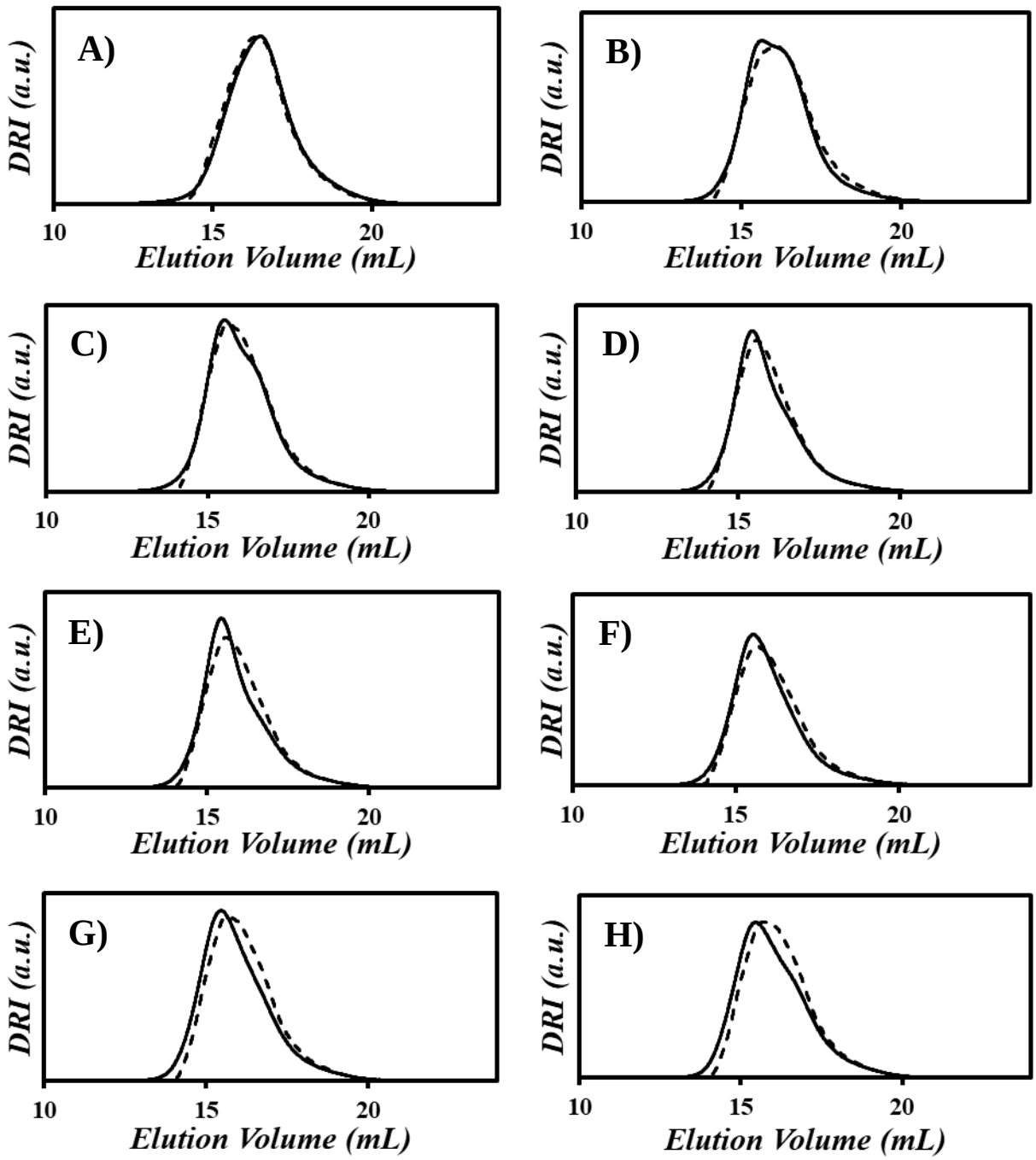

Figure B3. Comparison of (- - - -) the simulated DRI traces obtained from the molar fractions obtained with reaction4, and w_{PIB} = 0.30 using the simulated traces of *m*- and *b*-PIBSI from prod-dis2 and (———) the experimental DRI traces fitted with the *x*gaussSNP programs of the PIBSA-2-H(*X*) products. The N_{Am}/N_{SA} ratios equal A) 0.25, B) 0.5, C) 0.75, D) 1.0, E) 1.25, F) 1.5, G) 1.75, and H) 2.0.

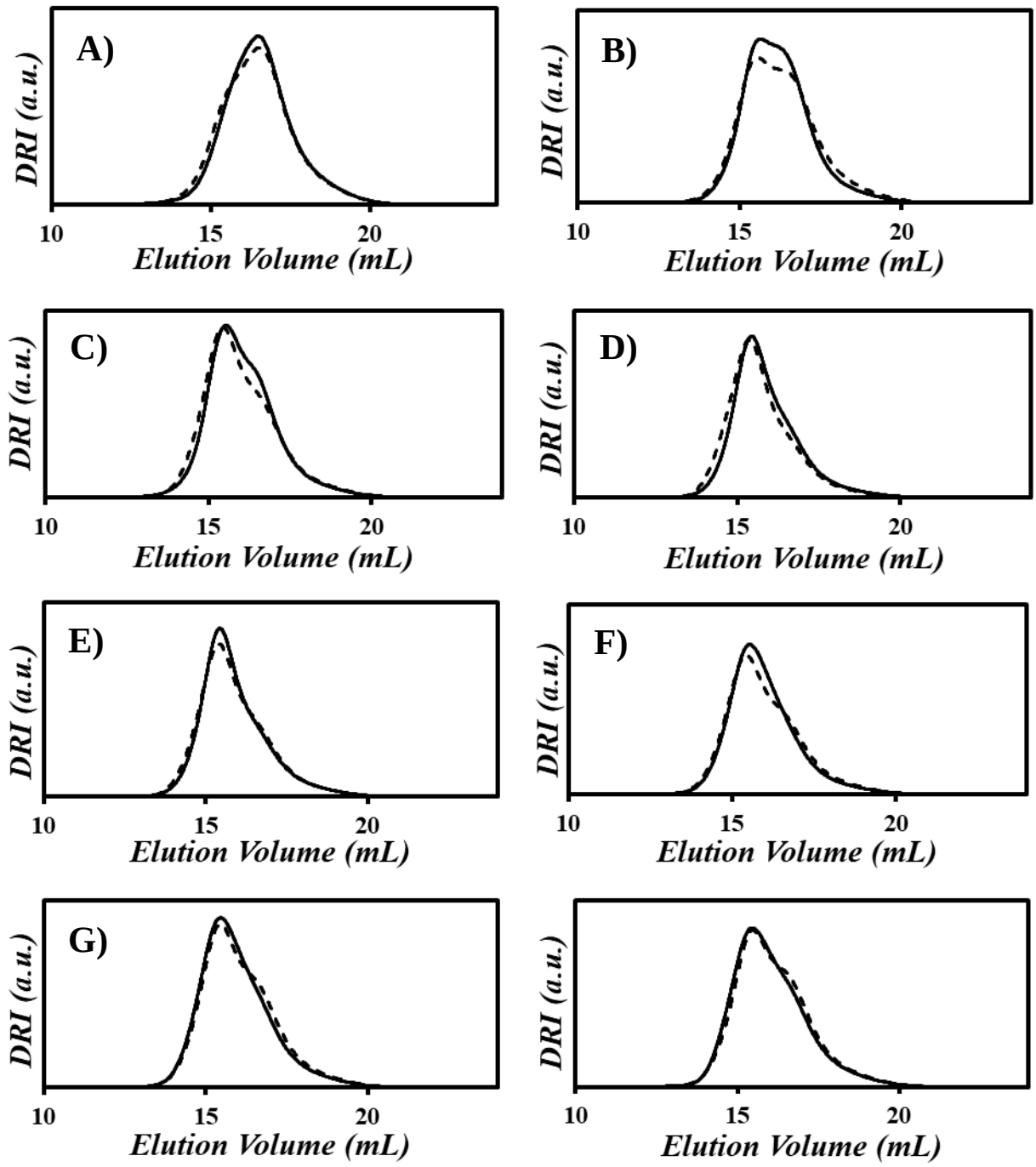

Figure B4. Comparison of (- - - -) the simulated DRI traces obtained from the molar fractions obtained with reaction3, and w_{PIB} = 0.30 using the experimental *m*- and *b*-PIBSI traces and simulated traces of *tri*- and *tet*-PIBSI from prod-dis2, and (———) the experimental DRI traces fitted with the *x*gaussSNP programs of the PIBSA-2-H(*X*) products. The N_{Am}/N_{SA} ratios equal A) 0.25, B) 0.5, C) 0.75, D) 1.0, E) 1.25, F) 1.5, G) 1.75, and H) 2.0.

Appendix C – Supporting Information for Chapter 4

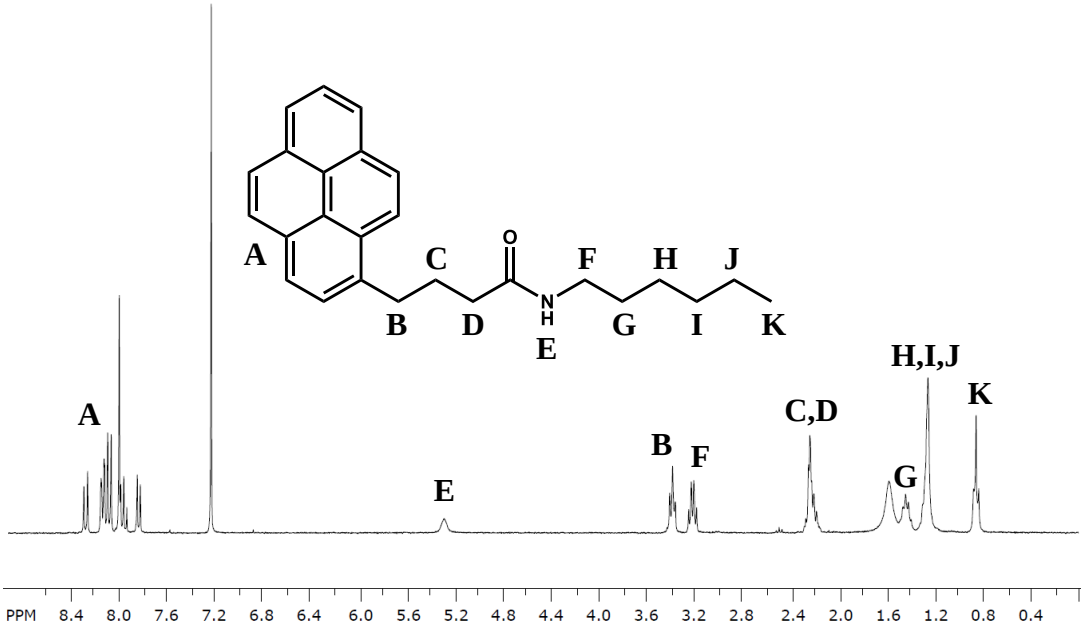

Figure C1. ^{1}H NMR spectrum of Py_1-HA in $CDCl_3$. The peaks at 7.27 and 1.58 ppm are from $CHCl_3$ and H_2O, respectively.

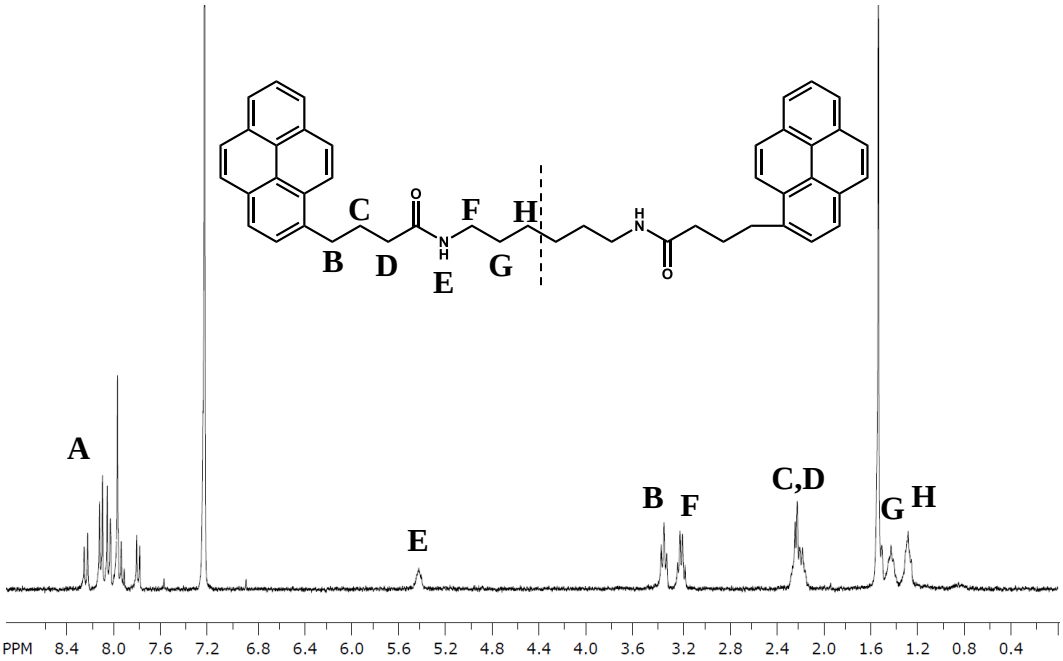

Figure C2. ^{1}H NMR spectrum of Py_2-HMDA in $CDCl_3$. The peaks at 7.27 and 1.56 ppm are from $CHCl_3$ and H_2O, respectively.

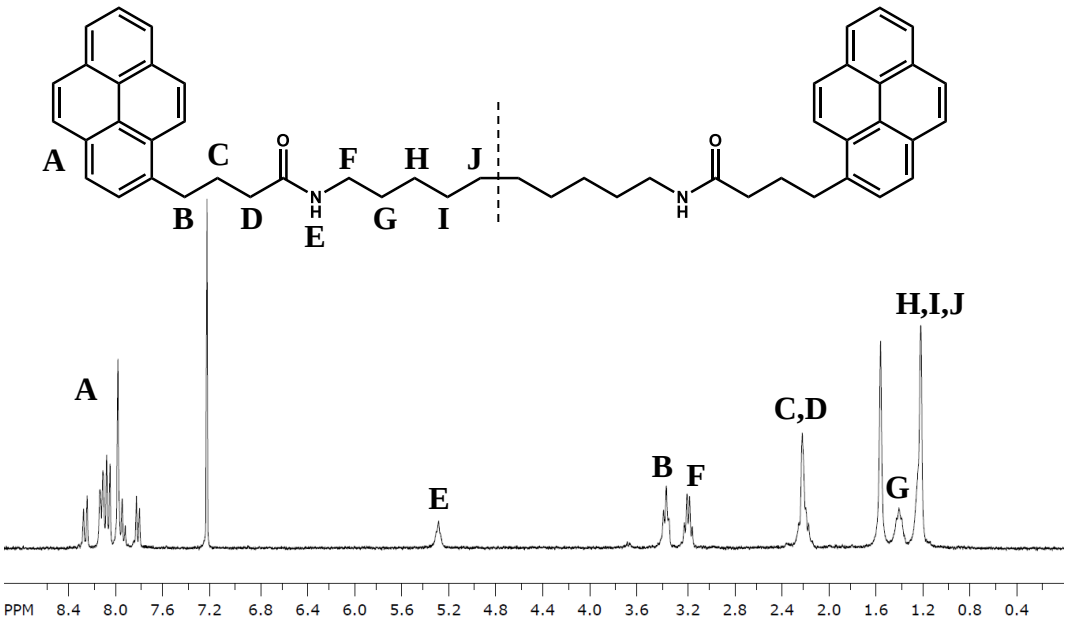

Figure C3. ^{1}H NMR spectrum of Py_2-DEC in $CDCl_3$. The peaks at 7.27 and 1.58 ppm are from $CHCl_3$ and H_2O, respectively.

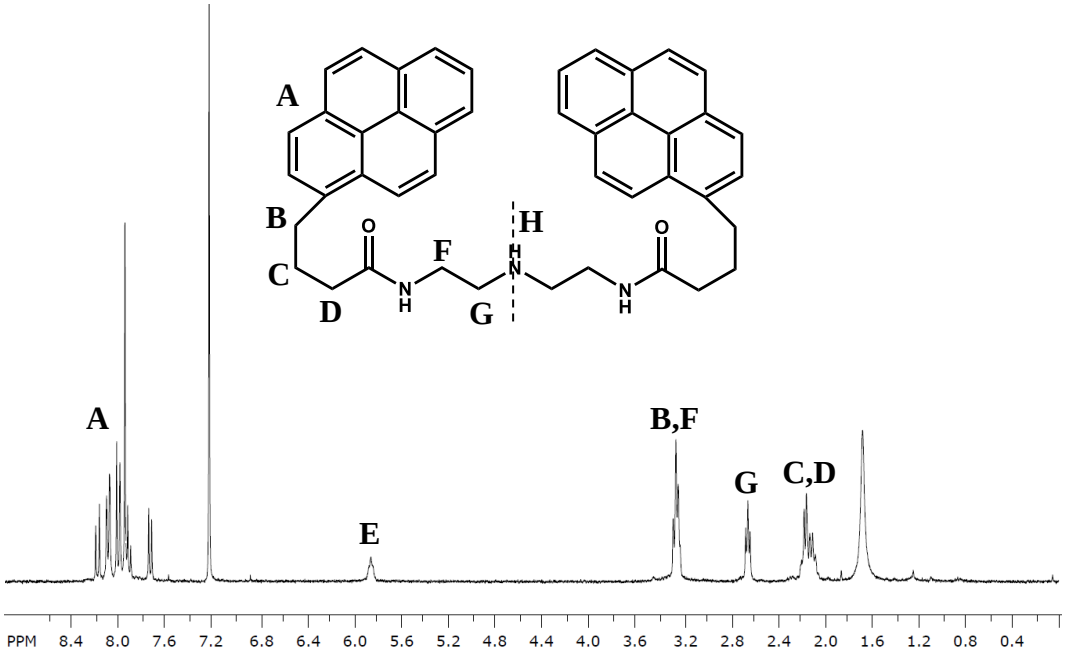

Figure C4. ^{1}H NMR spectrum of Py_2-DETA in $CDCl_3$. The peaks at 7.27 and 1.63 ppm are from $CHCl_3$ and H_2O, respectively. The secondary amine proton of DETA is exchanging with the solvent.

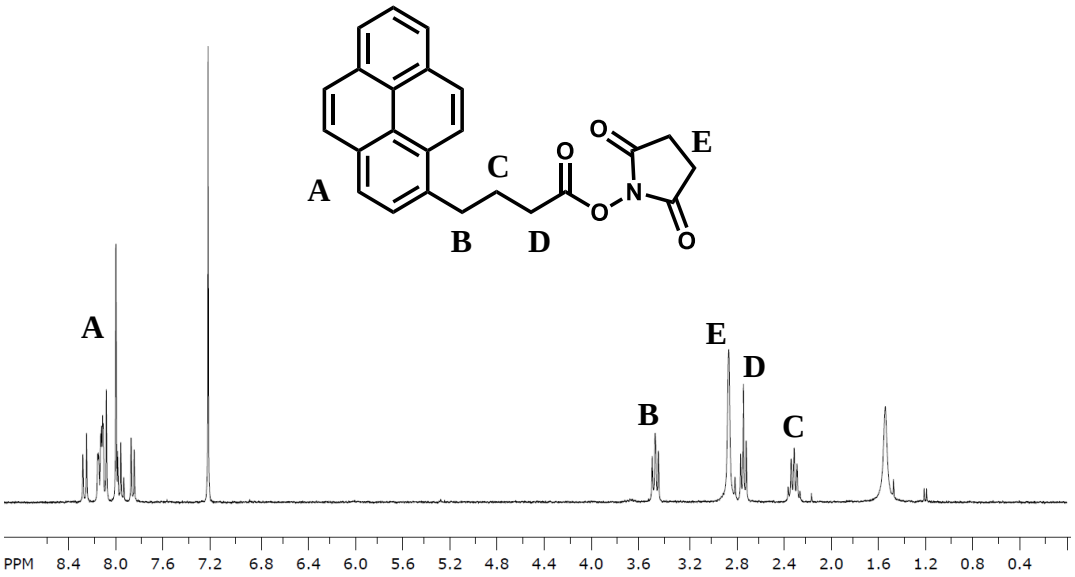

Figure C5. ^{1}H NMR spectrum of PyBA-OSu in $CDCl_3$. The peaks at 7.27 and 1.56 ppm are from $CHCl_3$ and H_2O, respectively.

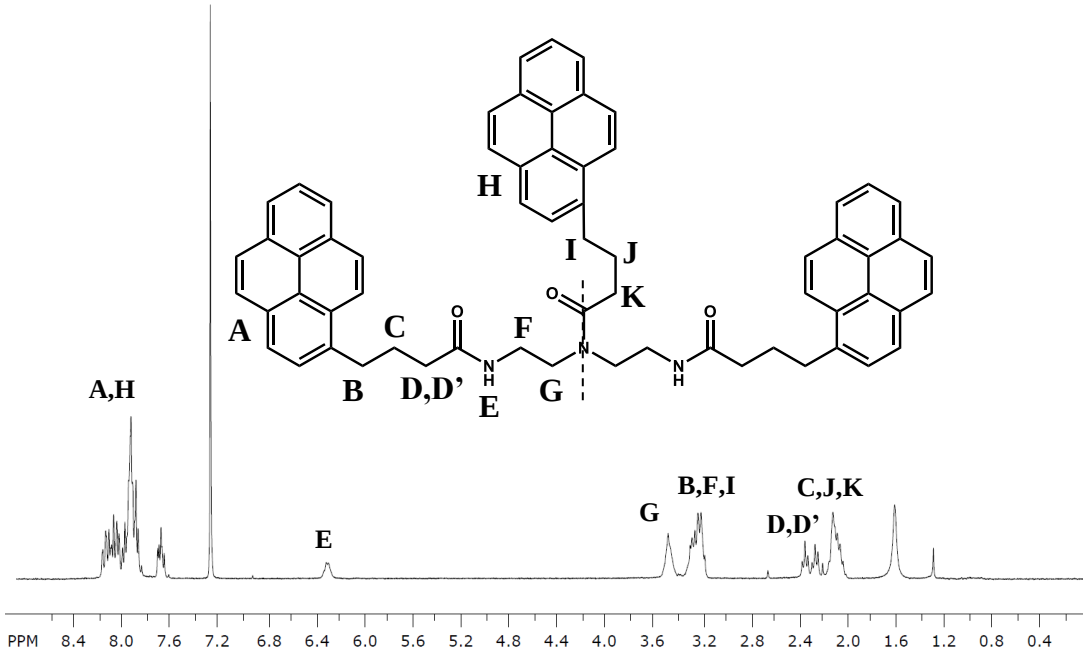

Figure C6. ^{1}H NMR spectrum of Py_3-DETA in $CDCl_3$. The peaks at 7.27 and 1.60 ppm are from $CHCl_3$ and H_2O, respectively.

Table C1. Pre-exponential factors, decay times, and <*k*> retrieved from MFA with Equations 4.5 and 4.6 for the Py-PAs.

Sample	Solvent	a_{M1}	a_{M2}	a_{M3}	a_M	τ_{M1} (ns)	τ_{M2} (ns)	τ_{M3} (ns)	τ_M (ns)	f_{diffE0}	f_{diffD}	f_{E0}	f_D	τ_{E0} (ns)	τ_D (ns)	<k> (μs^{-1})	χ^2
Py_2-HMDA	THF	0.92	0.04	\	0.03	9.2	57	\	203	0.36	0.55	0.09	0.00	67	46	83	1.27
	DMF	0.92	0.05	\	0.03	16.2	63	\	175	0.42	0.53	0.04	0.00	62	45	48	1.23
	DMSO	0.94	0.03	\	0.03	23	70	\	137	0.35	0.60	0.05	0.00	58	45	34	1.25
Py_2-DEC	THF	0.87	0.08	\	0.05	17.9	71	\	203	0.96	\	0.04	\	55	\	39	1.22
	DMF	0.84	0.10	\	0.06	25	62	\	175	0.97	\	0.03	\	54	\	29	1.11
	DMSO	0.87	0.07	\	0.06	31	66	\	137	0.96	\	0.04	\	52	\	22	1.12
Py_2-DETA	THF	0.91	0.02	0.04	0.03	5.9	34	82	203	0.73	0.18	0.08	0.00	58	31	98	1.13
	DMF	0.92	0.04	0.02	0.02	10.4	58	117	175	0.54	0.36	0.10	0.00	56	42	63	1.17
	DMSO	0.86	0.07	0.05	0.03	17.2	17.2	59	137	0.46	0.46	0.09	0.00	54	40	45	1.15
Py_3-DETA	THF	0.61	0.36	0.02	0.01	2.9	5.3	43	203	0.82	0.08	0.06	0.04	54	29	210	1.04
	DMF	0.91	0.07	0.02	0.00	4.7	10.7	52	175	0.60	0.31	0.08	0.00	52	41	163	1.02
	DMSO	0.35	0.63	0.02	0.00	5.4	8.9	53	137	0.49	0.41	0.10	0.00	50	40	112	1.07